Imperial College London
Department of Mechanical Engineering

Flywheel Energy Storage Systems for Rail

Matthew Read

November 2010

Thesis submitted for the Diploma of the Imperial College (DIC),

PhD degree of Imperial College London

I declare that the research presented in this Thesis is my own work and that the work of others is properly acknowledged and referenced.

Matthew Read

Abstract

In current non-electrified rail systems there is a significant loss of energy during vehicle braking. The aim of this research has been to investigate the potential benefits of introducing onboard regenerative braking systems to rail vehicles.

An overview of energy saving measures proposed within the rail industry is presented along with a review of different energy storage devices and systems developed for both rail and automotive applications. Advanced flywheels have been identified as a candidate energy storage device for rail applications, combining high specific power and energy.

In order to assess the potential benefits of energy storage systems in rail vehicles, a computational model of a conventional regional diesel train has been developed. This has been used to define a base level of vehicle performance, and to investigate the effects of energy efficient control strategies focussing on the application of coasting prior to braking. The impact of these measures on both the requirements of an energy storage system and the potential benefits of a hybrid train have been assessed.

A detailed study of a range of existing and novel mechanical flywheel transmissions has been performed. The interaction between the flywheel, transmission and vehicle is investigated using a novel application-independent analysis method which has been developed to characterise and compare the performance of different systems. The results of this analysis produce general 'design tools' for each flywheel transmission configuration, allowing appropriate system configurations and parameters to be identified for a particular application. More detailed computational models of the best performing systems have been developed and integrated with the conventional regional diesel train model. The performance of proposed flywheel hybrid regional trains has been assessed using realistic component losses and journey profiles, and the fuel saving relative to a conventional train quantified for a range of energy storage capacities and power-train control strategies.

Acknowledgments

I would like to thank my supervisor, Roderick Smith, for his support and guidance. I am also very grateful to Keith Pullen for his invaluable knowledge, advice and enthusiasm.

Many thanks go to my colleague and friend Pablo Martinez. His knowledge and insight has resulted in many thought-provoking conversations and fruitful ideas. I would also like to thank Catherine Griffiths for her advice during the writing-up process and all the members of the Future Railway Research Centre for providing such a stimulating research environment.

Finally, I owe an enormous debt of gratitude to my parents. This would not have been possible without their endless support and encouragement.

Nomenclature

Symbol	Unit	Meaning
E	J	Energy
fc	litres/car-km	Fuel consumption
F	N	Force
G	-	Speed ratio of gear pair in control gearbox
GPE	J	Gravitational potential energy
h	m	height
J	kg m^2	Moment of inertia
K	-	Speed ratio of gear pair
KE	J	Kinetic energy
m	kg	Mass
P	W	Power
R	-	Characteristic gear ratio of planetary gearset
r	-	Overall transmission speed ratio
t	s	Time
T	Nm	Torque
U	-	Flywheel utilisation factor
v	m/s	Velocity
x	m	Displacement
η	-	Efficiency
φ	-	Variator speed ratio
ω	rad/s	Angular velocity

Abbreviations

Abreviation	Meaning
ATOC	Association of Train Operating Companies
BL	Branch-line
CGB	Control gearbox
CVT	Continuously variable transmission
DDC	Dual differential coupled
DMU	Diesel multiple unit
DOD	Depth of discharge
ESS	Energy storage system
FC	Fluid coupling
FDC	Final drive coupled
FESS	Flywheel energy storage system
FHRT	Flywheel hybrid regional train
FMG	Flywheel motor generator
FWC	Flywheel coupled
GA	Genetic algorithm
GHG	Greenhouse gas
GM	General Motors
HRDT	Hybrid regional diesel train
IAM	Independent Analysis Method
ICE	Internal combustion engine
IEA	International Energy Authority
IPCC	Intergovernmental Panel on Climate Change
IVT	Infinitely variable transmission
LDV	Light duty vehicle
Li-ion	Lithium ion
LPG	Liquid petroleum gas
ML	Main-line
NiMH	Nickel metal hydride
OC	Output couped
PGS	Planetary gearset
PST	Power-split transmission
RSSB	Rail Safety and Standards Board
RTRI	Railway Technical Research Institute
SE	Specific energy
SOC	State of charge
TC	Torque converter
ULEV	Ultra low emission vehicle
UMTA	Urban Mass Transportation Administration
VRLA	Valve regulated lead acid

Table of contents

Abstract **3**

Acknowledgments **4**

Nomenclature **5**

Abbreviations **6**

List of figures **11**

List of tables **18**

1. Introduction **20**

1.1. Background to energy consumption in the UK rail network 24

1.2. Proposed energy saving options 26

1.3. Objectives of the research 28

1.4. Overview of Thesis structure 29

2. Literature review **31**

2.1. Hybrid power-train technology 31

2.1.1. Overview of hybrid vehicle classification 32

2.1.2. Energy storage devices 36

2.1.2.1. Energy and power capabilities of storage devices 40

2.1.2.2. Additional considerations 41

2.1.3. Developments in hybrid rail vehicles 47

2.1.4. Continuously variable transmissions for flywheel energy storage systems 54

2.1.4.1. Fixed ratio gearbox with slipping clutch 54

2.1.4.2. Variator technology 55

2.1.4.3. Power-split principles for a simple differential 58

2.1.4.4. Advanced power split configurations 61

2.1.5. Mechanical flywheel hybrid vehicles 62

2.2. Rail vehicle energy modelling 67

2.2.1. Optimised control 68

2.2.2. Hybrid rail vehicle analysis 69
2.2.3. Rail vehicle modelling 71
2.3. Summary 74
3. Effects of driving strategy on conventional and hybrid diesel regional trains 75
3.1. Approach to vehicle modelling 75
3.1.1. Vehicle dynamics module 76
3.1.2. Power-train module 77
3.1.3. Vehicle control module 79
3.1.4. Description of route data 81
3.2. Driving strategies for conventional vehicles 82
3.2.1. Effect of timetabling constraints on fuel consumption 84
3.3. Simple vehicle model of a hybrid regional train 86
3.3.1. Constant force regenerative braking with coasting 86
3.3.2. Constant power regenerative braking with coasting 88
3.3.3. Effect of timetable restrictions on performance of hybrid regional train 89
3.3.4. Requirements for HRDT regenerative braking system 92
3.4. Summary 92
4. Independent analysis of clutch and brake controlled flywheel transmissions 94
4.1. Brake-controlled flywheel transmissions 95
4.1.1. Connection options for differential gearing 97
4.1.2. Approach to independent analysis of PGS transmissions 97
4.1.3. Analysis of multi-PGS brake-controlled transmission 100
4.1.4. Results for single PGS brake-controlled flywheel transmission 106
4.1.5. Results for multiple PGS brake-controlled transmissions 114
4.1.6. Regional rail application of flywheel system with brake-controlled transmission 116
4.2. Independent analysis of clutch-controlled flywheel transmissions 121
4.2.1. Clutch-controlled power-split transmission modes 121
4.3. Multi-PGS clutch/brake controlled PST 133

4.3.1. CGB kinematic requirements 134
4.3.2. Performance of CGB-controlled PST 137
4.3.3. CGB torque and speed requirements 140
4.3.4. Strategy for limiting CGB mass 142
4.3.5. Regional rail vehicle application of CGB-controlled PST 144
4.4. Summary 146
5. Independent analysis of variator-controlled transmissions 148
5.1. Direct variator-controlled transmission 149
5.2. Single regime variator-controlled power-split transmissions 152
5.2.1. Ideal variator-controlled power-split phase 153
5.2.2. Independent analysis of single regime variator-controlled PSTs 156
5.2.3. Comparison of single regime variator-controlled transmissions 168
5.3. Single PGS, 2-regime variator-controlled transmissions 171
5.3.1. Combined FDC/FWC 2-regime transmission 172
5.3.2. Synchronous shift 2-regime transmissions 174
5.3.3. Comparison of multiple regime variator-controlled transmissions 177
5.4. Multiple-regime FDC/DDC transmissions 179
5.5. Regional rail application of variator-controlled PSTs 182
5.6. Summary 183
6. Effect of vehicle and flywheel losses on FESS performance 185
6.1. Characterisation of vehicle and flywheel losses 185
6.1.1. Flywheel resistance losses 186
6.1.2. Vehicle resistance losses 187
6.2. Methodology for assessing accuracy of Independent Analysis Method 188
6.3. FESS performance for regional train application including losses 190
6.4. FESS performance for passenger car application including losses 194
6.5. Summary 196
7. Investigation of flywheel hybrid regional train 197

7.1. FESS configurations considered for hybrid train 197
7.2. Integration of FESS and conventional diesel regional train models 198
7.2.1. Torque and speed dependence of FESS component efficiencies 198
7.2.2. FESS control strategy 201
7.3. Results of FHRT modelling 203
7.3.1. Effect of FESS control strategy on FHRT performance 205
7.3.2. Effect of initial FESS condition on FHRT performance 208
7.3.3. Comparison of mechanical FESSs for regional rail application 209
7.4. Summary 213
8. Summary and conclusions 215
8.1. Summary of research and contributions 215
8.2. Recommendations for future work 218
Appendices 220
Appendix A – Identifying expression for normalised CGB speed 220
Appendix B – Further results from the Dependent Analysis Method 221
Appendix C – Consideration of PGS meshing losses 223
Bibliography 225

List of figures

Figure 1-1 – Proposed reductions in energy related CO_2 emissions in order to stabilise atmospheric concentration at 450 ppm [3] 21

Figure 1-2 – (a) World energy-related CO_2 emissions [4] and (b) Global transport energy use by mode in 2000 [2] 21

Figure 1-3 – Average energy intensity of passenger and freight transportation in IEA member countries [3] 22

Figure 1-4 – Proposed CO_2 reduction measures for transport in order to meet BLUE Map scenario [3] 23

Figure 1-5 – Estimated breakdown of UK electric train energy usage after power generation losses [11] 25

Figure 1-6 – Estimated breakdown of UK diesel train energy usage after engine losses [11] 25

Figure 2-1 – Classification of hybrid electric vehicles [16] 33

Figure 2-2 – Typical series electric hybrid architecture 34

Figure 2-3 – Parallel hybrid architecture 35

Figure 2-4 – Example of complex 'power-split' hybrid architecture 35

Figure 2-5 – Examples of flywheel design for (a) mechanical [33] and (b) electrical [34] FESSs 38

Figure 2-6 – Comparison of specific energy and power for energy storage devices 40

Figure 2-7 – Typical charge and discharge efficiency of a lead-acid battery as a function of *SOC* [51] 41

Figure 2-8 – Effect of *SOC* on specific power of a Li-ion cell at 25°c [52] 42

Figure 2-9 – Effect of temperature on specific power of a NiMH battery at 60% *SOC* [52] 42

Figure 2-10 – Implementation of Li-ion battery modules in a vehicle application [49] 43

Figure 2-11 – Typical power-train efficiencies for electrical and mechanical FESSs during discharge 45

Figure 2-12 – Overview of the NE Train layout and operational performance [67] 48

Figure 2-13 – (a) Lithium-ion battery system developed by RTRI [70] and (b) Mitrac supercapacitor based energy storage unit [71] 49

Figure 2-14 – Illustration of conventional and hybrid shunting locomotives [75] 50

Figure 2-15 – (a) Illustration of ACT-1 flywheel-motor-generator unit [78] and (b) ULEV-TAP2 complete electrical flywheel system [61] 51

Figure 2-16 – PPM vehicle and power-train configuration [79] 52

Figure 2-17 – Specific energy, specific power and energy density for Li-ion supercapacitor and advanced flywheel devices and integrated units (arrows show the effect of control and packaging requirements) 53

Figure 2-18 – Illustration of a full toroidal variator [82] 55

Figure 2-19 – (a) Illustration of push-belt variator operation showing low and high gear ratios [84] and (b) details of push-belt construction 56

Figure 2-20 – Toroidal variator efficiency for an output/input speed ratio of 1 [85] 57

Figure 2-21 – Description of generic differential gearing unit 58

Figure 2-22 – Possible range of *R* values for practical simple and idler PGSs [95] 59

Figure 2-23 – Illustration of the possible operating regions for a variator-controlled 'output coupled' power-split transmission with arrows showing direction and magnitude of power flow (adapted from [96]) 60

Figure 2-24 – Proposed flywheel hybrid power-train for passenger car [93] 61

Figure 2-25 – Example of the operation of the Gyreacta in vehicle acceleration mode (simplified diagram does not include PGS-flywheel gearbox) [103] 63

Figure 2-26 – Illustration of proposed flywheel hybrid power-train [104] 64

Figure 2-27 – Illustration of flywheel hybrid power-train proposed by General Motors 65

Figure 2-28 – Flybrid mechanical FESS developed for Formula 1 application [109] 66

Figure 2-29 – Illustration of longitudinal dynamic forces 71

Figure 3-1 – Flow chart of calculation procedure for forward-facing model structure consisting of control, power-train and vehicle dynamics modules 76

Figure 3-2 – Specific fuel consumption and max torque curve for a 315kW engine 77

Figure 3-3 – Power-train output values of (a) tractive effort, (b) SFC, (c) transmission efficiency and (d) tank-to-wheel efficiency as a function of vehicle speed for power notches 1, 3, 5 and 7 78

Figure 3-4 – Schematic illustration of vehicle control subsystem operation 80

Figure 3-5 – Data for (a) Main-line and (b) Branch-line routes used in the simulations 81

Figure 3-6 – Examples of calculated vehicle speed profiles for main-line route with no coasting (flat out) and coasting trigger deceleration values (D_{coast}) of 0.1 and 0.07 m/s^2 81

Figure 3-7 – Comparison of measured fuel consumption (fc) with results of model using 'flat-out' vehicle operation matching the time-tabled departure times for main-line (ML) and branch-line (BL) routes 82

Figure 3-8 – Effect of increasing coasting and reducing maximum vehicle speed on relative journey time and fuel consumption for main-line operation with station dwell time of 60s 83

Figure 3-9 – Effect of increasing coasting and reducing maximum vehicle speed on relative journey time and fuel consumption for branch-line operation with station dwell time of 30s..... 83

Figure 3-10 – Illustration of the cause of fuel consumption increase when timetable-limited coasting is used to achieve overall journey time..... 85

Figure 3-11 – Effect of coasting on main-line hybrid performance with ESS power limitations..... 87

Figure 3-12 – Effect of coasting on branch-line hybrid performance with ESS power limitations..... 87

Figure 3-13 – Calculated fuel saving and required energy capacity for hybrid train with 1MW ESS using constant power and constant force braking strategies with various degrees of coasting on main-line (ML) and branch-line (BL) routes 88

Figure 3-14 – Braking energy available during approach to (a) ML and (b) BL stations using uniform and timetable-limited coasting to achieve overall journey time; dotted lines shows minimum ESS capacity required to capture all available energy with uniform coasting (assuming 100% ESS efficiency) 90

Figure 3-15 – Hybrid fuel savings relative to conventional vehicle using timetable-limited coasting to achieve overall journey time (assuming 100% ESS efficiency) 91

Figure 3-16 – ML and BL fuel consumption for conventional and hybrid vehicles using uniform and timetable (TT) limited coasting strategies (ESS power and energy capacities as stated and assuming 100% efficiency)..... 91

Figure 4-1 – Examples of (a) brake and (b) clutch controlled flywheel transmissions..... 96

Figure 4-2 – Definition of relationship between the flywheel rotor and the output characteristics of the flywheel unit 99

Figure 4-3 – Schematic diagram of brake-controlled flywheel transmission with m differentials (arrows show the direction of power flow during flywheel discharge using PGS 1) 101

Figure 4-4 – Example of a possible configuration for 2-PGS ring-brake controlled transmission (note: $0 < R_1 < R_2 < 0.5$ in this configuration)..... 101

Figure 4-5 – Illustration of simple flywheel discharge/charge cycle with a 2-PGS ring-brake transmission, constant T_{fd} and DOD_{ov} = 75% 102

Figure 4-6 – Value of $|R^*|/\sqrt{\eta_{pgs}}$ as a function of DOD_{ov} for a single PGS brake-controlled transmission 107

Figure 4-7 – (a) discharge and (b) charging efficiency as a function of η_{pgs} and DOD_{ov} for a 1-PGS brake-controlled transmission 108

Figure 4-8 – Round-trip efficiency of the 1-PGS brake-controlled transmission as a function of η_{pgs} and DOD_{ov}..... 109

Figure 4-9 – The value of U/η_{pgs} as a function of DOD_{ov} for the 1-PGS brake-controlled transmission 109

Figure 4-10 – Normalised energy dissipation at the control brake during discharging and charging of flywheel, as a function of η_{pgs} and DOD_{ov} for a 1-PGS brake-controlled transmission 111

Figure 4-11 – Total energy dissipation in the control brake during a full charge/discharge cycle per unit energy delivered to the vehicle during flywheel discharge as afunction of η_{pgs} and DOD_{ov} for a 1-PGS brake-controlled transmission 112

Figure 4-12 – Values of $|R_n^*|/\sqrt{\eta_x}$ required to achieve maximum $\eta_{discharge}$ as a function of DOD_{ov} for a 5-PGS brake-controlled transmission 115

Figure 4-13 – $\max(\eta_{discharge}/\eta_x)$, $\max(U/\eta_x)$ and round-trip efficiency as functions of DOD_{ov} for a 5-PGS brake-controlled transmission (using the R_n^* values specified in Figure 4-14) 115

Figure 4-14 – Total energy dissipated at transmission brakes in a full charge/discharge cycle per unit energy delivered to the vehicle during flywheel discharge as afunction of η_x and DOD_{ov} for a 5-PGS brake-controlled transmission 116

Figure 4-15 – Limitations on the specific energy capacity (*SE*) of a 1-PGS brake-controlled flywheel system for a regional rail application (E_{avail} = 40 MJ, η_{pgs} = 100%) 119

Figure 4-16 – Limitations on the specific energy capacity of 1-5, 10 and 15 PGS brake-controlled flywheel systems for a regional rail application (E_{avail} = 40 MJ, η_{pgs} = 100%) 120

Figure 4-17 – FDC clutch-controlled PST (arrows show direction of power-flow during flywheel discharge) 122

Figure 4-18 – FWC clutch-controlled PST (arrows show direction of power-flow during flywheel discharge) 126

Figure 4-19 – Illustration of DDC clutch-controlled PST (arrows show direction of power-flow during flywheel discharge) 128

Figure 4-20 – Example of a 3-PGS power-split transmission with 4-speed CGB 133

Figure 4-21 – Influence of DOD_{ov} on the CGB gearing ratios required for maximum efficiency 136

Figure 4-22 – The values of η_{eq} for a 3-PGS, 4-speed CGB controlled transmission during flywheel discharge with gear ratios chosen for maximum efficiency (η_A, η_B, η_C and η_{cgb} are equal to 95%) 138

Figure 4-23 – Overall charge, discharge and round-trip efficiencies for the 3-PGS, 4-speed CGB-controlled transmission (with η_{pgs}'s and η_{cgb} = 95%) 139

Figure 4-24 – Comparison of maximum possible discharge efficiency as a function of DOD_{ov} between 15-phase brake-controlled and 3-PGS, 4-speed CGB-controlled transmissions 139

Figure 4-25 – Maximum values of normalised speed, torque and rated power at CGB 141

Figure 4-26 – Comparison of normalised rated variator power as a function of U, calculated to achieve maximum discharge efficiency or equal max *CGB* torque (defined as the 'equalised modes' case) in each power-split mode 143

Figure 4-27 – Values of normalised PGS ratio required to achieve equalised maximum CGB torques in all modes, and the resulting transmission efficiency 144

Figure 4-28 – Mass of system components as a function of DOD_{ov} using a 3-PGS, 4-speed CGB transmission providing a useful energy capacity of 30 MJ 145

Figure 4-29 – Maximum specific energy of FESS as a function of available energy using a brake/clutch controlled transmission with 4-speed CGB and 3 PGSs, and a 4-PGS ring-brake transmission (E_{avail} = 40 MJ, η_{pgs}'s and η_{cgb} = 100%) 146

Figure 5-1 – Configuration for a direct (toroidal type) variator-controlled transmission 149

Figure 5-2 – Performance characteristics of the direct variator flywheel transmission as functions of normalised gear ratio, K^* (η_{var} = 85%) 152

Figure 5-3 – Definition of input and output coupled configurations with arrows showing direction of power-flow with no power recirculation 153

Figure 5-4 – Characteristics of simple input and output coupled PSTs operating with no power recirculation (φ_t = 6.25) 154

Figure 5-5 – Schematic diagram of FDC variator-controlled PST configuration (arrows show direction of power-flow during clutch/variator controlled flywheel discharge) 158

Figure 5-6 – Contour maps for a FDC variator-controlled PST showing (a) $\eta_{discharge}$, (b) DOD_{ov}, (c) $\eta_{round\text{-}trip}$, (d) U and (e) $P_{var,\,rated}^*$ as functions of R^* and R_{eq}^* (with η_{var} = 0.85, η_{pgs} = 0.95) – dotted line shows min($P_{var,\,rated}^*$) w.r.t. U 162

Figure 5-7 – Illustration of the effect of R_{eq}^* values on transmission losses (shown as percentage of transmission input energy dissipated in components) 163

Figure 5-8 – Characteristics of FDC variator-controlled PST when $P_{var,\,rated}^*$ is minimised for a given U 164

Figure 5-9 – Values of R_p^* and R_{eq}^* which minimise $P_{var,\,rated}^*$ for a given U 164

Figure 5-10 – FWC variator-controlled PST (arrows show direction of power-flow during flywheel discharge) 165

Figure 5-11 – Characteristics of FWC variator-controlled PST when $P_{var,\,rated}^*$ is minimised for a given U 167

Figure 5-12 – R_p^* and R_{eq}^* of a FWC variator-controlled PST which minimise $P_{var,\,rated}^*$ for a given U 168

Figure 5-13 – Normalised rated variator power as a function of U for 1-regime flywheel transmissions 169

Figure 5-14 – Transmission efficiencies as a function of U for 1-regime flywheel transmissions 169

Figure 5-15 – Variator speed ratio as function of time for the three single regime transmissions during flywheel discharge with optimum conditions for U = 60% and the same maximum flywheel KE 170

Figure 5-16 – Normalised rated variator power and breakdown of transmission losses for single regime variator-controlled transmissions during flywheel discharge with U = 60% (transmission losses expressed as % of total transmission input energy) 171

Figure 5-17 – Schematic diagram of possible combined FDC/FWC variator-controlled PST configuration 173

Figure 5-18 – Schematic diagram of FDC synchronous shift PST configuration (arrows show direction of power-flow during both regimes of flywheel discharge) 175

Figure 5-19 – Schematic diagram of FWC synchronous shift PST configuration (arrows show direction of power-flow during flywheel discharge) 176

Figure 5-20 – Normalised rated variator power and discharge efficiency as a function of U for 1 and 2 regime flywheel transmissions 177

Figure 5-21 – Variator speed ratio as function of time for the three 2-regime PSTs during flywheel discharge with 'minimised power' conditions for U = 60% using the same maximum flywheel KE 178

Figure 5-22 – Breakdown of losses for 2-regime variator-controlled PSTs during flywheel discharge with U = 60% (losses expressed as % of total transmission input energy) 178

Figure 5-23 – Possible configuration for a 3-PGS FDC/DDC variator-controlled PST 180

Figure 5-24 – Variator speed ratio as function of time during flywheel discharge with 'equalised modes' for U = 60% 181

Figure 5-25 – Efficiencies, normalised rated variator power and normalised PGS ratios as functions of U for 3-PGS FDC/DDC variator-controlled PST (η_{var} = 0.85, η_{pgs} = 0.95) 181

Figure 5-26 – Specific energy capacity of variator-controlled PSTs (E_{avail} = 40 MJ, η_{pgs}'s = 95%, η_{var} = 85%) 182

Figure 5-27 – Specific energy capacity of 3-PGS variator and CGB controlled PSTs (E_{avail} = 40 MJ, η_{pgs}'s and η_{cgb} = 95%, η_{var} = 85%) 183

Figure 6-1 – Schematic illustration of time parameters for analysis of FESS performance including vehicle and flywheel losses 189

Figure 6-2 – (a) Flywheel utilisation and (b) transmission discharge (solid) and round-trip (dashed) efficiencies as a function of R^* for 1-regime FDC variator-controlled PST (E_{useful} = 20 MJ using IAM design tool) 191

Figure 6-3 – (a) Rated variator power and (b) useful energy delivered to vehicle during flywheel discharge (E_{useful}, solid line) and minimum braking energy required to fully recharge flywheel ($E_{recharge}$, dashed line) as functions of R^* for 1-regime FDC variator-controlled PST (E_{useful} = 20 MJ using IAM design tool) 191

Figure 6-4 – (a) Overall round-trip system efficiency and (b) specific energy of FESS as a function of R^* for 1-regime FDC variator-controlled PST (E_{useful} = 20 MJ using IAM design tool) 193

Figure 6-5 – Maximum *SE* as a function of useful energy capacity for regional train application using 1-PGS FDC and 3-PGS FDC/DDC variator-controlled FESSs with available braking energy limited to 40 MJ 194

Figure 6-6 – Typical discharge/charge event for passenger car in urban driving (extracted from ECE urban drive cycle) and associated drive cycle characteristics used in the DAM 195

Figure 6-7 – Maximum *SE* as a function of useful energy capacity for 3-PGS variator-controlled PST in a passenger car application with available braking energy limited to 60 kJ 195

Figure 7-1 – Variator efficiency map (in percent, including hydraulic control system) as a function of speed ratio and normalised input torque [133] 199

Figure 7-2 – PGS efficiency as a function of maximum torque in the three PGS branches divided by the PGS torque rating (experimental data from Mantriota [139]) 200

Figure 7-3 – Overview of the FHRT model structure 201

Figure 7-4 – Effect of FESS control strategy on fuel saving for 3-PGS variator-controlled FESS relative to conventional vehicle using a range of 'uniform coasting' conditions 205

Figure 7-5 – Effect of FESS control strategy 1 on the maximum operating speed of the variator (relative to the rated value) in a 3-PGS variator-controlled FESS using a range of 'uniform coasting' conditions 206

Figure 7-6 – An example of the effect of FESS control strategy (CS) on FHRT performance (with $D_{coast} = 0.1$ m/s^2) 207

Figure 7-7 – Fuel saving relative to conventional vehicle using 3-PGS variator-controlled transmission and the stated FESS useful energy capacities with flywheel initially either fully charged or empty 209

Figure 7-8 – Fuel saving relative to conventional vehicle for main-line operation using 4-PGS brake-controlled and 3-PGS variator-controlled PSTs and the stated FESS useful energy capacities with equal initial and final flywheel *SOC* 212

Figure 7-9 – Fuel saving relative to conventional vehicle for branch-line operation using 4-PGS brake-controlled and 3-PGS variator-controlled PSTs and the stated FESS useful energy capacities with equal initial and final flywheel *SOC* 212

List of tables

Table 1-1 – The relationship between emissions and climate change [2] 20

Table 1-2 – Traction energy consumption in the UK railways (primary fuel energy) [10-11] 24

Table 2-1 – Potential fuel savings for diesel light-duty vehicle (LDVs) using range of currently available technologies, and associated cost increase [3] 32

Table 2-2 – Feasible energy storage devices and the required ESS transmissions for passenger vehicle applications 36

Table 2-3 – Comparison of cell characteristics for the main battery chemistries 43

Table 2-4 – Relationship between *R* and simple PGS [95] 59

Table 2-5 – Relationship between *R* and PGS with idler planets [95] 59

Table 3-1 – Vehicle parameters for model of 3-car diesel-hydrodynamic vehicle 77

Table 3-2 – Effect of coasting strategy and timetable restrictions on fuel consumption 85

Table 4-1 – Direction of power flow in PGS branches (+ve in, -ve out) and associated torque equations including the effect of constant PGS transmission losses for all possible cases 98

Table 4-2 – Torque and energy dissipation relationships for a phase of operation using brake-controlled transmission 103

Table 4-3 – Summary of normalised parameter dependence for 1-PGS brake-controlled transmission 113

Table 4-4 – Expressions for R_{eq} and η_{eq} for FDC, FWC and DDC clutch-controlled power-split modes 130

Table 4-5 – Expressions for ($\omega_{cgb,o}$*) and ($T_{cgb,o}$*) for FDC, FWC and DDC clutch-controlled power-split modes 131

Table 4-6 – The limiting values of R_{eq} and η_{eq} for the equivalent PGS brake-controlled transmission 132

Table 4-7 – Control sequence for 3-PGS, 4-speed CGB clutch/brake controlled PST during flywheel discharge (X indicates the element is engaged) 134

Table 4-8 – Expressions for CGB gear ratios (where $R_{eq,\,j}$* is the equivalent *R** value of the operating phase using the *j*'th CGB gear in the respective power-split mode) 135

Table 4-9 – Required spread of gear ratios in the CGB for DOD_{ov} = 80% (assuming a constant actual or equivalent PGS efficiency of η_x for all phases) – brake-controlled phases are shown in bold 136

Table 4-10 – Normalised torque expressions for 3-regime (FDC/DDC/DDC) CGB-controlled PST 140

Table 4-11 – Parameters of 3-regime CGB controlled transmission used in 'equalised modes' analysis 143

Table 4-12 – Values used in analysis of 3-regime CGB-controlled flywheel transmission for a regional rail vehicle..... 144

Table 5-1 – Characteristic relationships for simple input and output coupled PSTs [94]..... 154

Table 6-1 – Vehicle data for Ford Focus passenger car [107] 188

Table 7-1 – Specifications for a 3-PGS variator-controlled FESS with a range of useful energy capacities in order to achieve minimum mass (using the design tool data presented in Chapter 5 with the stated maximum variator speed and PGS torque) 204

Table 7-2 – Specifications for a 4-PGS brake-controlled FESS with a range of useful energy capacities in order to achieve minimum mass (using the design tool data presented in Chapter 4 with the stated maximum PGS torque) 204

Table 7-3 – Energy breakdown (in MJ's) for conventional and flywheel hybrid regional trains on main-line (ML) and branch-line (BL) routes using uniform coasting driving strategy (FESS useful energy capacity of 20 MJ, equal initial and final flywheel *SOC*) 210

1. Introduction

This Thesis describes an investigation into how novel flywheel energy storage systems may provide a means of reducing energy consumption in rail vehicles through the implementation of regenerative braking. This technical challenge is connected to both the environmental and economic pressure to reduce vehicle emissions and energy consumption related to transport. In recent years, the issue of global warming has generated great scientific and public interest regarding the effects of human activity on the environment. The production of greenhouse gasses (GHGs) has been linked with climate change, and in the light of scientific evidence and reports such as the Stern Review on the economic impacts of climate change [1], a general consensus appears to have been reached on the need to limit such emissions. Table 1-1 shows the relationship between global temperature rises and the atmospheric concentration of GHGs as predicted by the Intergovernmental Panel on Climate Change (IPCC) [2]. The target levels of CO_2 emissions required by the year 2050 in order to limit these temperature rises are also shown relative to 2000 levels. Figure 1-1 is taken from a 2008 International Energy Agency publication [3] and presents a roadmap for limiting global GHG emissions over this period in order to stabilise atmospheric CO_2 concentrations at 450 ppm, as illustrated by the 'BLUE Map' scenario. This is shown relative to a 'Baseline' scenario, which corresponds to the predicted global emissions that will occur with the energy and climates policies that were implemented by 2008. It is clear that in order to limit CO_2 levels, large reductions in emissions are required from both the power generation sector and end-users. The reduction of transport emissions is a key element in meeting this target, and illustrates the pressing need to develop technologies and strategies to improve vehicle energy efficiency.

Temperature increase (°C)	All GHGs (ppm CO_2 eq.)	CO_2 (ppm CO_2)	CO_2 emissions 2050 (% of 2000 emissions) (%)
2.0-2.4	445-490	350-400	–85 to –50
2.4-2.8	490-535	400-440	–60 to –30
2.8-3.2	535-590	440-485	–30 to +5
3.2-4.0	590-710	485-570	+10 to +60

Table 1-1 – The relationship between emissions and climate change [2]

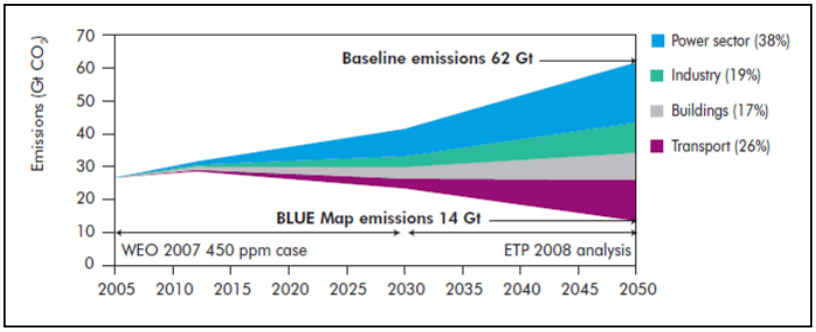


Figure 1-1 – Proposed reductions in energy related CO_2 emissions in order to stabilise atmospheric concentration at 450 ppm [3]

Transport represents a large proportion (23% in 2007) of global energy-related CO_2 emissions, as shown in Figure 1-2. There has also been steady growth in transport emissions since the 1970s, driven primarily by increasing car ownership in both developed and developing countries.

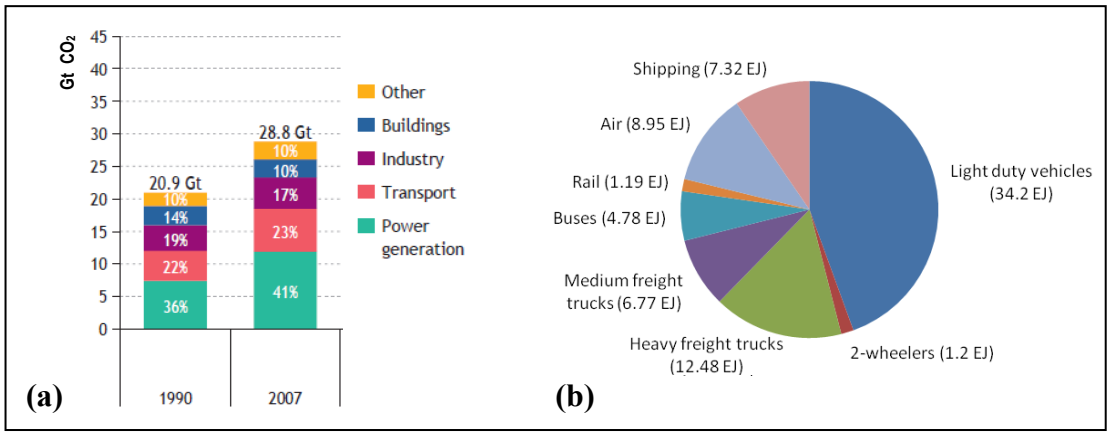


Figure 1-2 – (a) World energy-related CO_2 emissions [4] and (b) Global transport energy use by mode in 2000 [2]

Figure 1-2(b) shows the breakdown of global primary energy use in the transport sector by mode. It is clear that transport energy use is dominated by road vehicles, especially passenger cars (LDVs). The large market for these vehicles, combined with rising fuel costs and tightening emissions legislation has driven research and development within both industry and academia focussed on improving the efficiency of road vehicles. The small contribution of rail (1.5% of transport energy use) illustrates its limited potential to affect overall GHG emissions. The relatively small market and long service life of rail vehicles also mean that opportunities for improving energy efficiency are restricted.

Rail does however have an important role to play in current and future transport strategy due to its inherent advantages as a mass transportation system. These include;

i. The efficiency of the steel-on-steel wheel-rail contact which avoids the hysteresis losses associated with pneumatic tyres,
ii. The aerodynamic profile of rail cars in convoy leading to low vehicle drag per unit mass,
iii. The use of an electrical power delivery system which allows high energy efficiency and the exploitation of low carbon power generation.

These advantages lead to low energy intensity (defined here as the primary energy use per passenger-km) compared to other modes of transport. This is shown in Figure 1-4 for passenger and freight transportation modes using data for member countries of the International Energy Agency.

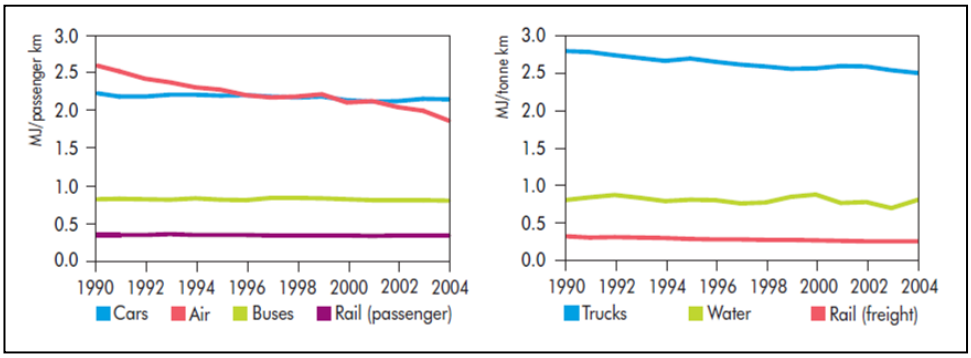


Figure 1-3 – Average energy intensity of passenger and freight transportation in IEA member countries [3]

The advantages of rail transport mean that it is set to play an important role in achieving the transport emissions reduction required to meet the 'BLUE Map' scenario described in Figure 1-1. These reductions can be achieved through improving engine and power-train efficiencies, using alternative fuels (i.e. bio and synthetic fuels) and enabling shifts between different transport modes. The required contribution of these measures is shown in Figure 1-5.

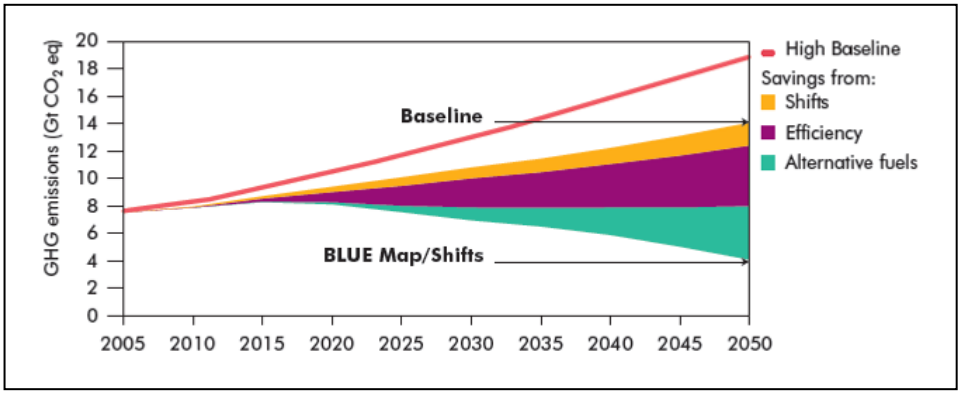


Figure 1-4 – Proposed CO_2 reduction measures for transport in order to meet BLUE Map scenario [3]

The emission reduction due to modal shifts shown in Figure 1-5 is achieved largely through the greater use of high speed rail for journeys up to 750 km, greater use of rail to transport freight and the greater use of trams, buses and light rail in urban areas. These modal shifts are combined with predicted improvements in the energy efficiency of rail transportation. In order to achieve these targets growth is required in international railway capacity. The cost of building the required infrastructure is however relatively high, with high speed rail costing in the region of 5 to 50 million US$/km [5-6] depending on topography, the cost of land (which can be particularly high around urban areas) and labour costs. The cost of conventional rail systems are significantly lower, but are still affected by these factors. The development of existing rail networks is also constrained by the need to maintain rail services. This can be seen in the UK, where the percentage of electrified track is currently only 40% and plans to increase electrification are limited to a few mainline routes [7-8].

Rather than relying on electrification to improve energy efficiency, an alternative and potentially more cost-effective approach is to develop clean and fuel efficient self-powered rail vehicles. This requires a thorough understanding of current traction systems in order to identify the main areas of energy loss and assess the benefits of potential future technologies and operating strategies aimed at improving fuel efficiency. The analysis presented in this Thesis has been performed in the context of the UK railways, the key features of which are described in the following sections.

1.1. Background to energy consumption in the UK rail network

Transport accounted for 21% of total greenhouse gas emissions in the UK [9], and has seen steady growth over the last 20 years. The total energy consumed by rail vehicles in the UK is around 15 million MWh per year, and is divided approximately equally between electric and diesel traction [10]. Electric vehicles can be subdivided into high voltage (25kV AC) intercity trains, and both high and low voltage (750V DC) multiple units which operate predominantly regional and commuter services. A relatively small amount of energy is used by electric freight locomotives. Diesel passenger vehicles can be divided according to the transmission and service type, with diesel-electric trains providing intercity services and diesel-hydrodynamic vehicles providing the majority of regional services. A considerable amount of energy is also used by diesel freight trains. The Association of Train Operating Companies (ATOC) produce yearly energy consumption data for rail vehicle in the UK, and the figures for 2004/05 are shown in Table 1-2. This data is for the primary fuel energy consumed which includes losses associated with the generation and distribution of electricity, but does not include the energy use associated with the production and distribution of the diesel fuel or the fuel used at the power station.

		Energy consumption (million MWh)
Diesel	Intercity DEMU	2.2
	Regional DHMU	2.5
	Total passenger	**4.7**
	Freight	**2.7**
Electric	Intercity 25kV	2.3
	EMU 25kV	1.3
	EMU 750V	3.9
	Total passenger	**7.5**
	Freight	**0.3**
Total		**15.2**

Table 1-2 – Traction energy consumption in the UK railways (primary fuel energy) [10-11]

A 2007 report by the Railways Safety and Standards Board (RSSB) [11] provides detailed estimates of the total energy losses for UK rail vehicles. The estimated power generation efficiencies for both electric and diesel traction are as follows:

Average electric power generation efficiency = 40%

Average diesel engine fuel efficiency = 32%

These estimates are made on the basis of current technology (and typical duty-cycle in the case of diesel engines), and will be subject to future developments in electrical generation (such as the possible expansion of renewable and nuclear capacity) and IC engine technology respectively. A shift in power-train technology to hybrid or fuel cell systems also has the potential to raise the average operating efficiency of self-powered trains, thereby reducing primary energy consumption. Once the power generation losses have been taken into account, a breakdown of where the supplied electrical or mechanical energy is used in the vehicle gives an indication of where efforts to improve efficiency should be focussed. This is shown according to vehicle and service types in Figures 1-6 and 1-7 for electric and diesel trains respectively.

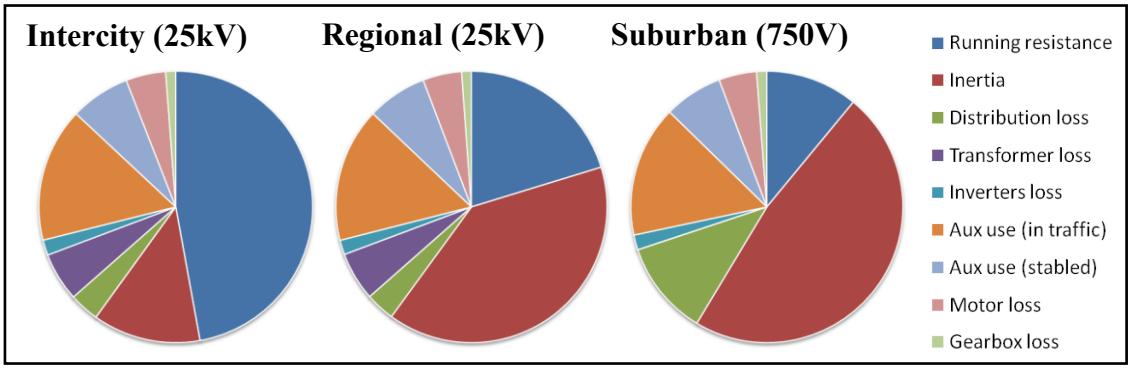


Figure 1-5 – Estimated breakdown of UK electric train energy usage after power generation losses [11]

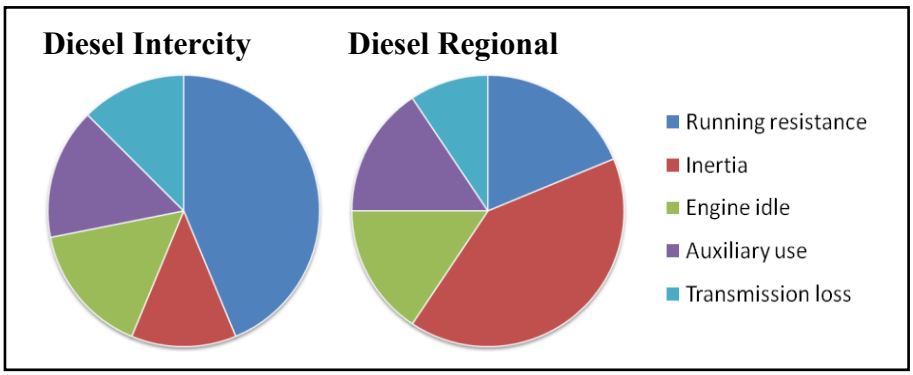


Figure 1-6 – Estimated breakdown of UK diesel train energy usage after engine losses [11]

It is clear from Figures 1-6 and 1-7 that after power generation losses (at either a power station or the diesel engine) the combined traction requirements of accelerating the vehicle and overcoming running resistance account for the majority of energy used. The balance

between these inertia and resistance losses is seen to depend on the service type. For intercity services the train is likely to spend long periods at high speed, leading to high resistance losses. For regional and suburban services the train is likely to stop more frequently, dissipating large amounts of kinetic energy.

As of 2009 all the 25kV AC network and a large proportion of the 750V DC network is compatible with regenerative braking [8]. The inertia losses shown in Figure 1-6 are therefore likely to be higher than current levels, although factors such as power and efficiency limitations in the electrical power-train limit the proportion of braking energy that can be regenerated. A further issue known as 'line receptivity' also limits regeneration in DC systems, resulting in regenerated electrical energy being dissipated in resistors if there is insufficient power demand from other vehicles in the same section of track. While this issue can be tackled by using inverting equipment at the DC substation [12-13] this technology is not used in the UK railways.

For diesel trains, it is clear from Figure 1-7 that significant fuel savings could be achieved through the efficient capture and reuse of vehicle braking energy. This can be achieved (along with a range of other potential benefits) by implementing hybrid power-train systems in self-powered rail vehicles. In fact, the potential of hybrid technology to reduce fuel consumption and emissions has been given as one of the reasons for not pursuing wide-spread electrification of the UK network [14]. Hybridisation is therefore included in the range of measures which have been identified as suitable for reducing the energy consumption of the UK railways, as discussed in the following section.

1.2. Proposed energy saving options

The desire for a sustainable and efficient UK railway network has led to the investigation of measures aimed at reducing the traction energy consumption of both electric and diesel rail vehicles. A 2007 report produced by the Rail Safety and Standards Board (RSSB) [11] has identified a wide range of strategies and technologies which could be implemented to reduce overall energy consumption in the UK railways. The potential of each option was assessed in terms of estimated network-wide energy savings and timescale for introduction. Each measure considered was then ranked on a cost-benefit basis. The results suggest that the opportunities to reduce energy consumption in a cost effective way fall into one of two categories – 'short term' which involves changes to the way current vehicles are operated, and 'long term' which relates to new technologies which require more development or can

only be introduced on new rolling-stock. The most promising measures identified in the report are summarised below;

Short term energy saving measures

- Energy efficient driving techniques and timetabling
- Matching train capacity to demand (e.g. shorter trains during off-peak periods)
- Reducing diesel engine idling

Long term energy saving measures

- Regenerative braking with on-board energy storage for diesel trains
- Intelligent engine control on vehicles with distributed power-train
- Reducing vehicle weight per seat
- Reducing vehicle drag

It is important to note that some of these measures are inter-related. For example, the introduction of hybrid systems is likely to be combined with efficient power-train control strategies, while the additional components (particularly the energy storage devices) will tend to increase the mass of the vehicle power-train.

The focus of this Thesis is on assessing the potential of implementing regenerative braking with on-board energy storage for diesel trains. Analysis has therefore been performed using detailed computational modelling of a typical UK regional diesel train, where the benefits of this technology are expected to be greatest due to the high braking losses that occur in conventional vehicles of this type. The development of systems to capture, store and reuse energy that would otherwise be lost is constrained by a wide range of technological and practical issues. The type of energy storage device used and the transmission connecting it to the vehicle drive are critical in determining the hybrid system characteristics and ultimately the fuel consumption of the vehicle. Many different types of energy storage device are available. Selection of the most appropriate device for a given application is achieved by consideration of the following:

- The vehicle characteristics and duty cycle requirements
- The degree of hybridisation and the power-train control strategy
- The efficiency of the energy storage system
- Practical issues relating to safety, reliability, weight and installation requirements
- The cost, lifespan and maintenance requirements of the system

The possibility of using diesel-electric hybrid technologies similar to those developed in the automotive industry has been investigated by the RSSB for a new fleet of UK diesel regional trains [15]. This report concluded that new hybrid vehicles represented poor value for money due to the small order size combined with uncertainties over possible future electrification and options to extend the life of existing vehicles. Simpler hybrid systems involving intelligent control of conventional distributed power-trains and self contained 'bolt-on' regenerative braking systems should therefore be considered as an alternative means of reducing fuel consumption.

The research described in this Thesis identifies advanced flywheel energy storage technology and diesel hybrid power-train architectures as suitable for rail vehicles, and the potential application of appropriate systems to diesel-powered trains operating UK regional services is investigated at both system and operational levels. A key relationship which has not been fully addressed in the literature is the effect of driving strategy on the design requirements and potential benefits of hybrid regional diesel trains (HRDTs). As energy efficient driving has been identified as a short term measure which can be applied to existing vehicles through improved driver training and/or in-cab advisory systems, this should be considered as a baseline against which to assess the fuel savings possible through hybridisation. This has also been assessed using detailed computational modelling of a conventional diesel-hydrodynamic regional train operating a representative UK service, allowing the effect of hybridisation to be isolated for a range of driving strategies.

1.3. Objectives of the research

The research described in this Thesis focuses on assessing the performance of hybrid diesel regional train (HRDTs) and a range of flywheel energy storage systems using mechanical transmissions. The aims are summarised below;

1. Investigate the effect of driving strategy on the fuel consumption of conventional and hybrid diesel regional trains in order to identify the realistic fuel savings possible through hybridisation, and the energy and power requirements of appropriate regenerative braking systems.
2. Investigate the compromises in the specification of a mechanical flywheel energy storage system (FESS) and identify flywheel and transmission parameters in order to maximise the specific energy capacity of the system.

3. Develop design tools to allow the comparison of different transmission systems, and specify appropriate FESS parameters for a given application.
4. Assess the benefits of the best performing mechanical FESSs through detailed computational modelling of a flywheel-hybrid regional diesel train.

A summary of the Thesis content is presented below, providing an overview of the methods used to achieve these objectives.

1.4. Overview of Thesis structure

Chapter 2

A review of hybrid systems (including consideration of energy storage devices and transmission options), computational methods for calculating rail vehicle energy consumption and the potential of efficient driving strategies.

Chapter 3

An analysis of the effect of driving strategy on vehicle fuel consumption using detailed computational models of a conventional diesel-hydrodynamic regional train and a generic hybrid diesel train.

Chapter 4

An analysis of a range of clutch and brake controlled mechanical transmissions for FESS applications. A novel independent analysis method (IAM) has been implemented to provide an absolute basis for the comparison of different transmission configurations and to identify appropriate system parameters for a given application.

Chapter 5

An analysis of a range of variator-controlled transmissions for mechanical FESS applications using the IAM.

Chapter 6

Validation of the IAM results through the detailed computational analysis of the effect of flywheel losses and vehicle resistance on the performance of mechanical FESSs for specific applications.

Chapter 7

A detailed computational analysis of proposed mechanical hybrid regional diesel trains, integrating the mechanical FESS models (using parameters identified from the IAM) with the conventional diesel regional train model. The effect of driving strategy and energy storage capacity on fuel consumption is investigated for realistic main-line and branch line services.

Chapter 8

Conclusion, contributions of the research and recommendations for future work.

2. Literature review

Regenerative braking and energy efficient driving have been identified in Chapter 1 as two key measures for reducing rail energy consumption and harmful emissions. This literature review is therefore divided into two main sections. Section 2.1 comprises an overview of hybrid power-train systems and components, while Section 2.2 considers methods of analysing rail vehicle dynamics, power-train operation and driving strategies in order to assess energy consumption.

2.1. Hybrid power-train technology

As discussed in Chapter 1, this Thesis focuses on the fuel consumption of regional rail vehicles where there is a strong case for implementing hybrid systems to capture braking energy that would otherwise be dissipated. The recovery, storage and reuse of braking energy can be implemented using a wide range of technologies and control systems, and has the potential to allow some or all of the following benefits to be achieved;

Potential benefits of hybridisation

- Reduced fuel use and emissions due to;
  - The capture and reuse of braking energy
  - Reduced engine idling when no traction power is required
  - More efficient provision of auxiliary power requirement
  - Efficient control of the engine during powering
  - Downsizing of the installed engine capacity
- Improved vehicle acceleration
- Reduced engine noise and emissions around stations
- Reduced wear on friction brake components

The viability of these benefits depends upon the type of regenerative braking system implemented. A simple 'bolt-on' system operating in parallel with a conventional power-train may allow the recovery of braking energy and achieve a reduction in fuel consumption, but will be less flexible than a fully integrated hybrid power-train where the capacity and operating range of the engine can be optimised. There are also a number of limiting factors when considering regenerative braking systems for regional rail vehicles, as discussed below.

Constraints on the hybridisation of rail vehicles

- Increasing vehicle mass (as this affects traction energy consumption and infrastructure maintenance)
- Increasing vehicle complexity (as this affects the vehicle reliability and maintenance costs)
- Increasing life cycle costs
- Vehicles are required to operate on a range of routes and services, which limits the potential optimisation of power-train components and control strategies

The choice of energy storage device and the architecture of the regenerative braking system will have a strong influence on these factors, and are therefore extremely important considerations. Existing and proposed devices and systems for both rail and automotive vehicles are explored in the following literature review.

2.1.1. Overview of hybrid vehicle classification

Much of the development of hybrid power-train technology has been focussed on automotive vehicles. It is therefore instructive to consider the potential of hybrid systems for this application alongside a range of other proposed technologies aimed at improving fuel efficiency. The data in Table 2-1 is taken from a recent IEA report [3] and shows the potential fuel savings and the predicted cost of vehicle and diesel power-train technologies.

Energy Saving Measures	**Diesel hybrid**
Non-engine improvements	
Tyres	0.5 - 4%
Aerodynamics	0.5 - 4%
Lights	0 - 2%
Efficient aux.	0.5 - 4%
25% weight reduction	10 - 11%
Engine improvements	
Higher compression ratio, no throttle	2 - 3%
Direct injection	7 - 8%
Improved combustion	3 - 4%
Hybrid system	15 - 17%
Total improvement compared to baseline vehicle	**40 - 55%**
Cost of improvements ($)	**4200 - 5600**

Table 2-1 – Potential fuel savings for diesel light-duty vehicle (LDVs) using range of currently available technologies, and associated cost increase [3]

Many of these measures are equally applicable to diesel-powered rail vehicles, although the resulting improvements in fuel economy will obviously differ. With respect to automotive vehicles Table 2-1 shows that hybridisation can achieve large fuel savings, especially when combined with other measures. This however, results in a considerable estimated increase in vehicle cost of around 20% for a typical US vehicle price of $25,000. It is clear that there is a compromise between improving vehicle efficiency and increasing the vehicle cost which is highly dependent on the characteristics of the hybrid system used. A range of hybrid-electric systems have been proposed and developed for automotive applications as shown in Figure 2-1. This provides a good basis for understanding different hybrid configurations and system requirements.

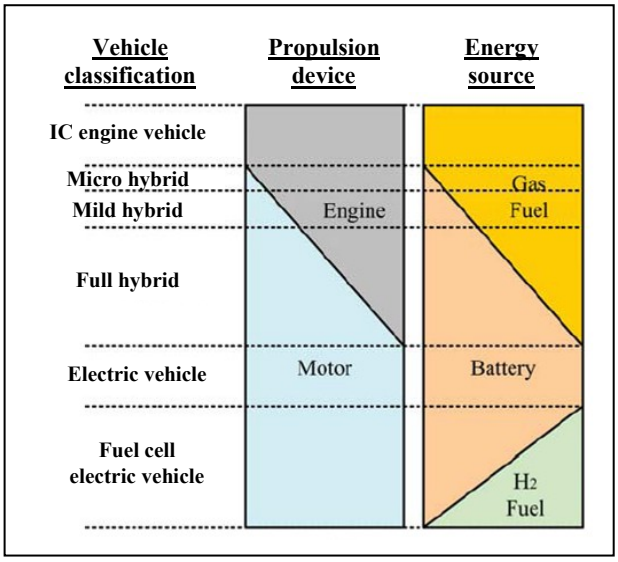


Figure 2-1 – Classification of hybrid electric vehicles [16]

While Figure 2-1 is focussed on hybrid-electric systems, the vehicle classifications also apply to more general hybrid configurations using different transmission types and energy storage devices, and are discussed in more detail below.

Series Hybrid

The series hybrid vehicle is possible when the medium of energy transfer in the vehicle transmission is the same as that of the energy storage device. This can be achieved using either a hydraulic or electrical system, where energy storage is achieved using a hydro-pneumatic accumulator or batteries/capacitors respectively. An example of this

configuration is shown below, with arrows illustrating the possible direction of power flows in the system.

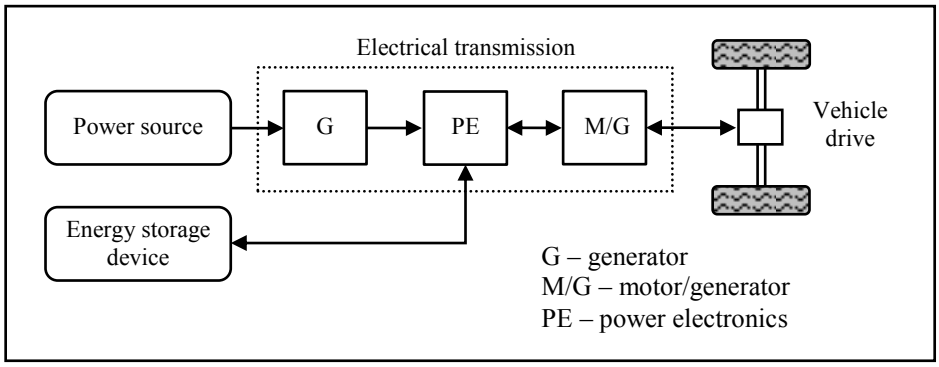


Figure 2-2 – Typical series electric hybrid architecture

Automotive vehicles using the electric hybrid architecture shown in Figure 2-2 are often referred to as 'plug-in hybrids', as they are designed to operate primarily as electric vehicles. In this case, the ICE or fuel cell has a relatively low power rating, and is used to extend the range of the vehicle by supplementing the tractive power and/or recharging the battery. The series hybrid architecture can also be used for multiple energy storage devices with complementary characteristics [17]. An example of this approach is the use of batteries to achieve good energy storage capacity and allow a long vehicle range, combined with super-capacitors [18-19] or flywheel motor/generator devices [20] to allow high transient power flows during acceleration and braking.

Full Hybrid

As illustrated in Figure 2-1, a full hybrid can be defined as a power-train where the power source can deliver power to the vehicle via a separate path than the energy storage device. In the simplest form, this corresponds to a parallel hybrid configuration where the engine/fuel cell and energy storage devices have separate transmissions.

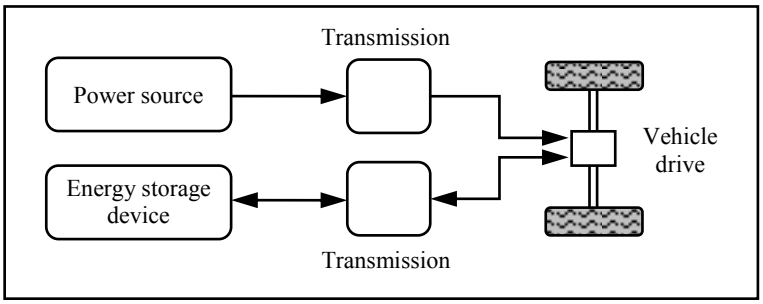


Figure 2-3 – Parallel hybrid architecture

More complex full hybrid configurations are also possible through the use of mechanical differentials such as planetary gear sets (PGSs) to provide multiple paths for power-flow. An example of this is the complex 'power-split' hybrid architecture shown in Figure 2-4.

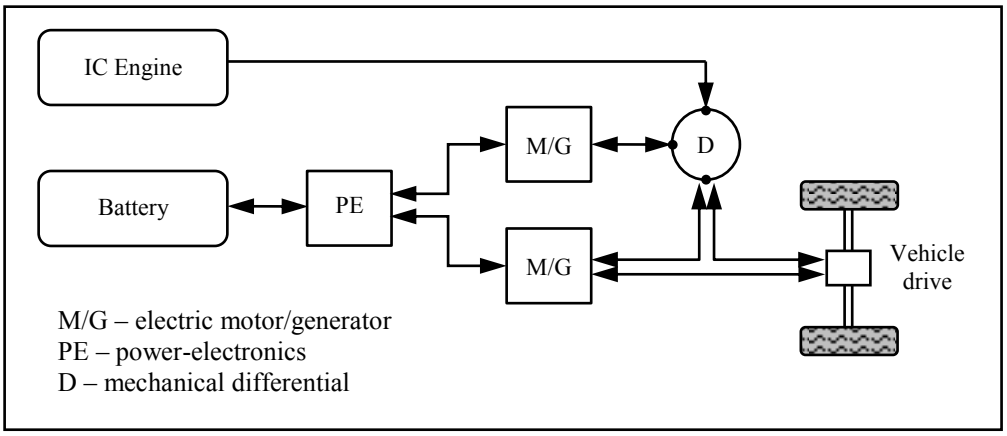


Figure 2-4 – Example of complex 'power-split' hybrid architecture

This arrangement provides a greater degree of flexibility in the operation of the engine and power-train than is possible with a parallel hybrid, allowing fuel consumption to be optimised through the use of appropriate control strategies [21].

Mild Hybrid

Hybrid vehicles of this classification are essentially conventional, ICE powered vehicles with a low powered electrical motor/generator and limited energy storage capacity arranged in a parallel hybrid configuration. The energy storage device can be recharged from the engine or by regenerative braking, and can be used to provide auxiliary power load (enabling engine shut down when stationary) and limited tractive power assistance during acceleration (enabling a small degree of engine down-sizing).

Micro Hybrid

Micro hybrid vehicles are similar to mild hybrids but the energy storage devices have a smaller capacity, can only be recharged from the engine and do not provide any tractive power to the vehicle. Fuel savings are achieved through the application of engine shutdown to minimise fuel consumption when no tractive power is required.

A key component of all these hybrid power-trains is the energy storage device. This is likely to account for a significant proportion of the additional cost and weight of a hybrid vehicle, and will strongly influence the transmission, configuration and packaging of the power-train. The different energy storage options are discussed in the following section.

2.1.2. Energy storage devices

Developments in the automotive industry have largely focussed on using electrical systems and battery technology to compliment internal combustion engines, which has become the most established hybrid technology [22]. There are however a range of practical energy storage options, each of which have advantages and disadvantages. The four most established types of energy storage device are shown in Table 2-2, along with the type of transmission required for integration in an energy storage system (ESS).

Energy storage device	ESS transmission
Electro-chemical battery	Electrical
Capacitor	Electrical
Flywheel	Electrical or Mechanical
Hydro-pneumatic accumulator	Hydrostatic

Table 2-2 – Feasible energy storage devices and the required ESS transmissions for passenger vehicle applications

A brief description of each of these energy storage technologies is given below.

Batteries

For practical hybrid vehicle applications three main types of electro-chemical battery have been identified; lead-acid, nickel-metal-hydride (NiMH) and lithium-ion (Li-ion) [23-25].

Lead-acid batteries are a well established technology, and are widely used as an auxiliary storage device in automotive applications. They consist of lead and lead oxide

electrodes with a liquid electrolyte containing sulphuric acid. Modern valve-regulated lead-acid (VRLA) batteries are sealed units which are more robust than a simple lead-acid cell and provide an economical, low maintenance option for applications where energy capacity per unit mass is not critical.

Nickel-metal-hydride and lithium-ion are both types of 'dry cell' batteries where the electrolyte is in the form of a paste. For NiMH the electrodes consist of nickel oxide-hydroxide and an intermetallic compound, with an alkaline electrolyte. These batteries are widely used in consumer electronics and electric vehicles due to their reasonable cost and good energy storage capacity. Li-ion batteries consist of carbon and metal-oxide electrodes with a lithium salt electrolyte, and achieve better energy capacity than NiMH batteries but at a higher cost. They are also used in consumer electronics (especially in products where low size and mass are important), and are beginning to see use in electric and hybrid vehicles such as the Tesla sports car [26] and the Nissan Leaf passenger car [27].

Supercapacitors

Supercapacitors are high performance electrolytic capacitor devices consisting of two electrodes of activated carbon (which has a very high surface area) separated by an electrolyte layer. Unlike in an electro-chemical battery, no chemical reactions occur during operation and the boundary between the electrolyte and electrode acts as an insulator. Applying a voltage across the electrodes therefore causes charge to accumulate, storing electrical energy. The high surface area of the electrode and the thin insulating boundary layer result in a very high capacitance. The energy storage capacity of these devices is however limited by a maximum cell voltage of around 3V [28].

Advanced flywheels

Advanced flywheels use rotors constructed from high strength composite materials which rotate at high speed (typically 10,000 to 100,000 rpm), thereby storing kinetic energy. The rotor is contained within a vacuum environment in order to minimise aerodynamic losses, and the flywheel casing is designed to contain the rotor in the event of a catastrophic failure. This type of flywheel technology has been developed and demonstrated in several research programs [29-32], and advanced flywheels have been shown to achieve much higher energy storage per unit mass than conventional steel flywheels.

The energy capacity of a flywheel depends on both the rotor inertia (related to the material density and geometric shape) and the maximum safe rotational speed (related to material strength and shape of the rotor, the applied safety margin and the bearing system used). The design of the flywheel will therefore affect the specific energy, but a range of other factors such as controlling failure modes and the costs of components, materials and manufacturing must also be considered. The design and performance of advanced flywheels are also dependent on the choice of transmission system. Practical options for transferring power to and from the flywheel involve the use of either;

i. An electrical motor/generator integrated with the rotor
ii. A mechanical transmission capable of operating over a continuous ratio range

Figure 2-5 shows examples of advanced flywheel devices developed for electrical and mechanical systems.

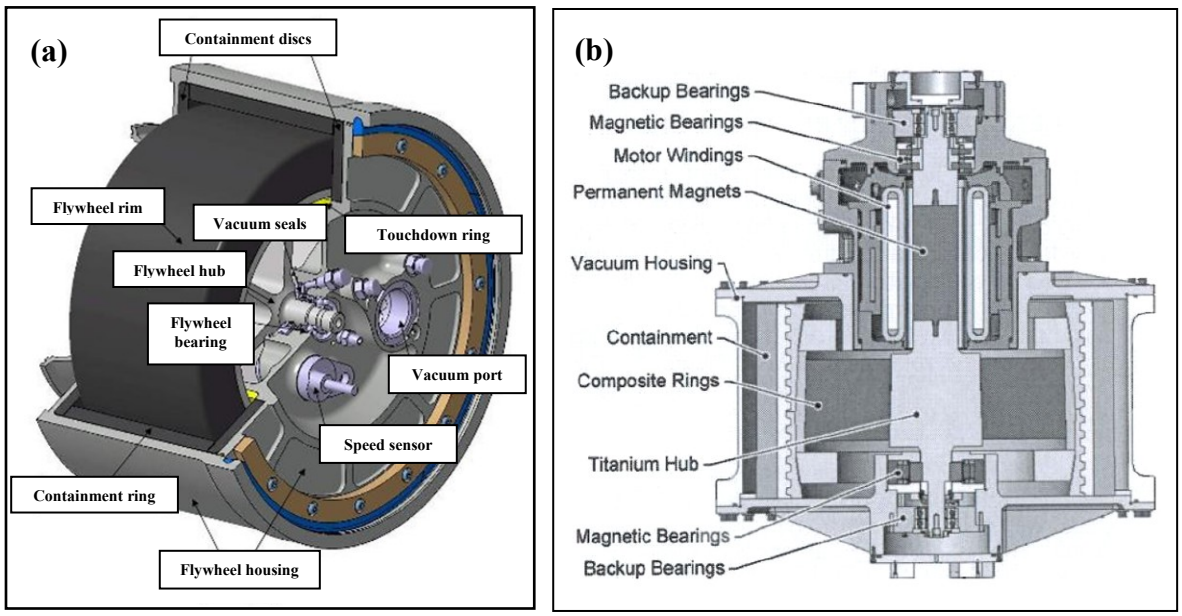


Figure 2-5 – Examples of flywheel design for (a) mechanical [33] and (b) electrical [34] FESSs

The 'electrical flywheel' option can only operate in a system with a full electrical transmission. The flywheel-motor-generator (FMG) unit is therefore sometimes referred to as a 'mechanical battery', due to its conversion of electrical energy to kinetic energy (rather the chemical energy as in an electro-chemical battery). With suitable control

electronics the FMG can therefore be considered as a direct competitor to battery or supercapacitor units for hybrid electric vehicle applications.

The 'mechanical flywheel' option relies on a direct mechanical link between the high speed flywheel and a continuously variable transmission (CVT) capable of transmitting power over a continuous range of gear ratios. While the FMG requires an external electrical traction system, the mechanical flywheel can connect directly to the vehicle drive shaft via the CVT, and has the advantage of reduced complexity of the flywheel rotor. The mechanical flywheel is therefore suitable as a 'bolt-on' FESS to enable regenerative braking on existing vehicle architectures.

A general discussion of all aspects of the design process for advanced flywheels is given by Genta [35], while detailed descriptions of the design and testing of mechanical and electrical flywheels for vehicle applications are given by Shah [29] and various publications by researchers at the Center for Electromechanics, University of Texas at Austin [32, 34, 36] respectively.

Hydro-pneumatic accumulator

Hydraulic energy storage systems can be implemented in hybrid vehicles through the use of a high pressure accumulator and a low pressure reservoir [37-38]. The accumulator is a pressure vessel partly containing a quantity of gas which is sealed by a membrane. Hydraulic fluid can then be pumped from the low pressure reservoir into the accumulator, compressing the gas and thereby storing energy. By allowing the pressurised hydraulic fluid to flow out of the accumulator and through a hydraulic motor the stored energy can be recovered as mechanical work. The energy storage efficiency of accumulator devices can be improved thorough the use of an elastomeric foam in the gas section of the accumulator to minimise thermal losses [39]. The maximum round-trip efficiency of this type of energy storage system can be as high as 80% [40-41]. A conventional variable-displacement hydraulic pump/motor suffers from relatively low efficiency at part load, although developments in 'digital displacement' hydraulic pump technology can achieve high efficiency over a wider power range [42-43]. The energy storage capacity of the system is however fundamentally limited by the maximum and minimum allowable volume and pressure of the gas contained in the accumulator.

The characteristics of these devices are described in the following sections and considered in terms of the suitability for application in rail vehicles.

2.1.2.1. Energy and power capabilities of storage devices

While many factors are important when selecting an energy storage device for a given application, an initial assessment can be made by considering the energy and power capacity per unit mass of a device. This can be achieved by performing Ragone tests, where the energy that can be extracted from a fully charged device at constant power demand is measured. This data can then be used to construct a Ragone plot [44-45]. Figure 2-6 shows energy storage device data from a range of sources for Ragone plots [46-47] and manufacturer's data [28, 48-50]. A key feature of Ragone plots is the fact that the ratio of specific energy to specific power defines a characteristic discharge time for a given device, which can be seen as dashed diagonal lines in Figure 2-6. By identifying the typical duration of charge and discharge events for an energy storage device in a given application, the type of device capable of meeting these requirements with minimum mass can be identified.

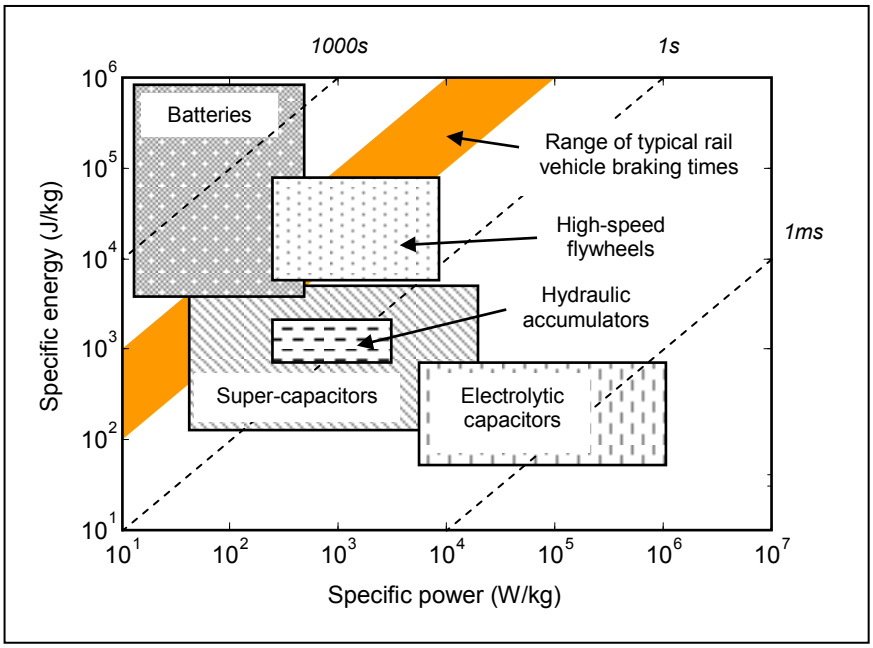


Figure 2-6 – Comparison of specific energy and power for energy storage devices

Electro-chemical batteries, capacitors (electrolytic and developments in super-capacitor technology), advanced flywheels and hydro-pneumatic accumulators are shown in Figure 2-6. The characteristic discharge times are also shown for the range of typical rail vehicle braking times (with upper and lower limits representing intercity and metro type services respectively). Currently batteries and super-capacitor devices can provide the energy and

power capacity required to store the braking energy of the vehicle. Advanced flywheels however can meet these requirements with the highest specific energy and power, and therefore with the lowest mass. The hydro-pneumatic accumulator is seen to have a very low specific mass (10-100 times lower than advanced flywheels) which limits its application in regenerative braking systems. This type of energy storage device has therefore not been considered in any further detail.

2.1.2.2. Additional considerations

There are a range of additional factors relating to the implementation of an energy storage device in a hybrid power-train including;

i. The safety requirements of the device,
ii. The efficiency with which energy can be stored,
iii. The cost, lifespan and maintenance requirements,
iv. The system integration and control requirements.

These issues are discussed below for battery, supercapacitor and advanced flywheel systems.

Electro-chemical batteries

An important feature of all batteries is the effect that state-of-charge (*SOC*) has on the charge/discharge efficiency, charge acceptance and the lifespan of the device. A limitation of batteries is that increasing *DOD* tends to reduce both the efficiency and life [51], although the magnitude of this effect depends on the battery chemistry. The effect of *SOC* on charge and discharge efficiency is illustrated in Figure 2-7 for a lead-acid battery.

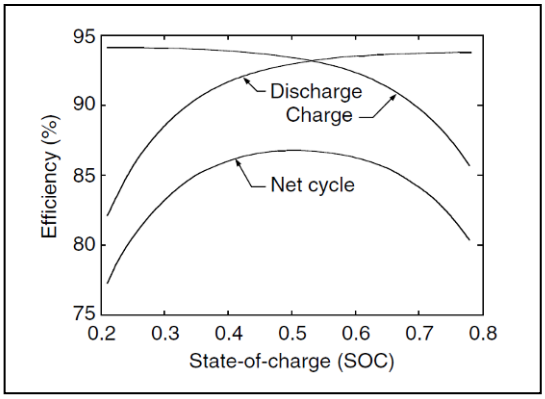


Figure 2-7 – Typical charge and discharge efficiency of a lead-acid battery as a function of *SOC* [51]

The power that can be delivered or accepted by the battery is also strongly dependent on the *SOC* as illustrated for a Li-ion battery in Figure 2-8.

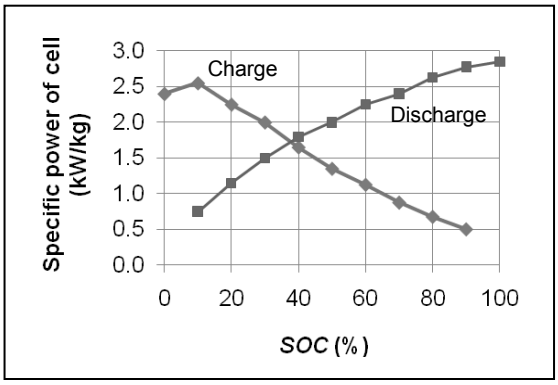


Figure 2-8 – Effect of *SOC* on specific power of a Li-ion cell at 25°c [52]

A suitable compromise is therefore required to identify appropriate operating conditions for a particular battery type in a given application. An example of this is the NiMH battery pack used in the Toyota Prius hybrid electric vehicle, where the control strategy maintains a *SOC* of between 50-70% at all times [51]. The actual specific energy of the battery pack is therefore only a fifth of the maximum energy capacity per unit mass. Another important factor affecting the performance of all batteries is the operating temperature. This is a particular problem with NiMH batteries where low temperatures can significantly reduce the power capacity of the battery, as illustrated in Figure 2-9. NiMH batteries also suffer from low charging efficiency at high temperature (>50°c) [52]. Careful monitoring and control of cell temperatures is therefore a necessary feature of battery packs for vehicle applications.

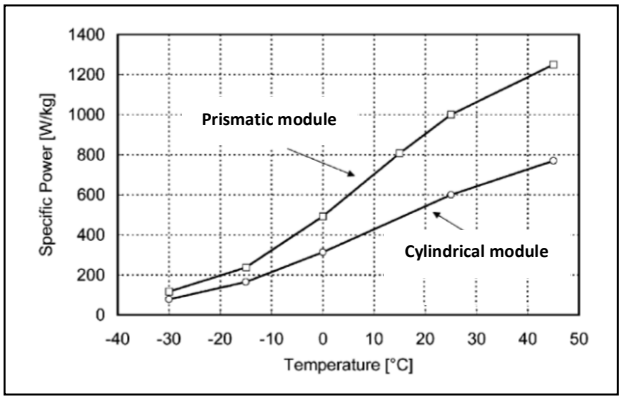


Figure 2-9 – Effect of temperature on specific power of a NiMH battery at 60% *SOC* [52]

Another issue with battery packs is the need to prevent significant variation in *SOC* between cells, which occurs through differences in the self discharge rates of the cells due to manufacturing or temperature variations. A battery pack for vehicle applications therefore needs careful management in order to maintain a consistent *SOC* in all cells, and prevent overcharging or fully discharging cells which cause permanent damage. In the Li-ion vehicle battery pack described by Saft et al [49] each module allows the charge and discharge of the individual cells to be controlled and monitored by the vehicle control systems. Each module is also designed to provide over-charge detection and short-circuit protection. The modules are liquid cooled to enable thermal management during both warm and cold weather operation. The integration of batteries in a vehicle system is illustrated in Figure 2-10. These requirements add to the overall weight and cost of battery systems, but are necessary to ensure safe and reliable operation.

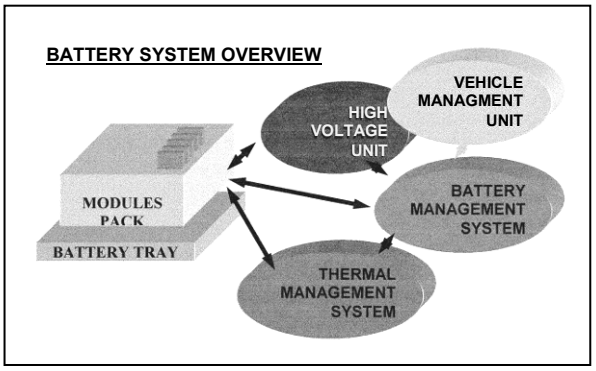


Figure 2-10 – Implementation of Li-ion battery modules in a vehicle application [49]

A comparison of the key performance parameters of the different battery chemistries is presented in Table 2-3. This comparison of different battery types provides representative data which has been collated from a several sources [24, 51, 53-54].

		Lead-acid	NiMH	Li-ion
Specific energy	Wh/kg	35-50	70-95	80-130
Specific power	W/kg	200-300	150-300	250-450
Energy density	Wh/litre	60-90	130-170	140-200
Normal life	years	-	-	-
Cycle life (at 80% DOD)	cycles	400-600	600-1200	800-1200
Actual cost	US$/kWh	120-150	200-350	500-750

Table 2-3 – Comparison of cell characteristics for the main battery chemistries

The cost of different battery systems depends on a number of factors including material and manufacturing costs and production volumes [55], and are therefore likely to vary with demand and technological developments [56]. The values of cost/kWh given in Table 2-3 reflect the current cost of the different battery systems, although lower costs (particularly for Li-ion technology) are being targeted. The self-discharge rate is highest for Ni-MH batteries, but in all cases the losses will be insignificant for hybrid vehicles applications as the battery is unlikely to be left fully charged for long periods, and will be recharged quickly during use.

Supercapacitor

As no chemical reactions take place within a supercapacitor device there is little material degradation over time, and a long lifespan (>100,000 cycles) without significant loss of performance is possible [57]. The lack of an electrical-chemical energy conversion also means that supercapacitors can achieve high discharge efficiencies of >95% when operating within the rated power [58], although this decreases during higher power operation. However, as with battery systems there is significant variation in cell properties which can lead to uneven *SOC* (and therefore voltage) within a pack of supercapacitor cells. Charge equalisation circuits are therefore used to balance the cells and prevent damage [59]. These control circuits are required to manage the performance and lifetime of the supercapacitor devices, but add to both the cost and size of supercapacitor systems. The cost of supercapacitors in US$/kWh is currently much higher than batteries [57], and they are more suited to higher power applications where the cost in US$/kW is critical. Costs are however expected to improved, with a target of < £50/kWh expected to be achieved in the next 5-10 years [47].

Advanced flywheel

The energy storage efficiency of a FESS depends largely on the characteristics of the transmission used. A comparison of the two transmission options in terms of the flywheel-to-wheel efficiency of the devices is illustrated in Figure 2-11 using representative motor-generator and gearing efficiencies.

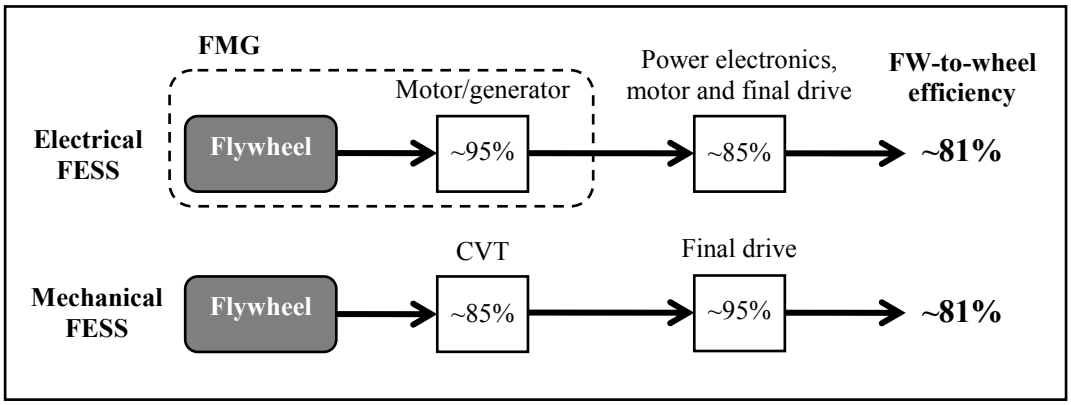


Figure 2-11 – Typical power-train efficiencies for electrical and mechanical FESSs during discharge

While the efficiency values stated in Figure 2-11 are approximate, and will depend on factors such as vehicle speed and applied tractive effort as well as the details of the power-train components and configuration, it is clear that the efficiencies of the two systems are broadly comparable. These efficiency values do not include the effect of flywheel self discharge due to aerodynamic and bearing losses. For a well designed flywheel operating in a low pressure environment these losses are typically in the region of 2-4% per minute [33] which is much higher than self-discharge rates for batteries or supercapacitors. While this makes FESSs unattractive as long-term storage devices, these losses are unlikely to have a large impact in hybrid vehicle applications where the flywheel is only fully charged for short periods – for example, station dwell times for trains are typically around 1 minute. These losses should however be taken into account when considering the system design and control strategy for hybrid flywheel vehicles. Other factors such as the ease of integration, mass, cost and auxiliary requirements of the flywheel system depend on the transmission system and are discussed below.

a) Ease of integration

For FMGs the integration of an electrical machine with the flywheel adds further design constraints to the flywheel geometry and increases the cooling requirements due to electrical motor-generator losses occurring within the vacuum containment. The speed range of the motor/generator required to maintain the required power flow also limits the speed range of the flywheel, leading a typical *DOD* of around 60% [60]. The FMG approach does however allow flexibility in the positioning of the energy storage device within the vehicle, and allows gimbal mounting in order to reduce both the flywheel bearing loads and the gyroscopic forces

transmitted to the vehicle [61-62]. The mechanical flywheel system requires a precision high-speed vacuum seal to allow a direct shaft connection between the flywheel and CVT [29], and is more restricted in the positioning and orientation of the flywheel unit. If necessary the gyroscopic forces acting on the vehicle can be eliminated by using two counter-rotating flywheels with parallel axes, although bearing loads must still be considered. The *DOD* of the flywheel is constrained by the characteristics of the mechanical transmission. The choice of flywheel *DOD* for a particular mechanical FESS and application is not clearly defined or justified in the literature.

b) Mass

The electrical FESS developed for the ULEV-TAP2 project [61, 63] (see Section 2.1.3 for more details) has an installed mass of around 1 tonne, only 35% of which is due to the FMG including the containment and gimbal mount. The remaining mass is largely due to the power electronics required to integrate the FESS with the diesel-electrical power-train. An argument in favour of mechanical flywheel transmissions over electric systems on the ground of reduced mass and cost is presented by Cross and Hilton [64]. Both the specific energy and specific power of the Flybrid mechanical FESS (see Section 2.1.5 for more details) are higher than those of the ULEV-TAP2 electrical flywheel unit, despite the fact that the electrical system requires separate electric traction motors in order to achieve regenerative braking. This illustrates the high specific torque that can be achieved with modern mechanical continuously variable transmissions.

c) Cost

The cost of FESSs for vehicle applications is difficult to specify as no system is currently in production. Whether the high cost of prototype systems can be reduced depends on the size of the market, and whether components (particularly the flywheel rotor) can be standardised for a range of applications. This may prove difficult in applications where a uniquely optimised flywheel capacity and geometry is necessary or beneficial. The flywheel device developed by Flybrid Systems for F1 applications has been designed to minimise the carbon-fibre content of the flywheel rotor, as this has been identified as a major component of the cost [64]. For electrical FESSs, a recent RSSB study into energy storage technologies for rail [47] suggests that the cost per unit energy capacity of FMGs could potentially be considerably lower than supercapacitors due to the relatively low material costs. The overall cost of electrical systems should however also be considered. In a report to the California

Energy Commission [65] one of the major manufacturers of stationary electrical flywheel systems for the power generation sector estimated that 60% of the total system cost is associated with the power electronics, while the remaining 40% is the FMG unit. These systems operate with a similar range of charge/discharge times (10-100s) to those required in regenerative braking systems for rail vehicles, and so the ratio of flywheel energy capacity to power requirement of the electronics will be similar. It is therefore reasonable to expect that the cost of a flywheel device for use with a mechanical transmission will be significantly lower than the electrical option, due to the low materials cost of the transmission and the simpler flywheel rotor design (which does not require an integrated motor and electrical control system).

d) Safety and reliability

The safety and reliability of the system is essential. This has been achieved through the use of careful design and control of the flywheel rotor in order to ensure that it is not exposed to dangerous stresses. Furthermore, containment systems have been designed and tested in order to ensure that the kinetic energy of the flywheel can be safely dissipated in the case of a catastrophic rotor or bearing failure [36, 53, 64]. As the operating range of the flywheel is constrained to ensure safety, there is little material degradation during use. This means that there is no decrease in performance over time, and the lifespan of these devices is expected to be high. Regular maintenance of the bearings and seals is however likely to be required [47].

In conclusion, while there are still challenges relating to the mass production and long-term reliability of advanced flywheels for vehicle application, they have been shown to represent a technically viable, efficient and potentially cost-effective technology for hybrid vehicles.

2.1.3. Developments in hybrid rail vehicles

The requirements of hybrid systems for rail are summarised by Lu et al. [66] in terms of the power-train configuration, energy storage device, vehicle control strategy, system optimisation and practical implementation. It is clear that there is a great deal of flexibility in the way that hybridisation can be implemented. This is illustrated by the range of hybrid systems that have been proposed and developed for rail applications, although none are currently in wide-spread use. Overviews of the different systems are presented below.

Hitachi hybrid trains

The Japanese manufacturer Hitachi has developed a single-car diesel-electric hybrid commuter train called the New Energy Train [67]. This vehicle has a maximum speed of 100 km/h and the power-train consists of a 331 kW diesel engine with an electrical transmission and a 10 kWh Li-ion battery pack, arranged as shown in Figure 2-12. The power-train control strategy limits the *DOD* of the battery pack to around 30% in order to achieve a predicted life of over 5 years. During operation, regenerated energy has been shown to provide 14-33% of the total energy demand on the routes shown in Figure 2-12.

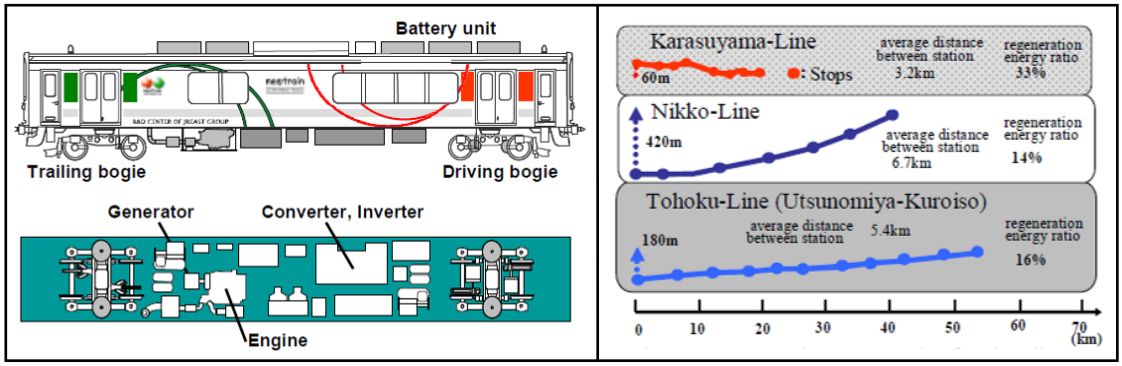


Figure 2-12 – Overview of the NE Train layout and operational performance [67]

It is interesting to note that there is no significant downsizing of the diesel engine – for comparison the 160 km/h UK Class 170 DMU (diesel multiple unit) has a similar installed engine capacity of 315 kW per car. This is probably due to the need to meet the maximum tractive power requirement on a range of routes with different characteristics in terms of gradient and stopping pattern. It does however suggest that the primary benefit of hybridisation for rail vehicle is the recovery and reuse of braking energy rather than improving the engine operating efficiency.

Hitachi have also been involved with the development of the hybrid diesel-electric power-train used in the unique 'Hyabusa' track measurement train operated in the UK by Network Rail [68]. This is a diesel-electric locomotive with Li-ion battery storage rated at 48 kWh. The battery pack weighs around 1 tonne and has an expected life of 8-10 years, suggesting that a relatively low *DOD* is used during operation. Around 80% of the regenerated braking energy was predicted to be recovered for the next powering cycle, which suggests that the energy storage system has an overall round-trip efficiency of around 70%. The vehicle was operated on all main-line routes around the UK as part of the routine track inspection programme between mid 2007 and late 2008. Reported fuel savings of 12-

20% were achieved depending on route [69], although no information is available regarding the effect of the drive cycle or the baseline fuel consumption figures used.

RTRI Li-ion Research

The Japanese Railways Technical Research Institute (RTRI) have conducted research investigating the use of Li-ion batteries in an electric tram [70]. While this is an electric rather than hybrid vehicle, the research provides useful information about the requirements of relatively large scale Li-ion energy storage systems. The battery system tested includes a battery protection management system and battery management units for each module of Li-ion cells, and is shown in Figure 2-13(a). The specific energy and power of the system is therefore significantly lower than for a single Li-ion cell. As the battery system was used as the primary energy source for the electric tram it was discharged from 100% *SOC* to around 60% *SOC* through a series of small discharge/charge cycles with *SOC* variations of around 2.5%/1.5% respectively, corresponding to vehicle powering and braking. In this application a life of over 100,000 cycles was expected. For a hybrid diesel application a change in *SOC* of around 30% of capacity would be expected during charge and discharge events (as seen with the Hitachi NE Train), reducing the lifespan. The specific energy and power of this system with a 30% *DOD* can be estimated from the data given.

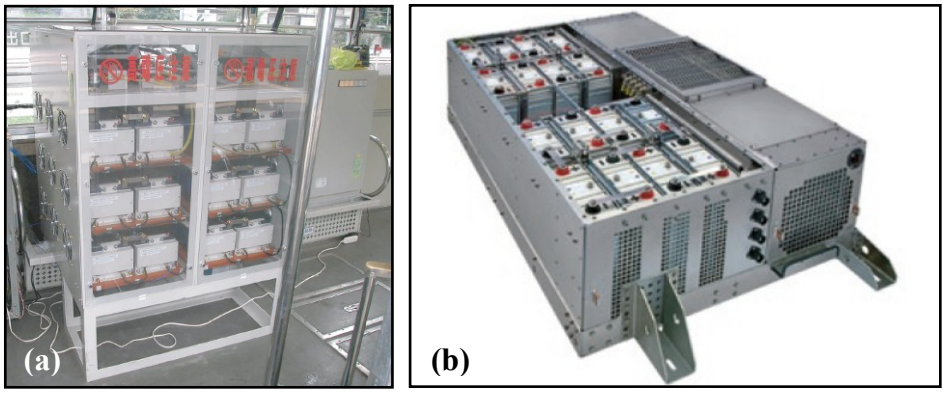


Figure 2-13 – (a) Lithium-ion battery system developed by RTRI [70] and (b) Mitrac supercapacitor based energy storage unit [71]

Bombardier Mitrac energy storage system

Bombardier Transportation have developed a supercapacitor based energy storage unit (shown in Figure 2-13(b)) which can be integrated with their 'Mitrac' range of electric power-train components [72]. Measurements of the energy storage device in operation on a

DC electric light train have been published [73], showing a reduction in both the peak power demand at the line and net energy consumption. The system is also proposed as a solution to regenerative braking in diesel-electric vehicles. When compared to other energy storage systems, the mass and volume of the supercapacitor unit are however very large for its energy capacity.

Green Goat hybrid shunting locomotive

The Green Goat hybrid shunting locomotive has been developed for use in railway switching yards [74-75]. This type of application with low mean power and short periods of high power operation is particularly suited to a hybrid power-train. A small diesel engine is used at optimum efficiency to charge a large bank of VRLA batteries, as shown in Figure 2-14.

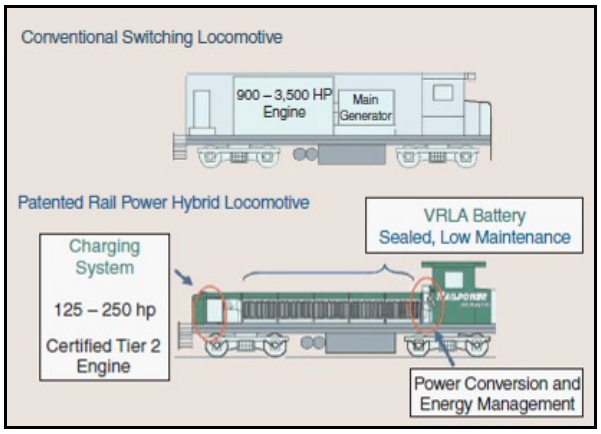


Figure 2-14 – Illustration of conventional and hybrid shunting locomotives [75]

These batteries then provide auxiliary and traction power for the vehicle. This achieves a reduction in fuel consumption and emissions compared to a conventional shunting locomotive which requires a much higher installed engine capacity. The requirements of the power-train for this type of application are particularly appropriate for fuel cells operating at constant power, and analysis of a fuel cell-battery hybrid has also been performed [76]. Both these systems work well in situations with intermittent operation at low speed, but are of limited potential for main-line diesel vehicles.

AiResearch ACT-1 electric flywheel unit for rail

In 1972 the Urban Mass Transportation Administration (UMTA) initiated the ACT-1 program to develop an efficient DC electric light rail vehicle with an onboard electric FESS

[77]. The flywheel energy storage device was developed by the company Garrett AiResearch [78], and is illustrated in Figure 2-15(a). The unit consists of a laminated steel rotor with a design speed of 11,000 rpm providing maximum kinetic energy storage of 4.5 kWh. The rotor is connected to a 600 kW DC motor-generator via a fixed ratio gearbox. The rotor operates within a vacuum environment to reduce aerodynamic drag, resulting in losses of around 3% per minute at design speed. The FESS unit weighs around 3 tonnes resulting in a relatively low specific energy of 1.45 Wh/kg. In operation, the unit was mounted with the axis of flywheel rotation parallel to the longitudinal axis of the vehicle. Under expected operating conditions, the gyroscopic forces acting at the mounting points of the FESS were found to be less than the weight of the unit, producing no noticeable effect on the vehicle dynamics or the operating life of the system.

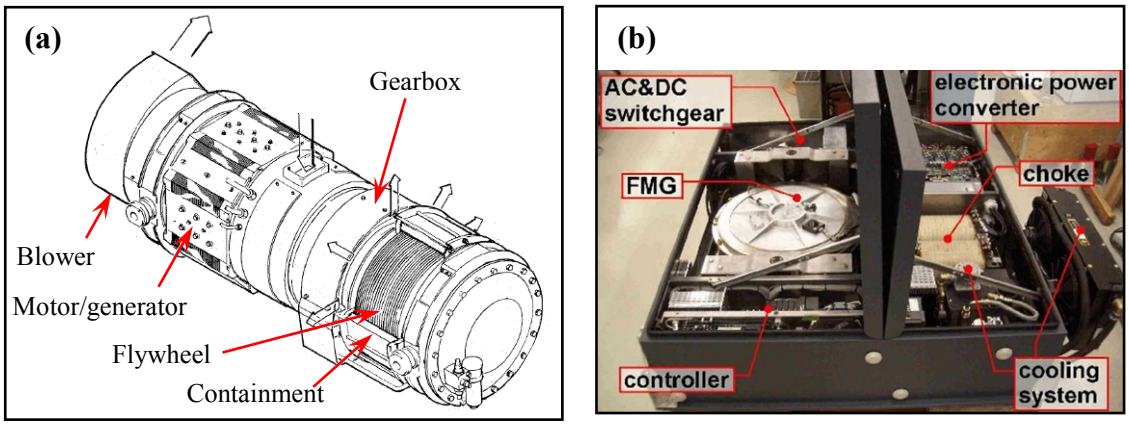


Figure 2-15 – (a) Illustration of ACT-1 flywheel-motor-generator unit [78] and (b) ULEV-TAP2 complete electrical flywheel system [61]

ULEV-TAP2 light rail power-train

During 2002-2005 a hybrid diesel-electric ultra-light rail vehicle with electric FESS was developed through the European Commission sponsored ULEV-TAP 2 project [61, 63]. The aim of the project was to develop an efficient alternative to electrified systems, which could also meet strict emissions and noise limits. The electric FESS unit developed for this application is shown in Figure 2-15(b). The FMG device uses a composite rotor with a maximum speed of 22,000 rpm to achieve a useful energy capacity of 4 kWh. This results in a specific energy of 10.6 Wh/kg for the FMG. However, it is clear from Figure 2-15(b) that many other components (predominantly power-electronics) are required in order to integrate the FMG with the vehicle power-train. The FMG accounts for only 38%

of the total component weight, and the specific energy of the FESS unit is therefore considerably lower than that of the FMG, at around 4 Wh/kg. A power-train using the FESS with an efficient diesel-generator unit was predicted to achieve a 40% fuel saving and 50% reduction in emissions compared to a conventional diesel-electric light rail vehicle, although no details of the drive cycle are given.

Parry People Mover light rail vehicle

A simple flywheel energy storage concept has been developed for light rail applications by Parry People Movers [79]. The vehicle contains a conventional low speed flywheel constructed from laminated steel and weighing around 0.5 tonnes (giving a relatively low specific energy of 2 Wh/kg for the rotor alone). This flywheel can be charged either from an external electric power source or through regenerative braking. A small LPG engine acts as a range extender, providing additional tractive power to the vehicle through an automatic gearbox and shared mechanical driveline.

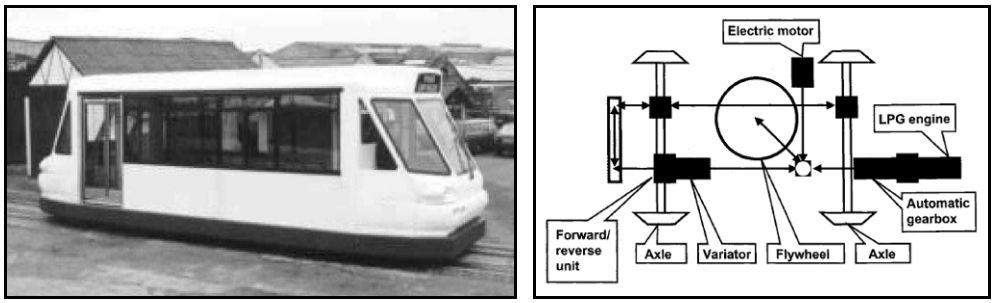


Figure 2-16 – PPM vehicle and power-train configuration [79]

The vehicle is currently operating a single niche application, providing a regular service on a 1.3 km stretch of isolated branch line at Stourbridge, UK. The size, weight and relatively low efficiency of the flywheel system however make it unattractive for use on larger and higher speed DMU type vehicles.

Voith hybrid systems for rail

The company Voith Turbo Ltd have developed a range of energy saving features for their rail power-train systems [80]. The conventional power-train consists of a diesel engine with a hydrodynamic transmission. Voith have included 'Microbrid' and Hydrobrid' options which both utilise a degree of onboard energy storage with a hydrostatic pump/motor and a hydro-pneumatic accumulator. The Microbrid system is a micro hybrid with the ability to

provide auxiliary loads, while the Hydrobrid is a mild hybrid capable of providing a degree of traction boost. Few details are available regarding the capability of the systems, and neither system appears to be in current service.

The available data for energy storage systems that have been developed for rail applications can be used to assess the effect of system requirements on the overall energy and power capacity of the Li-ion, supercapacitor and electric flywheel storage devices. Figure 2-17 shows the specific energy and energy density plotted against specific power for both the device and the complete energy storage unit operating with practical *DOD*.

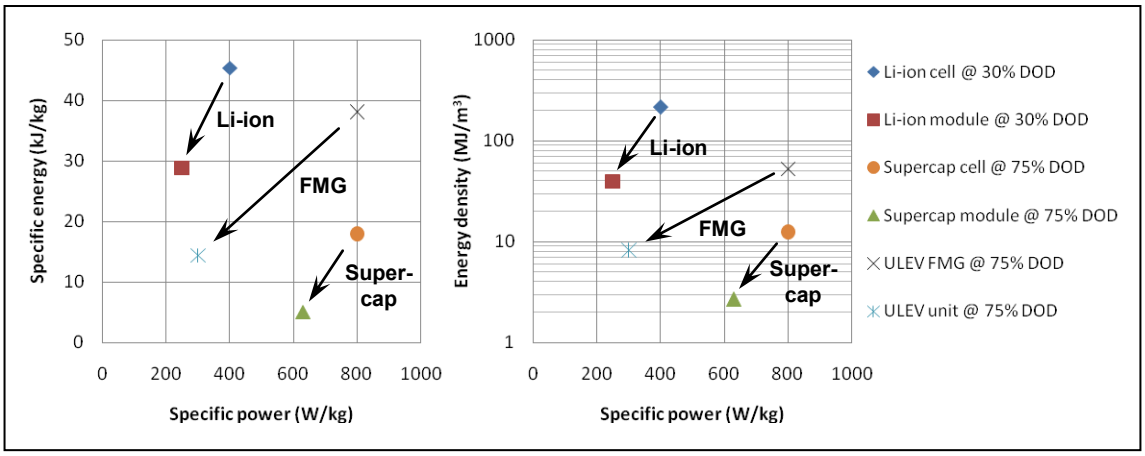


Figure 2-17 – Specific energy, specific power and energy density for Li-ion supercapacitor and advanced flywheel devices and integrated units (arrows show the effect of control and packaging requirements)

For the energy storage devices operating with practical *DOD* limits, the ULEV FMG is seen to combine high specific energy and specific power. When the mass of the FMG control systems are included, the specific energy is still much higher than the supercapacitor unit but drops to about half that of the Li-ion battery unit. However, the higher specific power of the ULEV system compared to the Li-ion unit means that it could still be the lighter option for regenerative braking applications with a characteristic charging time of up to 50 seconds.

This comparison of systems shows that advanced flywheels are a viable and attractive energy storage device for rail vehicles. The control requirements for an electrical flywheel device have been seen to represent a significant proportion of the weight and cost of the system. While mechanical flywheel systems have been identified as potentially low-cost, efficient and easily integrated method of enabling regenerative braking on vehicles with any

power-train, no such systems have been developed for rail applications. The following sections therefore consider relevant transmission technology and mechanical flywheel systems that have been developed for other applications.

2.1.4. Continuously variable transmissions for flywheel energy storage systems

While the design challenges of the advanced flywheel device have to a large extent been overcome, there are considerable difficulties associated with the design of a transmission to allow efficient transfer of energy between the vehicle and flywheel over a wide range of operating conditions. A complete transmission system capable of achieving this continuous variation in speed ratio is referred to in this Thesis as a 'continuously variable transmission' (CVT). Different options for achieving a mechanical CVT are discussed in the following sections.

2.1.4.1. Fixed ratio gearbox with slipping clutch

One of the simplest ways of implementing a CVT is through the use of a fixed ratio gearbox with a clutch designed to operate with continual slip. This allows the CVT to achieve any speed ratio within the range of the gearbox. As the torque exerted on each side of a slipping clutch is equal and opposite it can be used to transfer energy from a higher speed input shaft to a lower speed (or stationary) output shaft. This results in a proportion of the input energy being dissipated due to friction in the slipping clutch. These losses can be reduced by using multiple gear ratios, reducing the average speed difference between the input and output shafts during operation. A CVT consisting of a 12-speed gearbox and a hydraulically actuated wet multi-plate clutch has been investigated for use in automotive flywheel energy storage applications by Beachley et al. [81]. An average transmission efficiency of over 90% was predicted for this system, and potential advantages in terms of reliability and ease of development (due to the use of conventional automotive power-train components) were identified. The rapid gear changes required during acceleration (several times a second during high power operation) and during the switch from acceleration to regenerative braking were however felt to require a sophisticated control system in order to achieve good driveability and smooth power transfer.

2.1.4.2. Variator technology

A variator is defined here as a device capable of transmitting power while achieving a continuous variation in speed ratio (output speed divided by input speed). The term 'variator' should not be confused with the term CVT which is a complete transmission system which may or may not contain a variator device.

There are two main types of mechanical variator that have been developed for practical vehicle implementation. The first of these is the toroidal variator, an example of which is illustrated in Figure 2-18. This type of variator transmits power via a traction fluid under high pressure at the contact points between 'roller' elements and toroidal cavities located on an input and output disc. Varying the angle of the rollers about a fixed axis (perpendicular to the rotational axis of both the roller and the input/output discs) changes the radius of the contact points on the two toroidal surfaces. This allows a continuous variation in the ratio of output to input rotational speed between a maximum and minimum ratio defined by the geometry of the roller and toroidal surface.

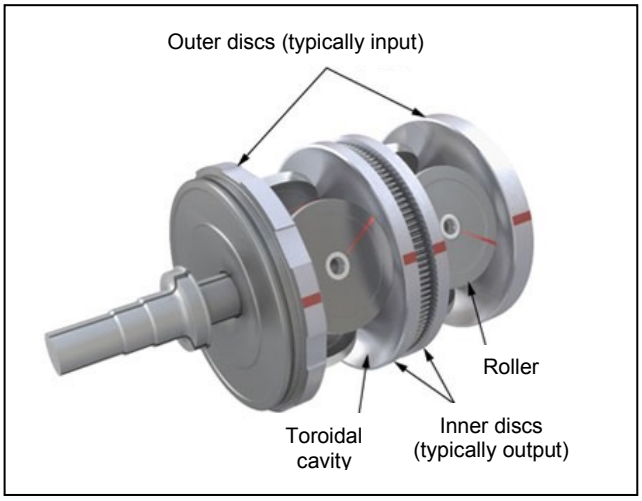


Figure 2-18 – Illustration of a full toroidal variator [82]

The torque transmitted by the toroidal variator is dependent on the contact pressure between the rollers and the inner/outer discs. By controlling this pressure, the rollers automatically assume the position required to achieve the necessary speed ratio between the input and output discs – the variator is therefore described as 'torque controlled', and can be implemented with a simple control system without feedback [83].

The second type of practical variator is the 'push-belt' design, and has been developed by companies including Bosch/Van Doorne for automotive applications with maximum torques of up to 400 Nm [84]. The components of the push-belt variator are illustrated in Figure 2-19.

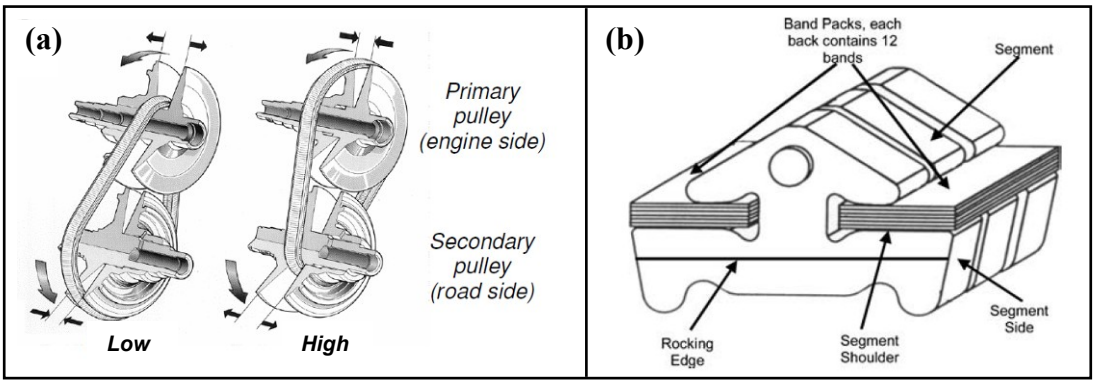


Figure 2-19 – (a) Illustration of push-belt variator operation showing low and high gear ratios [84] and (b) details of push-belt construction

This device uses two v-pulleys with variable spacing mounted on parallel shafts, connected with a v-belt consisting of a large number of metal segments mounted on steel bands (seen in Figure 2-19). Power is transmitted through compression of these elements, allowing much higher torques than can be achieved with a tensioned v-belt drive. The spacing of the two v-pulleys is controlled simultaneously using hydraulic actuators in order to vary the gear ratio between the secondary and primary pulleys. The variator is therefore 'ratio-controlled', and requires a feedback control system in order to maintain a demanded output torque.

Both toroidal and push-belt variators have similar performance and operating limitations. The range of ratio coverage that can be achieved is limited by the roller/cavity and pulley geometry respectively. For both types, a maximum practical gear spread of around 6.25 is possible, centred around a 1:1 gear ratio [64, 84]. Both devices are potentially bi-directional (i.e. power can flow in either direction) but are not reversible, as the sign of the speed ratio is fixed by the mechanism.

The maximum efficiency of variator devices is typically lower than that of fixed ratio gearing. While the loss mechanisms for toroidal and push-belt variators are different, the overall effect of losses is similar, with efficiency varying as a function of input speed, input torque and speed ratio. In toroidal variators the main losses are due to slippage at the roller

contact points and friction in bearings. Experimental tests show that maximum efficiencies of around 95% can be achieved [85], as shown in Figure 2-20.

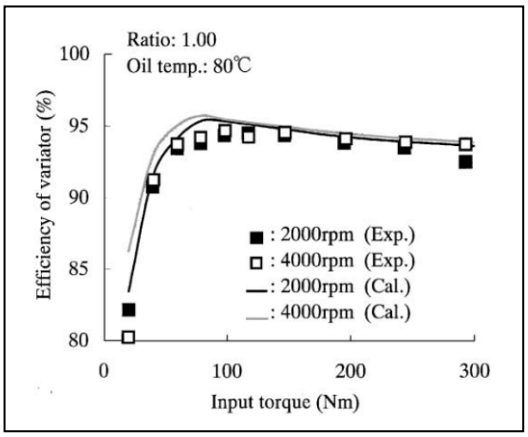


Figure 2-20 – Toroidal variator efficiency for an output/input speed ratio of 1 [85]

It is clear from Figure 2-20 that toroidal variator efficiency is only weakly dependent on the actual input speed, but decreases significantly at low input torque. The loss mechanisms for push-belt variators are discussed in some detail by Akehurst et al. [86-88], and are dominated by friction in the push-belt, at the belt/pulley contact points and in the bearings. This results in similar maximum efficiency levels as the toroidal variator, and the effect of input speed on the efficiency is again seen to be small [89]. For the modelling of CVT power-trains, the efficiency of mechanical variators is therefore often assumed to be a function of only speed ratio and input torque. This allows a quasi-static approach to be applied using experimentally derived efficiency maps.

The variable speed ratio of variators means that they can be used as a CVT. However, as the minimum speed ratio possible is greater than zero, it is apparent that a slipping clutch is required to transfer power to a low speed output shaft (e.g. for the initial acceleration of a vehicle) until the minimum speed ratio is reached. The energy dissipated in the clutch during this period of operation will reduce the overall efficiency of the CVT. Another issue relating to this type of 'direct variator' CVT is that the variator is required to transmit the full power flowing through the CVT. For high power applications (such as regenerative braking in rail vehicles) this could result in a heavy and costly system. Finally, the losses in the variator and the power demand of the variator control system may result in a relatively low CVT efficiency, particularly when operating at low torque.

2.1.4.3. Power-split principles for a simple differential

It is clear that there are a number of limitations regarding the use of a variator device as a CVT. Some of these issues can be addressed by considering mechanical power-split transmissions (PSTs). These are achieved by using a differential gearing unit with 2 degrees-of-freedom to split the main power flow into two paths. The kinematic and torque relationships that exist between the branches of the differential allow the overall power flow to be controlled by controlling the power flow in one of the two power-split branches. Fundamental analysis of power-split transmissions has been performed for a range of configurations consisting of a variator and PGS [90-93]. The way in which the three branches of a PGS are connected in these transmissions affects the overall operation, but the general analysis method used by White [94] allows an analysis of the system to be performed for the generic differential unit shown in Figure 2-21.

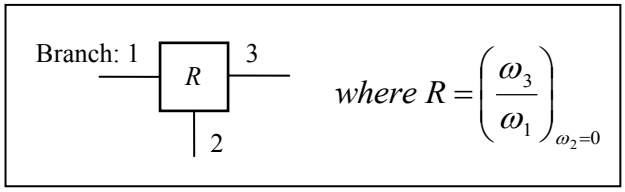


Figure 2-21 – Description of generic differential gearing unit

The kinematic and ideal torque relationships for the generic differential illustrated in Figure 2-21 are shown in Equation 2-1 and 2-2 respectively.

$$R = \frac{\omega_3 - \omega_2}{\omega_1 - \omega_2} \qquad \text{Or alternatively...} \quad \omega_3 = (1-R)\omega_2 + R\omega_1 \tag{2-1}$$

$$T_3 = -\left(\frac{1}{1-R}\right)T_2 = -\frac{1}{R}T_1 \tag{2-2}$$

These equations apply to any type of differential in any configuration. It has been shown [95] that the relationship between the ratio of ring to sun diameter of a planetary gearset (PGS) type differential and the value of R can be defined for each of the six possible configurations, as shown in Table 2-4 for a simple PGS and Table 2-5 for a PGS with idler planet gears.

Basic ratio	Branch connections			Value of R	Limits for $2 < (r/s) < 3.5$	Connection type
	Branch 1	Branch 2	Branch 3			
$R > 1$	Carrier	Ring	Sun	(r+s)/s	$3 < R < 4.5$	α
	Carrier	Sun	Ring	(r+s)/r	$1.29 < R < 1.5$	β
$0 < R < 1$	Ring	Sun	Carrier	r/(r+s)	$0.67 < R < 0.78$	γ
	Sun	Ring	Carrier	s/(r+s)	$0.22 < R < 0.33$	δ
$R < 0$	Sun	Carrier	Ring	- s/r	$-0.5 < R < -0.29$	ε
	Ring	Carrier	Sun	- r/s	$-3.5 < R < -2$	ξ

Table 2-4 – Relationship between *R* and simple PGS [95]

Basic ratio	Branch connections			Value of R	Limits for $2 < (r/s) < 3.5$	Connection type
	Branch 1	Branch 2	Branch 3			
$R > 1$	Ring	Carrier	Sun	r/s	$2 < R < 3.5$	ξ_1
	Ring	Sun	Carrier	r/(r-s)	$1.4 < R < 2$	γ_1
$0 < R < 1$	Carrier	Sun	Ring	(r-s)/r	$0.5 < R < 0.71$	β_1
	Sun	Carrier	Ring	s/r	$0.3 < R < 0.5$	ε
$R < 0$	Sun	Ring	Carrier	- s/(r-s)	$-1 < R < -0.4$	δ_1
	Carrier	Ring	Sun	- (r-s)/s	$-2.5 < R < -1$	α_1

Table 2-5 – Relationship between *R* and PGS with idler planets [95]

It can be seen that once an appropriate value of *R* has been identified for a given application, the most appropriate PGS configuration can be deduced for these types of differential by referring to Figure 2-22.

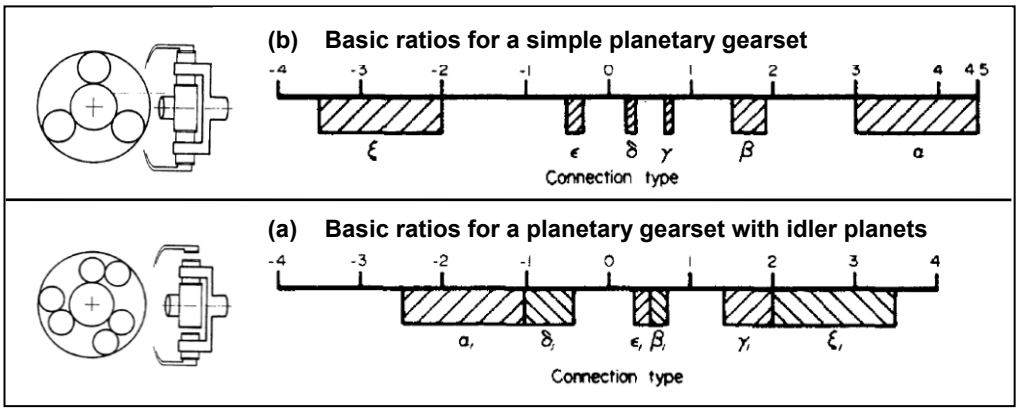


Figure 2-22 – Possible range of *R* values for practical simple and idler PGSs [95]

This allows a power-split system to be analysed for a given application as follows;

i. Analyse system using the equations for a generic differential,

ii. Identify an appropriate characteristic differential gear ratio for the application,

iii. Identify the most practical differential type and branch connections in order to achieve the required characteristic gear ratio

This is a powerful analysis method for understanding PSTs as it eliminates the need for an exhaustive study of all possible permutations of differential types and connection options.

Simple variator-controlled PSTs can be classified as either input or output coupled, depending on whether the variator connects between the control branch and the power input or power output branch of the PGS. Analysis of these configurations shows that several operating regions are possible, as illustrated in Figure 2-23 for the case of an output coupled PST.

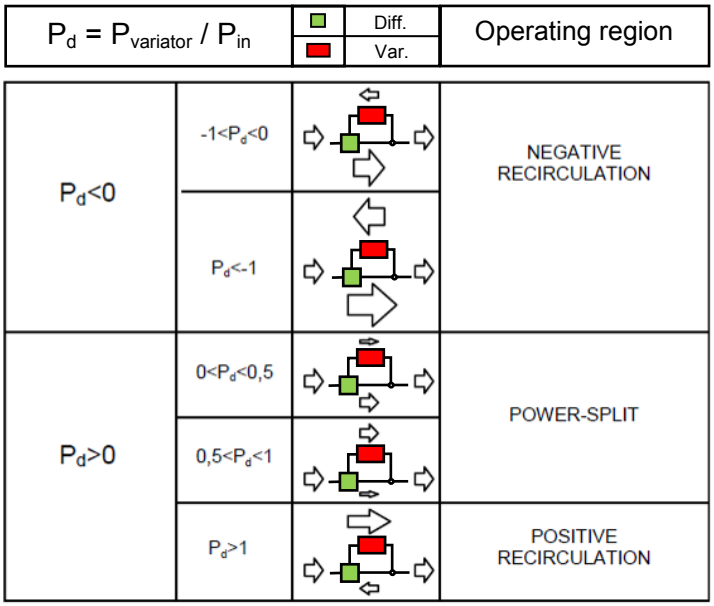


Figure 2-23 – Illustration of the possible operating regions for a variator-controlled 'output coupled' power-split transmission with arrows showing direction and magnitude of power flow (adapted from [96])

It can be shown (see Chapter 5) that in order to achieve genuine power-split operation (with power flow through each of the two branches being less than the overall power flow) the ratio spread of the PST is always smaller than the ratio spread of the variator. This spread can only be increased by allowing power-recirculation to occur. As well as extending the ratio spread, the presence of power-recirculation also makes it possible to achieve a geared neutral condition (i.e. zero transmission output speed with a non-zero input speed) and reverse drive (i.e. negative output speed for positive input speed) – these are often described as infinitely

variable transmissions (IVTs). This however requires the variator to be able to handle large power flows, and limits the overall efficiency of the PST due to high power losses in the variator and gearing. This reduction in efficiency has been demonstrated analytically and experimentally for the two main types of simple (single regime) power-split operation [97-99].

The compromise between ratio coverage and transmission efficiency has been investigated by Beachley et al. [93] for a flywheel hybrid passenger car application. The general hybrid power-train configuration used in the analysis is shown in Figure 2-24.

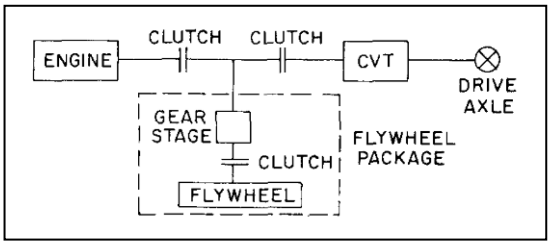


Figure 2-24 – Proposed flywheel hybrid power-train for passenger car [93]

A range of simple variator-controlled PSTs were considered for the CVT, with varying degrees of power-split and power-recirculation operation. The analysis focuses on the efficiency of the CVT rather than quantifying fuel savings. In order to produce general results that were independent of the control policy for the system, simulations were performed assuming a range of constant flywheel speeds. The results are therefore not useful in assessing the effect of factors such as energy storage capacity, flywheel self-discharge or the hybrid power-train control strategy on the overall FESS performance. They do however confirm that power-recirculation results in average CVT efficiencies considerably lower than average variator efficiencies. A 'load factor' (calculated assuming no transmission component losses and identical variator dimensions in all cases) was used to assess the relative variator size required for each case, which was shown to increase with the proportion of power flowing through the variator.

2.1.4.4. Advanced power split configurations

The compromise between overall ratio spread and the size and efficiency of the transmission which occurs with a simple variator-controlled PST can be addressed by considering more complex multiple-regime configurations. The simplest form of multiple-regime PST consists

of one regime of power-split operation and a second regime in which the variator provides a direct connection between the transmission input and output. This type of transmission has been investigated for both engine [100] and flywheel [93] applications. A fundamental analysis of a wide range of other 2-regime transmission configurations has been performed by White [92, 95], who identifies and characterises 48 different configurations for a 2-regime CVT with synchronous gear-change using only a variator, two coaxial differential gears and two clutches to engage each regime. This illustrates the complexity of identifying an appropriate configuration for a particular application, as there are a large number of ways that power-split operation can be achieved with multiple PGSs. Specific configurations of multiple-regime transmissions have been developed for use as a conventional IC engine transmission [96, 101-102] using mechanical variators or electrical motor/generator. Clutch and brake components are used to switch different differentials in and out of the power-flow path enabling several regimes of power-split operation to be achieved. These transmissions achieve high efficiency, and are compact and light enough to replace conventional automotive transmissions, although none are currently in production. There are no examples in the literature of applying these multiple-regime power-split transmissions to FESS applications.

In conclusion, mechanical CVTs can achieve high efficiency in a relatively compact and lightweight package and are therefore attractive for FESS applications. The use of a mechanical CVT does however impose kinematic restrictions on the operation of the FESS, which is related to the configuration and specification of the transmission components. It is therefore very important to be able to assess and compare a range of mechanical CVT systems, and identify the most appropriate system for a given application. Several transmissions have been developed specifically for FESSs in applications ranging from passenger buses to motorsports, and are discussed in the following section.

2.1.5. Mechanical flywheel hybrid vehicles

A range of hybrid vehicles utilising flywheel energy storage devices with mechanical transmissions have been proposed in the literature, and are described below. While some of these systems have been experimentally proven, none have achieved commercial production.

Gyreacta transmission

The Gyreacta transmission concept [103] operates with two differential gear units in the form of planetary gear sets (PGSs). These PGSs are used to achieve flywheel assisted acceleration or regenerative braking, with one PGS engaged in each mode (and the other allowed to freewheel). Each PGS has one of its three branches connected to the vehicle final drive and another to the flywheel (via a 4-speed gearbox). A clutch allows the engine to be connected to either of the remaining branches of the two PGSs.

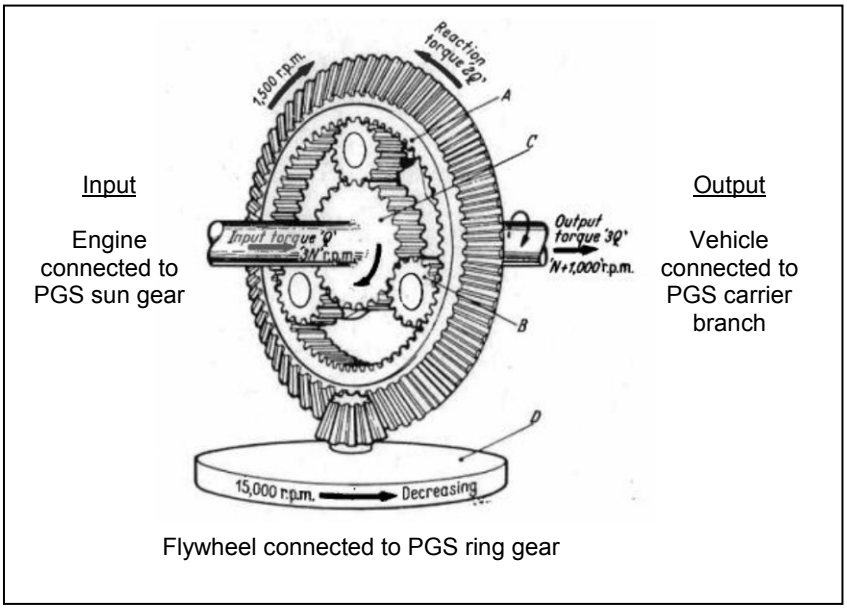


Figure 2-25 – Example of the operation of the Gyreacta in vehicle acceleration mode (simplified diagram does not include PGS-flywheel gearbox) [103]

These connections are made in such a way that during acceleration power flows from the engine and flywheel to the vehicle (as shown in Figure 2-25), while during regenerative braking power flows from the engine and vehicle to the flywheel (which is therefore referred to as 'power-assisted braking'). In either mode, the engine torque applied to one branch of the PGS establishes appropriate reaction torques at the vehicle and flywheel branches of the selected differential. The use of an additional 4-speed gearbox between the PGSs and the flywheel allows the engine to operate at appropriate speeds over the range of flywheel and vehicle operating speeds. A further mode of operation allows the flywheel to be charged from the engine while the vehicle is stationary.

The main drawback of this type of system is that the engine is required to operate during regenerative braking, and supplies a significant proportion of the energy stored in the

flywheel. This has two results; firstly, the energy capacity of the flywheel needs to be larger than the braking energy that is actually recovered (increasing the system mass and flywheel losses) and secondly, that significant transmission losses occur as energy is transferred between the engine, flywheel and vehicle.

University of Wisconsin research

A 1970s research program at the University of Wisconsin developed a flywheel hybrid system consisting of a 1-regime hydrostatic PST connected in series with a conventional 4-speed gearbox [81, 104]. This transmission was used to connect either an engine or a laminated steel flywheel to the final drive of the vehicle, as illustrated in Figure 2-26.

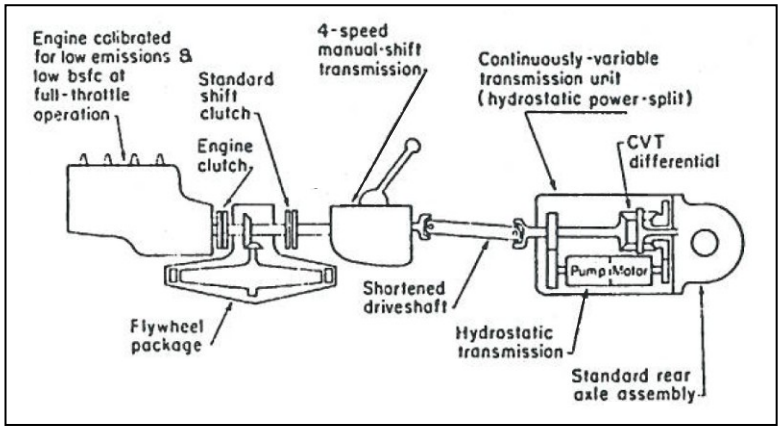


Figure 2-26 – Illustration of proposed flywheel hybrid power-train [104]

The flywheel had a useful energy capacity of 0.5 kWh and a self discharge rate of around 2% per min at the maximum speed of 10,000 rpm. When compared to a conventional vehicle, simulation results for the flywheel hybrid vehicle predicted an increase in fuel economy of 58% for an urban drive cycle. The majority of this fuel saving was achieved through more efficient operation of the engine. However, the transmission was found to operate with relatively low efficiency, with the total amount of regenerated energy being similar to the total losses at the flywheel and hydrostatic PST.

General Motors flywheel research vehicle

In the 1980's General Motors investigated the potential of FESSs and developed a hybrid passenger car with a direct-variator transmission [105]. This simple transmission was chosen over more flexible and efficient configurations due to its lower mechanical

complexity, size and cost. Figure 2-27 illustrates how the transmission connects either the flywheel or the engine to the final drive of the vehicle.

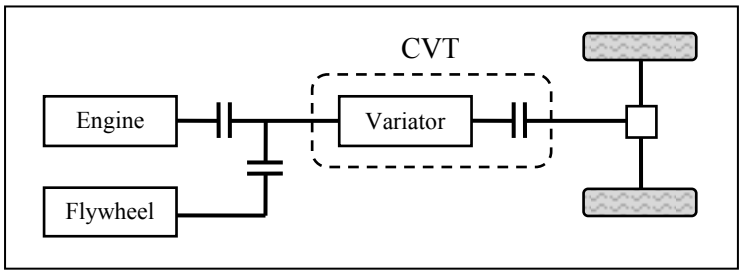


Figure 2-27 – Illustration of flywheel hybrid power-train proposed by General Motors

Computational modelling was used to assess the system performance of the flywheel hybrid power-train for both urban and highway drive-cycles. Compared to a conventional vehicle, the fuel consumption was found to be 36% lower for the urban cycle, but 11% higher for the highway cycle where transmission losses were high and little regenerative braking is possible. During the urban cycle 69% of braking energy was predicted to be available to charge the flywheel, 50% of which could then be used to deliver traction or auxiliary power. This gives a low overall regeneration efficiency of around 35%, and GM concluded that the improvements in urban driving efficiency were insufficient to justify further development of the concept.

Imperial College London 'Mechanical Hybrid Vehicle'

Research at Imperial College London has investigated the potential of a mechanical hybrid vehicle using a FESS [106-108]. Two flywheel transmission options have been considered; a simple friction-brake controlled PGS arrangement and a conventional single-regime variator controlled PST. The operating range of the PST was extended by considering additional periods of slipping-clutch and brake controlled operation. The performance of the two transmission systems was investigated through computational modelling and fuel savings were predicted for both passenger car and bus applications. The brake-controlled transmission was found to be very inefficient, with the calculated fuel savings largely due to reduced engine idling. The variator-controlled PST achieved much higher efficiency, resulting in fuel savings of 10-25% over a conventional vehicle. However, neither FESS was optimised in terms of transmission or system efficiency. This is seen in the low *DOD* of 25% that is achieved using the specified system parameters for the variator-controlled

PST, leading to high flywheel losses and an oversized energy storage capacity. Also, no information is provided regarding the design and control requirements of the transmission components (particularly the variator), making it difficult to assess the practicality of the system.

Flybrid Systems

The company Flybrid Systems have developed a FESS for use in a parallel hybrid configuration in motorsport applications [109]. The flywheel consists of carbon fibre wound around a steel hub and can operate at a maximum speed of 60,000 rpm. For racing cars, operation of the flywheel is rarely required to accelerate the vehicle from stationary and so a transmission with a geared neutral is not essential. Therefore, the transmission used is a direct toroidal variator with clutch. As shown in Figure 2-28 the flywheel is connected to one branch of the variator via a fixed gear ratio. The input drive to the FESS connects to the vehicle final drive.

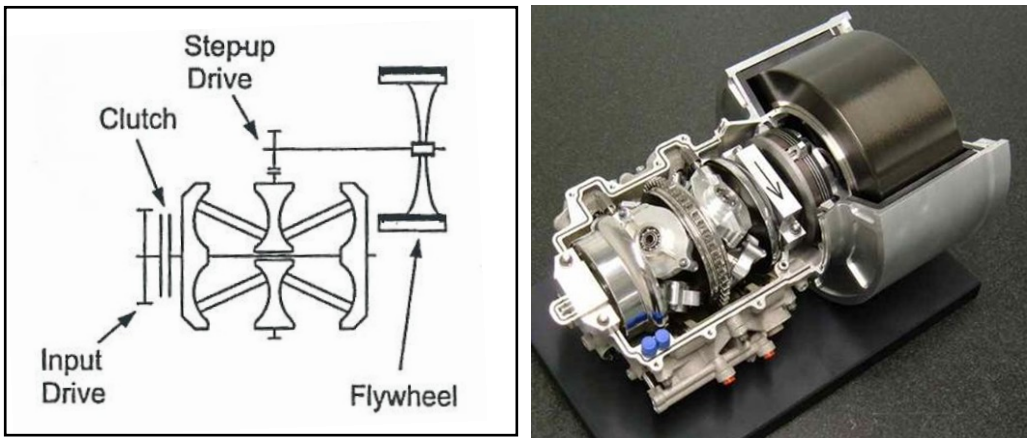


Figure 2-28 – Flybrid mechanical FESS developed for Formula 1 application [109]

This transmission provides sufficient ratio coverage to meet the application requirements, and operates with high efficiency due to the consistently high power demands. The differing requirements of a FESS for passenger car applications have however been acknowledged, and alternative transmissions have been proposed using a direct variator with a range-extending gearbox or single-regime power-split transmissions with a range of different connection points for the FESS within the vehicle power-train [110]. Results from this study suggest improvments in fuel efficiency of between 15-25% are possible over a conventional car for a range of standard urban and extra-urban drive-cycles, with over half

of the fuel savings shown to be a result of reduced engine idling when no engine power is required. No details are however given regarding the selection of gear ratios, component sizing or the power-train control strategy used in these simulations.

Conclusions on mechanical transmissions for FESS applications

It is very difficult to compare the different mechanical transmission systems in the literature, as they have all been developed and assessed for a specific application. When applied to FESSs, transmission efficiency has been identified as a critical factor in achieving effective regenerative braking, suggesting that PSTs should be designed to minimise or avoid power-recirculation in order to reduce losses and achieve a lightweight and compact transmission. The design of the transmission will however directly affect the operation range of the flywheel, and this interaction requires careful consideration in order to achieve good overall system performance in terms of energy capacity, regeneration efficiency, mass and cost. The identification of appropriate system parameters for high-power mechanical FESSs using a range of single and multiple regime transmissions is the focus of Chapters 4 and 5 of this Thesis.

2.2. Rail vehicle energy modelling

The assessment of the potential benefits of hybrid regional trains requires detailed modelling of the vehicle power-train and operating conditions. The performance of any rail vehicle is highly dependent on both the route considered and the way in which the vehicle is controlled. This is especially important in the case of hybrid vehicles where the requirement of the regenerative braking system and the amount of energy available for recovery depends on the braking strategy used by the driver. The relationship between control strategy and energy consumption must therefore be characterised for both conventional and hybrid trains in order to make a comprehensive comparison of vehicle performance.

A range of computational approaches are described in the literature to investigate the operation of electric and diesel powered rail vehicles. These can broadly be categorised as multiple vehicle 'system' models which tend to focus on the timetabling of services or the substation power demand on electric railways [111-112], and single vehicle models which focus on the control and energy consumption of an individual vehicle. In both cases, an accurate model must include details of the vehicle dynamics, the power-train, the route

profile (including station spacing and gradients) and the control strategy applied by the driver. The type of computational method applied depends on the aims and scope of the research. The two main areas of research in the literature are optimised control methods and hybrid rail power-trains.

2.2.1. Optimised control

A considerable amount of research effort has been focussed on identifying the most energy (or fuel) efficient driving profile for a single rail vehicle travelling along a defined route with specified timetable restrictions. The nonlinear nature of this problem means that optimisation methods are required. Both analytical methods (where a solution is calculated) and numerical methods (where a solution is reached iteratively) have been applied to this problem.

An analytical approach using differential equations to describe the vehicle trajectory and identify an optimum control strategy is described by Golovitcher and Lui [113]. This can be applied to a route with multiple stops and variable speed restrictions and gradient, and the proposed application of this method for use in automated train operation systems is described in some detail. The optimisation is however only performed to minimise the traction energy required at the wheel, and therefore assumes constant power-train efficiency under all operating conditions. The power delivered by the power-train is also assumed to be continuously variable, rather than notch-based as is common in diesel powered trains. The optimised control of notch-controlled diesel trains has been investigated by Howlett and colleagues [114-115]. A similar analytical approach is used to identify optimum trajectories for diesel trains with discrete control of the engine throttle, assuming each throttle setting allows a constant flow rate of fuel to the engine. The power-train efficiency is again assumed to be constant. Much of this research is embodied in the 'Metromiser' on-board computer system which can advise train drivers on fuel efficient driving strategies, mainly through the identification of appropriate coasting points. This system has been shown to achieve energy savings of 10-15% for metro and suburban type services [11].

Numerical optimisation methods have also been applied. Wong and Ho [116] assessed the feasibility and performance of classical and heuristic numerical searching methods in locating coasting points for a train travelling between two stations with a specified journey time. The analysis included the effects of speed restrictions, gradient and power-train characteristics, and was implemented using a time-step based single train model. They found that a heuristic 'genetic algorithm' (GA) search method achieved a robust and computational efficient

solution for the optimum coasting points. The research also showed that in cases with relatively short station spacing (less than 10 km) the optimal solution was achieved with a single coast point prior to braking on the approach to the station stop. Only with relatively long station spacing (~30 km) were multiple coast points required to achieve an optimum trajectory.

Hwang [117] describes an optimisation method using a combined fuzzy logic and GA hybrid scheme for identifying the optimal compromise between energy consumption and journey time in a high speed railway. An example case was presented and the location of appropriate 'coasting zones' were identified. A similar approach has been applied to DC suburban railways [118] using a detailed time-step based single-vehicle model. The use of fitness functions allowed weighting to be given to reducing either journey time or energy consumption, and the effect of regenerative braking on the optimum trajectory was also considered. In both these studies the optimum driving strategy was found to be achieved largely through the use of coasting prior to braking on the approach to speed reductions and station stops.

2.2.2. Hybrid rail vehicle analysis

Several computation studies have been performed to assess the potential benefits of applying hybrid power-trains to rail vehicles.

Hillmansen and Roberts [119] modelled a hybrid commuter train by assuming constant power output from a diesel engine and modelling the storage device as having constant efficiency and sufficient capacity to provide the fluctuating power demand over the course of a specified drive cycle. A constant regenerative braking efficiency was also used to define the fraction of available braking energy actually available at the storage device. Fuel consumption was calculated over representative commuter and high-speed drive cycles using the hybrid model and a standard diesel model to provide a basis for comparison. With a 50% regeneration efficiency and a storage device efficiency of 80% during both energy input and output, fuel savings of 35% and 28% were calculated for the high speed and commuter trains respectively. However, the fuel consumption was calculated for an optimised combination of engine capacity and energy storage capacity, which is highly dependent of the particular drive cycles used. This is unlikely to be possible in practice, as rail vehicles are required to operate a range of routes and services.

Jefferson and Marquez [120] described a Matlab/Simulink based generic ultra light rail vehicle (ULRV) hybrid model. Results were obtained for a diesel-mechanical vehicle with automotive gearbox and constant transmission efficiency of 85%, and a diesel-electric hybrid vehicle. The diesel engine in the hybrid was assumed to operate at constant power output and optimum efficiency, with energy storage provided by a FMG unit. Using simulations with the same operating conditions over a simple drive cycle, the hybrid vehicle was found to consume 36% less fuel than the conventional vehicle. The results are however calculated using a relatively simple power-train model, and are limited to light rail vehicles operating at low speed and with frequent stops.

Destraz et al. [121] have modelled a supercapacitor based energy storage system for a hybrid diesel-electric rail vehicle. A constant power output from the diesel engine was again assumed, and the relationship between required storage capacity and engine power output was investigated for a particular route. As engine size is decreased, both the fuel saving and the required storage capacity were shown to increase. An economic analysis was performed and the most appropriate configuration was predicted to achieve a 44% reduction in fuel consumption. This simulation work was however performed using drive cycle data for trains operating in a mountainous part of northern Italy, and the severe duty cycle is likely to have an influence on the performance of the hybrid vehicle. The optimised downsizing of the engine is again dependent on the particular drive cycle studied, and may limit the vehicle performance on other routes.

A major drawback of these three studies is the fact that the drive cycles used are representative of an aggressive driving strategy, with no coasting used on the approach to station stops and speed reduction. This effectively represents a ‘worst case’ driving strategy which maximises the fuel consumption of a conventional vehicle and maximises the proportion of fuel saved by the hybrid vehicle. A more efficient driving strategy aimed at closely matching the timetable for a given route is likely to decrease the amount of braking energy available for regeneration, and so reduce the percentage fuel saving associated with hybridisation. A more flexible approach to train control has been applied by Wen et al. [122] for the computational analysis of a hybrid-electric high speed intercity train. The inclusion of a driver module (discussed in more detail in Section 2.2.3) allows a range of driving strategies to be studied. A range of routes were considered, and both aggressive and efficient driving strategies applied. For the aggressive strategy the hybrid train was found to reduce fuel consumption by 15-25%, falling to 8-19% when the efficient strategy was applied.

It is clear that there is significant potential to reduce fuel consumption through the application of hybrid technology. However, the interaction between efficient driving and hybridisation needs to be characterised for regional rail vehicles in order to assess the realistic fuel savings possible and the requirements of the hybrid system. This can be achieved through detailed computational modelling.

2.2.3. Rail vehicle modelling

Computational modelling can be used assess energy consumption in rail vehicles by considering the following three areas; vehicle dynamics, power-trains and duty cycle analysis.

a) Vehicle dynamics

All rail vehicle energy models are based around the longitudinal motion of the vehicle, as illustrated in Figure 2-29.

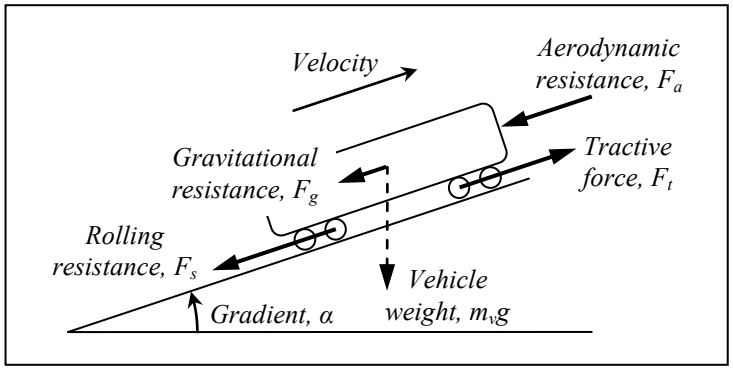


Figure 2-29 – Illustration of longitudinal dynamic forces

The longitudinal equation of motion can therefore be expressed as;

$$(m_v + m_r)\ddot{x} = F_t - (F_r + F_g) \tag{2-3}$$

where m_v is vehicle mass; m_r is equivalent mass of rotating components; x is the longitudinal vehicle displacement from an absolute reference point; F_r is the total resistance to motion (rolling and aerodynamic); F_g is force due to gravity and F_t is tractive force produced by the power-train.

The total resistance to motion is the sum of both rolling friction and aerodynamic drag forces. These resistance forces are functions of a large number of variables including vehicle

mass, length and profile; vehicle and wind velocity; condition of axles and bearings; curvature of track. As some of these conditions vary with time, an established method of characterising the vehicle resistance is to take a range of measurements during typical vehicle operation and identify the relationship between resistance force and vehicle speed for average conditions [123]. This average resistance curve can be approximated as a quadratic function of vehicle speed (the derivative of displacement) which is known as the Davis Equation, and is defined in Equation 2-2;

$$F_r = A + B\dot{x} + C\dot{x}^2 \tag{2-4}$$

The terms A, B and C are constants known as the Davis coefficients and can be empirically related to the aerodynamic and friction forces as discussed by Rochard and Schmid [124].

By assuming a lumped mass model for the train, the force due to gravity, F_g, can be approximated as a function of the vehicle mass, m_v, and the instantaneous angle of incline, $\alpha(x)$, which is +ve when travelling uphill. This is defined in Equation 2-3;

$$F_g = m_v \sin(\alpha(x)) \tag{2-5}$$

While this does not take into account the distributed mass of the vehicle along its length and therefore the continuous change in resistance force as the vehicle passes over a point where the gradient changes, the effect on energy calculations is negligible as the total change in gravitational potential energy over a route is unaffected.

b) Power-train modelling

This thesis focuses on the energy consumption of both conventional and proposed hybrid regional trains. The power-train in these vehicles consists of a number of distributed diesel engines with hydrodynamic transmissions. A suitable modelling approach is therefore required in order to assess the operation of the combined engine-transmission unit. In order to calculate fuel consumption, the dynamic operation of both the diesel engine and the transmission components (torques converter and fluid couplings) can be accurately modelled using empirical steady-state performance maps [46]. This is due to the fact that the rate of change of engine and transmission operating points are relatively low for rail vehicles, and so the power-train performance is close to the steady-state values. A standard time-step based quasi-static analysis method has therefore been used to create a detailed power-train model. This has been implemented using Matlab/Simulink software due to its simple graphical interface and provision of appropriate numerical solvers for time-step based analysis.

A steady-state fuel consumption map has been obtained for a 330 kW diesel engine from the ADVISOR automotive simulation software [125]. This has a similar power rating to the diesel engines used in DMUs, and can be scaled to achieve the required maximum power and maximum engine speed. This provides the fuel consumption (in g/kWh) as a function of engine torque and rotational speed. An important consideration in the modelling of a diesel-hydrodynamic power-train is the interaction between the engine and the hydrodynamic elements of the transmission. A standard approach to the analysis of torque converters and fluid couplings is described by several authors [46, 126-127]. Empirical data for the torque converter (TC) and fluid coupling (FC) components can be used to create a steady-state operating map defining the engine operating point as a function of the transmission output speed and the engine power setting.

c) Control/drive cycle

The calculation of fuel consumption for road vehicles relies on standard drive cycles (velocity-time profiles) which are often used to determine the tractive power required at the transmission output [46, 125]. This requires a backwards-facing calculation method which uses the required tractive power (calculated during each time-step) to deduce the operating point of the IC engine, and hence the fuel consumption. For a journey between two points, the constraints of rail vehicle operation mean that in theory the drive cycle can be predicted with more accuracy than is the case with road vehicles, where factors such as route selection, traffic intensity and signalling create considerable uncertainty. The slack in rail journey timetables does however allow variation in driving strategy, which has been shown to have a significant effect on the energy consumption of conventional diesel and electric trains [see section 2.2.1]. Furthermore, this variation in driving strategy can lead to significant variation in both the energy storage requirements and potential benefits of hybrid trains [see section 2.2.2]. A forwards-facing calculation procedure allows the vehicle power to be specified, and the resulting vehicle acceleration to be deduced. This method has been applied in a number of single-train models, where the locations at which braking must be initiated are found by performing a forward-facing calculation applied backwards in time to calculate the required velocity profile on the approach to a known speed limit when a specified braking force is applied [119-120]. This approach provides a means of obtaining a simple drive cycle, but does not allow the effect of different control strategies (especially those involving a degree of coasting) to be easily investigated. An alternative approach is described by Wen et al. [122] for the modelling of conventional and hybrid high speed diesel-electric trains. This uses a

forward-facing calculation procedure combined with a vehicle control subsystem. The tractive power delivered to the vehicle during a time-step is specified according to the current vehicle speed and position with reference to overall route profile (including consideration of gradients, speed limits and station locations), although the details of the control logic are not fully explained. This enables different driving styles to be investigated by varying a range of control parameters. A similar approach has therefore been used for analysing the performance of conventional and hybrid diesel regional trains in this Thesis.

2.3. Summary

Advanced flywheel energy storage devices have been identified as a candidate solution for regenerative braking systems due to their energy and power characteristics, long life and potentially low cost. Mechanical flywheel transmissions offer a means of achieving high regenerative braking efficiency with a lightweight and compact system that can be applied to any type of vehicle in a parallel-hybrid arrangement. The research presented in this Thesis therefore considers the application of mechanical FESSs to regional diesel-hydrodynamic trains where braking losses have been identified as a major source of inefficiency. The effect of regenerative braking on fuel consumption is however dependent on the driving strategy applied to the vehicle. Efficient driving strategies have been shown to significantly reduce braking losses, and have been identified as a short term measure to reduce the energy consumption of conventional rail vehicles. The interaction between efficient driving and regenerative braking must therefore be studied in a rigorous way in order to identify appropriate solutions and assess the realistic benefits of hybridisation.

3. Effects of driving strategy on conventional and hybrid diesel regional trains

Vehicle braking in non-electrified rail systems wastes energy. This Chapter considers two approaches to reducing braking losses in regional diesel trains; efficient driving strategies and regenerative braking. The interaction of these two approaches is critical in specifying the requirements of a hybrid train and assessing the relative fuel saving. Computational models of conventional and hybrid diesel-hydrodynamic regional trains have been developed using real route data to generate a simple control algorithm and investigate the effect of driving strategy on fuel consumption and journey time. The current modelling predicts fuel savings of up to 40% for the hybrid train when an aggressive control strategy is used. This fuel saving is halved when an efficient driving strategy is employed, which also reduces the required energy storage capacity. The model provides a tool for identifying effective control strategies which should be implemented to reduce fuel consumption for both conventional and hybrid trains. It also provides a realistic basis for assessing the potential of hybridisation for reducing fuel consumption, and allows an initial assessment of the energy and power requirements of the energy storage system.

3.1. Approach to vehicle modelling

The first stage in the development of a hybrid regional diesel train (HRDT) model has been the construction of a conventional diesel-hydrodynamic (non hybrid) model. This approach allows a direct comparison of the fuel consumption for both the conventional and hybrid trains. Matlab/Simulink software was chosen because of its simple graphical environment and the availablity of numerical solvers for discrete time-step based simulations. A forward facing model structure has been selected to allow a vehicle control module to be implemented, enabling the effect of different control strategies to be investigated. The modelling uses a standard quasi-static approach for the vehicle dynamics and power-train components. A control module has been created which specifies the required vehicle power or braking demand based on the current speed, position and the specified route data (including speed limits and station locations). Figure 3-1 illustrates the model structure which consists of three modules describing the vehicle dynamics, power-train and control.

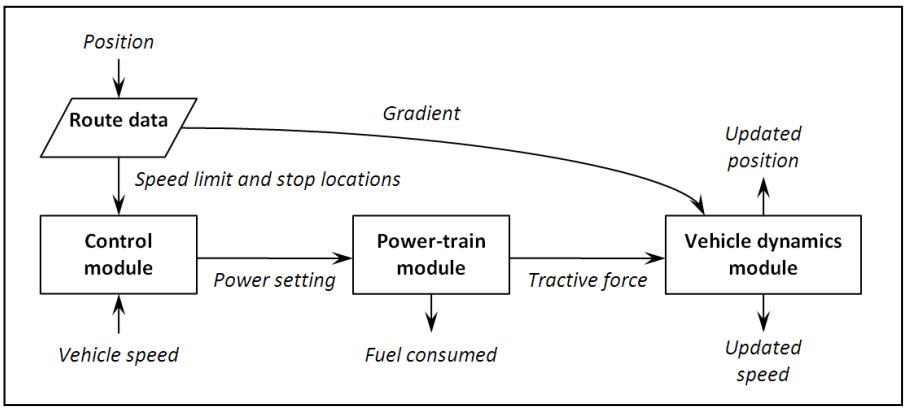


Figure 3-1 – Flow chart of calculation procedure for forward-facing model structure consisting of control, power-train and vehicle dynamics modules

The following three sections describe the standard approaches taken to modelling the vehicle and power-train, and the specific control approach applied in this study.

3.1.1. Vehicle dynamics module

The vehicle energy consumption is related to the longitudinal motion of the vehicle, as described by Equations (3-1).

$$\left(m_v + m_r\right)\ddot{x} = F_t - \left(A + B\dot{x} + C\left(\dot{x}\right)^2 + m_v \sin\left(\alpha\left(x\right)\right)\right) \qquad (3\text{-}1)$$

This ordinary differential equation can be solved within Matlab/Simulink using numerical integration methods when the tractive force, F_t, is specified. The vehicle parameters used in this analysis (including the empirical Davis equation coefficients) were specified using data for a typical UK 3-car diesel-hydrodynamic train with maximum speed of 160km/h [128-129] and are shown in Table 1. An equivalent rotational mass, m_r, of 10% of the actual vehicle mass, m_v, is used as this represents a typical value for mainline DMUs [123].

Vehicle Parameter	
Mass, m_v	133.7 tonnes
Equivalent rotational mass, m_r	0.1* m_v
Installed power	945 kW
Auxiliary power load	67.5 kW
Final drive ratio	2.6
Wheel radius	0.4 m
Davis equation coefficients:	
A [kN]	2.977
B [kN / (m/s)]	0.0345
C [kN / $(m/s)^2$]	0.00474

Table 3-1 – Vehicle parameters for model of 3-car diesel-hydrodynamic vehicle

3.1.2. Power-train module

The power-train provides the tractive power and consists of the diesel engine and hydro-dynamic transmission. This module defines the interaction between these components, and calculates the fuel consumption and tractive power delivered to the vehicle as a function of the vehicle speed and power setting. The fuel consumed by the engine is calculated using data from a 330 kW diesel engine map (obtained from the Advisor automotive vehicle simulation software [125]) which was scaled to match the installed power of a single 315 kW engine as shown in Figure 3-2. This map shows the operating efficiency of the diesel engine in terms of mass of fuel consumed per unit of energy generated as a function of the engine torque and speed.

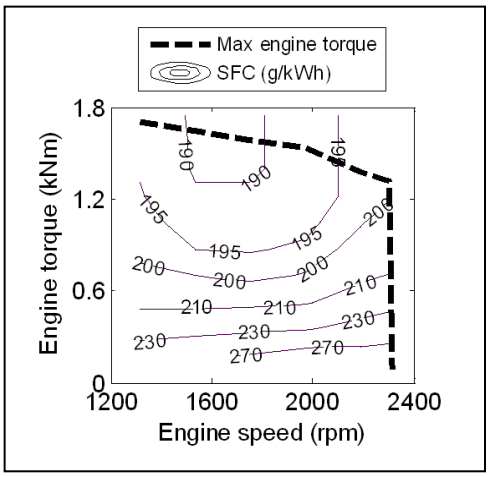


Figure 3-2 – Specific fuel consumption and max torque curve for a 315kW engine

Using a standard approach [126-127] a model of a 2-speed hydrodynamic transmission consisting of one torque converter and one fluid coupling has been developed. The torque converter and fluid coupling characteristics have been specified to match the published maximum tractive effort curve of the 3-car Class 170 Turbostar vehicle. Transmissions of this type are widely used in regional diesel vehicles in the UK, but have not been considered in previous analysis of HRDTs.

The power-train model allows the operating point of the engine and transmission to be defined for a given vehicle speed and power notch setting. A total of 7 power notch settings have been assumed for the transmission, with engine torques equal to the maximum torque shown in Figure 3-2 multiplied by 0.4 to 1 (in steps of 0.1) representing notches 1 to 7. The tractive effort, transmission efficiency, engine SFC (specific fuel consumption) and tank to wheel efficiency (assuming a specific energy of 12.1 kWh/kg for diesel fuel) are shown in Figure 3-3 as a function of vehicle speed for power notches 1, 3, 5 and 7.

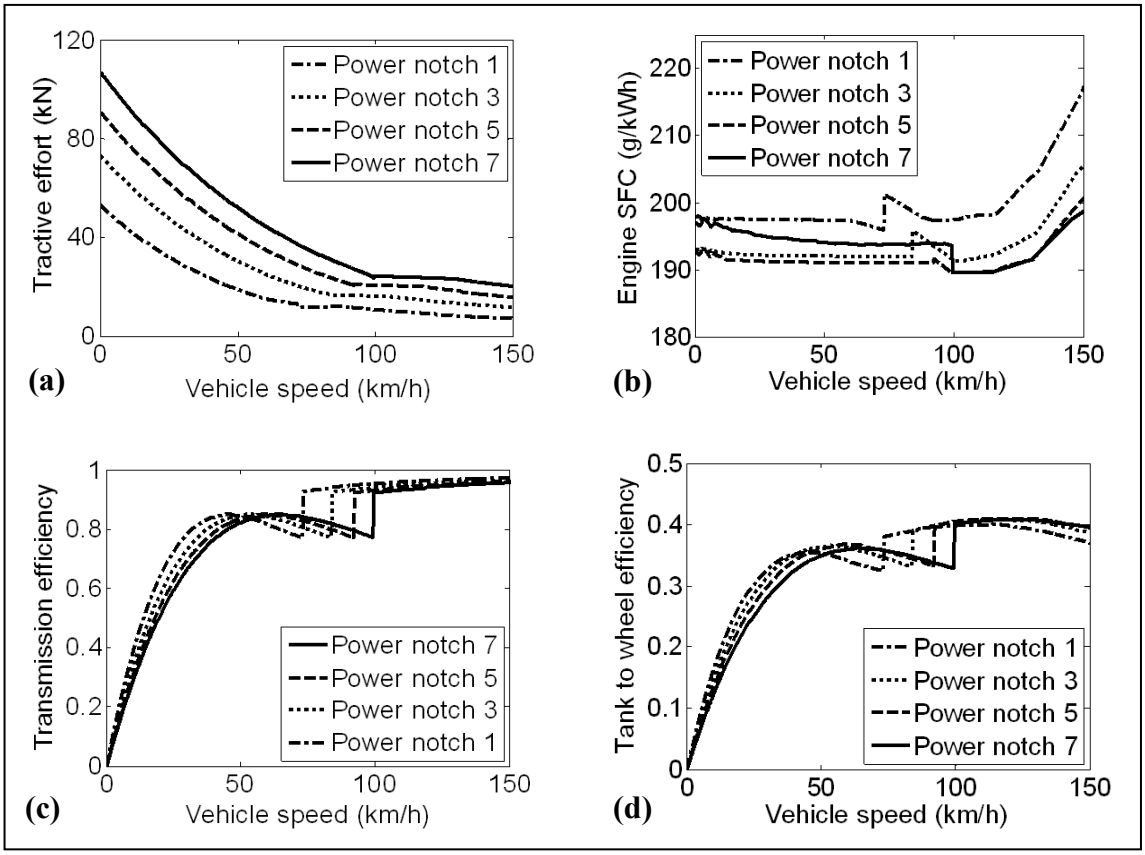


Figure 3-3 – Power-train output values of (a) tractive effort, (b) SFC, (c) transmission efficiency and (d) tank-to-wheel efficiency as a function of vehicle speed for power notches 1, 3, 5 and 7

The four diagrams in Figure 3-3 show the operating characteristics of the power-train. The fuel efficiency of the engine is relatively high under all operating conditions with the SFC varying between 190 and 218 g/kWh. This suggests that there will be little benefit from control strategies aimed at optimising the engine operating point. Transmission efficiency is found to be relatively high for vehicle speeds above 50km/h, but drops rapidly at lower speeds. These low speed losses are therefore significant, and can be reduced by either;

- Improving the low speed efficiency of the conventional power-train,
- Introducing a regenerative braking system to reduce or eliminate power delivery via the conventional power-train during low speed operation.

In terms of fuel consumption, hybridisation of this type of rail vehicle therefore has the dual benefits of recovering energy that would otherwise be dissipated during braking and using this energy to displace low efficiency operation of the conventional power-train.

The tractive force calculated by the power-train module is passed to the vehicle dynamics module allowing the vehicle acceleration, speed and position to be calculated. Introducing the control module then allows the required power setting to be defined, as described in the following section.

3.1.3. Vehicle control module

The vehicle control module has been constructed to use simple logic for powering, speed holding and speed reductions. Three scenarios are considered in order to define the power demand. These are:

i) *Acceleration* – during vehicle acceleration below the holding speed (where $v_{hold} < v_{line}$), the vehicle is commanded to operate at a specified engine power.

ii) *Speed holding* – as the vehicle reaches the holding speed the power notch is changed to the minimum setting which will maintain vehicle acceleration. When the line-speed is reached the maximum power setting to achieve deceleration is selected. If the gradient is sufficient to accelerate the vehicle beyond the line speed with no tractive power applied, braking is used to limit the vehicle speed.

iii) *Speed reduction* – this applies during the approach to reductions in line speed and station stops. Four trigger speeds are calculated during each time step based on the distance and height difference between the current vehicle position and;

   a) the next line speed reduction (Δx_{slow} and Δh_{slow})

b) the next stop location (Δx_{stop} and Δh_{stop}).

These trigger speeds represent a hypothetical vehicle speed at which a specified constant deceleration, D, would achieve the required speed reduction. For cases (a) and (b) two trigger speeds are calculated using a lower constant deceleration value for a 'coasting trigger speed', and a higher value for a 'braking trigger speed'. They are calculated by considering conservation of energy as defined in Equations 4-6.

$$(Energy\ dissipated\ during\ constant\ deceleration) + \Delta KE + \Delta GPE = 0 \qquad (3\text{-}2)$$

$$(m_v + m_r)D\Delta x + \frac{1}{2}(m_v + m_r)(v_{target}^2 - v_{trigger}^2) + m_v g\Delta h = 0 \qquad (3\text{-}3)$$

$$v_{trigger} = \sqrt{v_{target}^2 + 2(D\Delta x + \frac{m_v}{(m_v + m_r)} g\Delta h)} \qquad (3\text{-}4)$$

where v_{target} is the next line speed limit (zero when calculating trigger speeds for station stops). Once the vehicle speed equals the coasting trigger speed, the vehicle is allowed to coast until the braking trigger speed is reached. At this point a braking force is applied to the vehicle in order to achieve the specified constant deceleration.

All results presented for constant force braking use a moderate braking deceleration rate, D_{brake}, of 0.5m/s^2. By varying the coast trigger deceleration value, D_{coast}, different degrees of coasting can be applied for a specific route, and the effect on journey time and fuel consumption can be assessed. Figure 3-4 illustrates the operation of the vehicle in each of the three scenarios described.

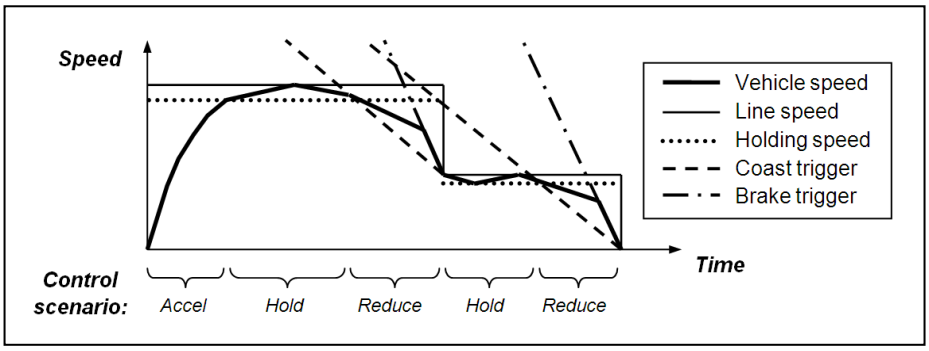


Figure 3-4 – Schematic illustration of vehicle control subsystem operation

This shows that the operation of the vehicle over a defined route can now be investigated using a range of simple vehicle control strategies. The effect of these strategies is assessed by comparing the calculated journey time and fuel consumption in each case.

3.1.4. Description of route data

The vehicle analysis is performed using route data for real sections of main-line and branch-line routes in the East Anglia region of the UK. The station locations, line speed limits and variation in height of both routes are shown in Figure 3-5.

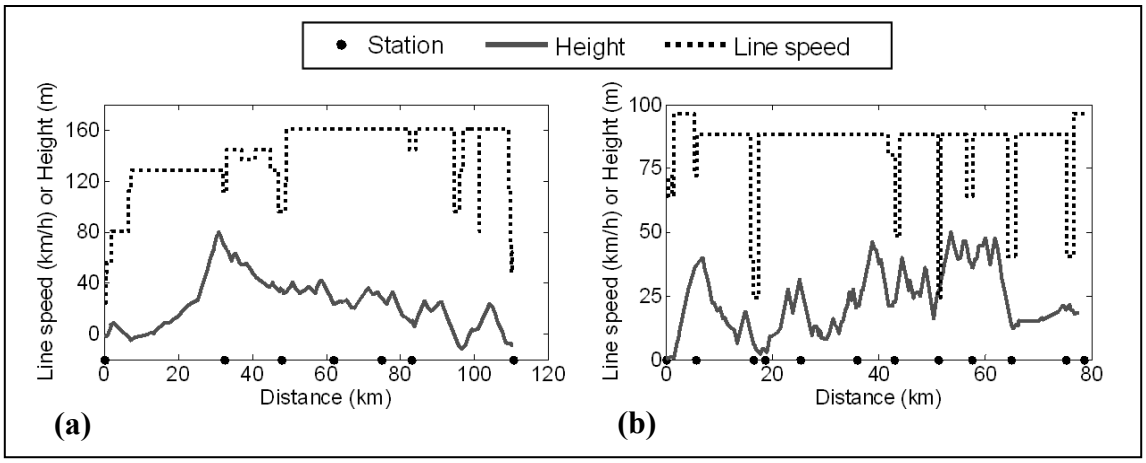


Figure 3-5 – Data for (a) Main-line and (b) Branch-line routes used in the simulations

An example of the output velocity profile calculated by the conventional vehicle model using the main-line route data and three different driving strategies is shown in Figure 3-6. This illustrates the effect of varying the D_{coast} parameter in the control module.

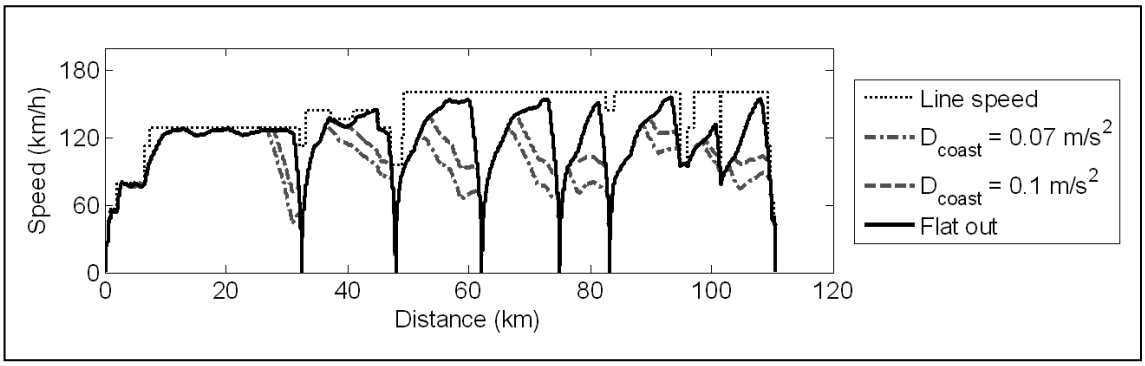


Figure 3-6 – Examples of calculated vehicle speed profiles for main-line route with no coasting (flat out) and coasting trigger deceleration values (D_{coast}) of 0.1 and 0.07 m/s^2

Using this real route data in the vehicle simulation allows the calculated fuel consumption to be compared to the time-averaged values reported in a recent industry study [128] for the small fleet of Class 170 diesel hydro-dynamic trains operating a range of services in this area (including these two routes). The results are shown in Figure 3-7 and are calculated for when the vehicle is driven 'flat out' (i.e. no coasting used during speed reduction) with station departure times matching the published time-table.

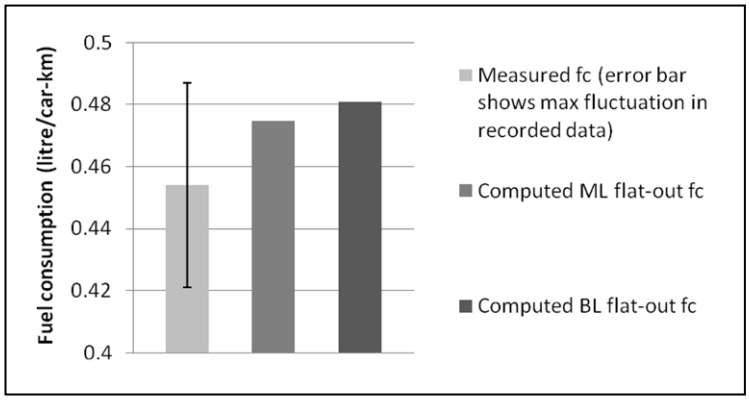


Figure 3-7 – Comparison of measured fuel consumption (fc) with results of model using 'flat-out' vehicle operation matching the time-tabled departure times for main-line (ML) and branch-line (BL) routes

The calculated fuel consumption per car-km (where car refers to a single carriage) is similar for both the main-line and branch-line routes, and lies towards the upper range of the time averaged fuel consumption measured in operational service. The results are sufficiently accurate for the investigation of relative fuel savings for efficient driving strategies and regenerative braking; however, more data is required for a full validation of the model.

3.2. Driving strategies for conventional vehicles

The model presented above can now be used to investigate the effect of driving strategies on conventional and hybrid regional trains. There are two simple driver control strategies considered for the conventional vehicle. These are:

i) Limiting the maximum allowable speed of the vehicle (subject to the line speed limit)

ii) Applying a degree of coasting prior to braking on the approach to speed reductions and station stops

These measures lead to reductions in both the energy dissipated during braking and the work done against resistance at the expense of increased journey time. Figures 3-8 and 3-9 show the calculated fuel consumption (in litres/car-km) against the calculated total journey time normalised by the scheduled journey time for the route. Constant station dwell times of 60s and 30s have been assumed for the main-line and branch-line routes respectively.

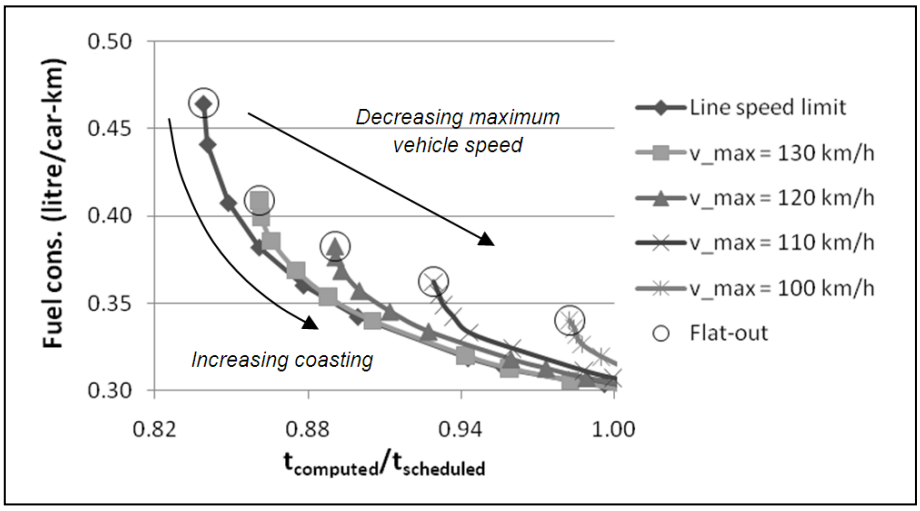


Figure 3-8 – Effect of increasing coasting and reducing maximum vehicle speed on relative journey time and fuel consumption for main-line operation with station dwell time of 60s

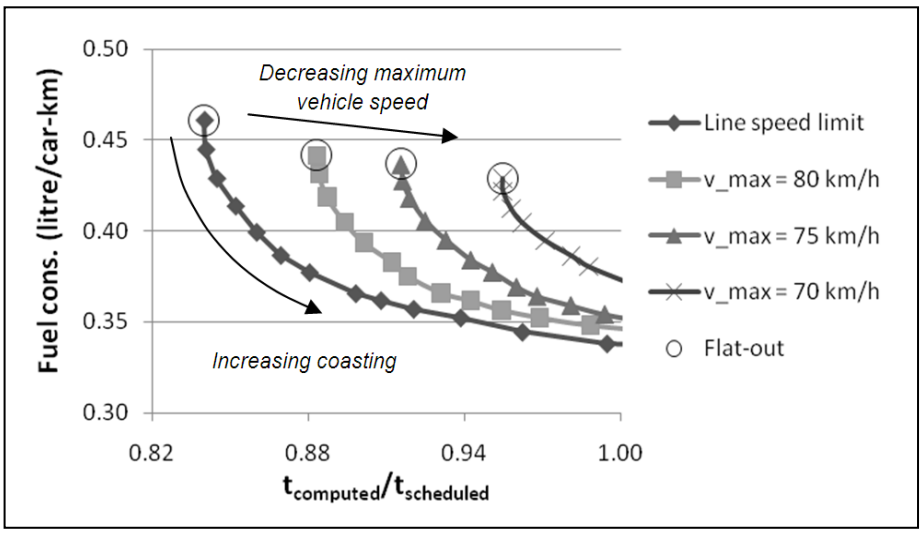


Figure 3-9 – Effect of increasing coasting and reducing maximum vehicle speed on relative journey time and fuel consumption for branch-line operation with station dwell time of 30s

Figures 3-8 and 3-9 show the effect of applying coasting and speed limits; each data point is calculated for a particular value of D_{coast} and maximum vehicle speed. The findings fall into the following three categories.

1. There is considerable scope to look at energy efficient driving techniques for these routes, as simulation with a flat out driving strategy takes around 85% of the scheduled journey time.

2. For a given journey time the maximum fuel saving is achieved by accelerating the vehicle to the full line speed limits and applying the required amount of coasting during deceleration.

3. There is a different effect on the two routes when applying the strategy of limited maximum vehicle speed. On the main-line route this results in a significant reduction in fuel consumption regardless of how much coasting is used. On the branch-line route however significant reductions in fuel consumption are only possible through coasting.

In summary, coasting is the most fuel efficient of the simple driving strategies considered. The vehicle control algorithm used here presents a simple method of identifying appropriate coasting points for drivers.

3.2.1. Effect of timetabling constraints on fuel consumption

The analysis presented in Section 3.2 assumes overall journey time is the only time constraint on the train services considered. A constant value of D_{coast} has therefore been used throughout the journey, defined here as a 'uniform coasting' strategy. However, the impact of driving strategies is also affected by timetabling constraints. When using coasting, these restrictions make it necessary to apply appropriate values of D_{coast} to meet the scheduled arrival times at each intermediate station, defined here as 'timetable-limited coasting' strategy. The calculated fuel consumption for three different driving techniques are shown in Table 3-2; flat out driving with scheduled intermediate departure times (the worst case driving style as shown in Figure 3-7), uniform coasting to achieve overall journey time (i.e. uniformly applied D_{coast} value) and timetable-limited coasting to achieve overall journey time (i.e. individual D_{coast} values for each inter-station route section).

Driving Strategy	Main-line		Branch-line	
	litres/car-km	saving*	litres/car-km	saving*
Flat out with scheduled intermediate departure times (worst case)	0.475	-	0.481	-
Uniform coasting to achieve overall journey time	0.302	36%	0.340	29%
Timetable-limited coasting to achieve overall journey time	0.334	30%	0.369	23%

** percentage saving relative to the worst case fuel consumption*

Table 3-2 – Effect of coasting strategy and timetable restrictions on fuel consumption

These results show that the fuel consumption is lowest when the uniform coasting strategy is used. Compared to timetable-limited coasting, uniform coasting achieves significant fuel savings of 10% and 8% on main-line and branch-line routes resepctively. This can be explained by considering the general form of the fuel consumption (*fc*) vs. journey time curve when coasting is applied for a journey between two stations, as shown in Figure 3-10.

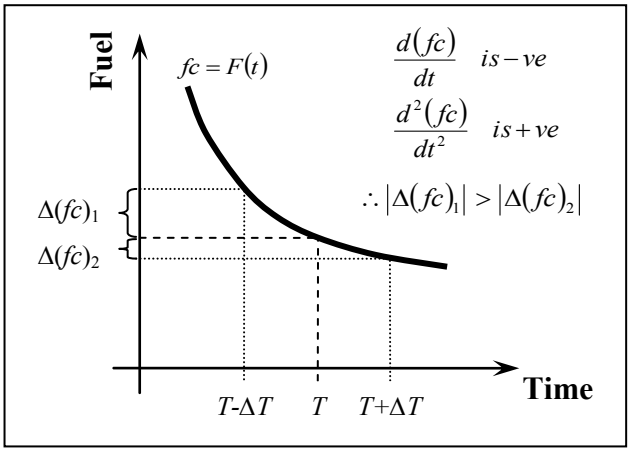


Figure 3-10 – Illustration of the cause of fuel consumption increase when timetable-limited coasting is used to achieve overall journey time

The general shape of *fc*-time curve means that the increase in *fc* for a time reduction, -ΔT, is more than the decrease in *fc* for a time extension, +ΔT. Hence using less coasting in one section of the route and more in another tends to increase the overall *fc* for the same overall journey time. Comparing the results of the uniform coasting analysis with the route timetable shows that shorter inter-station distances have less margin in the schedule and so less coasting can be used. The extra time available for coasting on longer sections makes little difference to the fuel consumption as significant coasting is already being used, and $\Delta(fc)/\Delta T$ is therefore small.

In practice this means that time-table restrictions should be relaxed where possible. This would be advantageous in reducing fuel use and encouraging drivers to take a consistent approach to energy efficient vehicle control. The issue of time-tabling also has a direct impact on the performance of hybrid trains due to the different braking strategies required. This is considered in Section 3.3.3.

3.3. Simple vehicle model of a hybrid regional train

The second section of this analysis focuses on hybrid trains. In this model a generic energy storage module calculates the recovery and reuse of vehicle braking energy. This allows the potential benefits and basic requirements of a hybrid train to be quantified without requiring detailed knowledge of a particular energy storage system (ESS) or hybrid power-train architecture. The performance of the regenerative braking is investigated by limiting the maximum power flow that the ESS can accept during braking; the results presented below show power limits of 0.5 MW , 1 MW and an unlimited case (representing maximum possible energy recovery). Two driving strategies are considered:

i) Coasting strategy with constant force braking (as this was seen to be most effective in reducing fuel use for the conventional vehicle)
ii) Coasting strategy with constant power braking and maximum deceleration limit of 0.5 m/s^2 (to maximise braking energy recovery with power-limited ESS)

The energy storage module uses the recovered vehicle braking to replace energy delivered to the vehicle by the conventional power-train operating at the average efficiency for the journey. This allows the fuel consumption of the hybrid train to be calculated.

3.3.1. Constant force regenerative braking with coasting

The coasting strategy (i) results in fuel consumption values shown in Figures 11a and 12a for the main-line and branch-line routes respectively. These values are calculated for the specified power limitations and assuming an ESS with 100% efficiency, allowing the maximum potential fuel savings to be identified. The energy storage capacity required in both cases is shown in Figures 11b and 12b.

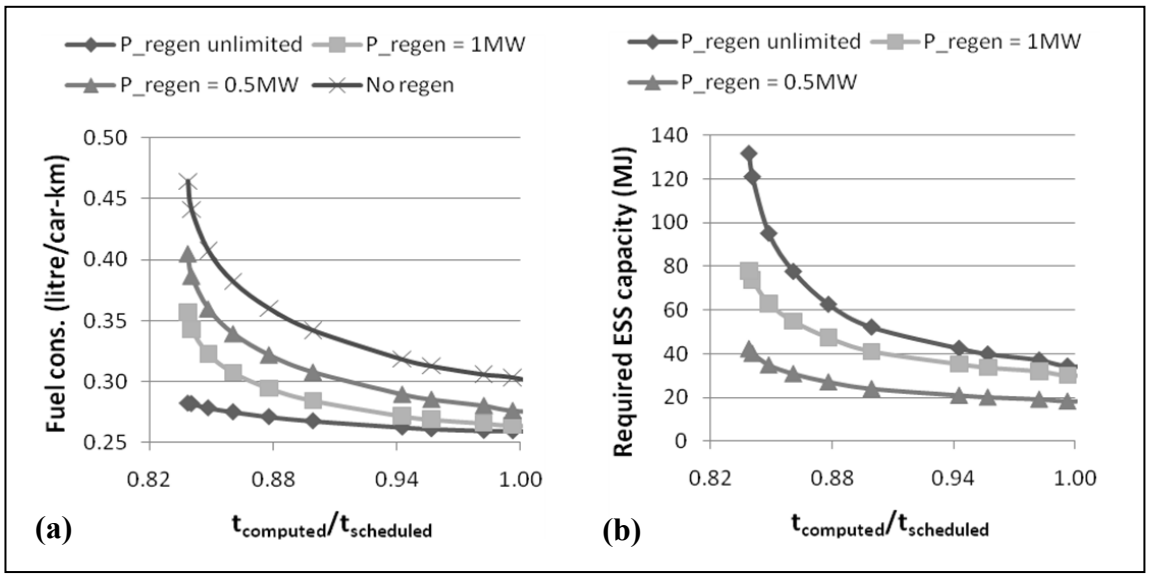


Figure 3-11 – Effect of coasting on main-line hybrid performance with ESS power limitations

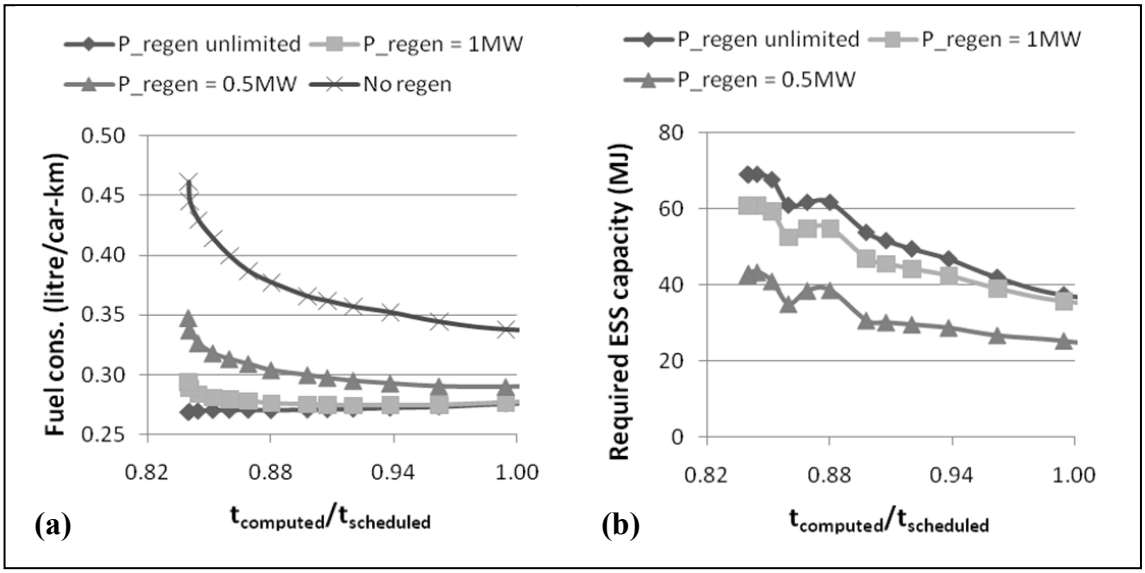


Figure 3-12 – Effect of coasting on branch-line hybrid performance with ESS power limitations

For both the main-line and branch-line routes the fuel consumption of the hybrid train with unlimited ESS power capacity is seen to be approximately constant across the range of coasting conditions. This illustrates the fact that coasting strategies and regenerative braking are alternative methods of utilising the finite kinetic energy of the vehicle prior to braking.

The power limitations of the ESS result in increased fuel consumption. This is most significant for the main-line route where the high vehicle speed leads to high initial braking power, severely limiting the amount of energy recovered.

3.3.2. Constant power regenerative braking with coasting

The outcome of the constant force braking analysis shows there is scope for further benefits if a constant power braking strategy (ii) is used. The trigger speed as a function of distance has been calculated for every station stop and change in line speed by performing back calculations (including the effects of resistance and local gradient) from these points, with the braking force limited by power (1MW has been considered) and a maximum vehicle deceleration of 0.5m/s^2. This braking strategy can again be combined with coasting.

An illustration of the effect of regenerative braking control strategies (i) and (ii) is shown in Figure 3-13 for an ESS power limit of 1MW. The fuel consumption is presented as a percentage saving relative to the conventional vehicle using coasting and constant force braking.

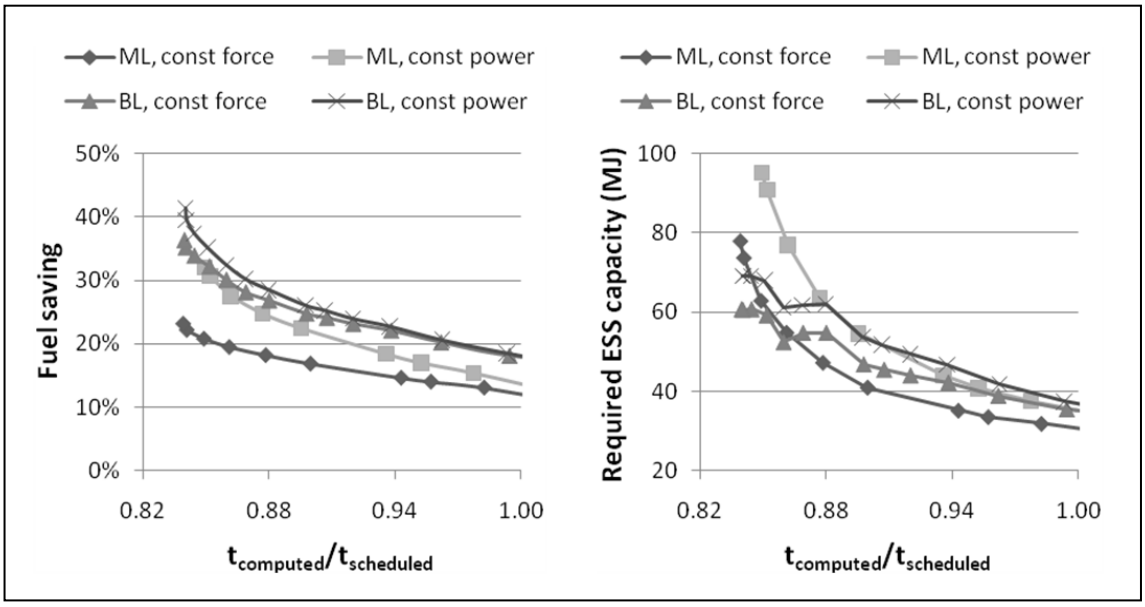


Figure 3-13 – Calculated fuel saving and required energy capacity for hybrid train with 1MW ESS using constant power and constant force braking strategies with various degrees of coasting on main-line (ML) and branch-line (BL) routes

Figure 3-13 shows that the constant power braking strategy increases the fuel saving for the HRDT on both routes. In total the benefit is however much smaller for the branch-line (BL) than the main-line (ML). Although the results have been calculated for an ESS efficiency of 100%, the nature of the analysis method means that the calculated fuel saving relative to the conventional vehicle can be scaled in proportion to the round-trip efficiency of the ESS, which is likely to be in the region of 50-80% for practical regenerative braking systems. In

summary the model shows that under the aggressive driving strategy up to 40% fuel savings are possible for the HRDT with an ideal ESS. However, when efficient driving strategies (i.e. coasting) are used the fuel savings are reduced by half. The model provides a tool for identifying effective control strategies which should be implemented to maximise the benefits of a HRDT. It also allows an assessment of the appropriate power and energy capacity of an ESS in order to minimise the additional cost and weight of a HRDT.

3.3.3. Effect of timetable restrictions on performance of hybrid regional train

The previous analysis of HRDTs assumes that a uniform coasting strategy is applied. It has already been shown in Section 3.2.1 that a timetable-limited coasting strategy significantly increases the fuel consumption for a conventional vehicle due to an increase in braking energy losses. While this means that more energy is available for regeneration, a larger energy storage capacity is required to capture this energy. Furthermore, the uneven nature of the coasting strategy means that available braking energy varies considerably along a route. This is illustrated in Figure 3-14 which shows braking energy available on the approach to each station stop using either uniform or timetable limited coasting with constant force braking.

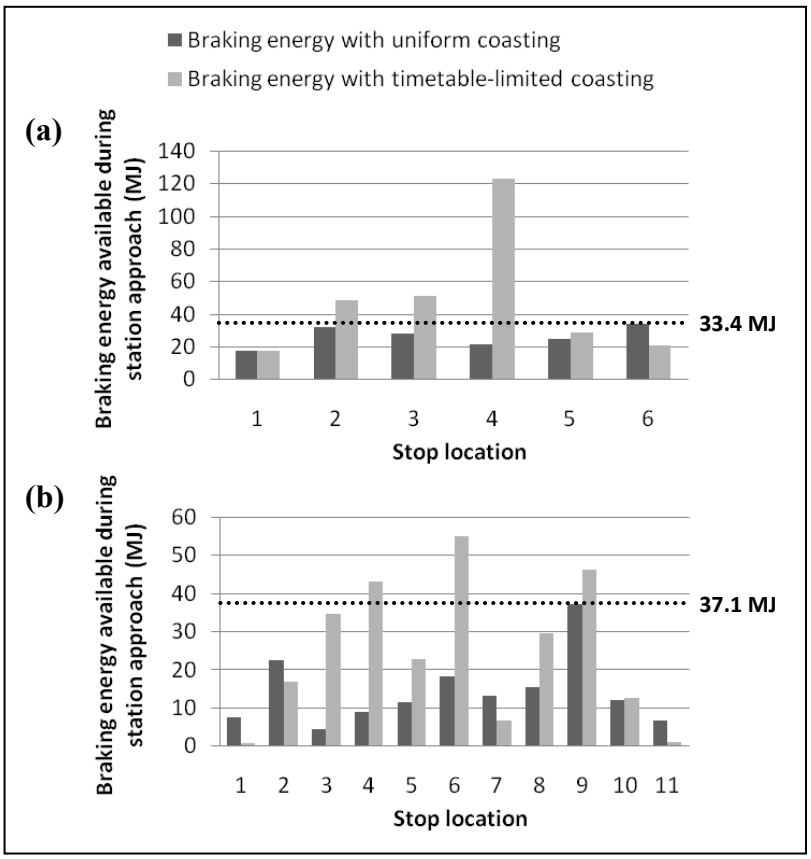


Figure 3-14 – Braking energy available during approach to (a) ML and (b) BL stations using uniform and timetable-limited coasting to achieve overall journey time; dotted lines shows minimum ESS capacity required to capture all available energy with uniform coasting (assuming 100% ESS efficiency)

It is clear from Figure 3-14 that in order to maximise braking energy recovery for the timetable-limited coasting strategy energy storage capacities of 125 and 55 MJ are required for the main-line and branch-line respectively. The effect of timetable-limited coasting on the fuel savings possible for the hybrid vehicle with a range of power capacity limitations is shown in Figure 3-15. The energy capacity is assumed to either be sufficient to store all available braking energy, or limited to the energy storage capacity values identified from the uniform coasting analysis for the main-line and branch-line routes.

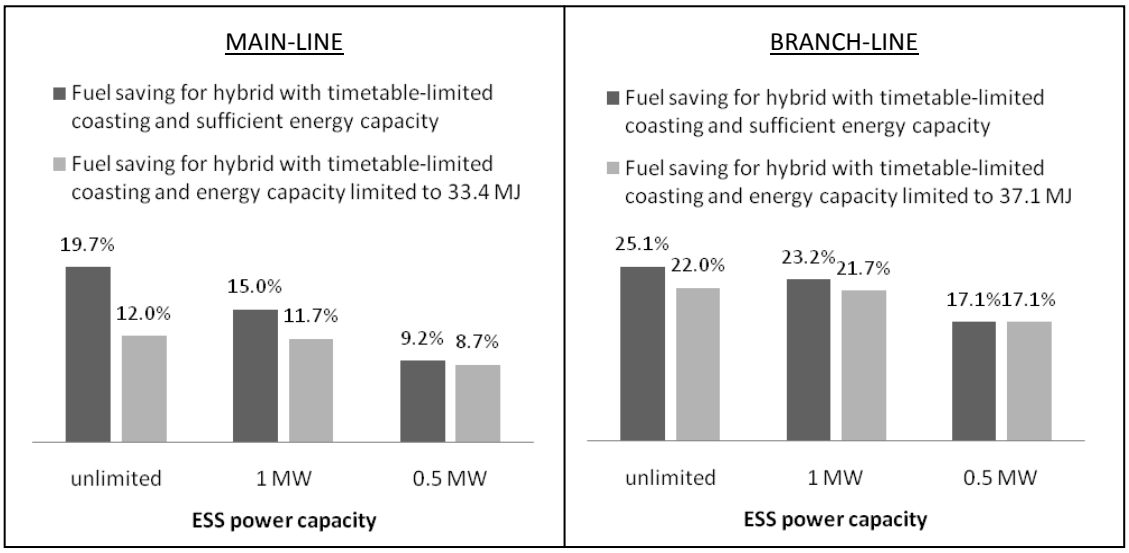


Figure 3-15 – Hybrid fuel savings relative to conventional vehicle using timetable-limited coasting to achieve overall journey time (assuming 100% ESS efficiency)

The values of fuel savings using the stated energy capacity limits and a power limit of 1MW are similar to those obtained for the uniform coasting strategy (see Figure 3-13). However, the timetable-limited coasting strategy causes an increase in the actual fuel consumption of the HRDT as shown in Figure 3-16.

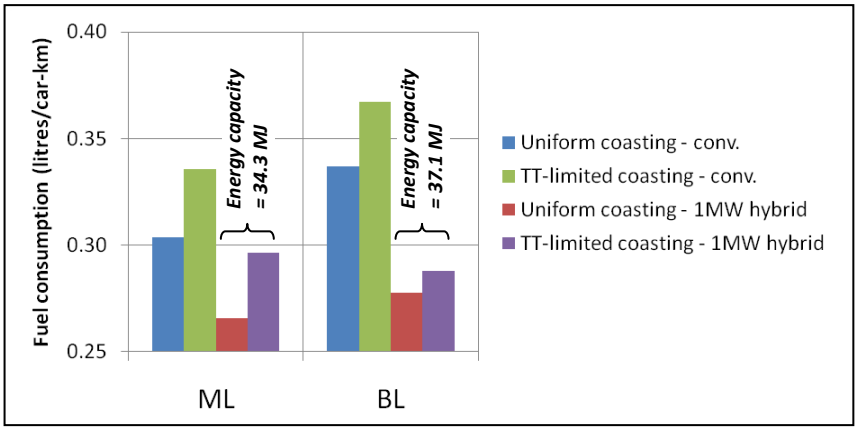


Figure 3-16 – ML and BL fuel consumption for conventional and hybrid vehicles using uniform and timetable (TT) limited coasting strategies (ESS power and energy capacities as stated and assuming 100% efficiency)

These results show that the uniform coasting strategy allows lower fuel consumption to be achieved with a HRDT through better utilisation of the available braking energy. However, significant fuel savings can also be achieved using timetable-limited coasting with practical ESS energy and power limitations.

3.3.4. Requirements for HRDT regenerative braking system

The results presented in this Chapter show that significant fuel savings can be achieved through the use of hybrid systems to enable regenerative braking. When combined with efficient driving strategies an ESS with energy capacity of around 40 MJ and power capacity of 1 MW (i.e. a characteristic discharge time of 40 seconds) has been identified as suitable to achieve high levels of braking energy recovery. As the conventional diesel-hydrodynamic power-train has been shown to operate with good efficiency over a wide range of operating conditions, the hybrid system can be designed as a pure regenerative braking system and used to deliver tractive power during (otherwise inefficient) low vehicle speed operation. The energy and power requirements combined with the short periods of energy storage and the high specific torque possible with mechanical transmissions mean that advanced flywheel systems are highly suited to this application, and are considered in more detail in the following Chapters.

3.4. Summary

In conclusion, there are a number of significant findings relating to both conventional and hybrid driving strategies.

- The most significant finding is that the potential savings for a hybrid regional diesel train (HRDT) using efficient control are around half of that found using an aggressive driving strategy. This saving is significantly lower than predicted by other models but is realistic considering there are a range of driving strategies in use. Fuel savings previously associated with hybrid trains can in fact be achieved through efficient control methods which can be implemented in the short-term at low cost. This must be taken into account when considering the case for implementing hybrid trains in the future.
- Different types of operation will require different amounts of energy storage capacity for the HRDT. This capacity should be tailored to specific routes in order to minimise the additional cost and weight of the hybrid train.

- The constant power braking strategy can increase energy recovery in cases where braking is implemented at high vehicle speed if sufficient storage capacity is available to store the additional energy.
- Of the strategies studied for conventional vehicles, the use of maximum line speed limits with coasting prior to braking can achieve the lowest fuel consumption for a given journey time with fuel savings of up to 36% relative to the worst case driving strategy.
- Advisory maximum speed limits are shown to be an effective means of regulating journey time and fuel consumption for the main-line route.
- Applying coasting to meet the fixed timetable for intermediate stops increases the fuel consumption of conventional vehicles by around 10% compared to a driving strategy where coasting is uniformly applied to achieve the overall journey time. This increases the available braking energy, but regeneration is limited by the HRDT energy and power capacity.

The results of the conventional vehicle model show that under a range of driving conditions significant fuel savings are possible using hybrid vehicles. Driving strategies governed by a simple control algorithm have been shown to achieve low fuel consumption when applied to both conventional and hybrid trains. The required energy capacity of a HRDT has been calculated as a function of the ESS power capacity and the driving strategy used.

It is important to now consider the components, configuration and control strategy of the ESS in order to more accurately assess the design requirements and performance of hybrid trains. For mechanical flywheel systems, a key element of the FESS is the mechanical CVT (continuously variable transmission). It is therefore essential to;

a) understand the interaction between the CVT, flywheel and vehicle
b) specify appropriate gearing ratios for a given CVT configuration
c) identify the power transmission efficiency of a given CVT configuration
d) identify the power and torque requirements of CVT components
e) Identify the most appropriate CVT configuration for a given application

These issues are addressed in Chapters 4 and 5 for FESSs containing CVTs controlled by brake, clutch and variator components.

4. Independent analysis of clutch and brake controlled flywheel transmissions

Advanced flywheel technology has been identified as a candidate for reducing the energy consumption of regional diesel trains. The challenge is to investigate how to use flywheel devices in a practical regenerative braking system to achieve energy efficiency. A key element is to explore the compromise between reducing vehicle fuel consumption and increasing the weight of the vehicle. This Chapter therefore aims to address mechanical flywheel transmission design and performance using planetary gearing controlled by brake or clutch components. The transmissions considered are similar to power-shift automatic transmissions widely used in automotive ICE (internal combustion engine) power-trains, but the requirements are different for flywheel applications. The transmission design is determined by the need to optimise system performance, as discussed below for the two cases;

i) ICE transmissions (current application)

An ICE is able to generate torque over a well defined range of speeds, with the transmission gearing ratios specified on the basis of overall fuel-efficiency (as the gear ratios affect the engine operating conditions) and driveability. The engine is connected to the vehicle through a fixed gear ratio for a large proportion of the time, while power-shifting is used intermittently to provide smooth gear changes. This means that the ICE actively controls the operating point of the transmission.

ii) Flywheel energy storage (proposed application)

In contrast, flywheels are passive devices which can only be charged and discharged when an appropriate torque is applied by the transmission. This can be achieved using fixed ratio gearing designed to operate with a continuous state of power-shift. The gearing ratios for this application are specified on the basis of maximising the useful energy storage capacity per unit mass of the FESS (flywheel energy storage system).

Previous approaches to analysing FESSs have focussed on detailed modelling of individual vehicles, drive cycles and systems [105-107, 109] in order to reduce fuel consumption for a particular ‘case study’. This approach has a number of drawbacks. Firstly, it results in a specific system being defined by a large number of parameters, making the optimisation

process computationally intensive and applicable only to the particular case considered. This tends to obscure the fundamental relationships between the key FESS design parameters and the system operating characteristics, making a general comparison of systems difficult. Secondly, an emphasis on minimising fuel consumption can fail to consider important system design compromises relating to the mass, cost and efficiency of components and the complexity of the transmission. In order to overcome these issues and assess the potential of a number of mechanical transmission configurations operating over a wide range of conditions a new design tool has been created. This design tool consists of normalised datasets that characterise the performance and design requirements of each transmission configuration. They are derived from analytical relationships between the key system parameters. By specifying the vehicle parameters and the required energy storage capacity for a given application, the design tool allows an initial estimate of the optimum gearing ratios required to achieve maximum specific energy for the FESS. This provides an absolute basis for the comparison of a range of mechanical transmissions, and a strong starting point for more detailed computational analysis of specific FESS applications.

The elements of the transmissions considered in this Chapter are all widely used in standard vehicle power-trains, and the systems presented therefore represent a practical, low-cost means of implementing efficient flywheel energy storage. The outcome of this analysis suggests high performance can be achieved using a simple and compact transmission consisting of a number of PGSs and a small counter-shaft control gearbox (CGB). These systems have the advantage of high specific energy when compared with published data for electrical flywheel systems.

4.1. Brake-controlled flywheel transmissions

This section analyses simple brake-controlled transmissions consisting of planetary gearing. In its simplest form, the transmission consists of a single PGS as shown in Figure 4-1(a). This system has been proposed by Diego-Ayala et al. [106] but for a specific automotive application which has very different energy and torque requirements than a rail vehicle. The system is controlled by applying a braking torque to the ‘control’ branch of the PGS (in this case the ring), which exerts opposite torques on the vehicle and flywheel. This allows the flywheel to be discharged, with a proportion of the energy being transferred to the vehicle while the remainder is dissipated due to friction at the control brake. This results in a fundamental limit on the overall efficiency of the transmission.

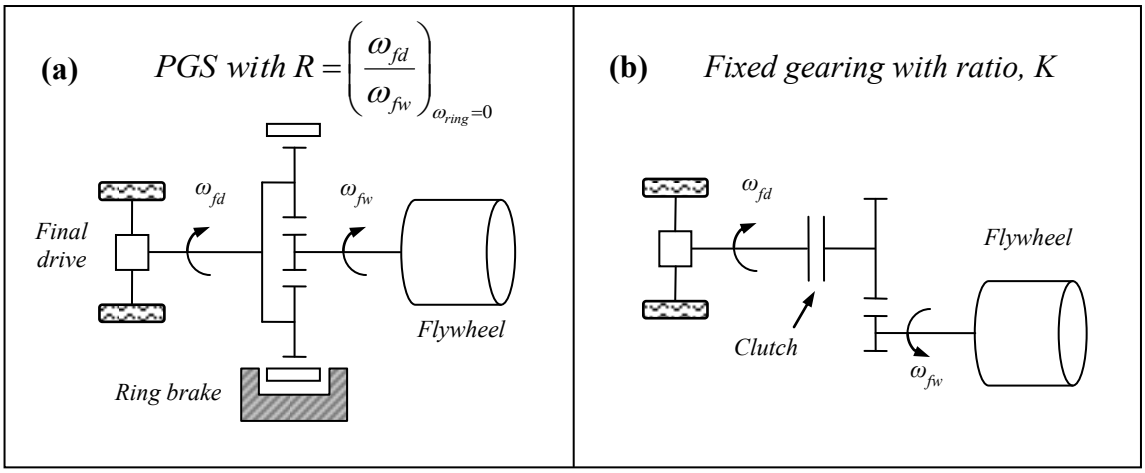


Figure 4-1 – Examples of (a) brake and (b) clutch controlled flywheel transmissions

An analysis of the systems illustrated in Figure 4-1(a) and 4-1(b) shows that they are equivalent when the gear ratios K and R are equal. When multiple gear ratios are used in either configuration the performance of the transmissions can be improved by reducing the total energy dissipated at the brake or clutch. Both types of transmission are attractive because of the mechanical simplicity and ease of control. PGSs are however preferred for the flywheel transmission, as they have the following advantages;

- They can achieve high gear ratios which are required when using high speed flywheels,
- A large range of gear ratios can be achieved using single and multiple stage PGSs,
- They can provide high torque capacity per unit mass due to load sharing in the multiple planet gears,
- It is easier to manage the cooling and maintenance of PGS brake components than clutches.

While the brake-controlled PGS transmission has been studied in its simplest form (using a single PGS), in this investigation a comprehensive analysis of multi-PGS brake-controlled transmissions has been performed in order to identify the requirements for optimum FESS performance, and to quantify the benefits of using multiple PGSs. It is found that the transmission parameters can be chosen to achieve optimum system performance within practical limitations (here considered in terms of system mass and energy available for recovery during braking). The analysis method below has been developed to provide these results in a generalised form which is independent of the application itself. The normalised

transmission parameters and associated performance provide a solid basis for comparing a range of mechanical transmission systems and allows the identification of appropriate gearing ratios for any vehicle application. The analysis of PGS brake-controlled transmissions is described in the following sections.

4.1.1. Connection options for differential gearing

Using the general approach to analysing differential gearing described by White [94] eliminates the need to specify the type of differential gearing used and the way it is connected to the vehicle and flywheel. The differential is simply considered to have three branches and a characteristic gear ratio, *R*, as defined in Chapter 2. The kinematic and ideal torque relationships for the generic differential are restated in Equation 4-1 and 4-2 respectively.

$$\omega_3 = (1-R)\omega_2 + R\omega_1 \tag{4-1}$$

$$T_3 = -\left(\frac{1}{1-R}\right)T_2 = -\frac{1}{R}T_1 \tag{4-2}$$

These equations apply to any type of PGS in any transmission configuration. A general analysis (using Equations 4-1 and 4-2) can be performed to identify an appropriate value of *R* for a given application, allowing the most appropriate PGS configuration to be deduced. In the case of a flywheel transmission this will depend upon the characteristics of both the vehicle and the flywheel unit. The results of a general analysis can therefore provide a design tool that illustrates the effect of these factors on the performance and the design requirements of various flywheel transmission configurations.

4.1.2. Approach to independent analysis of PGS transmissions

To generate this new design tool, the following analysis method is applied. The operation of a differential gearing unit is described by the kinematic relationship (Equation 4-1) and the ideal torque relationship (Equation 4-2). The effect of PGS gearing losses can be included in the analysis by using a simple assumption of constant transmission efficiency, η_{pgs}. The ideal torque equations can then be modified (depending on the direction of power flow in the three branches) to take these losses into account. The torque equations can therefore be defined as in Table 4-1 for all 6 possible cases of PGS power-flow (a-f).

Power-flow case	P_1	P_2	P_3	T_1 / T_2	T_3 / T_2
a	+	−	−	$\frac{1}{\eta_{pgs}}\left(\frac{R}{1-R}\right)$	$-\left(\frac{1}{1-R}\right)$
b	−	+	−	$\eta_{pgs}\left(\frac{R}{1-R}\right)$	$-\eta_{pgs}\left(\frac{1}{1-R}\right)$
c	+	−	+	$\frac{1}{\eta_{pgs}}\left(\frac{R}{1-R}\right)$	$-\frac{1}{\eta_{pgs}}\left(\frac{1}{1-R}\right)$
d	−	+	+	$\eta_{pgs}\left(\frac{R}{1-R}\right)$	$-\left(\frac{1}{1-R}\right)$
e	−	−	+	$\left(\frac{R}{1-R}\right)$	$-\frac{1}{\eta_{pgs}}\left(\frac{1}{1-R}\right)$
f	+	+	−	$\left(\frac{R}{1-R}\right)$	$-\eta_{pgs}\left(\frac{1}{1-R}\right)$

Table 4-1 – Direction of power flow in PGS branches (+ve in, -ve out) and associated torque equations including the effect of constant PGS transmission losses for all possible cases

In the ring-brake transmission illustrated in Figure 4-1(a) the sun gear can be defined as corresponding to branch 1 and the carrier to branch 3 of a generic differential. As power is always flowing out of the PGS at the ring (branch 2) and is dissipated in the brake, flywheel charging and discharging with this type of transmission therefore corresponds to power-flow cases (*e*) and (*a*) in Table 4-1 respectively. The kinematic and torque equations for the PGS are then identical to the specific case described by Diego-Ayala et al. [106] where the ratio of the PGS is defined in terms of the particular configuration and the number of teeth in the ring and sun gears. The general form of these equations are however used in all subsequent analysis due to the ability to identify both the most appropriate type of differential and how the branches should be connected to the vehicle and flywheel for a given application.

As the aim of this Chapter is to develop a generic design tool which is independent of the vehicle characteristics and drive cycle, the effects of dissipative losses at the vehicle (due to rolling and aerodynamic resistance) and flywheel (due to self-discharge) are disregarded. These assumptions can be justified as follows;

i. The maximum tractive effort is much greater than the force due to resistance at low vehicle speeds ($\max(T_{trac}) >> T_{veh\ res}$)

ii. Advanced flywheel self-discharge losses of 2-4% per minute are reported in the literature [109]. As typical acceleration and braking events will be of the order of 1

minute, this resistance torque is much lower than the maximum torque exerted on the flywheel by the transmission (max(T_{fw}) >> $T_{fw\ losses}$)

The effect of these assumptions will be assessed in Chapter 6. The simplification is however extremely useful, as by disregarding the losses at the vehicle and flywheel, the analysis corresponds to the case when vehicle and flywheel acceleration are infinite. The results are therefore independent of time, and so do not depend on any particular drive-cycle. With no vehicle or flywheel losses, the following equations apply at the input and output of the transmission (where the '*fd*' subscript refers to the conditions on the transmission side of the final drive gearing):

$$T_{fd} = J_{fd} \frac{d\omega_{fd}}{dt} \tag{4-3}$$

$$T_{fw} = J_{fw} \frac{d\omega_{fw}}{dt} \tag{4-4}$$

In Equation 4-4, J_{fw} and ω_{fw} represent the output inertia and speed of a flywheel unit, which can include a fixed gear ratio between the high speed rotor and the output as shown below in Figure 4-2;

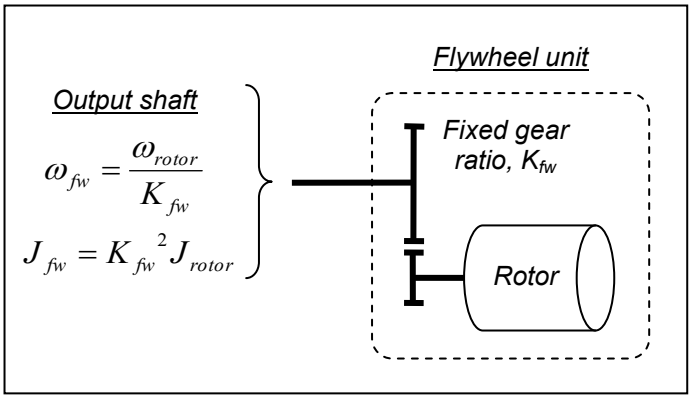


Figure 4-2 – Definition of relationship between the flywheel rotor and the output characteristics of the flywheel unit

Defining the flywheel in this way provides freedom to specify practical values for the PGS(s) and identify the required value of K_{fw} for a given maximum rotor speed and kinetic energy capacity.

Differentiating the PGS kinematic relationship (Equation 4-1) with respect to time results in;

$$\frac{d\omega_3}{dt} = (1-R)\frac{d\omega_2}{dt} + R\frac{d\omega_1}{dt} \tag{4-5}$$

For a specific transmission configuration we can now investigate the operation by combining Equations 4-1 and 4-3 to 4-5 with the appropriate torque relationships defined in Table 4-1. This approach is defined here as the Independent Analysis Method (IAM), and allows analytical expressions to be obtained which define the operation of the transmission. The effect of flywheel energy capacity, flywheel *DOD* (depth-of-discharge) and gear ratios on the transmission efficiency and system mass can be quantified, providing a fundamental basis for understanding and comparing the performance of different transmission configurations.

This approach allows exact analytical expressions to be derived to describe the performance of a brake-controlled transmission with *m* PGSs in terms of the following key system parameters;

i. The PGS characteristic gear ratios R_n (where n = 1, 2, ..., m)
ii. The estimated constant efficiency of each PGS
iii. The ratio of equivalent inertias at the transmission output (final drive) to input (flywheel unit)
iv. The ratio of the maximum to minimum transmission input (flywheel unit) speeds for a full discharge event as defined by the overall depth of discharge (DOD_{ov}) where;

$$DOD_{ov} = \frac{\Delta KE_{fw}}{\max(KE_{fw})} = 1 - \left(\frac{\omega_{fw,\min}}{\omega_{fw,\max}}\right)^2 \tag{4-6}$$

The performance of specific mechanical flywheel systems is considered in the following sections.

4.1.3. Analysis of multi-PGS brake-controlled transmission

The Transmission Configuration

Figure 4-3 illustrates the layout of a generic brake-controlled flywheel transmission using multiple PGSs. Sequential braking of branch 2 of each PGS allows a number of phases of transmission operation to be achieved; by increasing the number of PGSs (and therefore the number of operating phases) the total amount of energy dissipated in the brakes can be reduced for a given flywheel DOD_{ov}.

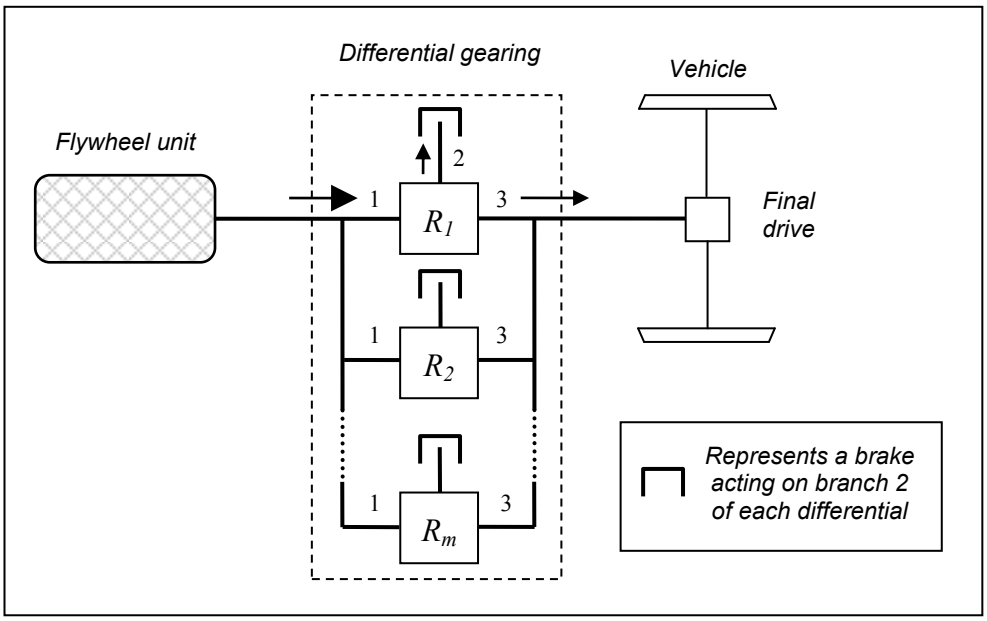


Figure 4-3 – Schematic diagram of brake-controlled flywheel transmission with *m* differentials (arrows show the direction of power flow during flywheel discharge using PGS 1)

Example of Transmission Operation

The operation of a brake-controlled transmission can be understood by considering a specific configuration. Figure 4-4 is a schematic illustration of a possible 2-PGS ring-brake transmission, while Figure 4-5 shows the operation of this system during a full flywheel discharge/charge cycle.

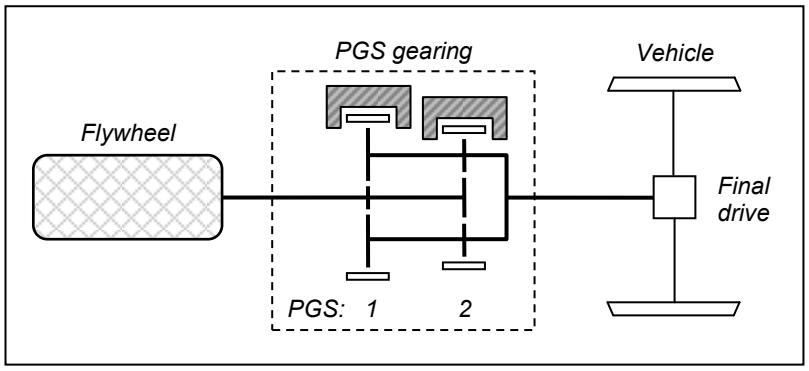


Figure 4-4 – Example of a possible configuration for 2-PGS ring-brake controlled transmission (note: $0 < R_1 < R_2 < 0.5$ in this configuration)

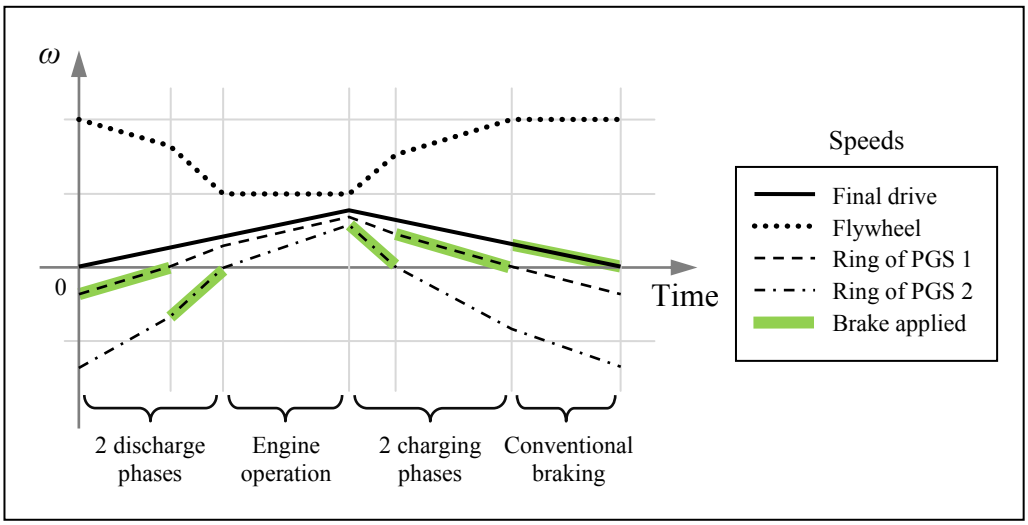


Figure 4-5 – Illustration of simple flywheel discharge/charge cycle with a 2-PGS ring-brake transmission, constant T_{fd} and DOD_{ov} = 75%

During flywheel powered vehicle acceleration, braking is applied at the ring rotating with negative speed of the smallest (non-zero) magnitude. Once all ring speeds are positive or zero the transmission can no longer discharge the flywheel and the conventional power-train must be used to continue accelerating to the vehicle. Regenerative braking is achieved by applying a braking torque to the ring rotating with the smallest positive (non-zero) speed. Once all the ring speeds are zero or negative conventional braking must be applied to bring the vehicle to a stop. The analysis of the system during both charging and discharging of the flywheel using the generic PGS equations follows.

Independent Analysis of Transmission Operation

By considering the balance of energy during each phase of transmission operation we can investigate the overall performance of the brake-controlled system. The generalised analysis procedure described earlier is therefore applied to each phase of a multi-PGS brake-controlled transmission with the appropriate initial conditions. The general expressions defining the operation of the transmission are as follows.

If the transmission consists of *m* PGSs, the ratio of output to input torque during brake-control of the *n*'th PGS is as follows;

$$\frac{T_{fd}}{T_{fw}} = \frac{T_{3,n}}{T_{1,n}} \tag{4-7}$$

Substituting Equations 4-3 and 4-4 into Equation 4-5 obtains;

$$\frac{d\omega_{2,n}}{dt} = \left(\frac{1}{1-R_n}\right)\frac{T_{3,n}}{J_{fd}} - \left(\frac{R_n}{1-R_n}\right)\frac{T_{1,n}}{J_{fw}} \tag{4-8}$$

The efficiency of the brake-controlled transmission is related to the total amount of energy dissipated in the brakes located on branch 2 of the m PGSs, $\Delta E_{2,\,tot}$. The total energy dissipated in the n'th transmission phase, $\Delta E_{2,n}$, is shown in Equation 4-9 where;

- t_i is the initial time at which $\omega_{2,n} = \omega_{2,i}$ (with $\omega_{2,(n+1)} = 0$ during charging and $\omega_{2,(n-1)} = 0$ during discharging)
- t_f is the final time at which $\omega_{2,n} = 0$

$$\Delta E_{2,n} = \int_{t_i}^{t_f} \left(\omega_{2,n} T_{2,n}\right) dt \tag{4-9}$$

Substituting Equation 4-8 into 4-9 allows the integration to be expressed w.r.t. the rotational speed of branch 2 of the n'th PGS, $\omega_{2,n}$, as shown in Equation 4-10.

$$\Delta E_{2,n} = \int_{\omega_{2,i}}^{0} \left(\omega_{2,n} T_{2,n}\right)\left(\frac{(1-R_n) J_{fd} J_{fw}}{\left(J_{fw} T_{3,n} - R_n J_{fd} T_{1,n}\right)}\right) d\omega_{2,n} \tag{4-10}$$

Equations 4-7 and 4-10 can be derived for the two cases of flywheel charging and discharging by using the appropriate torque ratios defined in Table 4-2. These results are shown in Table 4-3 below.

	Flywheel discharge	Flywheel charging
$\frac{T_{fd}}{T_{fw}} =$	$-\frac{\eta_{pgs,n}}{R_n}$	$-\frac{1}{\eta_{pgs,n} R_n}$
$\Delta E_{2,n} =$	$\frac{\eta_{pgs,n} J_{fw} J_{fd} (R_n - 1)^2}{2\left(\eta_{pgs,n} J_{fw} + R_n{}^2 J_{fd}\right)} (\omega_{2,i})^2$	$\frac{\eta_{pgs,n} J_{fw} J_{fd} (R_n - 1)^2}{2\left(J_{fw} + \eta_{pgs,n} R_n{}^2 J_{fd}\right)} (\omega_{2,i})^2$

Table 4-2 – Torque and energy dissipation relationships for a phase of operation using brake-controlled transmission

The expressions for $\Delta E_{2,n}$ are for a single phase of operation. The overall performance of the transmission can therefore be assessed by considering the total energy dissipated during flywheel charging or discharging, where;

$$\Delta E_{2,tot} = \sum_{n=1}^{m} \left(\Delta E_{2,n} \right) \tag{4-11}$$

These results make it clear that by assuming no losses at the flywheel or vehicle, the amount of energy dissipated at the ring is independent of the torque applied at the ring as a function of time, and depends only on the initial rotational speed of branch 2 in each phase of operation. This expression for the energy dissipated at branch 2 can be substituted into the overall energy balance for the *n*'th PGS during flywheel *discharge* (Equation 4-12) to obtain Equation 4-13.

$$\eta_{pgs,n} \Delta E_{1,n} = \Delta E_{3,n} + \Delta E_{2,n} \tag{4-12}$$

$$\eta_{pgs,n} \frac{1}{2} J_{fw} \left({\omega_{1,i}}^2 - {\omega_{1,f}}^2 \right) = \frac{1}{2} J_{fd} \left({\omega_{3,f}}^2 - {\omega_{3,i}}^2 \right) + \frac{\eta_{pgs,n} J_{fw} J_{fd} \left(R_n - 1 \right)^2}{2\left(\eta_{pgs,n} J_{fw} + {R_n}^2 J_{fd} \right)} \left(\omega_{2,i} \right)^2 \tag{4-13}$$

The following relationships apply for the initial and final speeds in the *n*'th transmission phase. The initial speeds of branches 1 and 3 corresponds to the final operating point of the *(n-1)*'th transmission phase. As the final speed of branch 2 of the *n*'th PGS is zero;

$$\omega_{3,i} = R_{n-1} \omega_{1,i} \tag{4-14}$$

$$\omega_{3,f} = R_n \omega_{1,f} \tag{4-15}$$

The initial speed of branch 2 can be defined in terms of the initial speeds of branches 1 and 3 according to Equation 4-1;

$$\omega_{2,i} = \left(\frac{1}{1 - R_n} \right) \omega_{3,i} - \left(\frac{R_n}{1 - R_n} \right) \omega_{1,i} = \left(\frac{1}{1 - R_n} \right) \left(R_{n-1} - R_n \right) \omega_{1,i} \tag{4-16}$$

Substituting Equations 4-14 to 4-16 into Equation 4-13 results in the following expression for the ratio of initial to final flywheel speeds during the n'th phase of flywheel discharge.

$$\left(\frac{\omega_{1,i}}{\omega_{1,f}} \right)_n = \frac{\left({R_n}^2 + \eta_{pgs,n} \dfrac{J_{fw}}{J_{fd}} \right)}{\left(R_n R_{n-1} + \eta_{pgs,n} \dfrac{J_{fw}}{J_{fd}} \right)} \tag{4-17}$$

Equation 4-17 shows that the ratio of initial to final flywheel speeds is a function of the PGS ratios, the 'inertia ratio' (defined here as J_{fd}/J_{fw}) and the efficiency of the PGS. Furthermore, a normalised PGS ratio, *R**, can be defined such that;

$$R_n^* = R_n \sqrt{\frac{J_{fd}}{J_{fw}}} \tag{4-18}$$

The performance of the transmission is then completely defined by the m values of R^* and η_{pgs}. Substituting Equation 4-18 into 4-17, the characteristic equation describing a phase of brake-controlled flywheel discharge is obtained;

Characteristic equation for the n'th phase of brake-controlled flywheel *discharge*

$$\left(\frac{\omega_{1,i}}{\omega_{1,f}}\right)_n = \frac{\left((R_n^*)^2 + \eta_{pgs,n}\right)}{\left((R_n^*)(R_{n-1}^*) + \eta_{pgs,n}\right)} \tag{4-19}$$

This analysis can be repeated for the case of flywheel charging, and a similar expression can be derived as shown in Equation 4-20.

Characteristic equation for the n'th phase of brake-controlled flywheel *charging*

$$\left(\frac{\omega_{1,i}}{\omega_{1,f}}\right)_n = \frac{\left(\eta_{pgs,n}(R_n^*)^2 + 1\right)}{\left(\eta_{pgs,n}(R_n^*)(R_{n+1}^*) + 1\right)} \tag{4-20}$$

For vehicle acceleration (flywheel discharge) from stationary, the initial vehicle speed in the first transmission phase (i.e. braking branch 2 of PGS 1) is zero, and so the value of R_0^* required in Equation 4-19 is zero (from Equation 4-15). For vehicle braking (flywheel charging) using the m'th PGS, the initial vehicle and flywheel speeds can be used to calculate a hypothetical value, R_h^*, for R_{m+1}^* (equal to $\omega_{3,i} / \omega_{1,i}$) which allows the final speeds of the vehicle and flywheel to be calculated for the phase of operation.

These two characteristic equations therefore completely define the operation of the brake-controlled flywheel transmission, and allow a thorough investigation of the effect of gearing ratios, PGS efficiency and inertia ratio on system performance. Expressions for the overall charging and discharging efficiencies can be derived as follows;

Overall brake-controlled transmission *discharge* efficiency

$$\eta_{discharge} = \frac{\Delta KE_{veh}}{\Delta KE_{fw}} = \frac{J_{fd}\left(\omega_{3\max}^{\ 2}\right)}{J_{fw}\left(\omega_{1\max}^{\ 2} - \omega_{1\min}^{\ 2}\right)} = \frac{(R_m^*)^2}{\left(\left(\frac{\omega_{1\max}}{\omega_{1\min}}\right)^2 - 1\right)} \tag{4-21}$$

Overall brake-controlled transmission *charging* efficiency

$$\eta_{charge} = \frac{\Delta KE_{fw}}{\Delta KE_{veh}} = \frac{J_{fw}\left(\omega_{1\max}{}^2 - \omega_{1\min}{}^2\right)}{J_{fd}\left(\omega_{3\max}{}^2\right)} = \frac{\left(\left(\frac{\omega_{1\max}}{\omega_{1\min}}\right)^2 - 1\right)}{\left(R_h{}^*\right)^2} \tag{4-22}$$

Equations 4-19 to 4-22 are key results, as they show that analytical expressions can be derived defining the normalised PGS ratios and the overall efficiency as functions of the *m* values of DOD_n. This allows the exact calculation of transmission performance which is independent of the application (defined by the actual vehicle and flywheel inertias), and provides a basis for the direct comparison of different transmission configurations. The results of this analysis follow for the two distinct cases of single and multiple PGS transmissions.

4.1.4. Results for single PGS brake-controlled flywheel transmission

The characteristic equations for flywheel discharging and charging (Equations 4-19 and 4-20 respectively) can now be applied to the case of a brake-controlled transmission consisting of a single PGS with gearing ratio *R*. This allows analytical expressions to be obtained for four key results;

i. A normalised gear ratio, *R**
ii. The transmission charge, discharge and round-trip efficiencies
iii. A flywheel utilisation factor, *U*
iv. A normalised energy dissipation at the control brake

These four areas are discussed below. A design method using these results is then described, which provides a means of identifying appropriate FESS design parameters for any application.

i) Normalised PGS gear ratio

From the characteristic discharge equation (Equation 4-19), it is clear that the normalised PGS gearing ratio, *R**, is defined as a function of the PGS efficiency, η_{pgs}, and the ratio of maximum to minimum flywheel speeds (a monotonic function of DOD_{ov}), as shown in Equation 4-23.

$$R^* = \sqrt{\eta_{pgs}\left(\frac{\omega_{1\max}}{\omega_{1\min}} - 1\right)} \tag{4-23}$$

It is clear from this result that the value of $R^*/\sqrt{\eta_{pgs}}$ is purely a function of DOD_{ov}. Figure 4-6 illustrates this relationship.

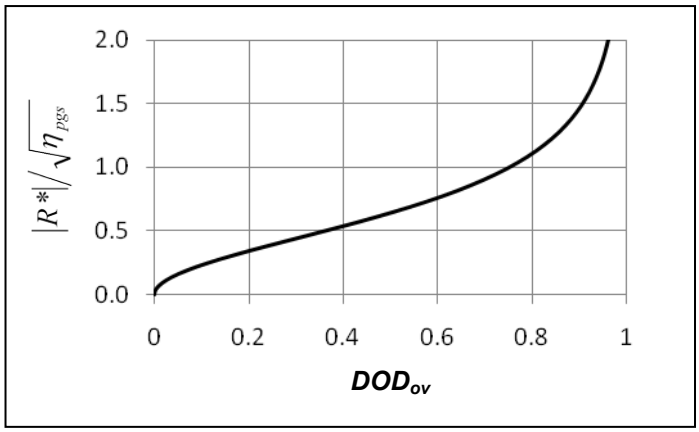


Figure 4-6 – Value of $|R^*|/\sqrt{\eta_{pgs}}$ as a function of DOD_{ov} for a single PGS brake-controlled transmission

Substituting the expression for R^* (Equation 4-23) into the characteristic equation for flywheel charging (Equation 4-20) allows an expression to be derived for the normalised hypothetical PGS ratio, R_h^*, which defines the initial braking conditions required to fully recharge the flywheel from minimum to maximum speed.

$$R_h^* = \left(\frac{\omega_{1\max}}{\omega_{1\min}} + \frac{1}{\eta_{pgs}^{\,2}}\right)\sqrt{\eta_{pgs}\left(\frac{\omega_{1\max}}{\omega_{1\min}} - 1\right)} \tag{4-24}$$

This expression for R_h^* allows the performance of the system to be assessed for a full flywheel recharge event.

ii) Transmission efficiencies

Equations 4-23 and 4-24 can now be substituted into the expressions for discharge and charge efficiency (Equations 4-21 and 4-22) respectively, resulting in Equations 4-25 and 4-26;

$$\eta_{discharge} = \frac{(R*)^2}{\left(\left(\frac{\omega_{1\max}}{\omega_{1\min}}\right)^2 - 1\right)} = \frac{\eta_{pgs}}{\left(\frac{\omega_{fw,\max}}{\omega_{fw,\min}} + 1\right)} \tag{4-25}$$

$$\eta_{charge} = \frac{\left(\left(\frac{\omega_{1\max}}{\omega_{1\min}}\right)^2 - 1\right)}{(R_h*)^2} = \frac{\left(\frac{\omega_{fw,\max}}{\omega_{fw,\min}} + 1\right)}{\eta_{pgs}\left(\frac{\omega_{fw,\max}}{\omega_{fw,\min}} + \frac{1}{\eta_{pgs}^2}\right)^2} \tag{4-26}$$

These discharge and charge efficiencies are illustrated in Figure 4-7 as functions of DOD_{ov} and constant PGS efficiency, η_{pgs}.

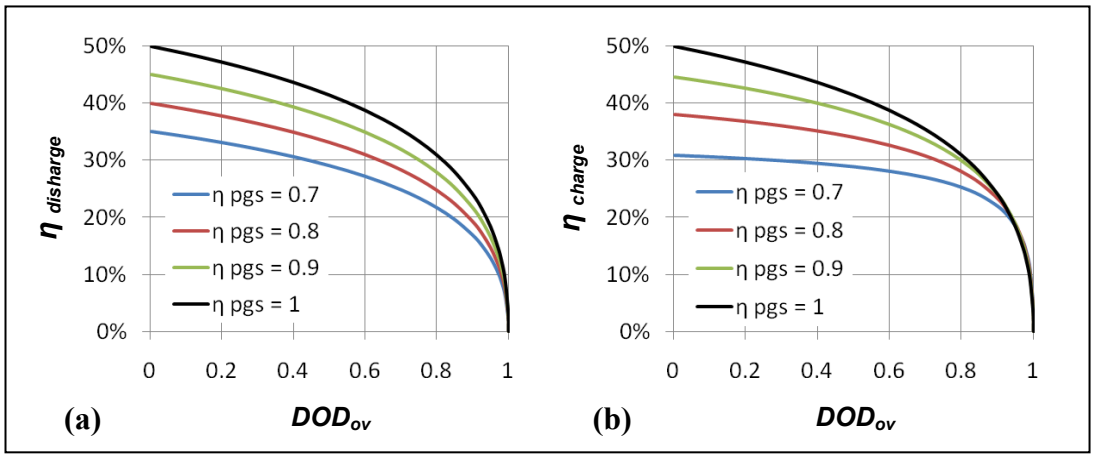


Figure 4-7 – (a) discharge and (b) charging efficiency as a function of η_{pgs} and DOD_{ov} for a 1-PGS brake-controlled transmission

The product of the overall charging and discharging efficiencies is defined as the round-trip efficiency, and is illustrated in Figure 4-8.

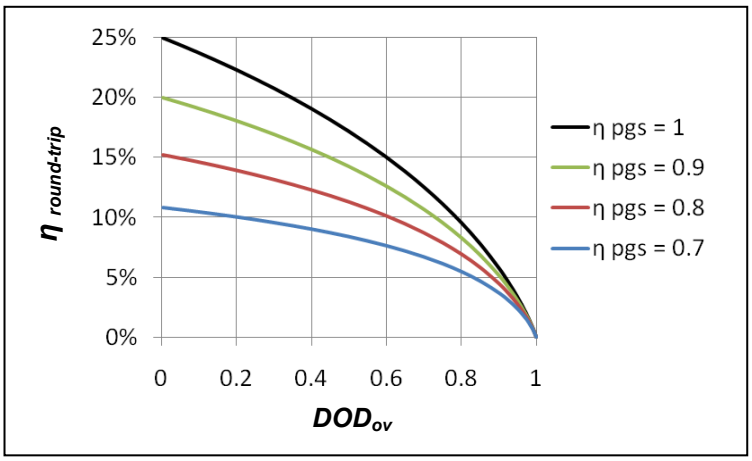


Figure 4-8 – Round-trip efficiency of the 1-PGS brake-controlled transmission as a function of η_{pgs} and DOD_{ov}

iii) Flywheel utilisation factor

It is apparent from these results that when choosing the PGS gear ratio there is a compromise between achieving a high transmission efficiency or a high DOD_{ov}. This is an important consideration as it will affect the useful energy that can be delivered to the vehicle per unit mass of the system, defined here as the specific energy capacity. A flywheel utilisation factor has therefore been defined as the proportion of the kinetic energy of the fully charged flywheel that can be delivered to the vehicle during a flywheel discharge event, as shown in Equation 4-27.

$$U = \frac{\left(\Delta KE_{veh}\right)_{discharge}}{\max\left(KE_{fw}\right)} = DOD_{ov}\frac{\left(\Delta KE_{veh}\right)_{discharge}}{\Delta KE_{fw}} = DOD_{ov} \times \eta_{discharge} \tag{4-27}$$

The value of U/η_{pgs} is therefore only a function of DOD_{ov} as shown in Figure 4-9.

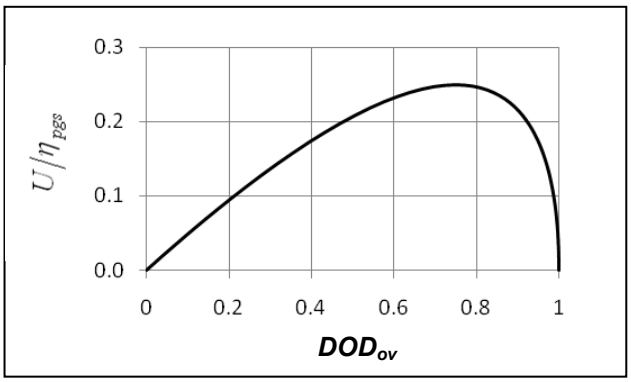


Figure 4-9 – The value of U/η_{pgs} as a function of DOD_{ov} for the 1-PGS brake-controlled transmission

The maximum flywheel utilisation is $U = 0.25\eta_{pgs}$ and occurs when $DOD_{ov} = 0.75$ and $R^* = \sqrt{\eta_{pgs}}$. For a known inertia ratio and PGS efficiency, the value of R required to achieve maximum U can be found. Operating with maximum U minimises the mass of the flywheel required for a particular useful energy capacity of the system. The requirements of the brake components in the transmission will however affect the total transmission mass, and depend on the amount of energy being dissipated in branch 2 of the differential, as discussed below.

iv) Normalised energy dissipation at control brake

The energy dissipated in the control brake can be evaluated by substituting the expressions for R^* and R_h^* (Equations 4-23 and 4-24) into the expressions for ΔE_2 during charge and discharge as defined in Table 4-2. Normalised values of energy dissipation at branch 2 of the differential, ΔE_2^*, can be defined by dividing ΔE_2 by the maximum kinetic energy of the flywheel, as shown below.

$$\left(\Delta E_2^*\right)_{discharge} = \frac{\Delta E_{2,discharge}}{\max\left(KE_{fw}\right)} = \eta_{pgs}\left(1 - \frac{\omega_{1\min}}{\omega_{1\max}}\right) \tag{4-28}$$

$$\left(\Delta E_2^*\right)_{charge} = \frac{\Delta E_{2,charge}}{\max\left(KE_{fw}\right)} = \frac{\eta_{pgs}^{\,2}\left(1 - \frac{\omega_{1\min}}{\omega_{1\max}}\right)\left(1 + \frac{\omega_{1\min}}{\omega_{1\max}}\left(\frac{1}{\eta_{pgs}^{\,2}} - 1\right)\right)^2}{\left(1 + \eta_{pgs}^{\,2}\left(\frac{\omega_{1\max}}{\omega_{1\min}} - 1\right)\right)} \tag{4-29}$$

The values of ΔE_2^* during both flywheel charging and discharging are functions of η_{pgs} and DOD_{ov}, as illustrated in Figure 4-10.

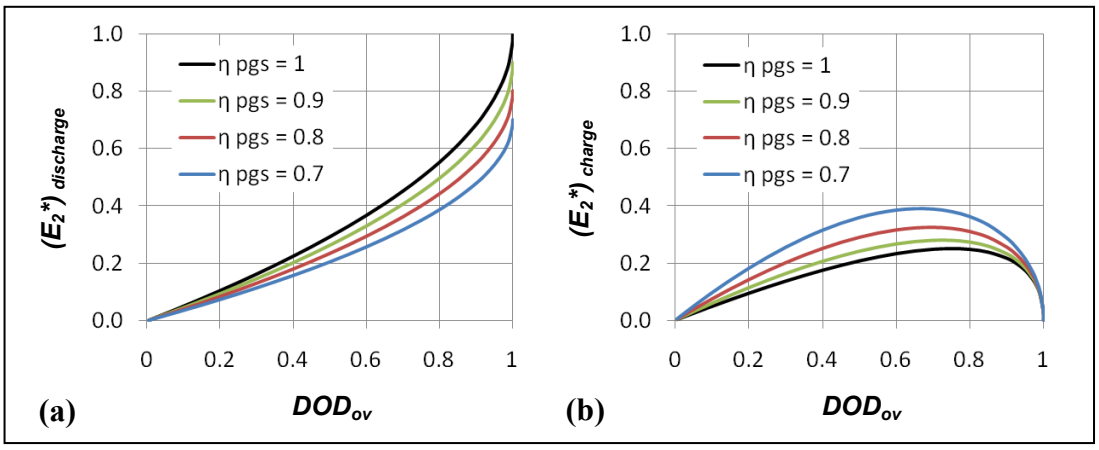


Figure 4-10 – Normalised energy dissipation at the control brake during discharging and charging of flywheel, as a function of η_{pgs} and DOD_{ov} for a 1-PGS brake-controlled transmission

An assumed worst case for energy dissipation at the control brake is here considered to be the case when a full flywheel charge/discharge cycle occurs in a short space of time. The following expression therefore represents the total amount of energy dissipated at the control brake during a charge/discharge cycle per unit of energy delivered to the vehicle during flywheel discharge;

$$\frac{(\Delta E_2)_{cycle}}{E_{useful}} = \frac{(\Delta E_{2,charge} + \Delta E_{2,discharge})}{(\Delta KE_{veh})_{discharge}} = \frac{(\Delta E_2{}^*)_{cycle}}{U} \tag{4-30}$$

This is an important factor, as it allows the brake components in the transmission to be sized for a given useful energy capacity of the FESS. It is a function of PGS efficiency and DOD_{ov} as illustrated in Figure 4-11.

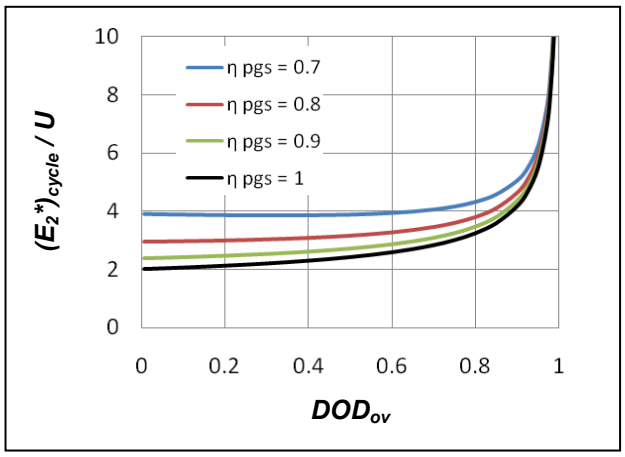


Figure 4-11 – Total energy dissipation in the control brake during a full charge/discharge cycle per unit energy delivered to the vehicle during flywheel discharge as afunction of η_{pgs} and DOD_{ov} for a 1-PGS brake-controlled transmission

The operating characteristics of the transmission are now completely defined. In summary, the 1-PGS brake-controlled transmission is seen to operate with low charge and discharge efficiencies, with a maximum of 25% of the flywheel kinetic energy being delivered to the vehicle. The large amount of energy dissipated at the control branch of the PGS also mean that relatively large brake components are required, adding to the mass of the system. This system is therefore unlikely to be a suitable choice for vehicle regenerative braking applications. There are however three important conclusions from the analysis of this transmission;

i. The analysis method described produces exact analytical expressions describing the performance of the flywheel system, and therefore provides a robust basis for the comparison of different transmission configurations.

ii. Normalising the key parameters that define the operation of the transmission allows the performance and design requirements to be characterised as functions of the overall flywheel depth of discharge, DOD_{ov}, and the PGS efficiency, η_{pgs}. The normalised parameters are therefore independent of the actual vehicle or flywheel characteristics. A summary of the parameter dependence for the 1-PGS brake-controlled transmission is presented in Table 4-3 to illustrate these relationships.

Parameter	*Flywheel discharging*	*Flywheel charging*
PGS gear ratio	$R^* / \sqrt{\eta_{pgs}} = fn(DOD_{ov})$	–
Efficiency	$\frac{\eta_{discharge}}{\eta_{pgs}} = fn(DOD_{ov})$	$\frac{\eta_{charge}}{\eta_{pgs}} = fn(DOD_{ov}, \eta_{pgs})$
Energy dissipated at control brake	$\frac{\Delta E_2{}^*_{discharge}}{\eta_{pgs}} = fn(DOD_{ov})$	$\frac{\Delta E_2{}^*_{charge}}{\eta_{pgs}} = fn(DOD_{ov}, \eta_{pgs})$
Flywheel utilisation	$\frac{U}{\eta_{pgs}} = fn(DOD_{ov})$	–

Table 4-3 – Summary of normalised parameter dependence for 1-PGS brake-controlled transmission

iii. The analysis generates a general 'design tool' which allows parameters to be specified for a particular application in order to achieve an optimum condition (for example, maximising the specific energy capacity of the FESS). This is achieved by performing the following procedure;

Design Method

1. Define J_{fd}, E_{useful} (the energy delivered to the vehicle during full flywheel discharge), max(ω_{fw}), max(T_{fd}) and η_{pgs} for a particular application
2. Use E_{useful} to find $\Delta E_{2,cycle}$ (from Figure 4-11) and calculate the mass of the brake components as a function of DOD_{ov}
3. Use E_{useful} and U (Figure 4-9) to find max(KE_{fw}) and calculate the mass of the flywheel as a function of DOD_{ov}
4. Use max(KE_{fw}) and max(ω_{fw}) to find the required J_{fw} as a function of DOD_{ov}
5. Use J_{fd} and J_{fw} to find R (from Figure 4-6) as a function of DOD_{ov}
6. Calculate the mass of the PGS(s) based on the maximum torque
7. Calculate the total system mass as a function of DOD_{ov} and identify the value of DOD_{ov} that results in minimum mass
8. Identify the $\pm R$ value required to achieve this DOD_{ov}
9. Use Figure 2-22 to identify suitable differential type and configuration to achieve the required R – if the required gear teeth ratios are impractical for both R's then adjust the value of max(ω_{fw}) and repeat steps 5-9 (note that this allows K_{fw} to be identified to allow a practical PGS to be used with a given maximum flywheel rotor speed)

10. Use Figure 4-8 to find the value of ($E_{useful} / \eta_{round\text{-}trip}$) for the chosen FESS design – if this is greater than the typical amount of energy available during vehicle braking the flywheel is over-sized and will not be fully charged during a typical braking event. One of the following measures should then be considered;
    - Decrease the required value of E_{useful}
    - Operate at lower DOD_{ov} and therefore higher $\eta_{round\text{-}trip}$ (although this will decrease the specific energy capacity of the system)
    - Use a more efficient transmission configuration

    Steps 1-10 are then repeated until a practical FESS design is identified.

The following Section discusses the use of the IAM to investigate brake-controlled transmissions containing multiple PGSs. The application of the design method described here is then performed for both single and multiple PGS brake-controlled transmissions in Section 4.1.6.

4.1.5. Results for multiple PGS brake-controlled transmissions

The characteristic charge and discharge equations for a phase of brake-controlled transmission operation can be applied in an iterative calculation procedure to investigate the performance of multiple-PGS transmissions. In the case of a transmission with m PGSs, the operation of the transmission is a function of the m values of R^* and η_{pgs}. Once these values are specified, the final flywheel SOC in each phase of brake-controlled operation can be calculated by specifying the initial value as equal to the final value of the previous phase. This allows the overall transmission efficiency and the normalised brake energy dissipation to be calculated. By specifying the value of the first PGS, R_1^*, a minimising search function can be used to identify the remaining $m\text{-}1$ values of R^* that result in maximum flywheel discharge efficiency. This can be performed for a range of R_1^* values. The maximum efficiency (along with the m values of R^* required to achieve this, and the normalised brake requirements) can therefore be defined as a function of DOD_{ov}.

Analysis has been performed using a representative value of $\eta_{pgs} = \eta_x$ for all of the m PGS units in the multi-PGS brake-controlled transmissions. This means that in order to achieve the maximum discharge efficiency;

- The values of $\frac{R_n^*}{\sqrt{\eta_x}}$, $\frac{\eta_{discharge}}{\eta_x}$, $\frac{U}{\eta_x}$ and $\frac{E_r{}^*{}_{discharge}}{U}$ are only functions of DOD_{ov}
- the value of η_x must be specified in order to evaluate η_{charge} and $\frac{(E_2{}^*)_{cycle}}{U}$

A detailed series of results is presented here for the case of a 5-PGS brake-controlled transmission

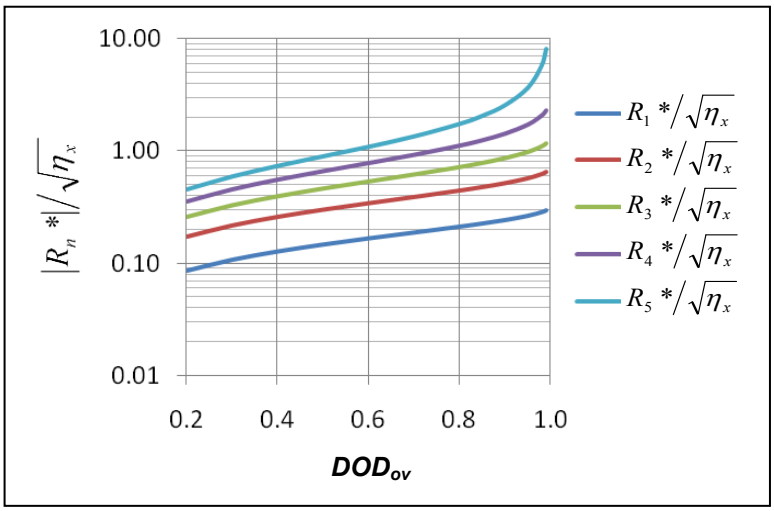


Figure 4-12 – Values of $|R_n^*|/\sqrt{\eta_x}$ required to achieve maximum $\eta_{discharge}$ as a function of DOD_{ov} for a 5-PGS brake-controlled transmission

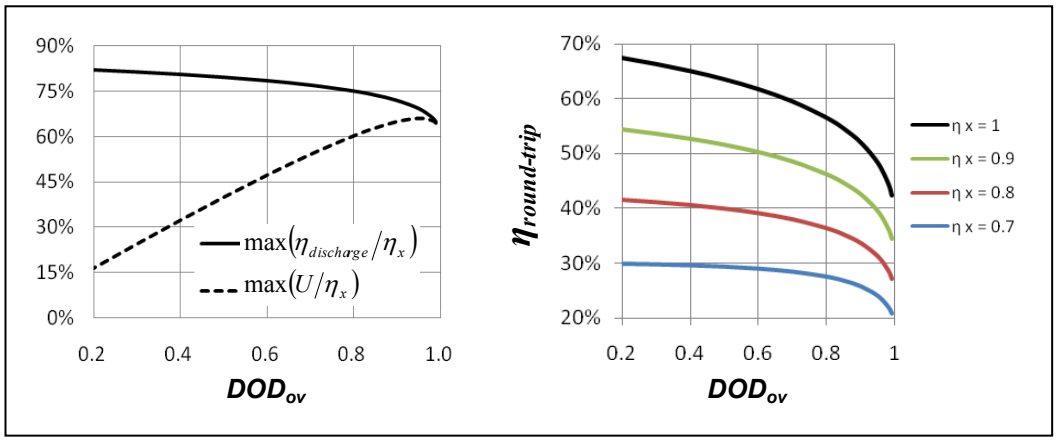


Figure 4-13 – $\max(\eta_{discharge}/\eta_x)$, $\max(U/\eta_x)$ and round-trip efficiency as functions of DOD_{ov} for a 5-PGS brake-controlled transmission (using the R_n* values specified in Figure 4-14)

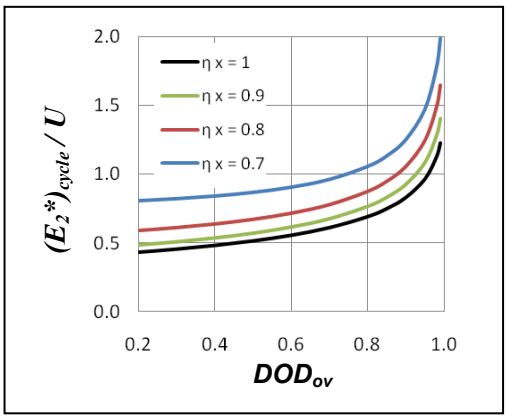


Figure 4-14 – Total energy dissipated at transmission brakes in a full charge/discharge cycle per unit energy delivered to the vehicle during flywheel discharge as afunction of η_x and DOD_{ov} for a 5-PGS brake-controlled transmission

These results show that the 5-PGS brake-controlled transmission can achieve significantly higher efficiency and lower total energy dissipation in the control brakes than the 1-PGS transmission. This is however achieved by increasing the number of transmission components which is likely to increase the total mass and cost of the system.

In summary, the analysis method presented above allows the key FESS parameters to be generated in a normalised form. A 'design tool' has therefore been created which consists of datasets describing the maximum value of $\eta_{discharge}$ (with the associated $\eta_{round\text{-}trip}$ and m values of R^*) and $\Delta E_{2,tot}^*$ as functions of the flywheel DOD_{ov} and the efficiencies of the m PGSs. This normalised data can then be used to identify the appropriate design point for a particular transmission configuration and application. By performing this analysis for a range of configurations, the most appropriate system for a given application can be identified.

The analysis presented in section 4.1.6 is for the application of brake-controlled flywheel transmissions to regional rail vehicles, and illustrates the compromise between the system mass and performance.

4.1.6. Regional rail application of flywheel system with brake-controlled transmission

The application of multi-PGS brake-controlled transmissions to regional rail vehicles can be investigated by considering the mass and efficiency of flywheel systems. Two factors are important when assessing the suitability of a particular system;

i. The mass of the system per unit of useful energy, E_{useful}, that can be delivered to the vehicle from a fully charged FESS
ii. The amount of braking energy which is available for regeneration

If a system is fully charged, then a given amount of energy can be delivered with minimum system mass by choosing the appropriate gearing ratio(s). It is however possible that the amount of energy available during vehicle braking may not be enough to fully recharge the system, in which case the flywheel is oversized for the application. Both of these issues can be illustrated by using the following factors to characterise the total mass (flywheel and transmission) of a given system;

- Specific torque of a single PGS (a value has been identifed which is consistent for both low speed industrial and high speed aerospace units [130-131], although the costs are likely to differ);

  $\overline{T_{pgs}}$ = 50 Nm/kg

- Specific energy dissipation for transmission brake disc and callipers (value identified from consideration of conventional rail vehicle brake components [132]);

  $\overline{E_{brake}}$ = 0.125 MJ/kg

- Specific energy of an advanced flywheel energy storage device (intermediate value selected from Figure 2-6);

  $\overline{E_{fw}}$ = 0.05 MJ/kg

These are representative values taken from the literature which when combined with the results of the preceding analysis allow the limitations of brake-controlled transmissions to be investigated. This approach offers a starting point for analysis, and can be refined as part of a design process for particular flywheel units and promising transmission configurations.

In the application of FESSs for regional rail vehicles it is assumed that the standard final drive gear unit (as found in conventional vehicles) is used. The actual PGS ratios used in the flywheel transmissions are constrained to have an absolute value of less than one. This constraint is applied to ensure that the speed of the PGS branch connected to the flywheel is greater than the speed of the branch connected to the final drive of the vehicle, reducing the gear ratio required in the flywheel unit, K_{fw}. The maximum torque in the PGS therefore always occurs at the branch connected to the vehicle final drive. The required maximum torque at this branch has been specified as 10 kNm in order to achieve a maximum constant

vehicle acceleration rate of ±0.5 m/s^2 for a typical 3-car regional diesel train. For a transmission with a specified number of PGSs, N_{pgs}, the mass of the PGS, brake and flywheel components (m_{pgs}, m_{brake} and m_{fw} respectively) can be estimated as follows;

$$m_{pgs} = \frac{N_{pgs} \max\left(T_{fd}\right)}{\overline{T_{pgs}}} \tag{4-31}$$

$$m_{brake} = \frac{E_{useful}}{\overline{E_{brake}}} \frac{\left(\Delta E_{2,tot}{}^{*}\right)_{cycle}}{U} \tag{4-32}$$

$$m_{fw} = \frac{E_{useful}}{U \times \overline{\overline{E_{fw}}}} \tag{4-33}$$

When the system is limited by the available vehicle braking energy, E_{avail}, the following equation defines the useful energy that can be returned to the vehicle;

$$E_{useful} = E_{avail}\,\eta_{round-trip} \tag{4-34}$$

The performance of the FESS can be characterised by defining a specific energy capacity, *SE*, as follows;

$$SE = \frac{E_{useful}}{m_{pgs} + m_{brake} + m_{fw}} \tag{4-35}$$

This defines the amount of energy that can be delivered to the vehicle from a fully charged flywheel per unit mass of the FESS. These equations can be applied to the results of the brake-controlled transmission analysis in order to compare the performance of different transmission configurations. Figure 4-15 shows a plot of *SE* against E_{useful} (the energy delivered to the vehicle during full flywheel discharge) using a 1-PGS brake-controlled transmission. Two conditions are illustrated;

1. The system is assumed to be initially fully charged and parameters are specified in order to minimise the mass for a given amount of useful energy delivered to the vehicle (solid line),
2. The energy available during braking is limited to 40 MJ (based on earlier vehicle analysis) and the useful energy that can be recovered and returned to the vehicle is limited by the round-trip efficiency of the transmission. The useful energy can be increased by reducing DOD_{ov}, which increases the transmission efficiency but also increases the required energy capacity (and mass) of the flywheel (dashed line).

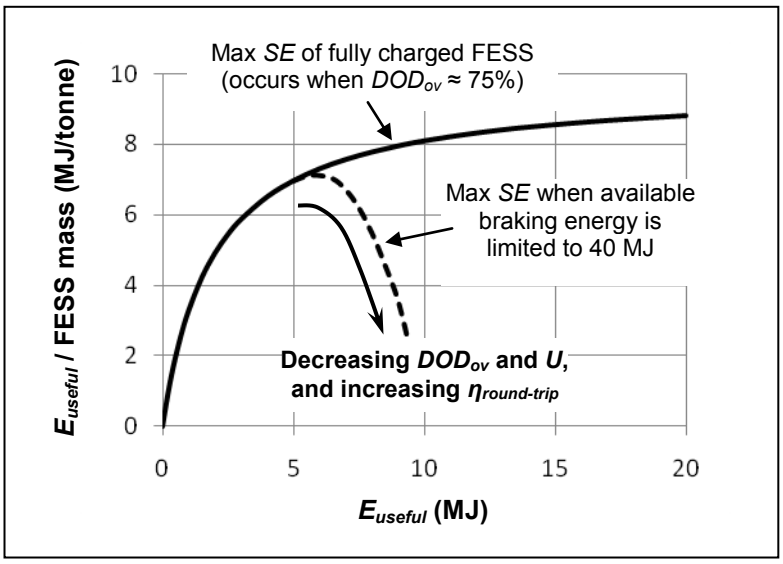


Figure 4-15 – Limitations on the specific energy capacity (*SE*) of a 1-PGS brake-controlled flywheel system for a regional rail application (E_{avail} = 40 MJ, η_{pgs} = 100%)

It is clear from Figure 4-15 that the 1-PGS brake-controlled transmission is limited in how much braking energy can be recovered and made available for the acceleration of the vehicle (less than 25% of the braking energy). The maximum specific energy of the system is around 8.5 MJ/tonne when the useful energy capacity is 6 MJ (15% of the available energy); this is achieved with DOD_{ov} = 60%. The increased efficiency that can be achieved using multiple PGSs allows a higher degree of braking energy recovery. Figure 4-16 shows the results of this analysis for 1-5, 10 and 15 PGS brake-controlled transmissions when E_{avail} = 40 MJ.

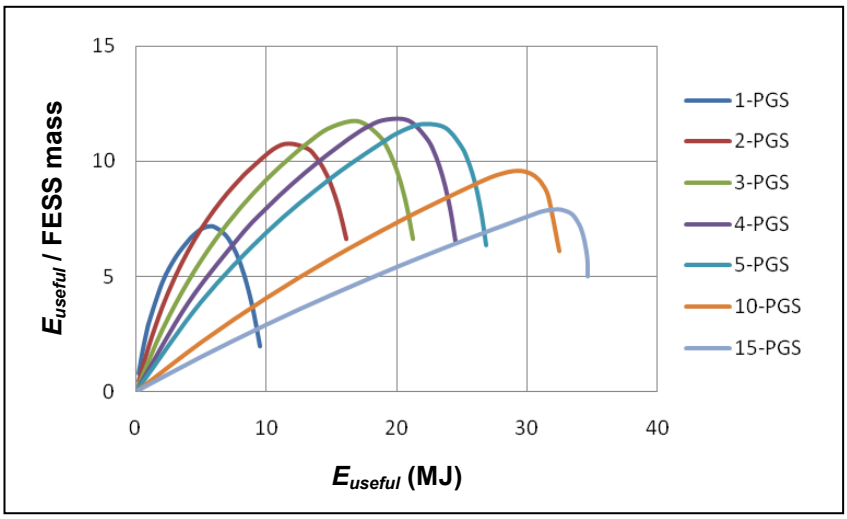


Figure 4-16 – Limitations on the specific energy capacity of 1-5, 10 and 15 PGS brake-controlled flywheel systems for a regional rail application (E_{avail} = 40 MJ, η_{pgs} = 100%)

Figure 4-16 shows that the highest specific energy capacity for a multi-PGS brake-controlled transmission is approximately 12 MJ/tonne and occurs when a 4-PGS transmission is used to achieve a useful energy capacity of 20 MJ (i.e. a round-trip efficiency of 50%). Using transmissions with more PGSs (and therefore higher charge/discharge efficiency) allows more braking energy to be recovered at the expense of increased transmission mass and reduced specific energy. In practical terms, a high number of PGSs (particularly multi-stage types) are likely to be difficult to connect together and idling losses in the gearing will be high. These results suggest that multi-PGS brake-controlled transmissions can provide a viable regenerative braking system when the chosen energy capacity is significantly lower than the available energy expected during a braking event, and the transmission efficiency is therefore not a critical factor. Alternative transmission systems are however required if both a high proportion of braking energy recovery and a high specific energy are to be achieved.

4.2. Independent analysis of clutch-controlled flywheel transmissions

The preceding analysis shows that a simple brake-controlled transmission consisting of a large number of PGSs can achieve high overall operating efficiency, and high utilisation of installed flywheel energy capacity. Increased efficiency is however gained at the expense of increased transmission size and weight, limiting the specific energy capacity of the system. This can be addressed by considering power-split configurations.

4.2.1. Clutch-controlled power-split transmission modes

Power-split configurations are often defined as 'input-coupled' or 'output-coupled', which describes whether the power-split branch connects to the input or output of the transmission. This is an important distinction, as these two configurations exhibit different characteristics. In a flywheel transmission, the definition of 'input' and 'output' is however confusing as power flows in different directions during charging and discharging. Also, power-split configurations are possible between two differential gearsets, which do not fall under either category. To ensure clarity, the following terminology is therefore used to describe three different power-split configurations analysed in this section. In all cases, the flywheel is assumed to be connected to branch 1 of the differential(s) and the final drive to branch 3.

a) Final-drive coupled (FDC) – power-split connection between branches 2 and 3
b) Flywheel coupled (FWC) – power-split connection between branches 2 and 1
c) Dual differential coupled (DDC) – power-split connection between branch 2 of two differentials

In all three cases, the power-split can be achieved by using fixed gearing with a slipping clutch to control the torque exerted on the vehicle. A detailed analysis of this type of system is presented below for the FDC configuration. It is shown that the operation of the clutch-controlled transmission can be related to the analysis of the brake-controlled transmissions discussed in Section 4.1. This is extremely useful as it allows the same simple characteristic charge and discharge equations (Equations 4-19 and 4-20) to be applied to the more complex power-split transmission configurations once 'equivalent' PGS ratio and efficiency parameters have been specified. The characteristics of the FWC and DDC configurations are

then briefly discussed, before a comprehensive results table for all three configurations is presented.

a) FDC clutch-controlled PST

The first power-split configuration considered is the 'final drive coupled' (FDC) transmission layout which uses a fixed gear ratio and clutch-control to achieve a power-split between branches 2 and 3 of the differential. This is illustrated in Figure 4-17, with the arrows defining the direction of power-flow with no power recirculation during flywheel discharge.

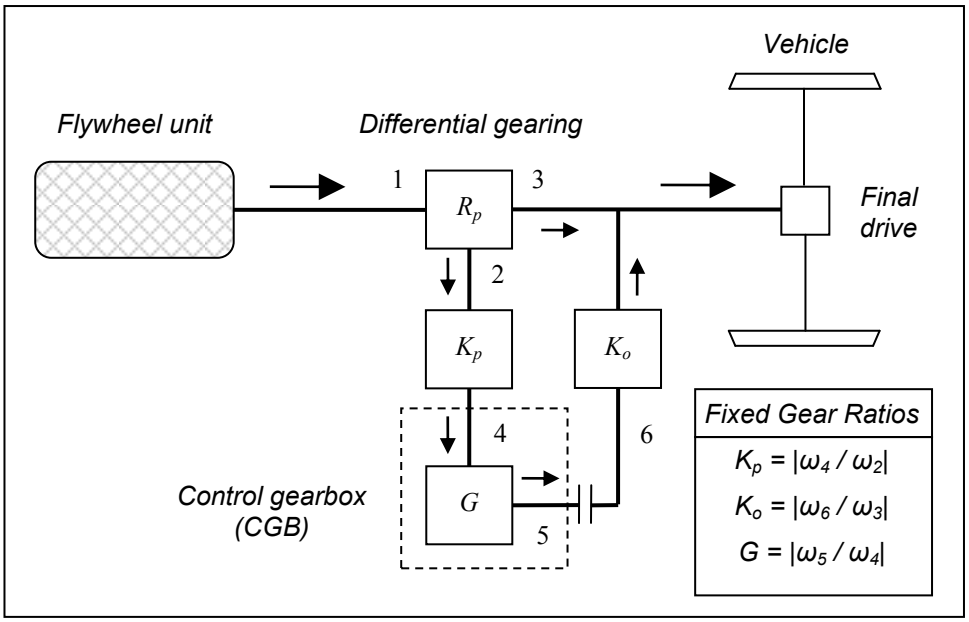


Figure 4-17 – FDC clutch-controlled PST (arrows show direction of power-flow during flywheel discharge)

In order to achieve the required power-split during flywheel discharge;

If $R_p > 1$, then $T_2/T_3 > 0$ (from Table 4-2), therefore $\omega_2/\omega_3 > 0$ for $P_2/P_3 > 0$

If $R_p < 1$, then $T_2/T_3 < 0$ (from Table 4-2), therefore $\omega_2/\omega_3 < 0$ for $P_2/P_3 > 0$

In either case, the power transfer from shaft 5 to shaft 6 via the clutch can only be achieved when;

$$0 < \left(\frac{\omega_6}{\omega_5} \right) < 1 \tag{4-36}$$

Substituting the expressions for the fixed gear ratios and considering the required sign of (ω_3/ω_2) results in;

$$0 < \left(\frac{\omega_3}{\omega_2}\right) < -\frac{\left|\left(1-R_p\right)\right|}{\left(1-R_p\right)}\frac{GK_p}{K_o} \tag{4-37}$$

The clutch therefore locks up when;

$$\left(\frac{\omega_3}{\omega_2}\right)_{lock} = -\frac{\left|\left(1-R_p\right)\right|}{\left(1-R_p\right)}\frac{GK_p}{K_o} \tag{4-38}$$

At this point, power flow through the fixed gear ratio G is no longer possible. In the configuration illustrated in Figure 4-17 the torques exerted at the transmission input and output during flywheel discharge are defined as follows:

$$\left(T_{fw}\right)_{discharge} = \frac{1}{\eta_p}\left(\frac{R_p}{1-R_p}\right)T_2 \tag{4-39}$$

$$\left(T_{fd}\right)_{discharge} = -T_2\left(\frac{1}{1-R_p}\right)\left(1+\left|\left(1-R_p\right)\right|\frac{\eta_{cgb}K_o}{GK_p}\right) \tag{4-40}$$

$$\left(\frac{T_{fd}}{T_{fw}}\right)_{discharge} = -\frac{\eta_p}{R_p}\left(1+\left|\left(1-R_p\right)\right|\frac{\eta_{cgb}K_o}{GK_p}\right) \tag{4-41}$$

The torque ratio defined here can also be achieved by using a brake-controlled PGS transmission, as described in Section 4.1. This occurs when the equivalent brake-controlled PGS has a ratio, R_{eq}, and efficiency, η_{eq}, such that,

$$\frac{\left(\eta_{eq}\right)_{discharge}}{R_{eq}} = \frac{\eta_p}{R_p}\left(1+\left|\left(1-R_p\right)\right|\frac{\eta_{cgb}K_o}{GK_p}\right) \qquad \textit{Torque relationship} \tag{4-42}$$

This 'torque relationship' suggests that the analysis method previously used for brake-controlled transmissions can be applied to clutch-controlled PSTs. In order to achieve the same overall performance as a brake-controlled transmission a 'speed relationship' must however also be defined. This ensures that the speed ratio $\left(\omega_3/\omega_1\right)$ is exactly the same at the end of the clutch-controlled phase (when the clutch locks up) as it is at the end of the equivalent brake-controlled phase (when the speed of branch 2 of the equivalent PGS reaches zero). By considering this final condition of the operating phase for both the brake-controlled transmission and the clutch-controlled PST, the following speed relationship can be derived;

$$\left(\frac{\omega_3}{\omega_1}\right)_{lock} = R_{eq} = \frac{R_p}{\left(1 + \left|\left(1 - R_p\right)\right| \frac{K_o}{GK_p}\right)} \qquad \textit{Speed relationship} \qquad (4\text{-}43)$$

If both the torque and speed relationships are obeyed, a clutch-controlled PST will therefore exert the same torques on the vehicle and flywheel over the same range of operating speeds as the equivalent brake-controlled transmission. The performance of the two systems is then identical, with an equal amount of energy being dissipated in the transmission of each. By substituting Equation (4-43) into Equation (4-42) it is clear that this is achieved when the efficiency of the PGS in the equivalent brake-controlled transmission, η_{eq}, is as follows;

$$\left(\eta_{eq}\right)_{discharge} = \eta_p \left(\eta_{cgb} + \left(\frac{R_{eq}*}{R_p*}\right)\left(1 - \eta_{cgb}\right)\right) \qquad \textit{Equivalent PGS efficiency} \qquad (4\text{-}44)$$

There are a number of interesting points to be drawn from these results;

- The FDC clutch-controlled PST always has a value of R_{eq} less than the actual ratio of the PGS used in the power-split, R_p
- The analysis of clutch-controlled PSTs can be performed using equivalent values of $R*$ and η with the characteristic equations previously derived for brake-controlled transmissions (Equations 4-19 and 4-20)
- Maximum possible value of η_{eq} occurs when; $R_{eq}* \to R_p*$, $\eta_{eq} = \eta_{pgs}$
- Minimum possible value of η_{eq} occurs when; $R_{eq}* \to 0$, $\eta_{eq} = \eta_{pgs}\eta_{cgb}$
- The efficiency of the equivalent brake-controlled PGS is therefore always less than the efficiency of the actual PGS in the clutch-controlled PST (due to additional losses that occur in the CGB)

The use of a multiple speed gearbox (with a range of discrete values of G) in this configuration can allow multiple phases of transmission operation using a single PGS. This potentially allows high transmission performance to be achieved with a significant reduction in gearing compared to the brake-controlled transmissions discussed earlier.

The torque and speed requirements of the CGB must now be considered, as this will affect the mass of the system. With reference to Figures 4-17 and using the speed relationship (Equation 4-43) the following expression can be derived for the ratio of CGB output torque to the transmission output torque in the FDC power-split mode;

$$\left(T_{cgb,o}*\right)_{discharge} = K_o\left(\frac{T_5}{T_{fd}}\right) = \frac{\dfrac{\eta_{cgb}K_o}{GK_p}\left|\left(1-R_p\right)\right|}{\left(1+\dfrac{\eta_{cgb}K_o}{GK_p}\left|\left(1-R_p\right)\right|\right)} = \frac{\eta_{cgb}\left(\dfrac{R_p*}{R_{eq}*}-1\right)}{\left(1+\eta_{cgb}\left(\dfrac{R_p*}{R_{eq}*}-1\right)\right)} \tag{4-45}$$

This normalised CGB output torque is therefore a function of the CGB efficiency and the actual and equivalent R* values.

The CGB output speed can be normalised relative to the maximum speed of the flywheel, as discussed in Appendix A. This normalised speed is defined in Equation 4-46 and is only a function of the actual and equivalent values of R* and PGS efficiency, and the CGB efficiency.

$$\omega_{cgb,o}* = \frac{1}{K_o}\left|\frac{\omega_{cgb,o}}{\omega_{1,\max}}\right|\sqrt{\frac{J_{fd}}{J_{fw}}} \tag{4-46}$$

Once the CGB gear ratio, G, is specified the normalised torque and speed at the CGB input can easily be found from;

$$\left(T_{cgb,i}*\right)_{discharge} = \frac{G}{\eta_{cgb}}\left(T_{cgb,o}*\right)_{discharge} \qquad \text{and} \qquad \omega_{cgb,i}* = \frac{\omega_{cgb,o}*}{G} \tag{4-47}$$

The equations presented here for η_{eq} and $T_{cgb,o}$* are for the case of flywheel discharge using a FDC clutch-controlled transmission, but the analysis can be repeated for operation during flywheel charging where the direction of power-flow in all branches is reversed. The full results (including charging and discharging cases) for R_{eq} and η_{eq} are presented in Table 4-5, while the expressions for $\omega_{cgb,o}$* and $T_{cgb,o}$* are presented in Table 4-6.

These results show that the normalised actual and equivalent PGS gearing ratios and actual component efficiencies can be used to completely characterise the transmission operation and the normalised torque and speed requirements of the CGB. The effect of the actual and equivalent R* values on transmission efficiency, flywheel utilisation and normalised CGB power rating can be investigated using the simple characteristic charge and discharge equations derived for brake-controlled transmission. As in Section 4.1, applying this analysis to a specific transmission configuration produces a general design tool, which can be used to identify appropriate values of R_p, G, K_o and K_p for a particular application. Before complete transmission systems are investigated, the operation other power-split configurations should

be considered. The derivation of the expressions for R_{eq}, η_{eq}, $\omega_{cgb,o}$* and $T_{cgb,o}$* for FWC and DDC clutch-controlled PSTs are presented below.

b) FWC clutch-controlled PST

The 'flywheel coupled' (FWC) transmission layout uses a fixed gear ratio and clutch-control to achieve a power-split between branches 1 and 2 of the differential, as presented in Figure 4-18.

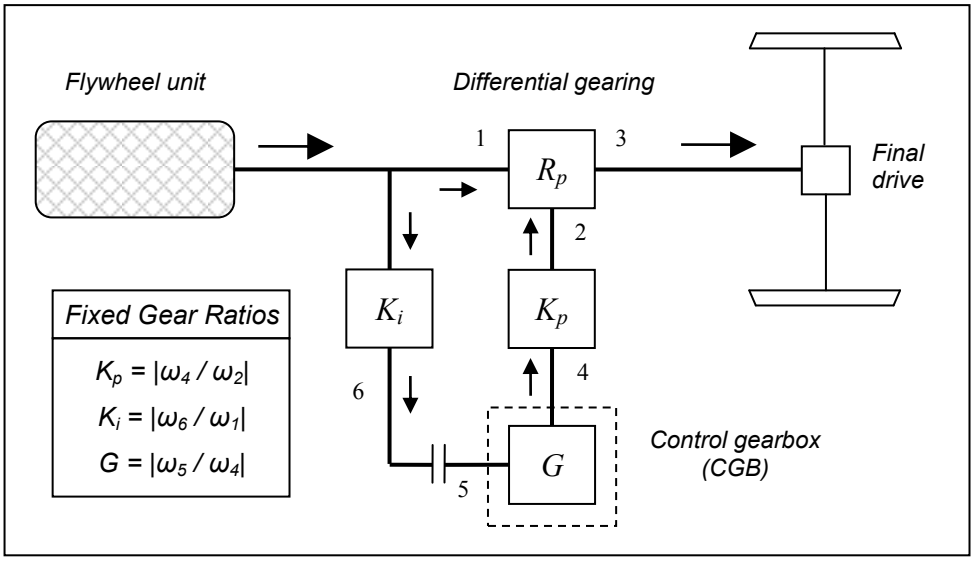


Figure 4-18 – FWC clutch-controlled PST (arrows show direction of power-flow during flywheel discharge)

By considering the PGS torque and speed relationships it can be shown that the illustrated power flow during discharge is only possible when;

$$\frac{\omega_2}{\omega_1}\frac{\left|R_p\left(1-R_p\right)\right|}{R_p\left(1-R_p\right)} \geq 0 \qquad (4\text{-}48)$$

This configuration cannot therefore be used for the initial acceleration of the vehicle from stationary (when $\omega_2/\omega_1 = - R_p /(1-R_p)$), and a phase of brake-controlled operation is required to accelerate the vehicle and reduce the speed of branch 2 to zero. The limiting condition in Equation 4-48 is then satisfied and a phase of FWC clutch-controlled operation is possible, ending when the clutch locks at the following speed ratio;

$$\left(\frac{\omega_1}{\omega_2}\right)_{lock} = \frac{\left|R_p\left(1-R_p\right)\right|}{R_p\left(1-R_p\right)}\frac{GK_p}{K_i} \tag{4-49}$$

The ratio between the torques exerted at the transmission input and output during flywheel discharge is defined as follows:

$$\left(\frac{T_{fd}}{T_{fw}}\right)_{discharge} = -\frac{\eta_p}{R_p\left(1+\left|\left(\frac{1-R_p}{R_p}\right)\right|\frac{K_i}{\eta_{cgb}GK_p}\right)} = -\frac{\eta_{eq}}{R_{eq}} \tag{4-50}$$

The torque ratio defined here can again be achieved by using a brake-controlled transmission, as described earlier. This equivalent differential must have a ratio, R_{eq}, and efficiency, η_{eq}, such that,

$$\left(\frac{\omega_3}{\omega_1}\right)_{lock} = R_{eq} = R_p\left(1+\left|\left(\frac{1-R_p}{R_p}\right)\right|\frac{K_i}{GK_p}\right) \qquad \textit{Speed relationship} \tag{4-51}$$

$$\left(\eta_{eq}\right)_{discharge} = \frac{\eta_p\eta_{cgb}}{\left(1-\left(\frac{R_p*}{R_{eq}*}\right)\left(1-\eta_{cgb}\right)\right)} \qquad \textit{Equivalent PGS efficiency} \tag{4-52}$$

The torque and speed at the CGB can be analysed in the same way as for the FDC configuration, and the full results (including charging and discharging cases) for R_{eq} and η_{eq} are presented in Table 4-5, while the expressions for $\omega_{cgb,o}$* and $T_{cgb,o}$* are presented in Table 4-6.

c) DDC clutch-controlled PST

The final configuration considered here is the 'dual differential coupled' (DDC) clutch-controlled PST. This is illustrated in Figure 4-19 where branch 1 of both differentials is connected to the flywheel and branch 3 to the final drive. Arrows again show the direction of power-flow during flywheel discharge; the direction of the power-flow between the two differentials now depends on the relative values of R_p and R_q as illustrated.

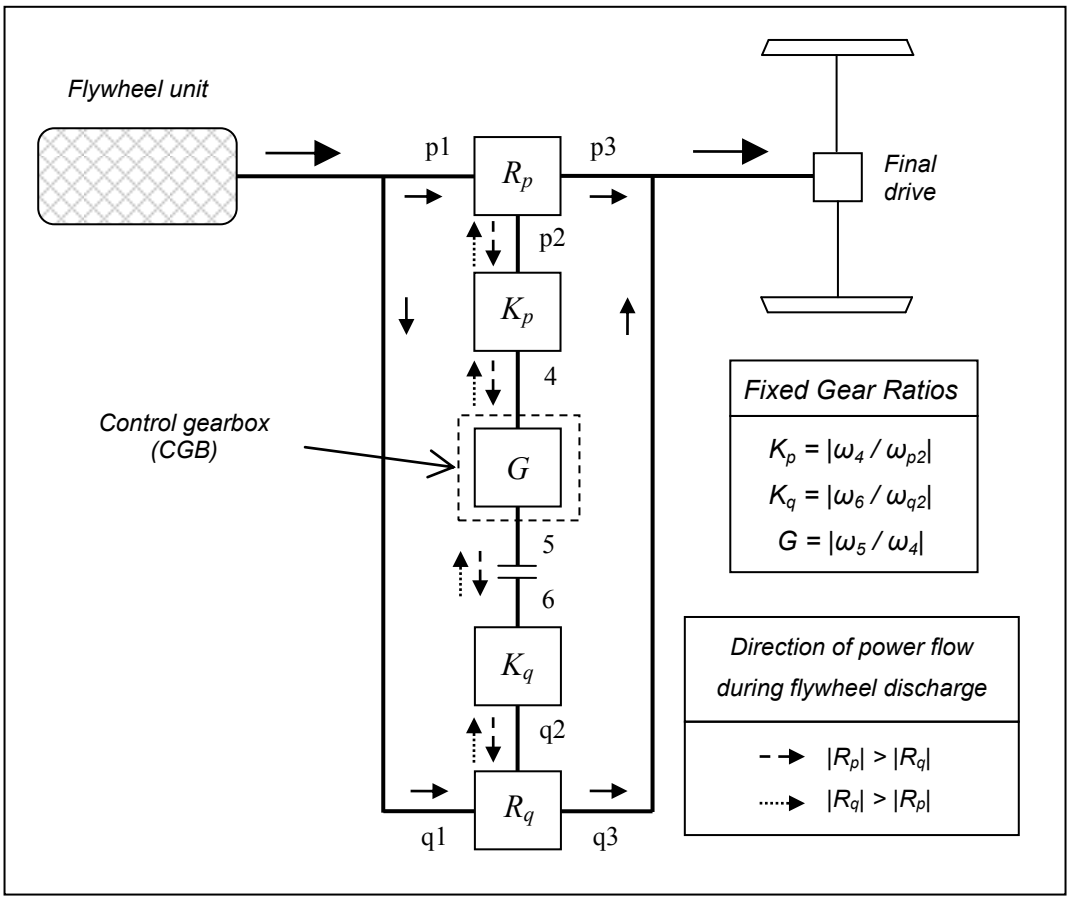


Figure 4-19 – Illustration of DDC clutch-controlled PST (arrows show direction of power-flow during flywheel discharge)

In order to achieve the power flow indicated in Figure 4-19 for flywheel discharge, the following speed relationship between branch 2 of the two differentials must apply;

$$\left(\frac{\omega_{q2}}{\omega_{p2}}\right)_{lock} = -\frac{\left|\left(1-R_p\right)\left(1-R_q\right)\right|}{\left(1-R_p\right)\left(1-R_q\right)}\left(\frac{GK_p}{K_q}\right) \tag{4-53}$$

and $R_p R_q > 0$ to ensure that the sign of ω_3/ω_1 is consistent for each differential; although additional gearing at branch 1 or 3 of one of the differentials could remove this constraint, the condition is required for a practical coaxial configuration of the two differentials.

If $\left|R_p\right| > \left|R_q\right|$ then power can only flow out of branch p2 and into branch q2 during discharge. The relationship between the torques at these two branches is then given by;

$$T_{q2} = \frac{\left|\left(1-R_p\right)\left(1-R_q\right)\right|}{\left(1-R_p\right)\left(1-R_q\right)}\left(\frac{K_q}{GK_p}\right)\eta_{cgb}T_{p2} \tag{4-54}$$

The speed relationship at lock-up (Equation 4-53) leads to the following speed relationship between the DDC clutch-controlled PST and an equivalent brake-controlled transmission;

$$\left(\frac{\omega_3}{\omega_1}\right)_{lock} = R_{eq} = \frac{\left(R_p + R_q\left|\left(\frac{1-R_p}{1-R_q}\right)\right|\frac{K_q}{GK_p}\right)}{\left(1+\left|\left(\frac{1-R_p}{1-R_q}\right)\right|\frac{K_q}{GK_p}\right)} \qquad \textit{Speed relationship} \qquad (4\text{-}55)$$

The necessary equivalent efficiency of the brake-controlled transmission can be found, as shown in Equation 4-56.

$$\left(\eta_{eq}\right)_{discharge(Rp>Rq)} = \frac{\eta_p\left(1+\eta_q\eta_{cgb}\left(\frac{R_p{}^* - R_{eq}{}^*}{R_{eq}{}^* - R_q{}^*}\right)\right)}{\left(\frac{R_p{}^*}{R_{eq}{}^*}\right)+\eta_p\eta_{cgb}\left(\frac{R_q{}^*}{R_{eq}{}^*}\right)\left(\frac{R_p{}^* - R_{eq}{}^*}{R_{eq}{}^* - R_q{}^*}\right)} \qquad (4\text{-}56)$$

It is clear that the equivalent efficiency is again only a function of the CGB and PGS efficiencies and the normalised PGS ratios, R_p*, R_q* and R_{eq}*. This analysis can be repeated in order to find expressions for η_{eq} during both charging and discharging when $|R_p| > |R_q|$ and $|R_q| > |R_p|$, as shown in Table 4-5. An analysis of the normalised CGB torque and speed produces the results shown in Table 4-6 for the same cases.

PS mode	PGS characteristics required to achieve equivalent performance using brake-controlled transmission		
	R_{eq}	η_{eq} *(charging)*	η_{eq} *(discharging)*
FDC	$\dfrac{R_p}{\left(1+\left\|\left(1-R_p\right)\right\|\dfrac{K_o}{GK_p}\right)}$	$\dfrac{\eta_p\eta_{cgb}}{\left(1-\left(\dfrac{R_{eq}*}{R_p*}\right)\left(1-\eta_{cgb}\right)\right)}$	$\eta_p\left(\eta_{cgb}+\left(\dfrac{R_{eq}*}{R_p*}\right)\left(1-\eta_{cgb}\right)\right)$
FWC	$R_p\left(1+\left\|\left(\dfrac{1-R_p}{R_p}\right)\right\|\dfrac{K_i}{GK_p}\right)$	$\eta_p\left(\eta_{cgb}+\left(\dfrac{R_p*}{R_{eq}*}\right)\left(1-\eta_{cgb}\right)\right)$	$\dfrac{\eta_p\eta_{cgb}}{\left(1-\left(\dfrac{R_p*}{R_{eq}*}\right)\left(1-\eta_{cgb}\right)\right)}$
DDC $R_p > R_q$	$\dfrac{\left(R_p+R_q\left\|\left(\dfrac{1-R_p}{1-R_q}\right)\right\|\dfrac{K_q}{GK_p}\right)}{\left(1+\left\|\left(\dfrac{1-R_p}{1-R_q}\right)\right\|\dfrac{K_q}{GK_p}\right)}$	$\dfrac{\eta_q\left(\eta_p\eta_{cgb}\left(\dfrac{R_p*}{R_{eq}*}\right)+\left(\dfrac{R_q*}{R_{eq}*}\right)\left(\dfrac{R_p*-R_{eq}*}{R_{eq}*-R_q*}\right)\right)}{\left(\eta_q\eta_{cgb}+\left(\dfrac{R_p*-R_{eq}*}{R_{eq}*-R_q*}\right)\right)}$	$\dfrac{\eta_p\left(1+\eta_q\eta_{cgb}\left(\dfrac{R_p*-R_{eq}*}{R_{eq}*-R_q*}\right)\right)}{\left(\left(\dfrac{R_p*}{R_{eq}*}\right)+\eta_p\eta_{cgb}\left(\dfrac{R_q*}{R_{eq}*}\right)\left(\dfrac{R_p*-R_{eq}*}{R_{eq}*-R_q*}\right)\right)}$
DDC $R_q > R_p$		$\dfrac{\eta_p\left(\left(\dfrac{R_p*}{R_{eq}*}\right)+\eta_q\eta_{cgb}\left(\dfrac{R_q*}{R_{eq}*}\right)\left(\dfrac{R_p*-R_{eq}*}{R_{eq}*-R_q*}\right)\right)}{\left(1+\eta_p\eta_{cgb}\left(\dfrac{R_p*-R_{eq}*}{R_{eq}*-R_q*}\right)\right)}$	$\dfrac{\eta_q\left(\eta_p\eta_{cgb}+\left(\dfrac{R_p*-R_{eq}*}{R_{eq}*-R_q*}\right)\right)}{\left(\eta_q\eta_{cgb}\left(\dfrac{R_p*}{R_{eq}*}\right)+\left(\dfrac{R_q*}{R_{eq}*}\right)\left(\dfrac{R_p*-R_{eq}*}{R_{eq}*-R_q*}\right)\right)}$

Table 4-4 – Expressions for R_{eq} and η_{eq} for FDC, FWC and DDC clutch-controlled power-split modes

PS mode	Definitions of normalised speed and torque at CGB output			
	$\omega_{cgb,o}$*	$T_{cgb,o}$*	*Expressions for* $T_{cgb,o}$*	
	fn(DOD_{ov}*, η's)*	*fn(*DOD_{ov}*, η's)*	*Charging*	*Discharging*
FDC	$\frac{1}{K_o}\left\lvert\frac{\omega_{cgb,o}}{\omega_{1\max}}\right\rvert\sqrt{\frac{J_{fd}}{J_{fw}}}$	$K_o\left\lvert\frac{T_{cgb,o}}{T_{fd}}\right\rvert$	$\frac{\left(\frac{R_p*}{R_{eq}*}-1\right)}{\left(\eta_{cgb}+\left(\frac{R_p*}{R_{eq}*}-1\right)\right)}$	$\frac{\eta_{cgb}\left(\frac{R_p*}{R_{eq}*}-1\right)}{\left(1+\eta_{cgb}\left(\frac{R_p*}{R_{eq}*}-1\right)\right)}$
FWC	$\frac{1}{K_i}\left\lvert\frac{\omega_{cgb,o}}{\omega_{1\max}}\right\rvert$	$K_i\left\lvert\frac{T_{cgb,o}}{T_{fd}}\right\rvert\sqrt{\frac{J_{fd}}{J_{fw}}}$	$\eta_p\eta_{cgb}\left(R_{eq}*-R_p*\right)$	$\frac{1}{\eta_p\eta_{cgb}}\left(R_{eq}*-R_p*\right)$
DDC $R_p > R_q$	$\frac{\lvert(1-R_q)\rvert}{K_q}\left\lvert\frac{\omega_{cgb,o}}{\omega_{1\max}}\right\rvert\sqrt{\frac{J_{fd}}{J_{fw}}}$	$\frac{K_q}{\lvert(1-R_q)\rvert}\left\lvert\frac{T_{cgb,o}}{T_{fd}}\right\rvert$	$\frac{\eta_q}{\left(1+\eta_{cgb}\eta_q\left(\frac{R_{eq}*-R_q*}{R_p*-R_{eq}*}\right)\right)}$	$\frac{\eta_{cgb}}{\left(\eta_{cgb}\eta_q+\left(\frac{R_{eq}*-R_q*}{R_p*-R_{eq}*}\right)\right)}$
DDC $R_q > R_p$			$\frac{\eta_{cgb}\eta_p}{\left(\eta_{cgb}\eta_p+\left(\frac{R_{eq}*-R_q*}{R_p*-R_{eq}*}\right)\right)}$	$\frac{1}{\left(1+\eta_{cgb}\eta_p\left(\frac{R_{eq}*-R_q*}{R_p*-R_{eq}*}\right)\right)}$

Table 4-5 – Expressions for ($\omega_{cgb,o}$*) and ($T_{cgb,o}$*) for FDC, FWC and DDC clutch-controlled power-split modes

PS mode	Limiting values of the equivalent PGS characteristics		
	R_{eq}	η_{eq} *(charging)*	η_{eq} *(discharging)*
FDC	$R_{eq} < R_p$	$\eta_{cgb}\eta_p < \eta_{eq} < \eta_p$	$\eta_{cgb}\eta_p < \eta_{eq} < \eta_p$
FWC	$R_{eq} > R_p$	$\eta_{cgb}\eta_p < \eta_{eq} < \eta_p$	$\eta_{cgb}\eta_p < \eta_{eq} < \eta_p$
DDC $R_p > R_q$	$R_q < R_{eq} < R_p$	$\eta_{cgb}\eta_p\eta_q < \eta_{eq} < \eta_p$	$\eta_{cgb}\eta_p\eta_q < \eta_{eq} < \eta_q$
DDC $R_q > R_p$	$R_p < R_{eq} < R_q$	$\eta_{cgb}\eta_p\eta_q < \eta_{eq} < \eta_q$	$\eta_{cgb}\eta_p\eta_q < \eta_{eq} < \eta_p$

Table 4-6 – The limiting values of R_{eq} and η_{eq} for the equivalent PGS brake-controlled transmission

There are two important points to note about the results in Tables 4-4 and 4-5;

- If η_{pgs} and η_{cgb} are assumed to be 100% then the value of η_{eq} is 100% for all three power-split modes – the operation of the power-split modes is then identical to the operation of a brake-controlled transmission with a PGS ratio of R_{eq}.
- If η_{pgs} and η_{cgb} are both less than 100% then the gearing ratios in the transmission must be specified in order to calculate the R_{eq} and η_{eq} values and hence assess the performance of the clutch-controlled transmission

In summary, these three different forms of clutch-controlled PST each allow a phase of flywheel discharge to be achieved which is exactly equivalent to a brake-controlled transmission using a PGS with characteristic gear ratio R_{eq} and efficiency η_{eq}. A range of transmissions can therefore be implemented using a conventional counter-shaft CGB with a number of discrete gear ratios to achieve multiple phases of flywheel discharge. Using the respective equations for R_{eq} and η_{eq}, appropriate values for the CGB gear ratios can be specified in order to achieve identical performance (with maximum efficiency for a given DOD_{ov}) to the multi-PGS brake controlled transmission described earlier. The most effective configuration uses a discrete ratio gearbox to achieve clutch-controlled FDC and DDC power-split modes as discussed in the following section.

4.3. Multi-PGS clutch/brake controlled PST

The suitability of the three different forms of clutch-controlled PST for use in flywheel transmissions can be considered by using the earlier results for a 15 phase brake-controlled transmission. These results provide the R^* values required to achieve maximum transmission efficiency for a given flywheel DOD_{ov}. By using multiple PGSs the power in the control gearbox (CGB) can be reduced, but this requires that the gear ratios, G_j, be consistent in all power-split modes. A transmission consisting of a combination of FDC and DDC power-split modes is the only configuration able to achieve the maximum efficiency with the same CGB gear ratios in all modes. An example of this configuration consisting of 3 PGSs and a 4-speed CGB is shown in Figure 4-20.

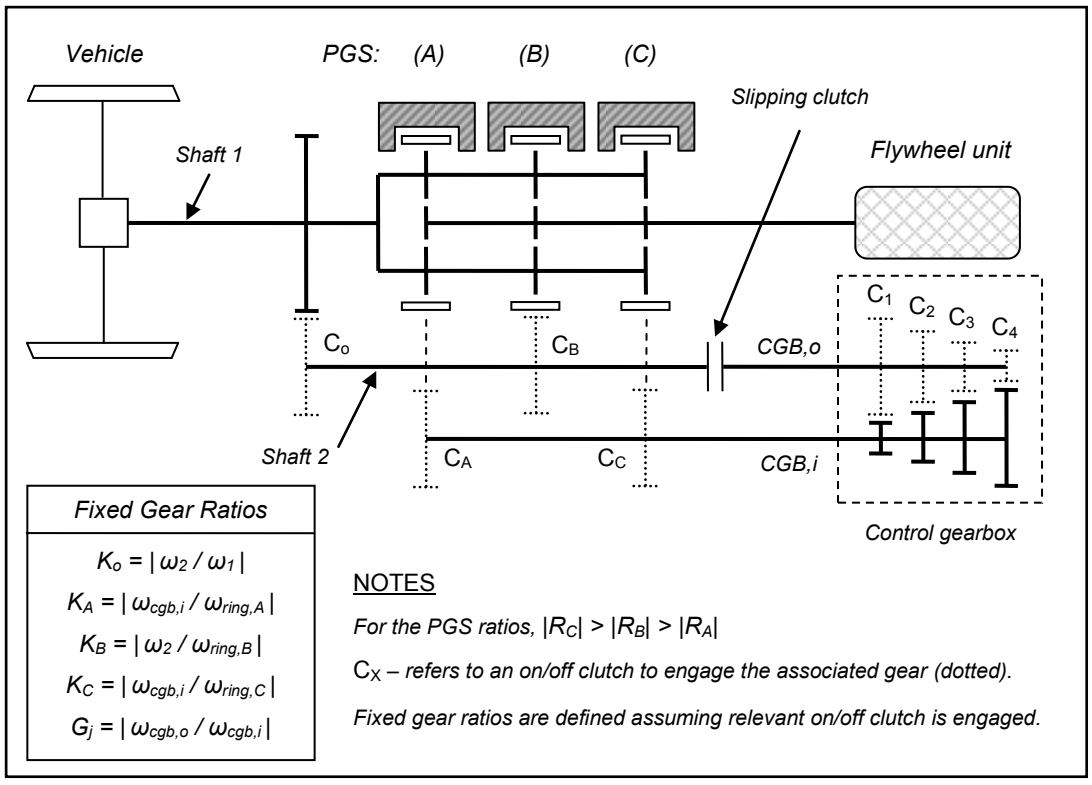


Figure 4-20 – Example of a 3-PGS power-split transmission with 4-speed CGB

During flywheel powered acceleration of the vehicle from stationary the particular transmission configuration shown in Figure 4-20 is operated according to the sequence described in Table 4-7. The 'connecting elements' are on/off clutches that engage and disengage the fixed ratio gearing. The 'control elements' are the clutch and brake

components which are used to generate torque at the transmission input and output via friction at a slipping interface leading to energy dissipation.

Phase	Connecting elements								Control element				Description of operation
	CGB gear clutch				Shaft clutch				PGS brake			Slipping clutch	
	C_1	C_2	C_3	C_4	C_o	C_A	C_B	C_C	A	B	C		
1	X				X	X						X	Power-split between FD and PGS A
2		X			X	X						X	
3			X		X	X						X	
4				X	X	X						X	
5				X		X			X				Brake-controlled at PGS A
6				X		X	X					X	Power-split between PGS A and B
7			X			X	X					X	
8		X				X	X					X	
9	X					X	X					X	
10	X						X			X			Brake-controlled at PGS B
11	X						X	X				X	Power-split between PGS B and C
12		X					X	X				X	
13			X				X	X				X	
14				X			X	X				X	
15				X				X			X		Brake-controlled at PGS C

Table 4-7 – Control sequence for 3-PGS, 4-speed CGB clutch/brake controlled PST during flywheel discharge (X indicates the element is engaged)

Once $(\omega_{ring,\,C}) \geq 0$ the transmission can no longer discharge the flywheel. It is clear that this type of configuration allows a large number of transmission phases to be achieved, as defined by the following equation;

$$N_{phases} = N_{PGS}(N_{CGB} + 1) \tag{4-57}$$

A clutch/brake controlled PST consisting of 3 PGSs and a 4-speed CGB therefore has the 15 operating phases shown in Table 4-7. While all the R^* values of a 15-PGS brake-controlled transmission can be optimised to achieve maximum efficiency (as shown earlier), the power-split transmission is constrained by the requirement that the same discrete gear ratios in the CGB must be used in all the power-split modes. The effect of this constraint on transmission operation is explored in the following section.

4.3.1. CGB kinematic requirements

The required values of the CGB gear ratio G_j (where j = 1 to 4) during each of the three power-split modes of the transmission illustrated in Figure 4-20 can be found by considering

the appropriate equation for R_{eq} (see Table 4-4) applied to each of the four gears. As the values of R_A, R_B, R_C, K_o, K_A, K_B and K_C remain constant during transmission operation in all CGB gears, a general expression for the ratio of the j'th gear ratio, G_j/G_1 can be derived for each power-split mode, as shown in Table 4-8.

Power-split mode	$\frac{G_j}{G_1} =$
1 (FDC between final drive and PGS A)	$\frac{R_{eq,j}*\left(R_{eq,1}*-R_A*\right)}{R_{eq,1}*\left(R_{eq,j}*-R_A*\right)}$
2 (DDC between PGSs A and B)	$\frac{\left(R_A*-R_{eq,1}*\right)\left(R_{eq,j}*-R_B*\right)}{\left(R_{eq,1}*-R_B*\right)\left(R_A*-R_{eq,j}*\right)}$
3 (DDC between PGSs B and C)	$\frac{\left(R_C*-R_{eq,1}*\right)\left(R_{eq,j}*-R_B*\right)}{\left(R_{eq,1}*-R_B*\right)\left(R_C*-R_{eq,j}*\right)}$

Table 4-8 – Expressions for CGB gear ratios (where $R_{eq,j}$* is the equivalent R* value of the operating phase using the j'th CGB gear in the respective power-split mode)

The results of Table 4-8 show that the CGB gear ratios are a function of the actual and equivalent R* values that characterise the transmission operation. The strength of the particular configuration shown in Figure 4-20 can be illustrated by calculating the values of the CGB gear ratios (relative to G_1) using the R* values that are found to achieve maximum efficiency as a function of DOD_{ov} using a 15 phase brake-controlled transmission. If a constant efficiency, η_x, is assumed for all the equivalent PGSs then the values of G_j/G_1 are independent of the inertia ratio and PGS efficiency, and depend only on flywheel DOD_{ov}. Table 4-9 shows the $\left|R_{eq}*\right|/\sqrt{\eta_x}$ values required to achieve maximum discharge efficiency for a DOD_{ov} of 80%, and the corresponding values of G_j/G_1 that are required for the three power-split modes.

PS mode	*Phase*	$\lvert R_{eq}\ast\rvert/\sqrt{\eta_x}$	G_j/G_1
1	1	0.073	1
	2	0.146	2.64
	3	0.221	5.90
	4	0.298	15.58
-	**5**	**0.379** $= \lvert R_A\ast\rvert/\sqrt{\eta_x}$	-
2	6	0.464	15.58
	7	0.556	5.90
	8	0.655	2.64
	9	0.764	1
-	**10**	**0.885** $= \lvert R_B\ast\rvert/\sqrt{\eta_x}$	-
3	11	1.024	1
	12	1.184	2.64
	13	1.375	5.90
	14	1.608	15.58
-	**15**	**1.903** $= \lvert R_C\ast\rvert/\sqrt{\eta_x}$	-

Table 4-9 – Required spread of gear ratios in the CGB for DOD_{ov} = 80% (assuming a constant actual or equivalent PGS efficiency of η_x for all phases) – brake-controlled phases are shown in bold

These results show that the required *G* values are consistent between all three power-split modes for a DOD_{ov} of 80%. Further analysis shows that this is true for any DOD_{ov} when the $\lvert R_{eq}\ast\rvert/\sqrt{\eta_x}$ values are chosen for maximum discharge efficiency. There is however a slight variation of G_j/G_1 with DOD_{ov} as shown in Figure 4-21.

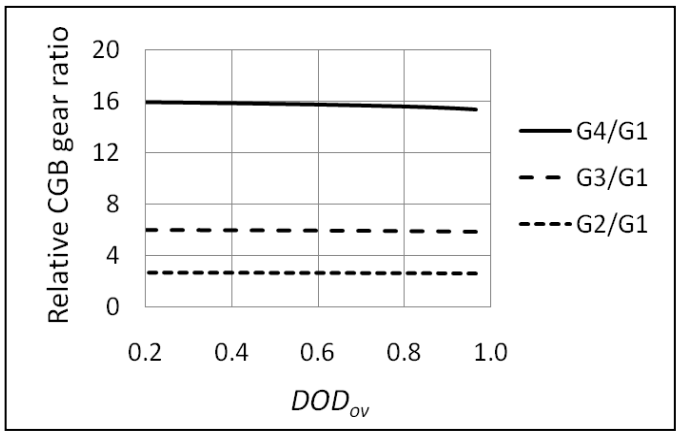


Figure 4-21 – Influence of DOD_{ov} on the CGB gearing ratios required for maximum efficiency

This variation in G_j/G_1 is relatively small (the maximum difference is 3.8% for G_4/G_1 over the range of DOD_{ov} shown in Figure 4-21), and the overall ratio spread required for the CGB is approximately equal to N_{CGB}^2 (i.e. 16 for a 4-speed CGB). Specifying the maximum gear ratio, G_4, equal to 4 results in a value of $G_1 \approx ¼$. The ratio of 4:1 is close to the maximum that can be achieved using a single stage of gearing, justifying the selection of a 4-speed CGB. This allows a compact counter shaft arrangement to be used, as illustrated in Figure 4-20.

This analysis shows that the 3-regime (FDC/DDC/DDC) transmission configuration illustrated in Figure 4-20 can achieve a similar maximum efficiency (as a function of DOD_{ov}) to the 15-PGS brake controlled transmission using only 3 PGSs and a 4-speed CGB. The kinematic viability of this particular transmission configuration has therefore been illustrated. Using the relationships defined in Table 4-4 it can be shown any other multiple-regime configuration of these components consisting of FDC, FWC or DDC power-split modes has a lower maximum efficiency due to the constraints of the CGB fixed gear ratios.

4.3.2. Performance of CGB-controlled PST

The performance of the CGB-controlled PST can be investigated in detail using the following procedure.

1. Specify value of R_A*, η_{pgs} (for A, B and C) and η_{cgb}
2. Estimate values of R_B*, and R_C*
3. Estimate values of $R_{eq,\,j}$* (j = 1, 2, 3, 4) for power-split mode 1 and the two values of $R_{eq,\,1}$* obtained using CGB gear G_1 in power-split modes 2 and 3
4. Use Table 4-8 to find required values of G_j/G_1 to achieve the mode 1 R_{eq}* values
5. Use Table 4-8 to find $R_{eq,\,j}$* (j = 2, 3, 4) for power-split modes 2 and 3
6. Use Table 4-5 with actual and equivalent R* values to calculate all η_{eq} values
7. Use characteristic discharge equations (Equation 4-19) to calculate transmission discharge efficiency, $\max(T_{cgb,o}*)_{\text{discharge}}$ and $\max(\omega_{cgb,o}*)_{\text{discharge}}$
8. Iterate steps 2-7 to identify values of R_B*, R_C*, ($R_{eq,\,1}$*) for modes 1, 2 and 3, and G_j/G_1 (j = 2, 3, 4) that result in maximum discharge efficiency for the specified value of R_A*
9. Use characteristic charging equations (Equation 4-20) to calculate transmission charge and round-trip efficiencies, $\max(T_{cgb,o}*)_{\text{charge}}$ and $\max(\omega_{cgb,o}*)_{\text{charge}}$

10. Record all values of actual and equivalent R^*, DOD_{ov}, $\eta_{discharge}$, $\eta_{round\text{-}trip}$, max($T_{cgb,o}$*), max($\omega_{cgb,o}$*)
11. Repeat steps 2-10 for a range of R_A* values

This calculation procedure allows the operation of the transmission to be completely characterised as a function of DOD_{ov} with the gear ratios chosen for maximum discharge efficiency. A constant component efficiency of 95% has been assumed for all four gears of the CGB and the three PGSs (as suggested by White [133] for typical operation in vehicle transmission applications). The resulting values of $(\eta_{eq})_{discharge}$ for a range of DOD_{ov} are shown in Figure 4-22. While the efficiency of all three actual PGSs in the 3-regime PST is 95%, during power-split operation the efficiency of the equivalent brake-controlled PGSs are up to 4% lower, illustrating the effect of the additional losses that occur in the CGB. The CGB losses during DDC power-split operation are seen to increase with DOD_{ov} due to the higher proportion of power flowing through the CGB.

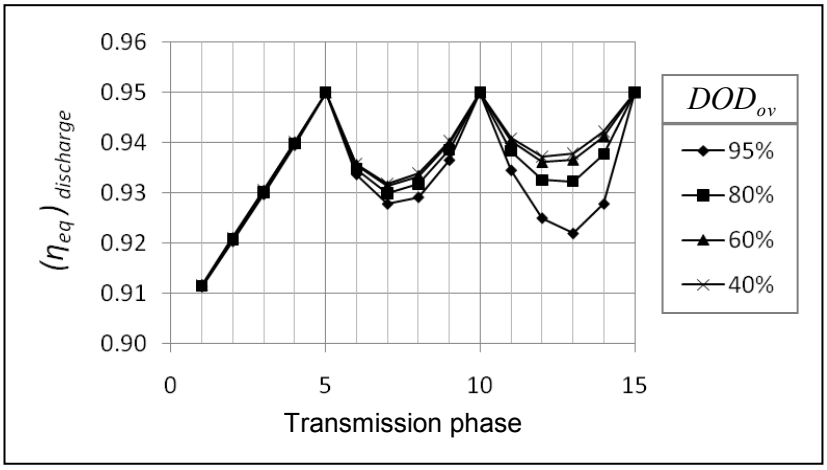


Figure 4-22 – The values of η_{eq} for a 3-PGS, 4-speed CGB controlled transmission during flywheel discharge with gear ratios chosen for maximum efficiency (η_A, η_B, η_C and η_{cgb} are equal to 95%)

While results can also be obtained for $(\eta_{eq})_{charge}$ using the same values of R^*, R_{eq}* and PGS/CGB efficiencies, these are found to be extremely close to the discharge values in each phase, with a maximum difference of 0.1% over the range of DOD_{ov} considered. The values of R^*, η_{pgs}, R_{eq}* and η_{eq} are used with the characteristic equations derived for the brake-controlled transmission (Equations 4-16 and 4-17) to calculate the overall charge and

discharge efficiencies of the CGB-controlled PST as a function of DOD_{ov}. These efficiencies are shown in Figure 4-23 for the case when PGS and CGB gear ratios are chosen to achieve the maximum possible discharge efficiency as a function of DOD_{ov}.

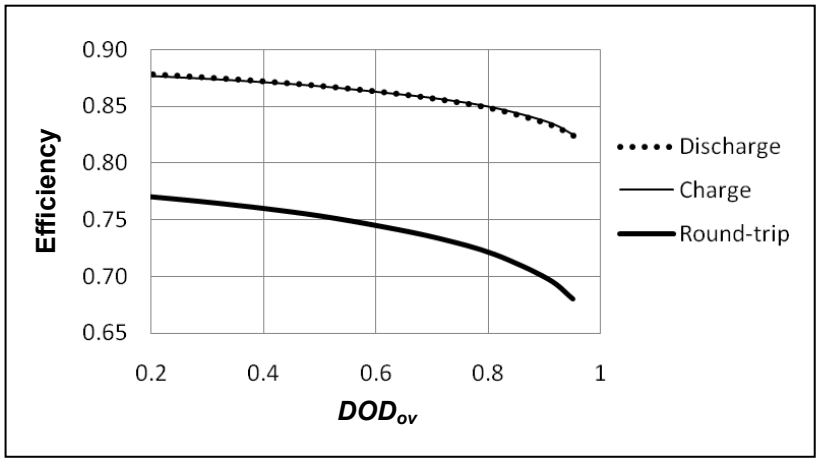


Figure 4-23 – Overall charge, discharge and round-trip efficiencies for the 3-PGS, 4-speed CGB-controlled transmission (with η_{pgs}'s and η_{cgb} = 95%)

Figure 4-24 shows the maximum discharge efficiency of the 3-PGS, 4-speed CGB controlled transmission compared with the 15-PGS brake-controlled transmission. Over the range of DOD_{ov} considered, the discharge efficiencies are very similar with the additional losses in the power-split branches of the CGB-controlled transmission reducing efficiency by around 1%.

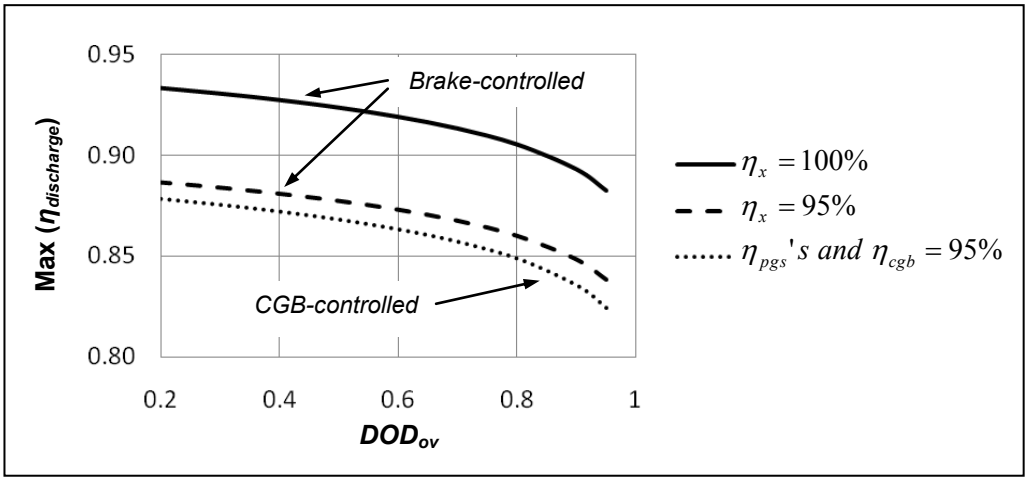


Figure 4-24 – Comparison of maximum possible discharge efficiency as a function of DOD_{ov} between 15-phase brake-controlled and 3-PGS, 4-speed CGB-controlled transmissions

While the CGB-controlled PST has been shown to achieve similar (although slightly lower) overall efficiency as the brake-controlled system, its main advantage is that the total mass of the transmission can be substantially lower due to the reduced amount of gearing. In order to quantify this, the torque and speed requirements of the CGB must be characterised.

4.3.3. CGB torque and speed requirements

In order to estimate the mass of the CGB component, the maximum torque and speed requirements must be identified. This can be achieved by applying the the expressions for normalised CGB torque and speed defined for the different power-split modes in Table 4-5. For the three power-split modes the following expressions apply for the normalised CGB torque apply;

Power-split mode	$T_{cgb,o}{}^{*} =$
1 (FDC between final drive and PGS A)	$K_o \left\| \frac{T_{cgb,o}}{T_{fd}} \right\|$
2 (DDC between PGSs A and B)	$\frac{K_B}{\left\|(1-R_B)\right\|} \left\| \frac{T_{cgb,o}}{T_{fd}} \right\|$
3 (DDC between PGSs B and C)	$\frac{K_B}{\left\|(1-R_B)\right\|} \left\| \frac{T_{cgb,o}}{T_{fd}} \right\|$

Table 4-10 – Normalised torque expressions for 3-regime (FDC/DDC/DDC) CGB-controlled PST

For CGB-controlled operation in gear G_j the following expressions for the corresponding $R_{eq,j}$ in power-split modes 1 and 2 apply;

$$\left(R_{eq,j}\right)_{mode\,1} = \frac{R_A}{\left(1+\left|(1-R_A)\right|\frac{K_o}{G_j K_A}\right)} \tag{4-58}$$

$$\left(R_{eq,j}\right)_{mode\,2} = \frac{\left(R_A + R_B\left|\left(\frac{1-R_A}{1-R_B}\right)\right|\frac{K_B}{G_j K_A}\right)}{\left(1+\left|\left(\frac{1-R_A}{1-R_B}\right)\right|\frac{K_B}{G_j K_A}\right)} \tag{4-59}$$

Combining these equations results in an expression for K_o;

$$K_o = \frac{K_B}{\left|(1-R_B)\right|}\left(\frac{R_A^* - \left(R_{eq,j}\right)_{mode\,1}^*}{\left(R_{eq,j}\right)_{mode\,1}^*}\right)\left(\frac{R_A^* - \left(R_{eq,j}\right)_{mode\,2}^*}{\left(R_{eq,j}\right)_{mode\,2}^* - R_B^*}\right) \tag{4-60}$$

A similar expression can be derived for power-split mode 3, where;

$$K_o = \frac{K_C}{\left|(1-R_C)\right|}\, fn\left(R^{*'}s,\ R_{eq}^{*'}s\right)$$

This allows the normalised CGB torques and speeds in all three power-split modes to be expressed relative to K_o. These are still only functions of the PGS and CGB efficiencies and the actual and equivalent R^* values (which are themselves only a function of DOD_{ov} for maximum $\eta_{discharge}$). Figure 4-25 shows the maximum values of $T_{cgb,o}^*$ and $\omega_{cgb,o}^*$ that occur during charge or discharge as a function of DOD_{ov} when η_A, η_B, η_C and η_{cgb} are all 95%. The product of the maximum normalised torque and speed is also shown. This is effectively a maximum normalised CGB power rating (although the maximum torque and speed do not occur simultaneously during operation), and is defined as follows;

$$P_{cgb,\,rated}^* = \left|\frac{\max\left(T_{cgb}\right)\max\left(\omega_{cgb}\right)}{T_{fd}\,\omega_{fw,\max}}\right|\sqrt{\frac{J_{fd}}{J_{fw}}} \tag{4-61}$$

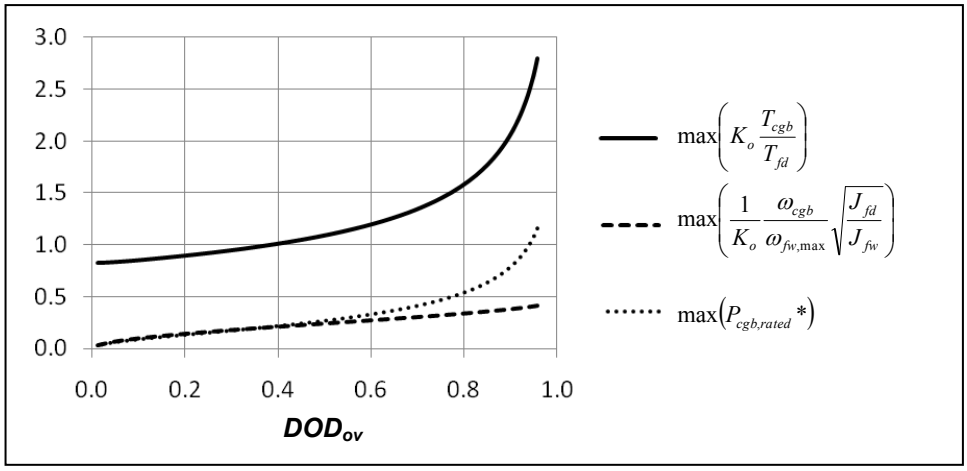


Figure 4-25 – Maximum values of normalised speed, torque and rated power at CGB

The value of $P_{cgb,rated}^*$ as a function of DOD_{ov} is very useful, as it allows the required torque capacity of the CGB to be identified once the other variables have been specified for a particular application. The plot of normalised CGB torque can then be used to find the required value of K_o.

The data in Figure 4-25 has been calculated for the case when the gear ratios (K_A/K_o, K_B/K_o, K_C/K_o, R_A*, R_B*, R_C* and G_1-G_4) have been chosen to achieve maximum discharge efficiency for a given DOD_{ov}. There is however a compromise between choosing gear ratios to maximise efficiency, or to minimise the rated power of the CGB. The extreme case of minimising CGB rated power occurs when the transmission gear ratios are chosen so that the power flow in each power-split phase falls to zero, and the transmission becomes a simple 3-PGS brake-controlled configuration. This compromise between transmission efficiency and CGB power-rating is investigated in the following section.

4.3.4. Strategy for limiting CGB mass

The maximum torque requirement of the CGB can be reduced by adjusting the gearing ratios K_A/K_o, K_B/K_o and K_C/K_o along with the PGS ratios R_B*/R_A* and R_C*/R_A*. While this will reduce the efficiency of the transmission for a given DOD_{ov} it has the advantage of reducing the required mass of the CGB, and can therefore increase the specific energy capacity of the FESS. There is obviously a compromise between reducing the mass and the efficiency of the system; the flywheel utilisation factor provides a basis for comparing the system performance and the CGB requirements. A simple approach to identifying appropriate gearing ratios and the associated system performance can be implemented by equalising the maximum CGB torque and speed achieved in each power-split modes, as follows;

1. Choose a value of $|(1\text{-}R_A)|K_o/K_A$ in order to achieve equal maximum T_{cgb}* at input and output during mode 1 operation
2. Choose values of $|(1\text{-}R_B)|K_o/K_B$ and $|(1\text{-}R_C)|K_o/K_C$ to achieve the same maximum T_{cgb}* at input or output during mode 2 and mode 3 operation
3. Perform iteration to find values of R_B* and R_C* that result in minimum P_{cgb}* for a given value of R_A*

By considering the expressions for normalised CGB torque during mode 1 operation, it can be seen that $\max(T_{cgb,o}^*)_{mode\ 1} = \max(T_{cgb,i}^*)_{mode\ 1}$ when;

$$\left|\left(1-R_A\right)\right|\frac{K_o}{K_A}=\frac{G_4\left(1-\eta_{cgb}G_1\right)}{\left(G_4-\eta_{cgb}\right)}, \quad \text{which equals 1 when } G_1 = 1/G_4. \tag{4-62}$$

If the CGB and PGS efficiencies are assumed to be 100% the maximum input and output CGB torques in modes 2 and 3 are exactly the same as in mode 1 when;

$$\left|(1-R_B)\right|\frac{K_o}{K_B}=1 \quad \text{and} \quad \left|(1-R_C)\right|\frac{K_o}{K_C}=1 \tag{4-63}$$

These values are therefore used to achieve an approximately equal maximum torque in each power-split mode when realistic CGB and PGS efficiencies are used.

The iterative procedure has been implemented using the data specified in Table 4-11. The resulting values for the maximum torque (which is now independent of DOD_{ov}) and $P_{cgb,\,rated}$* using this 'equalised modes' approach are shown in Figure 4-26 as a function of the flywheel utilisation, alongside the values of $P_{cgb,\,rated}$* obtained when the gearing ratios are selected to maximise discharge efficiency.

Parameter	G_1	G_2	G_3	G_4	$\eta_{pgs's}$	η_{cgb}
Value	1/4	2/3	3/2	4	0.95	0.95

Table 4-11 – Parameters of 3-regime CGB controlled transmission used in 'equalised modes' analysis

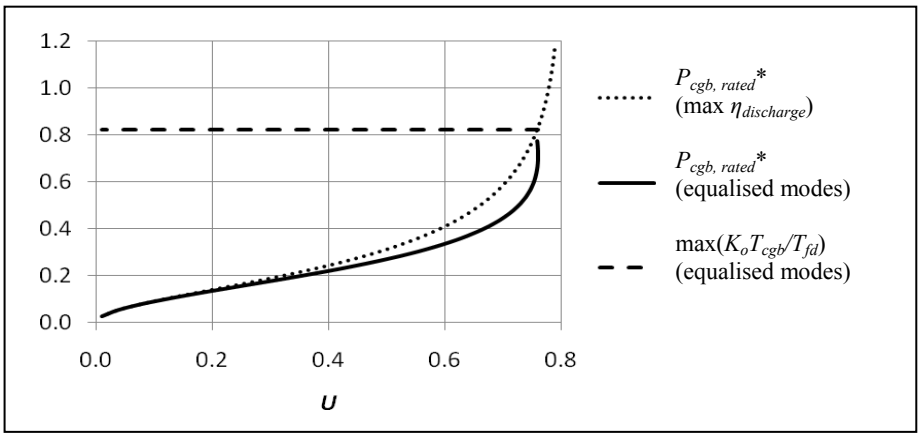


Figure 4-26 – Comparison of normalised rated variator power as a function of *U*, calculated to achieve maximum discharge efficiency or equal max *CGB* torque (defined as the 'equalised modes' case) in each power-split mode

The normalised power and torque data in Figure 4-26 shows that the 'equalised modes' method of gearing selection achieves the same flywheel utilisation with a lower maximum CGB power than the 'maximum $\eta_{discharge}$' method. The slight reduction in transmission efficiency does however mean that a slightly lower maximum U is possible. The three normalised PGS gear ratios required for this method are shown in Figure 4-27(a), with the discharge and round-trip efficiencies shown in Figure 4-27(b).

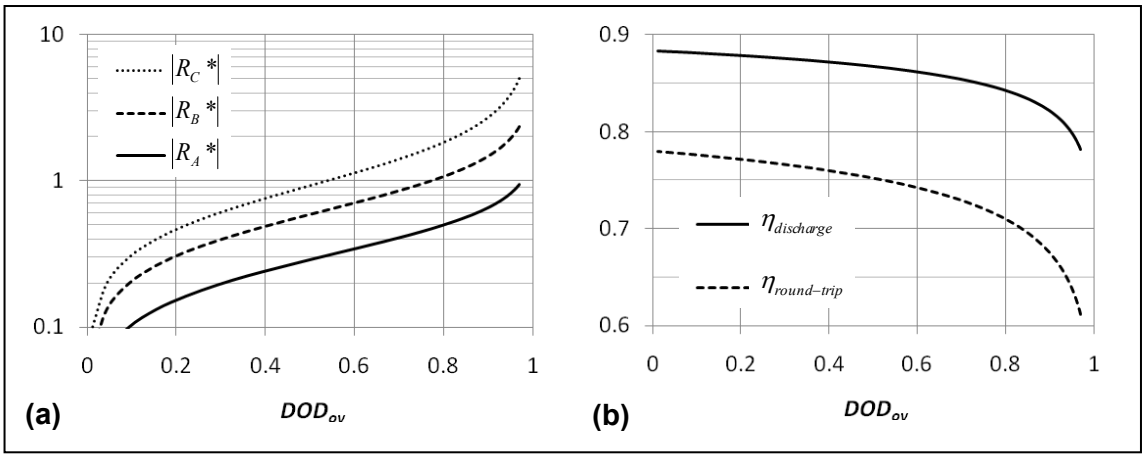


Figure 4-27 – Values of normalised PGS ratio required to achieve equalised maximum CGB torques in all modes, and the resulting transmission efficiency

Figures 4-26 and 4-27 (together with the 'equalised modes' conditions described in Equations 4-62 and 4-63) provide the information required to implement a design tool for the 3-PGS CGB-controlled flywheel transmission, allowing a direct comparison with the brake-controlled transmissions described in Section 4.1.

4.3.5. Regional rail vehicle application of CGB-controlled PST

The design tool data for the 3-regime CGB-controlled flywheel transmission can be used to find appropriate system parameters for the specific application of a regional rail vehicle, as characterised by the data in Table 4-12.

Parameter	Value	Unit
J_{fd}	3670	kgm²
T_{fd}	10	kNm
max(ω_{cgb})	300	rad/s
Single PGS specific torque	50	Nm/kg
CGB specific torque	5	Nm/kg
Flywheel specific energy	0.05	MJ/kg

Table 4-12 – Values used in analysis of 3-regime CGB-controlled flywheel transmission for a regional rail vehicle

The flywheel and transmission parameters are chosen in order to achieve maximum specific energy capacity for a given useful energy capacity, E_{useful} (the energy that can be delivered to

the vehicle from a fully charged flywheel). This is found by calculating the mass of the flywheel, PGSs and CGB as a function of DOD_{ov} in order to achieve a given value of E_{useful}. The mass of the PGS brake components are neglected as the energy dissipated is small. An example of the component masses as a function of DOD_{ov} is given in Figure 4-28 for the case of E_{useful} = 30 MJ.

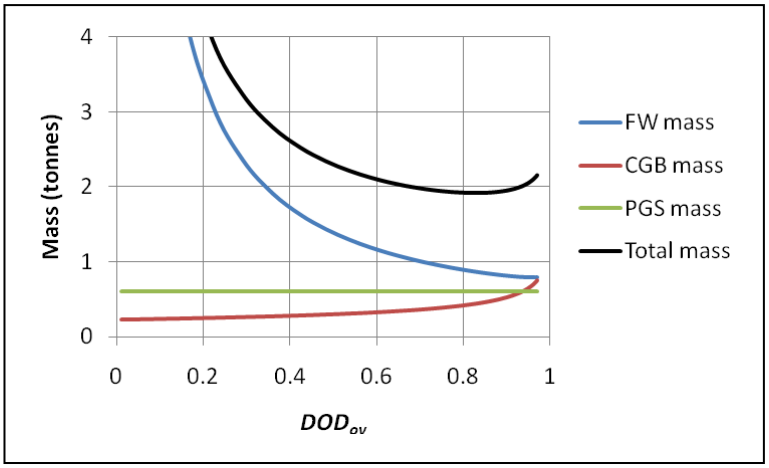


Figure 4-28 – Mass of system components as a function of DOD_{ov} using a 3-PGS, 4-speed CGB transmission providing a useful energy capacity of 30 MJ

These results are independent of the specified maximum flywheel speed (which does however affect the required gear ratios), and depend only on the required torque at the transmission output, the useful energy capacity and the inertias of the vehicle and flywheel. Increasing the specified maximum CGB speed also affects the CGB mass, reducing the maximum CGB torque that occurs with the same power flow. For E_{useful} = 30 MJ the minimum total mass (and therefore maximum specific energy capacity) is seen to occur for a DOD_{ov} of around 80%. Figure 4-29 shows the maximum specific energy capacity as a function of useful energy capacity using the 3-PGSs CGB-controlled transmission.

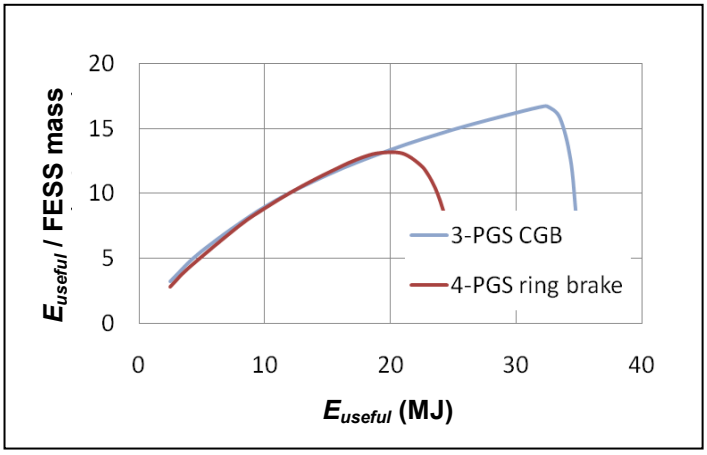


Figure 4-29 – Maximum specific energy of FESS as a function of available energy using a brake/clutch controlled transmission with 4-speed CGB and 3 PGSs, and a 4-PGS ring-brake transmission (E_{avail} = 40 MJ, η_{pgs}'s and η_{cgb} = 100%)

This result shows that when the braking energy is limited to 40 MJ, the maximum specific energy of the 3-regime CGB-controlled transmission is around 17 MJ/tonne which occurs when the useful energy capacity of the system is equal to 32.5 MJ. This is significantly higher than the efficiency and specific energy than can be achieved by a practical brake-controlled transmission, illustrating the advantages of the CGB controlled power-split. However, if a round-trip efficiency of less than 50% is acceptable then the mechanically simpler 4-PGS brake-controlled transmission can provide the same useful energy storage capacity and system mass as the CGB-controlled transmission, and is therefore an attractive option.

4.4. Summary

An analysis method for mechanical flywheel systems has been described, which allows the performance of specific transmission configurations to be characterised. Simple brake-controlled transmissions and clutch-controlled PSTs have been investigated using this method, which is independent of the application (i.e. the vehicle type and drive cycle) and allows a thorough investigation of the interaction between the flywheel, vehicle and transmission. A flywheel utilisation factor has been defined and shown to be a useful measure of the compromise between transmission efficiency and flywheel depth-of-discharge. Furthermore, in power-split transmissions the flywheel utilisation factor also provides a basis for investigating the compromise between transmission efficiency and

component power rating. The results of applying the independent analysis method (IAM) to a particular transmission configuration produce a design tool consisting of normalised system parameters as a function of the overal flywheel depth-of-discharge, DOD_{ov}, achieved during operation. These design tools are extremely useful as they allow an absolute basis for the comparison of different transmission configurations, and also provide a simple means of specifying appropriate transmission parameters for a particular application. This has been demonstrated for the case of a diesel regional train, with flywheel energy storage system (FESS) parameters chosen in order to maximise the specific energy capacity of the system. It has been shown that mechanical flywheel transmissions consisting of brake and clutch controlled PGSs can achieve high efficiency with relatively low mass, leading to high specific energy capacity for the FESS. A novel transmission configuration using a control gearbox (CGB) with slippling clutch has been investigated. This CGB-controlled FESS consists of multiple power-split modes and has been shown to perform particularly well for flywheel applications. An advantage of these mechanical transmissions is the fact that they consist of standard components that are currently widely used in conventional automatic transmissions for IC engines. The cost of developing and manufacturing transmissions for flywheel applications is therefore expected to be relatively low. Transmission systems using variator components (a more specialist technology) are more commonly proposed for flywheel applications. A range of variator-controlled transmissions are therefore investigated using the IAM in the following Chapter.

5. Independent analysis of variator-controlled transmissions

The previous Chapter illustrated an independent analysis technique for brake and clutch controlled transmissions. The value of this method was demonstrated by producing results in the form of normalised 'design tools' that allow a comparison of the performance of different transmission configurations and the identification of appropriate gearing ratios for any application (as characterised by the inertial loads at the transmission input and output). The aim of this Chapter is to implement a similar technique to investigate a range of variator-controlled transmissions. The limited range of gear ratios that can be achieved using a variator means that clutch and brake controlled transmission phases are useful for increasing the overall transmission speed ratio range. In the case of flywheel systems for rail vehicles, the resulting decrease in transmission efficiency is acceptable as the increased ratio range can eliminate the need for low speed (and therefore inefficient) operation of the conventional power-train. The analysis of these clutch and brake controlled operating modes is identical to that discussed in Chapter 4. When analysing the variator-controlled operating phases, the specific configuration of the transmission is an important factor. Three configuration categories are discussed in this Chapter. These are:

i. A direct variator connection between the flywheel unit and final drive
ii. Single regime power-split transmissions
iii. Multiple regime power-split transmissions

In the context of these transmissions, a 'regime' of variator-controlled operation relates to a power-split transmission phase in which the variator speed ratio varies between the maximum and minimum values. Multiple regime transmissions can be achieved by allowing a range of different power-split configurations to be implemented in a single transmission. This increases overall efficiency and/or decreases the required rated variator power, but it can only be achieved with increased system complexity. The independent analysis method (IAM) previously applied in Chapter 4 is again used to generate a design tool for each of the transmission configurations considered here. This method defines the transmission performance and allows appropriate design variables to be specified for any application. An important contribution of this research is that it provides an absolute basis for assessing the strengths and weaknesses of different configurations. Finally, the last section of this Chapter illustrates the use of these design tools to identify the most appropriate systems for regional rail vehicle applications.

5.1. Direct variator-controlled transmission

A simple single-path transmission can be achieved by using a variator to provide a direct connection between the flywheel and vehicle. The input of the variator is connected to the flywheel unit via a fixed gear ratio, K_i, and the output to the final drive via a gear ratio, K_o, and a clutch as shown in Figure 5-1. As the variator has limited maximum and minimum gear ratios the clutch is required in order to transmit power during both low speed acceleration and high speed deceleration of the vehicle. The analysis of this type of flywheel transmission is important as it provides a base case for quantifying the benefits of various power-split transmissions and identifying the most appropriate configuration for a given application.

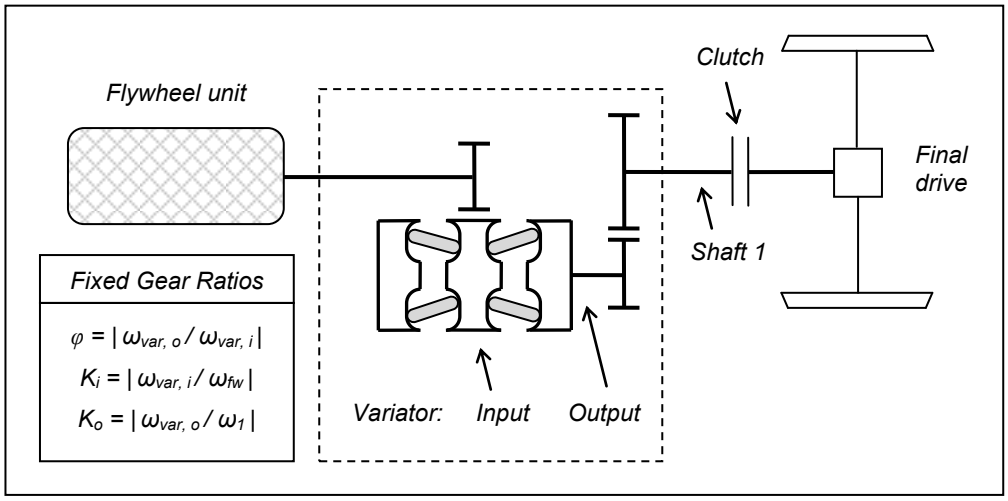


Figure 5-1 – Configuration for a direct (toroidal type) variator-controlled transmission

An analysis has been performed assuming an overall variator ratio spread, φ_t, of 6.25 (a typical value for toroidal and push-belt type variators), and with the following operating limits;

Variator speed ratio limits; $\varphi_{\max} = 2.5$ and $\varphi_{\min} = 0.4$

A constant variator efficiency, η_{var}, of 85% has been applied throughout the analysis presented in this Chapter. The operation of the direct variator transmission during flywheel discharge consists of the following phases;

Direct variator operating phases during flywheel discharge

For $0 \leq |(K_{fw}\,\omega_{fd} / K_{fd}\,\omega_{fw})| < 0.4$

In this phase of operation the variator is held at the minimum speed ratio ($\varphi_{\min}$) and the transmission is clutch-controlled. The phase ends when the slip speed in the clutch falls to zero. Applying the IAM to this phase results in the following expression relating the initial and final flywheel speeds for flywheel discharge;

$$\left(\frac{\omega_{fw,i}}{\omega_{fw,f}}\right)_{clutch} = 1 + \frac{\left(\varphi_{\min} K^*\right)^2}{\eta_{\text{var}}} \tag{5-1}$$

Where K^* is a normalised gear ratio defined as;

$$K^* = \frac{K_i}{K_o}\sqrt{\frac{J_{fd}}{J_{fw}}} \tag{5-2}$$

For $0.4 \leq |(K_{fw}\,\omega_{fd} / K_{fd}\,\omega_{fw})| \leq 2.5$

In this phase the clutch is locked and the variator is controlled to provide the required torque at the vehicle. The phase ends when the variator reaches its maximum speed ratio. Applying the IAM along with conservation of energy results in the following expression;

$$\left(\frac{\omega_{fw,i}}{\omega_{fw,f}}\right)_{variator} = \sqrt{\left(\frac{\eta_{\text{var}} + \left(\varphi_{\max} K^*\right)^2}{\eta_{\text{var}} + \left(\varphi_{\min} K^*\right)^2}\right)} \tag{5-3}$$

Otherwise

The transmission cannot be used to discharge flywheel

The results of Equations 5-1 and 5-3 allow the overall performance of the direct variator transmission to be assessed in terms of the normalised gear ratio, K^*, the maximum and minimum variator speed ratios and the variator efficiency. As the final flywheel speed in the clutch-controlled phase equals the initial speed in the variator-controlled phase, the ratio between the maximum and minimum flywheel speeds during discharge can be expressed as;

$$\frac{\omega_{fw,\min}}{\omega_{fw,\max}} = \frac{\eta_{\text{var}}}{\sqrt{\left(\eta_{\text{var}} + \left(\varphi_{\max} K^*\right)^2\right)\left(\eta_{\text{var}} + \left(\varphi_{\min} K^*\right)^2\right)}} \tag{5-4}$$

Equation 5-4 leads to the following expressions for the overall *DOD* and discharge efficiency of the transmission;

$$DOD_{ov} = 1 - \frac{\eta_{\text{var}}^{\,2}}{\left(\eta_{\text{var}} + \left(\varphi_{\max} K^*\right)^2\right)\left(\eta_{\text{var}} + \left(\varphi_{\min} K^*\right)^2\right)} \tag{5-5}$$

$$\eta_{discharge} = \frac{\left(\eta_{\text{var}} \varphi_{\max} K^*\right)^2}{\left(\eta_{\text{var}} + \left(\varphi_{\max} K^*\right)^2\right)\left(\eta_{\text{var}} + \left(\varphi_{\min} K^*\right)^2\right) - \eta_{\text{var}}^{\,2}} \tag{5-6}$$

It should be noted that the efficiency and DOD_{ov} achieved by the transmission depend on the ratio of the fixed gears, K_i/K_o, rather than the actual values. The actual values of K_i and K_o are however important in ensuring an appropriate range of operating torque and speed for the variator. This is apparent in the normalised expressions which can be derived for the maximum variator torque and speed as shown in Equations 5-7 and 5-8. As for the CGB in Chapter 5, a normalised rated power can again be defined as shown in Equation 5-9;

$$\left(T_{\text{var}}^*\right)_{direct} = K_o \frac{T_{\text{var}}}{T_{fd}} \tag{5-7}$$

$$\left(\omega_{\text{var}}^*\right)_{direct} = \frac{1}{K_i} \frac{\omega_{\text{var}}}{\omega_{fw,\max}} \tag{5-8}$$

$$P_{\text{var},rated}^* = \frac{\max\left(T_{\text{var}}\right)\max\left(\omega_{\text{var}}\right)}{T_{fd}\omega_{fw,\max}} \sqrt{\frac{J_{fd}}{J_{fw}}} = \max\left(T_{\text{var}}^*\right)_{direct} \max\left(\omega_{\text{var}}^*\right)_{direct} K^* \tag{5-9}$$

When a constant torque is applied to the final drive, the maximum variator torque will occur at the variator input during flywheel discharge;

$$\max\left(T_{\text{var}}^*\right)_{direct} = \frac{\varphi_{\max}}{\eta_{\text{var}}} \tag{5-10}$$

If $\left(\varphi_{\max}\sqrt{1 - DOD_{ov}} < 1\right)$ then the maximum variator speed occurs at the input and has the value;

$$\max\left(\omega_{\text{var}}^*\right)_{direct} = 1 \tag{5-11}$$

Otherwise, the maximum variator speed occurs at the output and has the value;

$$\max\left(\omega_{\text{var}}^*\right)_{direct} = \varphi_{\max}\sqrt{1 - DOD_{ov}} \tag{5-12}$$

These equations allow the direct variator transmission to be completely characterised as a function of the normalised gear ratio, K^*. Figure 5-2 shows the transmission discharge performance and the requirements of the variator, assuming constant variator efficiency, η_{var}, of 85%.

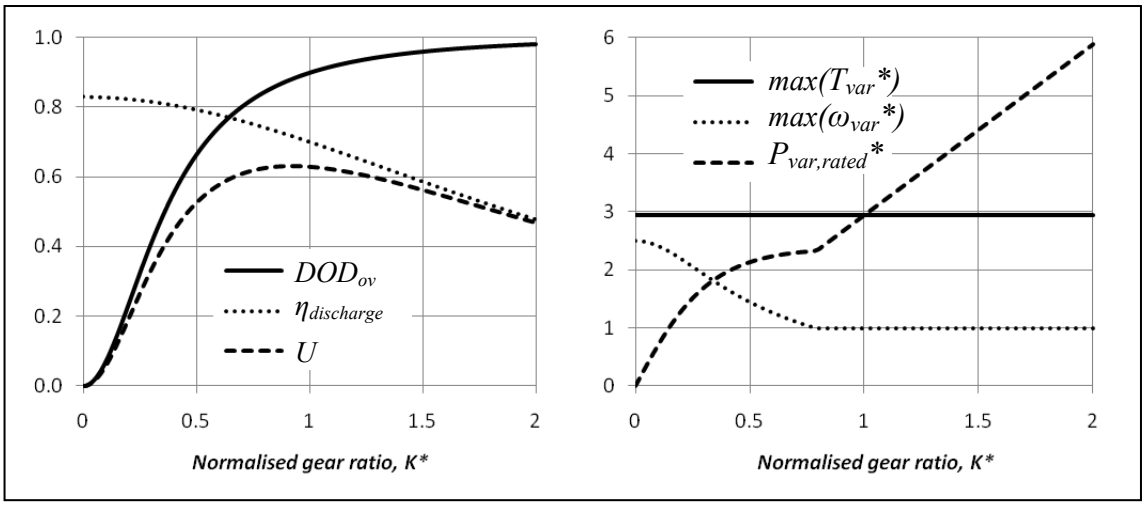


Figure 5-2 – Performance characteristics of the direct variator flywheel transmission as functions of normalised gear ratio, K^* (η_{var} = 85%)

The results show that the maximum U is achieved when $K^* \approx 0.95$. It is also clear that the preferred operating region for the transmission is in the range $0 < K^* < 0.95$, in order to achieve high efficiency and low rated variator power for a given U. There is no obvious advantage in operating with $K^* > 0.95$, and so this region should be avoided.

The problem with this direct variator-controlled transmission is that the variator is transmitting the full tractive/braking power between the vehicle and flywheel. This means that large and expensive variators are required to achieve full braking energy recovery (although a down-sized system could operate in conjunction with conventional braking for limited regeneration). Also, the transmission operates with relatively low efficiency due to the high power flow through the variator and the additional losses during clutch-controlled operation. Alternative systems which can achieve similar or improved efficiency with smaller variators are therefore attractive options for flywheel transmissions. Power-split transmissions can potentially achieve this, and are considered in the following sections.

5.2. Single regime variator-controlled power-split transmissions

An alternative to the direct variator transmission described above is a variator-controlled power-split arrangement. The limited ratio spread of mechanical variators means that variator-controlled PSTs are required to operate in clutch and brake controlled phases when outside the operating range of the variator. The analysis of transmission operation during

these phases is therefore the same as that described in Chapter 4. As with the clutch-controlled PST, a number of configurations of variator-controlled transmission can be achieved by connecting the variator between different branches of a PGS. Two possible configurations which avoid power-recirculation and consist of a single phase of variator-controlled operation are considered in this section;

a) FDC variator-controlled PST
b) FWC variator-controlled PST

Before applying the IAM to these power-split configurations, it is useful to first consider the characteristics of the variator-controlled phase using expressions derived for the case with no losses at the PGS or variator. The analysis of these 'ideal' variator-controlled PSTs is presented below.

5.2.1. Ideal variator-controlled power-split phase

In the literature [93-94] the simplest form of variator-controlled power-split transmissions have been considered and characterised for a single direction of power-flow as either input coupled (IC) or output coupled (OC) as defined in Figure 5-3. Simple relationships can be derived for each case relating the overall transmission speed ratio (r) and the ideal power ratio ($P_{variator}/P_{input}$, assuming no PGS or variator losses) to the PGS ratio (R) and the variator speed ratio (φ) as shown in Table 5-1.

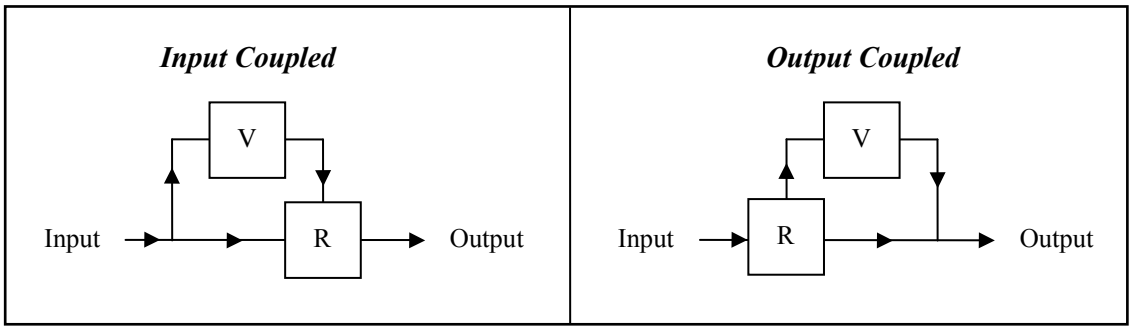


Figure 5-3 – Definition of input and output coupled configurations with arrows showing direction of power-flow with no power recirculation

Power-split configuration	***Input coupled***	***Output coupled***
Overall transmission ratio	$r = R + (1 - R)\varphi$	$r = \dfrac{\varphi R}{R - 1 + \varphi}$
Power-split ratio	$\dfrac{P_v}{P_i} = 1 - \dfrac{R}{r}$	$\dfrac{P_v}{P_i} = 1 - \dfrac{r}{R}$
Condition for no recirculation	$0 < \dfrac{R}{r} < 1$	$0 < \dfrac{r}{R} < 1$
Condition for $\max\left(\dfrac{P_v}{P_i}\right)$	$r = r_{\max}$	$r = r_{\min}$

Table 5-1 – Characteristic relationships for simple input and output coupled PSTs [94]

If the overall transmission speed range, r_t, and variator speed range, φ_t , are defined as;

$$r_t = \frac{r_{\max}}{r_{\min}} \quad \text{and} \quad \varphi_t = \frac{\varphi_{\max}}{\varphi_{\min}} \tag{5-13}$$

both r_t and the maximum value of P_v / P_i can be expressed as a function of $R/r_{\min}$ for the two cases, as shown in Figure 5-4 using a value of $\varphi_t = 6.25$. It is important to note that these results only cover the range of values of $R/r_{\min}$ in which no power-recirculation occurs.

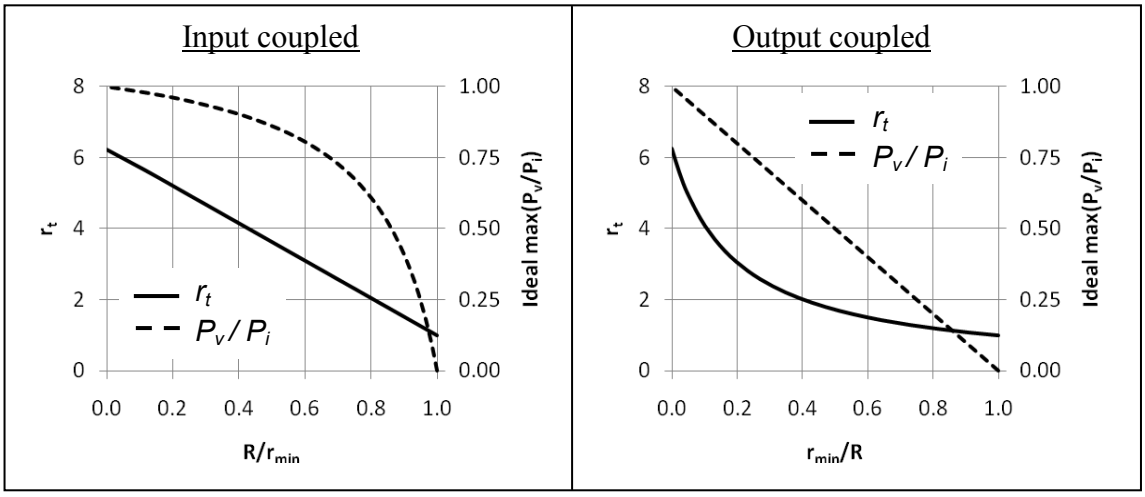


Figure 5-4 – Characteristics of simple input and output coupled PSTs operating with no power recirculation ($\varphi_t = 6.25$)

These Figures show that the value of r_t varies between the case of a direct variator transmitting 100% of the power ($r_t = \varphi_t$) and the case of a fixed gear ratio where no power flows through the variator branch ($r_t = 1$). Either the IC or OC configuration can achieve any

specified combination of r_t (between 1 and φ_t) and r_{min} resulting in the same maximum value of P_v / P_i (although the required value of R is different). The configurations are therefore kinematically equivalent, as either can be used to achieve the same overall transmission characteristics. The output coupled configuration is however likely to be more appropriate for achieving flywheel discharge in a FESS. This is because if a constant torque is required at the transmission output, the values of P_o and P_i will increase with vehicle speed and transmission speed ratio, r. In this situation the maximum actual variator power, P_v, can be minimised by using a system where the maximum value of P_v / P_i occurs at r_{min} (i.e. low vehicle speed and input power) rather than at r_{max} where vehicle speed and input power are higher. By considering the reverse case of flywheel charging (where the flywheel connection is the output and the vehicle connection is the input), it is clear that the maximum value of P_v / P_i should now occur at r_{max} (i.e. high flywheel speed and low vehicle speed), which is achieved using an input-coupled arrangement. The transmission configuration can therefore remain the same, while the direction of power-flow reverses, changing it from output-coupled during powering to input-coupled during regenerative braking. To ensure clarity, the term 'final-drive coupled' (FDC) is again used to define this particular configuration without needing to specify the direction of power-flow.

The results of this simple analysis highlight a number of important factors;

i. Power-split operation (without power recirculation) can only be achieved with a reduction in the transmission speed range relative to the variator itself (i.e. r_t is always less than φ_t). Compared to a direct variator transmission delivering the same amount of energy to the vehicle, the reduced ratio range means that a lower proportion of the flywheel energy is transmitted during the variator-controlled phase. This is likely to result in a lower overall efficiency due to losses during the brake and clutch controlled phases.

ii. IC and OC configurations are kinematically equivalent as they can be sized to achieve the same values of r_{min} and r_{max} by choosing an appropriate R for a given value of φ_t.

iii. In terms of variator power, the FDC configuration is likely to be more suited to flywheel transmission applications as the maximum value of P_v / P_i occurs at the minimum value of P_i (assuming constant output torque).

This analysis is limited as it considers only the variator controlled phase of operation, and provides no way of identifying a suitable compromise between transmission performance, variator power capacity and flywheel energy capacity. A thorough investigation is therefore required in order to quantify the effects of component efficiencies and gearing ratios on the overall performance of single regime variator-controlled flywheel transmissions. This is performed for both FDC and FWC transmissions using the independent analysis approach introduced in Chapter 4, as described in the following section.

5.2.2. Independent analysis of single regime variator-controlled PSTs

The IAM can be applied to the FDC and FWC variator-controlled PST configurations, with the results again providing a general FESS design tool. While the brake and clutch controlled phases of these transmissions can be analysed using the method described in Chapter 4, a different approach is required during the operating phase when the gear ratio of the variator is continuously changing. This is due to the fact that while the total energy dissipated in the variator during this phase is independent of time, it is not possible to derive an explicit expression for this. It is important however, that these variator losses are considered in the analysis as variator efficiencies can be significantly lower than those for fixed gearing, and their effect on the overall transmission operation should therefore be quantified. This can be done by creating a quasi-static time-step based model of each variator-controlled PST. A constant efficiency has been assumed for the variator component, allowing the losses to be quantified by numerically integrating the power-flow through the variator. The independent analysis method again assumes that there are no losses at the vehicle or flywheel, as justified for brake and clutch controlled transmission in Chapter 4.

Transmission operation during flywheel discharge is modelled by identifying the limiting overall transmission speed ratios for operation in brake, clutch and variator controlled phases. The initial conditions for the analysis are always a vehicle speed of zero, and a fully charged flywheel (i.e. SOC = 100%). A time-step based program has been developed using the Matlab/Simulink software, and consists of separate modules describing the operation of each phase (clutch, variator and brake controlled). These modules calculate the appropriate torque being exerted on the vehicle and flywheel during each time-step, and therefore the acceleration and speed of the vehicle and flywheel. Once the condition is reached where no

further discharge of the flywheel is possible, the program terminates and the overall discharge performance of the transmission is assessed.

The performance of the FESS during flywheel charging is assessed by identifying the limiting transmission speed ratios for operation in each phase. While the operating limits for the variator-controlled phase remain the same as during flywheel discharge, the reversal of power flow in the transmission changes the sequence in which clutch, variator and brake controlled operation is possible. Using these new operating limits, a backwards calculation can be performed using exactly the same modules as for the discharge case to describe each phase of operation, with the same initial conditions of zero vehicle speed and SOC = 100%, and a final condition of $DOD_{ov} = (DOD_{ov})_{\text{discharge}}$. This requires that the PGS and variator efficiencies used during the discharge calculation are inverted, due to the reversal of the direction of power-flow in all branches of the transmission. This method therefore identifies the minimum initial braking speed required to fully recharge the flywheel, ensuring that the overall charging performance of the transmission is assessed.

This analysis provides a well defined spectrum of operation for the system, and allows the performance and requirements to be characterised. The results therefore provide a rigorous basis from which a range of other factors can be investigated, including;

i. Regenerative braking and flywheel powered acceleration outside this range of operation (for example at higher vehicle speeds)
ii. The effect of losses at the vehicle and flywheel (which will increase the minimum vehicle speed required for full recharge of the flywheel)

These issues are considered in more detail in Chapters 6 and 7.

The calculation procedure for the independent analysis of power-split transmission is therefore as follows;

i. Specify values of η_{pgs} and η_{var}
ii. Specify values of R^* and R_{eq} * (which can be defined for FDC and FWC configurations as described in Chapter 4)
iii. Run time-step based computational model of a particular transmission configuration for flywheel powered acceleration to obtain DOD_{ov}, $\eta_{\text{discharge}}$, $\max(T_{var}^*)_{\text{discharge}}$ and $\max(\omega_{var}^*)_{\text{discharge}}$
iv. Run time-step based computational model of transmission configuration for flywheel charging to obtain η_{charge}, $\max(T_{var}^*)_{\text{charge}}$ and $\max(\omega_{var}^*)_{\text{charge}}$

v. Assess $\eta_{\text{round-trip}}$ and $P_{var,\ rated}$*

vi. Repeat steps (i) to (v) for a range of R* and R_{eq}* values to produce contour maps of the key performance parameters

This procedure is used to perform an independent analysis of both FDC and FWC variator-controlled PSTs as described in the following section.

a) FDC variator-controlled PST

The first PST considered is the FDC configuration, where a variator, V, is connected between branches 2 and 3 of a PGS is shown below.

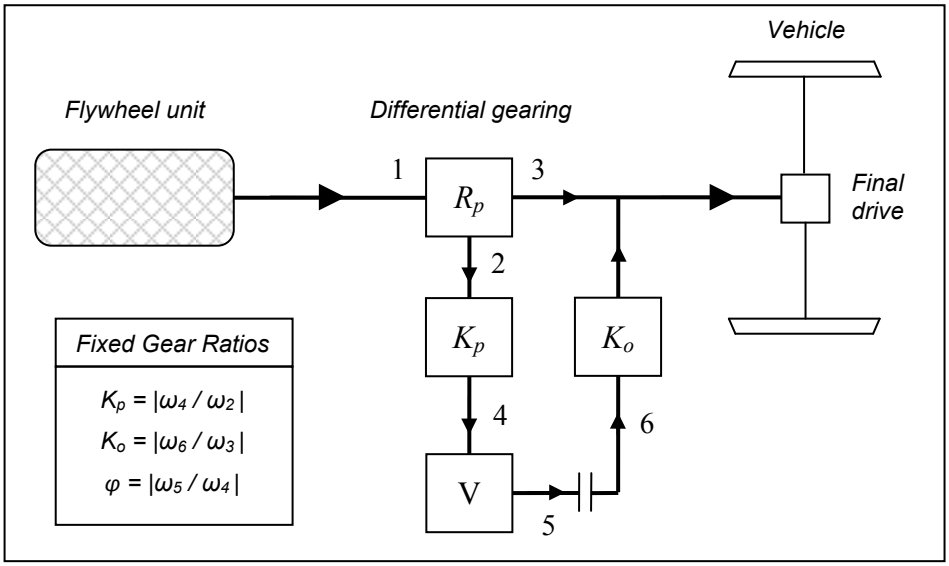


Figure 5-5 – Schematic diagram of FDC variator-controlled PST configuration (arrows show direction of power-flow during clutch/variator controlled flywheel discharge)

Transmission operating modes during flywheel discharge

i. Clutch-controlled operation phase

This occurs when the speed of shaft 6 is lower than the speed of shaft 5 using the minimum variator ratio;

$$\varphi_{\min} > \frac{K_o}{K_p} \frac{\left|\left(1 - R_p\right)\right|\omega_3}{\left(R_p \omega_1 - \omega_3\right)} \tag{5-14}$$

The output torque from the transmission is controlled by the torque at the clutch. The relationship between transmission input and output torque is given by;

$$\left(\frac{T_{fd}}{T_{fw}}\right)_{discharge} = -\frac{\eta_p}{R_p}\left(1+\left|\left(1-R_p\right)\right|\frac{\eta_{\text{var}}K_o}{\varphi_{\min}K_p}\right) \tag{5-15}$$

ii. Variator-controlled operation phase

This occurs when the clutch is locked and the required speed ratio across the variator lies within the operating limits;

$$\varphi_{\min} < \varphi < \varphi_{\max} \qquad \text{where} \qquad \varphi = \frac{K_o}{K_p}\frac{\left|\left(1-R_p\right)\right|\omega_3}{\left(R_p\omega_1-\omega_3\right)} \tag{5-16}$$

The output torque from the transmission is then equal to;

$$\left(\frac{T_{fd}}{T_{fw}}\right)_{discharge} = -\frac{\eta_p}{R_p}\left(1+\left|\left(1-R_p\right)\right|\frac{\eta_{\text{var}}K_o}{\varphi K_p}\right) \tag{5-17}$$

iii. Brake-controlled operation phase

Once the variator ratio required to connect the carrier and ring branches reaches the maximum limit ($\varphi = \varphi_{max}$) power can no longer be transmitted;

$$\varphi_{\max} < \frac{K_o}{K_p}\frac{\left|\left(1-R_p\right)\right|\omega_3}{\left(R_p\omega_1-\omega_3\right)} \tag{5-18}$$

The clutch is then disengaged and braking is applied at branch 2 of the PGS in order to continue discharging the flywheel. The output torque is therefore;

$$\left(\frac{T_{fd}}{T_{fw}}\right)_{discharge} = -\frac{\eta_p}{R_p} \tag{5-19}$$

FDC Results

As with the analysis of the brake/clutch controlled transmission described in Chapter 4, the transmission efficiency and flywheel DOD_{ov} of the FDC variator-controlled PST are found to be functions of the normalised PGS ratio, R_p*, and a normalised equivalent PGS ratio, R_{eq}*, relating to the final condition of the clutch controlled power-split phase between branches 2 and 3. The value of R_{eq} is therefore a function of R_p, K_p, K_o and φ_{min} as defined in the previous chapter and restated in Equation 5-20;

$$R_{eq} = \frac{R_p}{\left(1+\left|\left(1-R_p\right)\right|\frac{K_o}{\varphi_{\min}K_p}\right)} \tag{5-20}$$

It should also be noted that R_{eq} represents the minimum overall transmission ratio that can be achieved during variator-controlled operation, and therefore corresponds to the variable $r_{\min}$ used in Section 5.2.1. The term R_{eq} is used in the subsequent analysis in order to maintain consistency with the analysis of clutch-controlled PSTs presented in Chapter 4. The normalised variator torque, speed and rated power are expressed in the same form as for the FDC clutch-controlled transmissions;

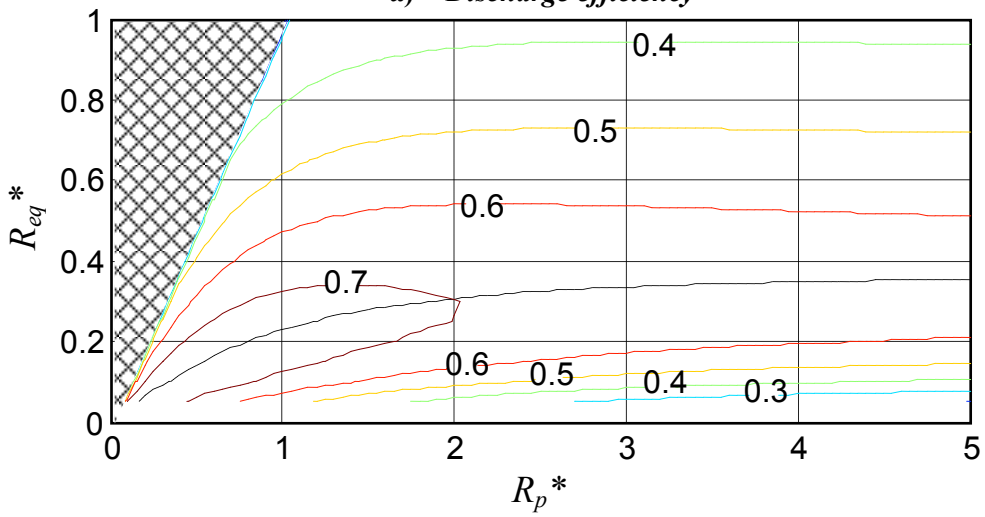
$$\left(T_{\text{var}}*\right)_{FDC} = K_o \left| \frac{T_{\text{var}}}{T_{fd}} \right| \tag{5-21}$$

$$\left(\omega_{\text{var}}*\right)_{FDC} = \frac{1}{K_o} \left| \frac{\omega_{\text{var}}}{\omega_{fw,\max}} \right| \sqrt{\frac{J_{fd}}{J_{fw}}} \tag{5-22}$$

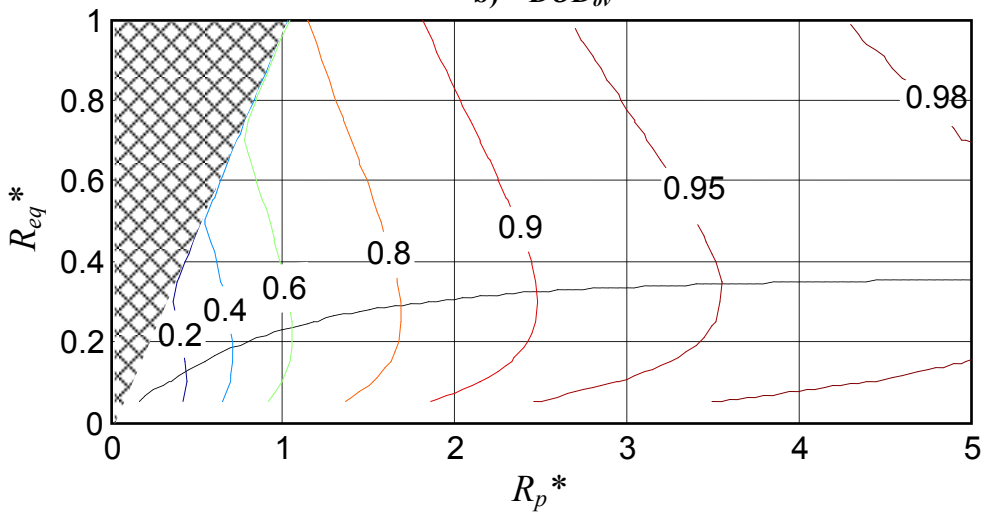
$$P_{\text{var},rated}* = \frac{\max\left(T_{\text{var}}\right)\max\left(\omega_{\text{var}}\right)}{T_{fd}\omega_{fw,\max}} \sqrt{\frac{J_{fd}}{J_{fw}}} = \max\left(T_{\text{var}}*\right)\max\left(\omega_{\text{var}}*\right) \tag{5-23}$$

By plotting discharge and round-trip efficiencies, DOD_{ov}, U and $P_{var,\,rated}$* as functions of R_p* and R_{eq}* a set of independent transmission performance maps can be produced for specified efficiencies of the PGS and variator. It is clear from Equation 5-20 that $|R_{eq}|$ must always be smaller than $|R_p|$ in order to prevent power recirculation. The performance maps are therefore only valid for the region in which $R_p* > R_{eq}*$. These results again form the basis of a design tool to identify suitable transmission parameters for any application of the proposed flywheel transmission, and are shown below for the FDC variator-controlled transmission with η_{var} = 0.85, η_{pgs} = 0.95.

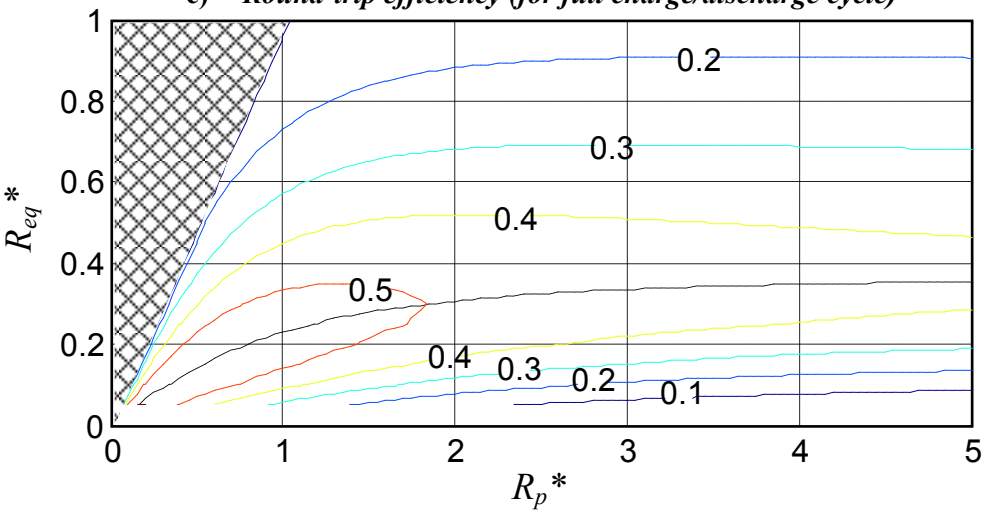
a) *Discharge efficiency*



b) *DOD_{ov}*



c) *Round-trip efficiency (for full charge/discharge cycle)*



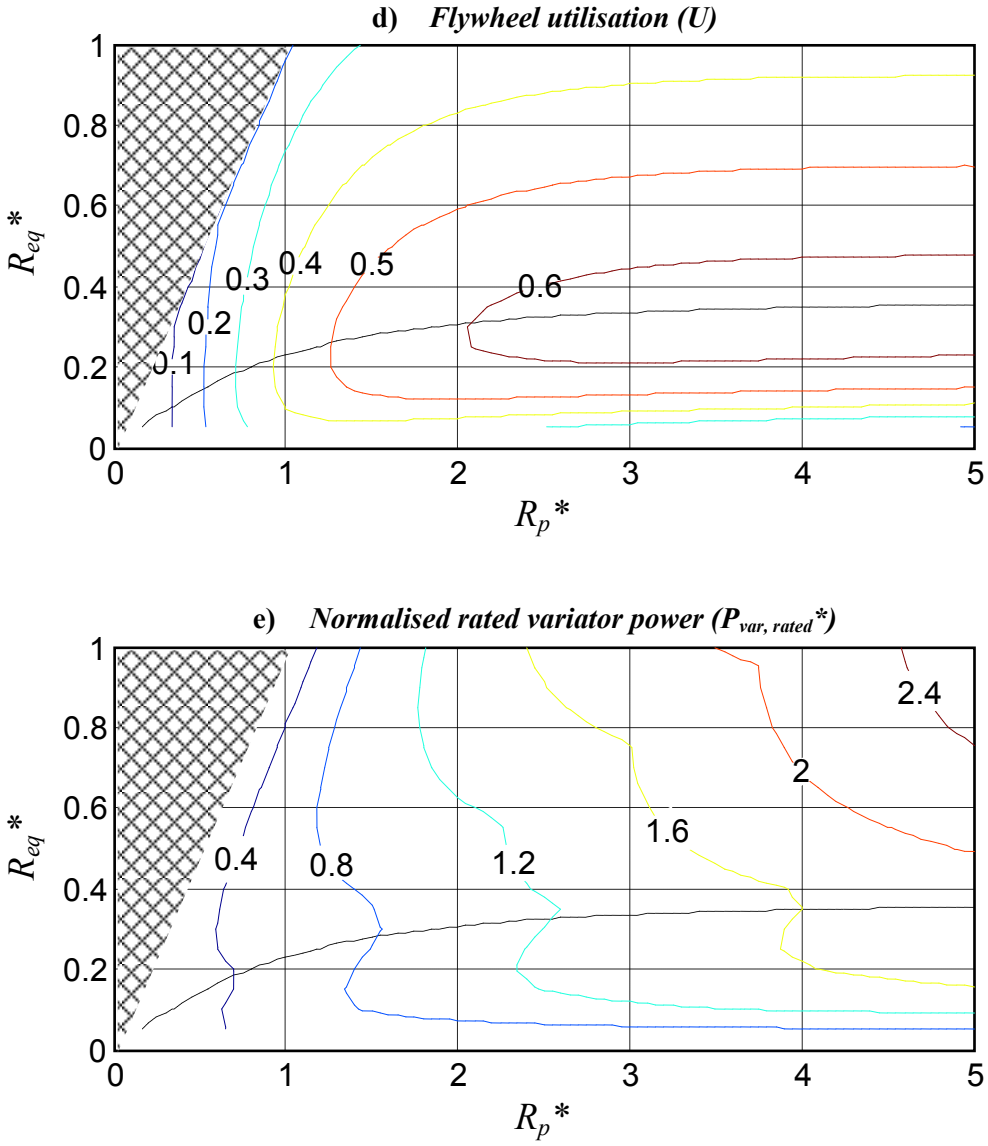


Figure 5-6 – Contour maps for a FDC variator-controlled PST showing (a) $\eta_{discharge}$, (b) DOD_{ov}, (c) $\eta_{round\text{-}trip}$, (d) U and (e) $P_{var, rated}$* as functions of R* and R_{eq}* (with η_{var} = 0.85, η_{pgs} = 0.95) – dotted line shows min($P_{var, rated}$*) w.r.t. U

Figures 5-6 (d) and (e) shows that values of R* and R_{eq}* can be chosen in order to achieve a particular flywheel utilisation with minimum normalised variator power. These values are indicated by the heavy dotted line in all the performance maps of Figure 5-6. Furthermore, it is apparent for Figure 5-6 (a) that these values coincide with the maximum possible values of transmission efficiency for a given U, which occurs when the losses in the brake and clutch controlled phases are equal as shown in Figure 5-7.

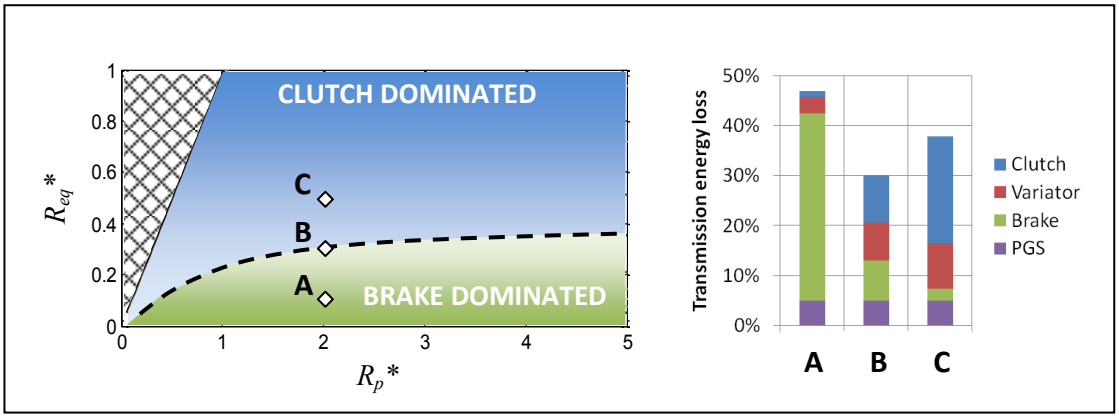


Figure 5-7 – Illustration of the effect of R_{eq}* values on transmission losses (shown as percentage of transmission input energy dissipated in components)

A conclusion of the independent analysis is therefore that the FDC variator-controlled flywheel transmission should always be sized to operate at a point on this 'minimised power' curve.

It is important to note that while the normalised rated variator power is almost identical during full charge and full discharge events, $\max(T_{var}^*)_{FDC}$ occurs during charging, and $\max(\omega_{var}^*)_{FDC}$ occurs during discharging. The overall rated variator power must therefore be calculated using these maximum values. This is encapsulated in the following two Figures which form the design tool for a FDC variator-controlled flywheel transmission and provide all the information required to characterise the gearing ratios, variator size and transmission performance for a particular application.

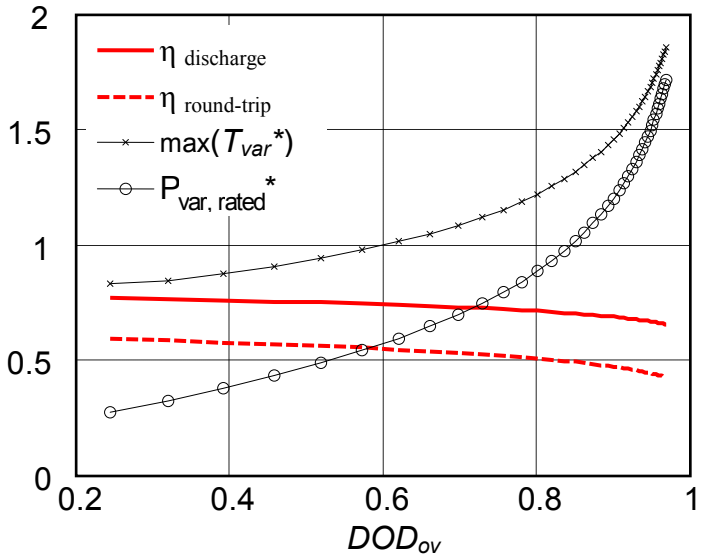


Figure 5-8 – Characteristics of FDC variator-controlled PST when $P_{var,\,rated}$* is minimised for a given U

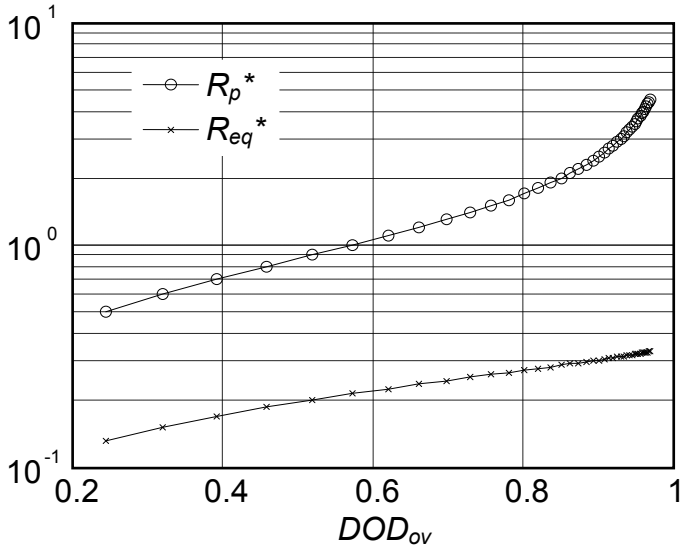


Figure 5-9 – Values of R_p* and R_{eq}* which minimise $P_{var,\,rated}$* for a given U

Figures 5-8 and 5-9 provide all the information necessary to define the performance and design requirements of the FDC variator-controlled PST.

b) FWC variator-controlled PST

An alternative configuration for a single regime PST is to connect the variator between branches 1 and 2 of the PGS, with associated fixed ratio gearing. This forms a 'flywheel-coupled' (FWC) variator-controlled PST as illustrated in Figure 5-10.

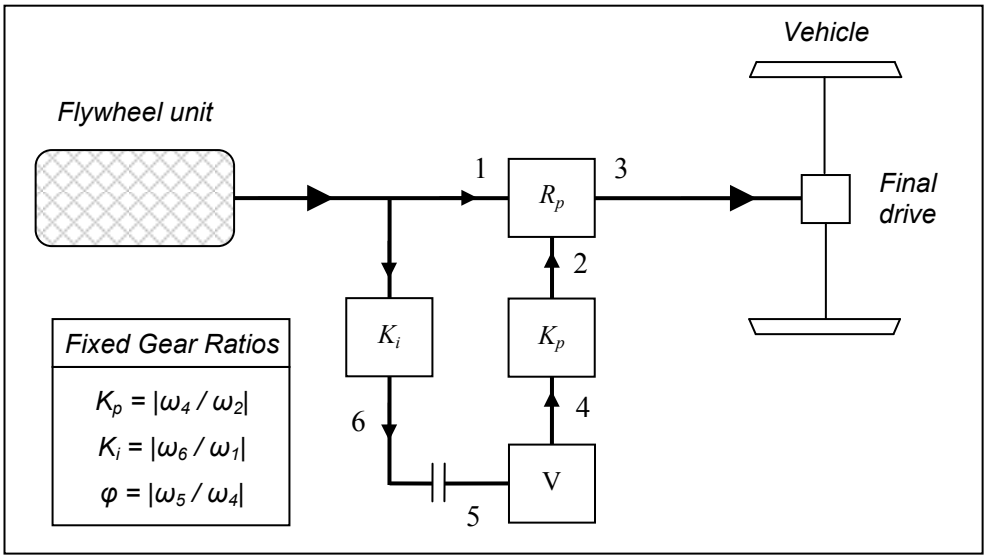


Figure 5-10 – FWC variator-controlled PST (arrows show direction of power-flow during flywheel discharge)

By considering the torque and speed relationships for the PGS, it can be shown that the power-split operation illustrated in Figure 5-10 is only possible when;

$$\frac{\omega_2}{\omega_1}\frac{\left|R_p\left(1-R_p\right)\right|}{R_p\left(1-R_p\right)} \geq 0 \qquad (5\text{-}24)$$

As this ratio is always negative for $\omega_3 = 0$ (i.e. when the vehicle is stationary), an initial phase of brake-controlled operation (with braking applied at branch 2) is required to accelerate the vehicle from stationary. Once $\omega_2 = 0$, clutch-controlled power-split is possible with the variator held at its maximum ratio, φ_{max}. When the clutch locks, the variator can be used to control the power flow through the transmission until the minimum ratio is reached, and the transmission can no longer discharge the flywheel.

Transmission operating modes during discharge

The three transmission operating modes are similar to the FDC variator-controlled PST described above, but are implemented in a different order;

i. Brake-controlled operation phase

While the following relationship between the speeds of branches 1 and 2 is true, power is transmitted by applying a braking torque at the ring.

$$\frac{\left|R_p\left(1-R_p\right)\right|}{R_p\left(1-R_p\right)}\left(\frac{\omega_2}{\omega_1}\right)<0 \tag{5-25}$$

ii. Clutch-controlled operation phase

This is required when the speed of shaft 6 is higher than the speed of shaft 5 using the maximum variator ratio;

$$\frac{\left|R_p\left(1-R_p\right)\right|}{R_p\left(1-R_p\right)}\left(\frac{\omega_1 K_i}{\omega_2 K_p}\right)>\varphi_{\max} \tag{5-26}$$

The output torque from the transmission is controlled by the torque at the clutch. The relationship between transmission input and output torque is then given by;

$$\left(\frac{T_1}{T_3}\right)_{discharge}=-\frac{R_p}{\eta_p}\left(1+\left|\left(\frac{1-R_p}{R_p}\right)\right|\frac{K_i}{\eta_{\text{var}}\phi_{\max}K_p}\right) \tag{5-27}$$

iii. Variator-controlled operation phase

This occurs when the clutch is locked and the required speed ratio across the variator lies within the following operating limits;

$$\varphi_{\max}>\varphi>\varphi_{\min} \qquad \text{Where} \quad \varphi=\frac{\left|R_p\left(1-R_p\right)\right|}{R_p\left(1-R_p\right)}\left(\frac{\omega_1 K_i}{\omega_2 K_p}\right) \tag{5-28}$$

The output torque from the transmission is then given by;

$$\left(\frac{T_1}{T_3}\right)_{discharge}=-\frac{R_p}{\eta_p}\left(1+\left|\left(\frac{1-R_p}{R_p}\right)\right|\frac{K_i}{\eta_{\text{var}}\phi\, K_p}\right) \tag{5-29}$$

FWC Results

The results from the analysis of the FWC variator-controlled PST can again be used to show transmission efficiency, DOD_{ov} and U as contour plots with axes R_p* and R_{eq}* for a given PGS and variator efficiency. The value of R_{eq}* now relates to the clutch controlled power-split phase between branches 1 and 2, and is therefore a function of R_p, K_p, K_i and $\varphi_{\max}$ as defined for FWC clutch-controlled transmissions in Chapter 4, and restated in Equation 5-30.

$$R_{eq}=\left(R_p+\left|\left(1-R_p\right)\right|\frac{K_i}{\varphi_{\max}K_p}\right) \tag{5-30}$$

The normalised variator torque and speed can be defined as below, allowing the normalised rated variator power to again be calculated.

$$\left(T_{\text{var}}*\right)_{FWC} = K_i \left|\frac{T_{\text{var}}}{T_{fd}}\right| \sqrt{\frac{J_{fd}}{J_{fw}}} \tag{5-31}$$

$$\left(\omega_{\text{var}}*\right)_{FWC} = \frac{1}{K_i} \left|\frac{\omega_{\text{var}}}{\omega_{fw,\max}}\right| \tag{5-32}$$

Using these contour maps, the minimum rated variator power required to achieve a particular value of U can again be identified. In contrast to the results for the FDC configuration, this 'minimised power' curve does not match the conditions for maximum efficiency. At maximum U a large degree of variator-controlled operation is achieved which results in a relatively high efficiency. As U decreases however, the brake-controlled phase begins to dominate leading to a sharp decrease in efficiency. These results are encapsulated in the following two Figures which form the design tool for the FWC variator-controlled PST.

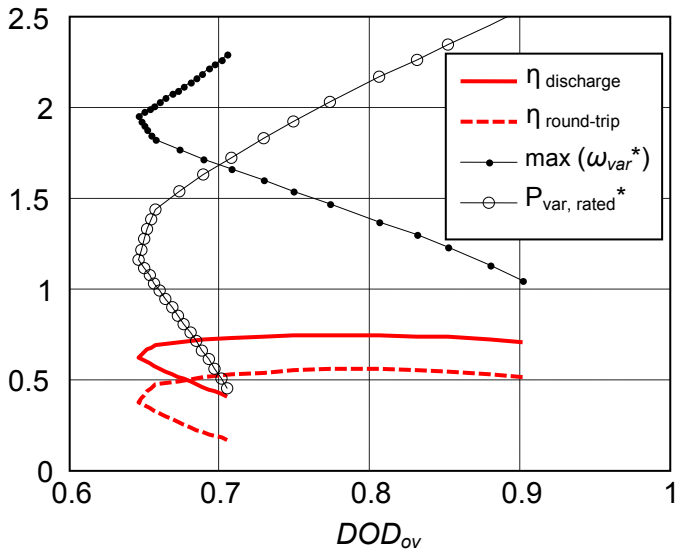


Figure 5-11 – Characteristics of FWC variator-controlled PST when $P_{var,\,rated}$* is minimised for a given U

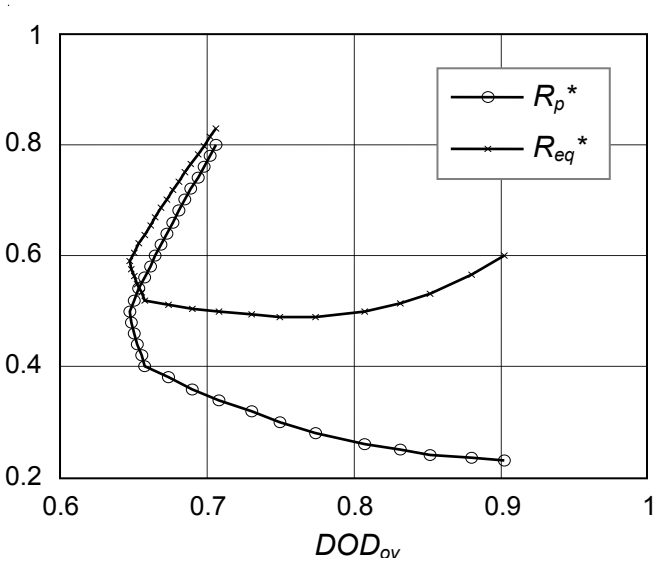


Figure 5-12 – R_p* and R_{eq}* of a FWC variator-controlled PST which minimise $P_{var,\ rated}$* for a given U

Figures 5-11 and 5-12 provide all the information necessary to define the performance and design requirements of the FWC variator-controlled PST. The two single regime variator-controlled PSTs can now be compared with the direct variator transmission.

5.2.3. Comparison of single regime variator-controlled transmissions

The strength of the independent analysis method presented in this Thesis is the ability to perform a rigorous comparison between flywheel transmissions of different configurations. The comparison of single regime transmissions is performed on the basis of flywheel utilisation by using the data obtained for the 'minimised power' lines (i.e. operating with minimum $P_{var,\ rated}$* for a given U) of the power-split configurations. The key parameters are the transmission efficiency and the required rated variator power, and these are shown as functions of U for each transmission in Figure 5-13 (note that the definition of $P_{var,\ rated}$* is the same for all three transmissions, although the definitions of T_{var}* and ω_{var}* are different).

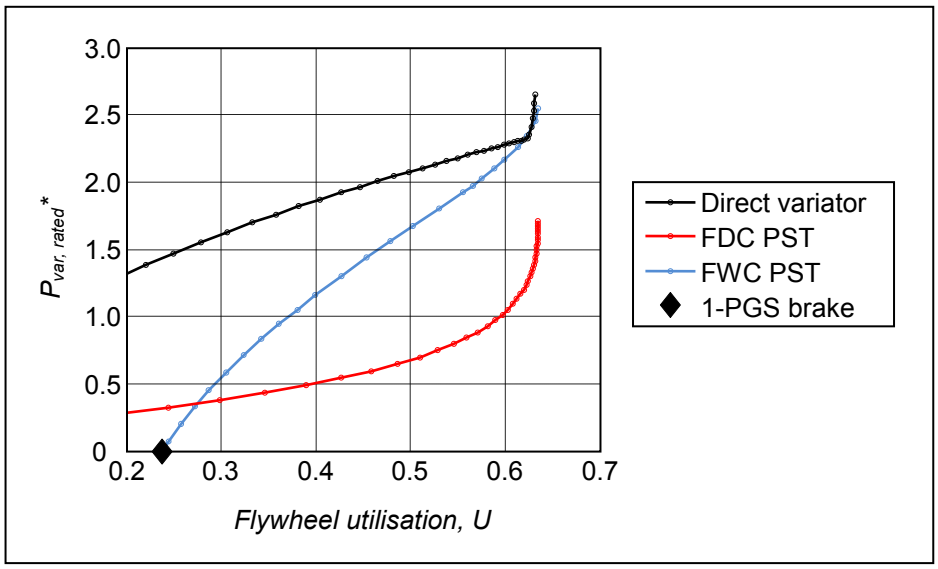


Figure 5-13 – Normalised rated variator power as a function of *U* for 1-regime flywheel transmissions

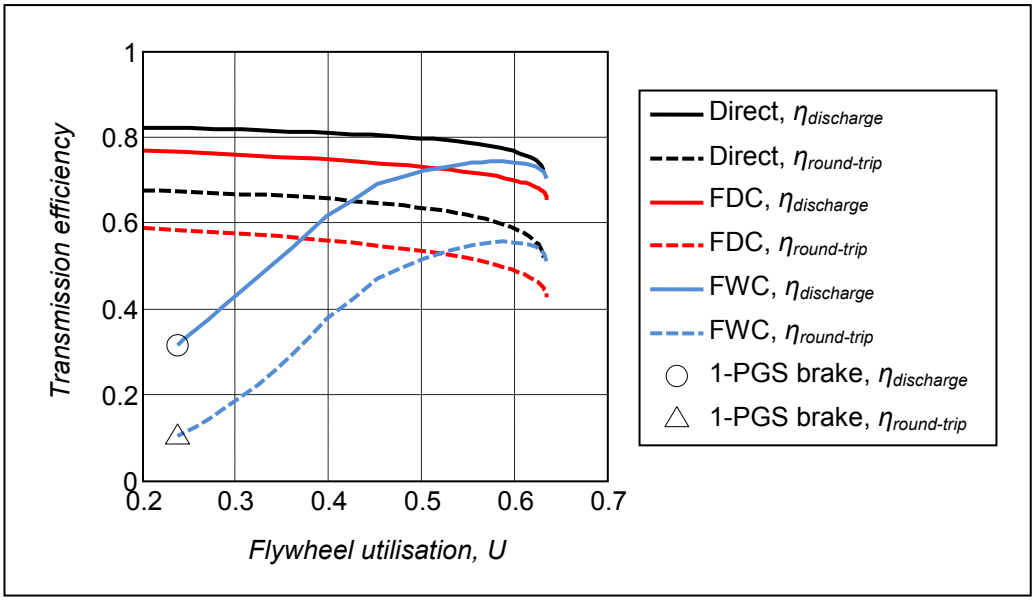


Figure 5-14 – Transmission efficiencies as a function of *U* for 1-regime flywheel transmissions

A constant value of *U* represents the case where each transmission has been sized in order to deliver the same amount of energy to the vehicle from identical flywheels. This would ideally be achieved with high efficiency (allowing a high degree of energy recovery during braking) and low rated variator power (reducing the size, cost and mass of the variator).

There are a number of conclusions to be made from the results shown in Figures 5-13 and 5-14, as discussed below.

i. Both single regime power-split variator-controlled transmissions can achieve the same U with lower rated variator power than the direct transmission

ii. Both FDC and FWC configurations have lower overall efficiency than the direct variator, as power-split reduces the ratio coverage of the variator-controlled phase. This is illustrated in Figure 5-15 for three configurations using an identical flywheel to achieve a flywheel utilisation of 60%. Constant and zero variator speed ratio values correspond to phases of clutch and brake controlled operation respectively. The reduced ratio coverage for the PSTs means that an increased proportion of the flywheel energy has to be delivered to the vehicle (with lower efficiency) during the clutch and brake controlled phases. A breakdown of the percentage of total transmission input energy dissipated in the transmission components of each configuration is shown in Figure 5-16.

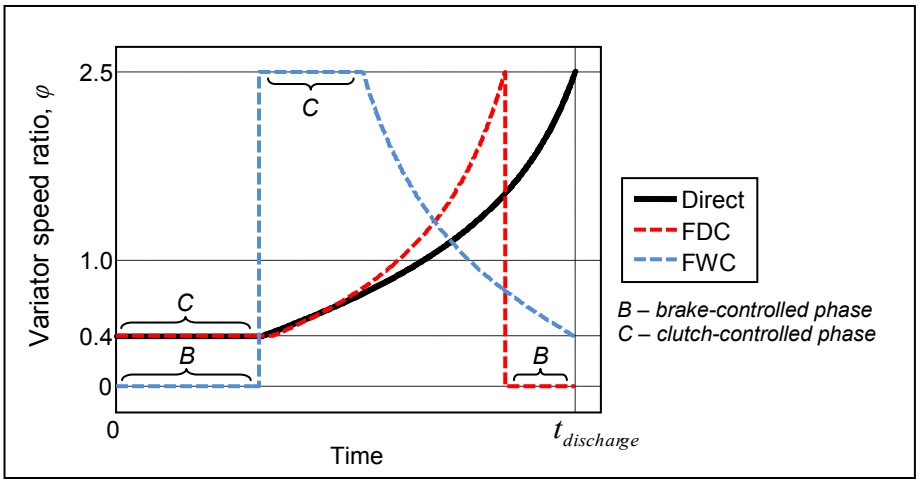


Figure 5-15 – Variator speed ratio as function of time for the three single regime transmissions during flywheel discharge with optimum conditions for U = 60% and the same maximum flywheel KE

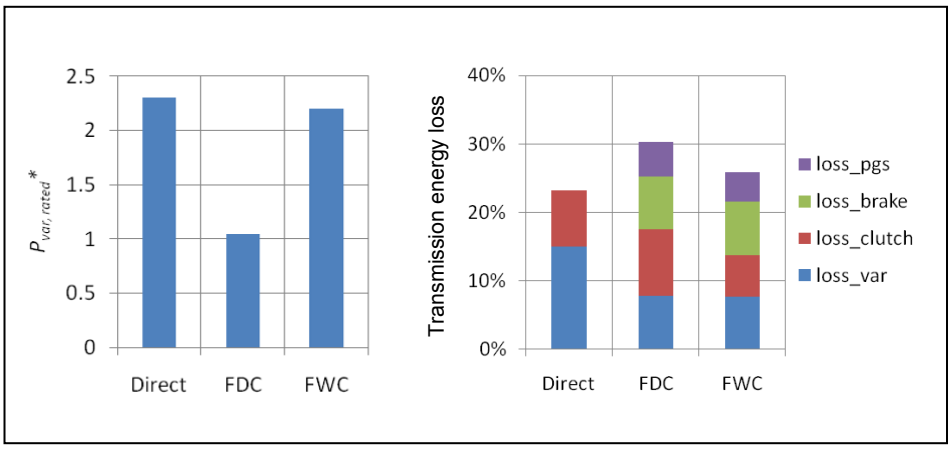


Figure 5-16 – Normalised rated variator power and breakdown of transmission losses for single regime variator-controlled transmissions during flywheel discharge with $U = 60\%$ (transmission losses expressed as % of total transmission input energy)

As expected from the ideal power-split analysis presented in Section 5.2.1 the FDC configuration achieves the lowest rated variator power for a given U, and provides a reasonable compromise between efficiency and variator size. This can be illustrated by considering the particular case when $U = 60\%$;

- FDC discharge efficiency is 8% lower than direct transmission
- FDC rated variator power is 60% lower than direct transmission

The round-trip efficiency of the FDC variator-controlled transmission is around 50% when $U = 60\%$. This is not particularly high, suggesting that there is scope for improvement in transmission performance using multi-regime PSTs.

5.3. Single PGS, 2-regime variator-controlled transmissions

The results of the previous section show that power-split arrangements can reduce variator losses and size, but that the reduction in the ratio coverage during variator-controlled operations leads to a relative decrease in overall transmission efficiency for a given U. Multi-regime transmissions allow the variator to operate for a larger proportion of the charge/discharge cycle. This can increase the overall efficiency of the transmission by reducing the proportion of energy dissipated in the brake and clutch controlled phases. The effect on the rated variator power requirement will depend on the configuration. Two classes of 2-regime transmission consisting of a single PGS are considered;

- Single PGS with combined FDC/FWC power-split regimes (described in Section 5.3.1)
- Single PGS with 2 variator-controlled regimes and synchronous gear shift which can be achieved in FDC and FWC arrangements (both of which are described in Section 5.3.2)

In order to assess the efficiency and rated variator power the independent analysis method has been applied to each of these transmissions, and a comparison of performance is made in Section 5.3.3.

5.3.1. Combined FDC/FWC 2-regime transmission

The first type of multiple regime power-split configuration considered is a combination of the two single regime PSTs analysed in Section 5.2. This is possible due to the limitations required to prevent power-recirculation in the FDC and FWC configurations, as restated below;

FDC: $$\frac{\omega_2}{\omega_1}\frac{\left|R_p\left(1-R_p\right)\right|}{R_p\left(1-R_p\right)} \leq 0$$

FWC: $$\frac{\omega_2}{\omega_1}\frac{\left|R_p\left(1-R_p\right)\right|}{R_p\left(1-R_p\right)} \geq 0$$

It is clear that power-split operation is possible with an FDC arrangement at low vehicle speeds when $\omega_3 \geq 0$ and $\omega_2/\ \omega_1 \leq 0$. Once the vehicle has reached a speed where $\omega_2/\ \omega_1 \geq 0$ then a FWC arrangement can be used to continue discharging the flywheel. The transmission therefore has 2 regimes of variator-controlled operation, although clutch and brake controlled phases are still required when operating outside the speed ratio limits of the variator. A possible configuration for this type of transmission is illustrated in Figure 5-16.

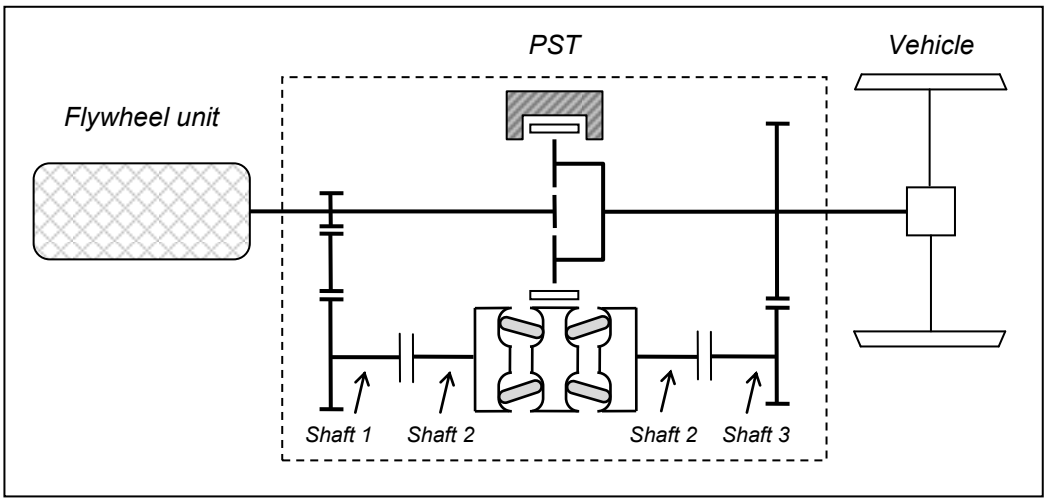


Figure 5-17 – Schematic diagram of possible combined FDC/FWC variator-controlled PST configuration

The sequence of operating phases during flywheel discharge is as follows;

i. Clutch-controlled FDC ($\varphi = \varphi_{min}$)
ii. Variator-controlled FDC ($\varphi_{min} < \varphi < \varphi_{max}$)
iii. Brake-controlled at PGS ring
iv. Clutch-controlled FWC ($\varphi = \varphi_{max}$)
v. Variator-controlled FWC ($\varphi_{max} < \varphi < \varphi_{min}$)

Phases 1 to 3 are identical to the single regime FDC PST. The operating range of the transmission is extended by using these phases to replace the initial brake-controlled phase of the FWC. Phases 4 and 5 are then identical to the single regime FWC PST. The combined FDC/FWC transmission now has 3 DOFs, corresponding to the values of R^*, $(R_{eq}^*)_{FDC}$ and $(R_{eq}^*)_{FWC}$. Analysis of this transmission is therefore performed using the following approach.

Analysis procedure for combined FDC/FWC 2-regime PST:

i. Use the relationship between R^* and $(R_{eq}^*)_{FDC}$ obtained in Section 5.2 for the single regime FDC transmission which gives minimum rated variator power and maximum discharge efficiency for a given U
ii. Vary the values of R^* and $(R_{eq}^*)_{FWC}$ and assess the performance of the combined transmission

By combining both FDC and FWC regimes of power-split in a single 'mode-switching'

transmission it can be shown that the transmission efficiency is improved with little additional gearing. This is due to the extended period of variator-controlled operation, and the reduced power flow thorough the variator which has the associated benefit of reducing the necessary power-rating of the variator device (compared to the FWC PST) when operated over the same range. The performance of this transmission is compared with the other single-PGS transmissions in Section 5.3.3.

5.3.2. Synchronous shift 2-regime transmissions

The second option considered for multi-regime flywheel transmissions is the synchronous gear change 2-regime configuration. This is an extension of the basic single-regime FDC and FWC PSTs described in Section 5.2, and allows an increased range of variator-controlled operation by providing two separate stages of power-split between the flywheel and vehicle. The key feature of these transmissions is that the variator speed ratio at the end of the first stage is the initial value required in the second stage, and that the switch between stages is achieved through the synchronous engagement of clutch elements. The fundamental requirements of this type of transmission for input and output coupled configurations have been characterised by White [92], and the efficiency of an input coupled version (described as a '2-stage PS-CVT') has been independently analysed by Mantriota [101]. The application of these transmissions for flywheel systems has not however been considered. This section therefore applies the independent analysis method to quantify the overall performance (including phases of brake and clutch control) for both FDC and FWC configurations and generate design tools for identification of appropriate system parameters for a given application.

a) FDC synchronous shift configuration

The fundamental constraints for a 2-regime synchronous shift FDC transmission are derived by White [92] for the simple case of a variator and PGS with no additional gearing. The key requirement is that the PGS gear ratio, $R_p > 1$, which is unaffected by the inclusion of the gear ratios shown in Figure 5-18. These gear ratios are required in order to ensure an appropriate range of operation for the variator, and that the synchronous gear change between regimes 1 and 2 is achieved at the point where the variator is operating at its limiting speed

ratio. The required value of K_2 must therefore be chosen so that $\omega_4 = \omega_6$ when operating in regime 1 with $\varphi = \varphi_{max}$. This is achieved when;

$$K_2/K_o = 1/\varphi_{max} \qquad \textit{Requirement for FDC synchronous shift} \qquad (5\text{-}33)$$

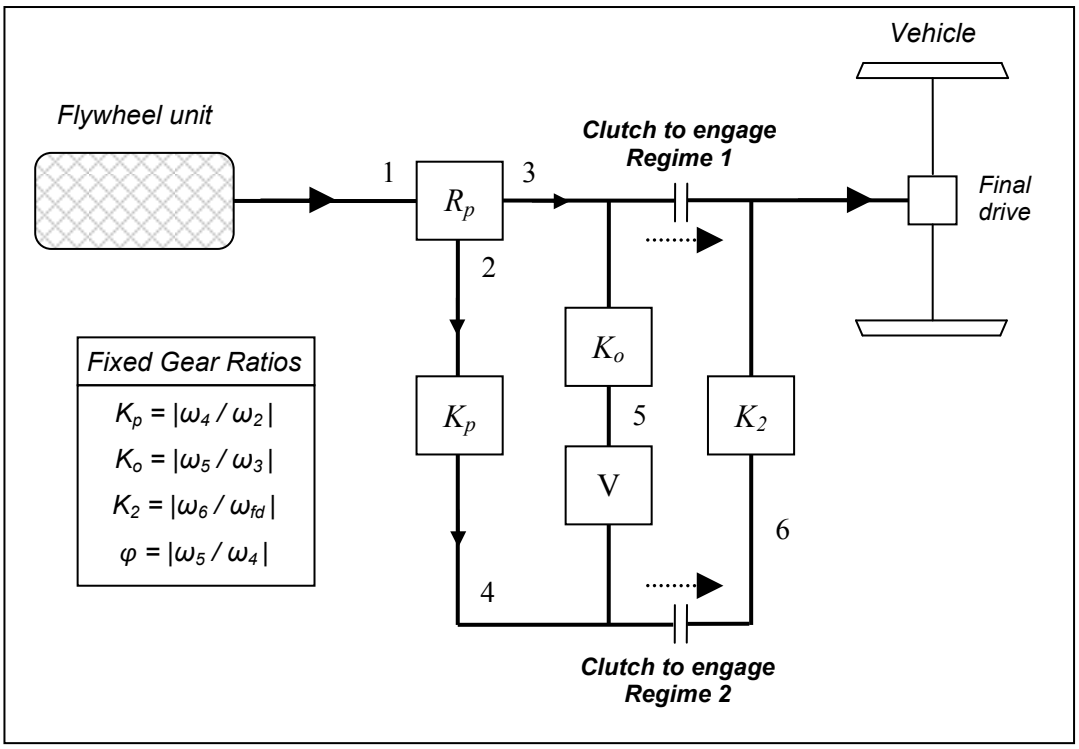


Figure 5-18 – Schematic diagram of FDC synchronous shift PST configuration (dashed arrows show direction of power-flow during each regime of flywheel discharge)

Regime 1 operation is identical to the single regime FDC transmission considered earlier (see Figure 5-5), as the different position of the clutch makes no difference to the proportion of energy dissipated during the clutch-controlled phase. For the case of flywheel discharge, the initial clutch and variator controlled phases of operation are therefore the same. When the variator ratio reaches φ_{max} (at the end of the regime 1 variator-controlled phase) the speeds of shafts 5 and 6 are exactly equal (using the K_2/K_o ratio specified in Equation 5-33) and a synchronous shift to regime 2 is achieved. A second stage of variator-controlled operation is now achieved as the variator speed ratio is decreased, until it reaches φ_{min}. As the vehicle is now connected to branch 2 of the PGS (via the variator), a final phase of flywheel discharge can be achieved by braking branch 3. The flywheel can no longer be discharged once the speed of branch 3 reaches zero.

The same analysis method can therefore be used as for the single stage FDC transmission with R^* and $(R_{eq}^*)_{FDC}$ values defining an operating point, and the conditions required to minimise $P_{var,\,rated}^*$ for a given U identified.

b) FWC synchronous shift configuration

The following constraints apply to the implementation of a 2-regime FWC synchronous shift PST. In order to achieve the required two phases of power-split operation, $0<R_p<1$, as derived by White [92]. Furthermore, to achieve a synchonous gear shift between power-split regimes;

$$K_2/K_i = 1/\varphi_{\min} \qquad \textit{Requirement for FWC synchronous shift} \tag{5-34}$$

A schematic illustration of the required transmission configuration is shown in Figure 5-19.

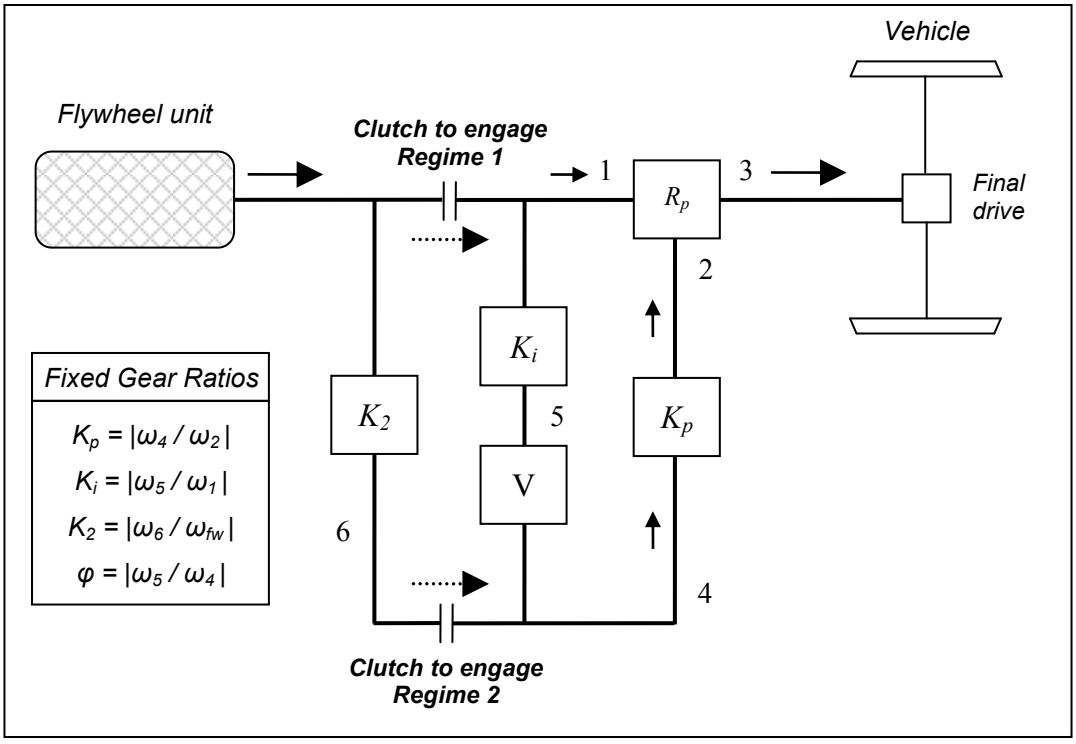


Figure 5-19 – Schematic diagram of FWC synchronous shift PST configuration (arrows show direction of power-flow during flywheel discharge)

This configuration can again be investigated by modifying the existing time-step based computation model of the single regime FWC variator-controlled PST to include the second regime of variator operation. The performance of the FWC 2-regime PST can therefore be

presented in terms of the normalised gear ratios, R^* and $(R_{eq}^*)_{FWC}$, and a 'minimised power' curve can again be identified .

5.3.3. Comparison of multiple regime variator-controlled transmissions

The performance of the three 2-regime PSTs can now be compared with the earlier results for the single regime PSTs as shown in Figure 5-20. This is achieved by using the 'minimised power' curves for each configuration, and comparing the values of discharge efficiency and rated variator power as functions of U.

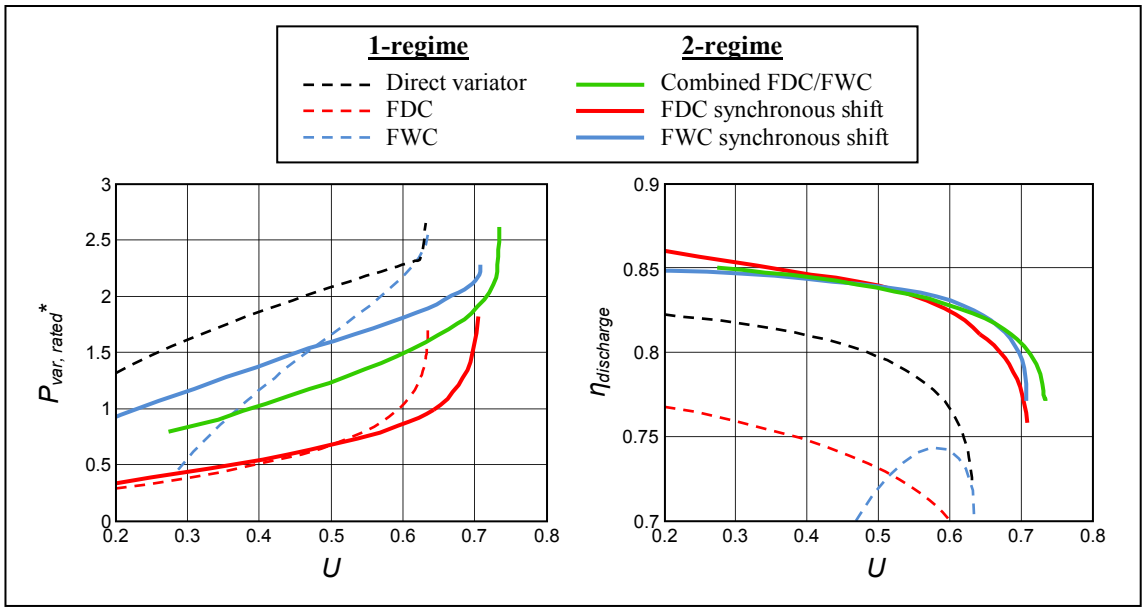


Figure 5-20 – Normalised rated variator power and discharge efficiency as a function of U for 1 and 2 regime flywheel transmissions

Similar values of efficiency as a function of U are obtained for all three 2-regime transmissions. These results illustrate that the efficiency of the transmissions is improved by increasing the proportion of variator-controlled operation. This is clearly seen in Figure 5-21 which shows the variator speed ratio during each of the brake, clutch and variator controlled phases for all 2-regime transmissions when sized to achieve U = 60% with the same flywheel unit.

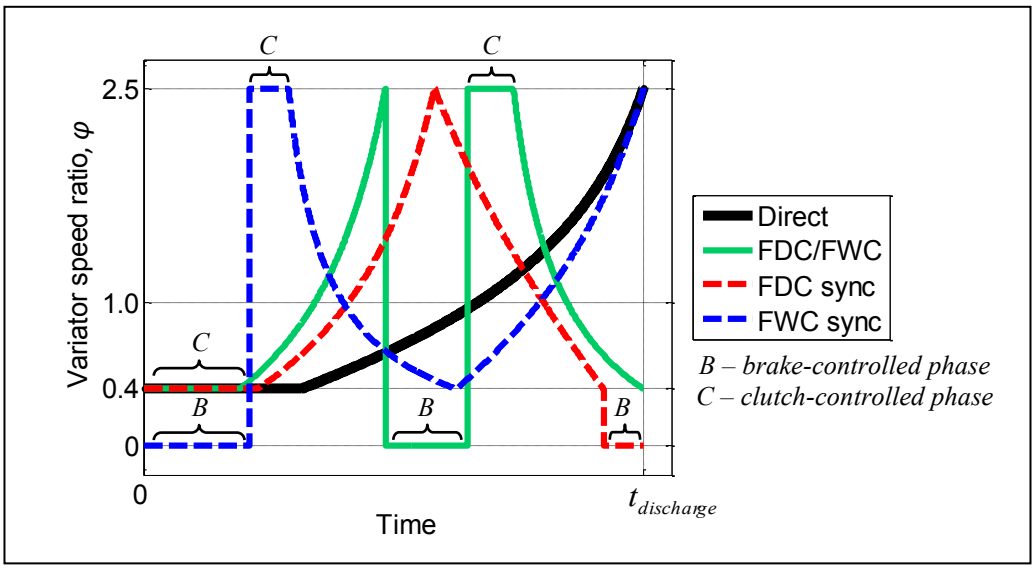


Figure 5-21 – Variator speed ratio as function of time for the three 2-regime PSTs during flywheel discharge with 'minimised power' conditions for U = 60% using the same maximum flywheel KE

A breakdown of the losses which occur in each component of the 2-regime transmissions is given in Figure 5-22.

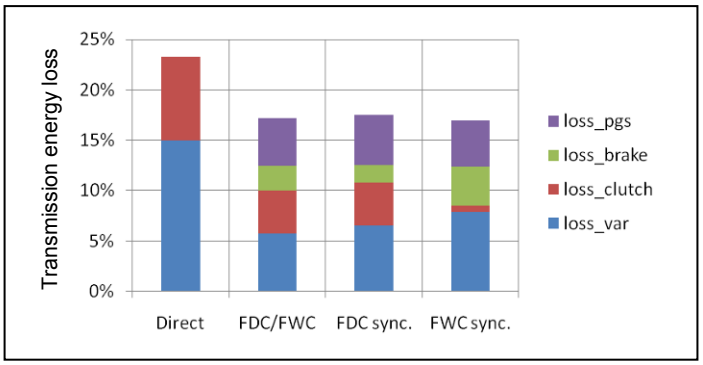


Figure 5-22 – Breakdown of losses for 2-regime variator-controlled PSTs during flywheel discharge with U = 60% (losses expressed as % of total transmission input energy)

The increase in efficiency which is achieved by all three 2-regime transmissions considered allows a higher maximum U to be achieved. There is however no significant decrease in rated variator power when compared with the 1-regime transmission. The FDC synchronous transmission achieves lowest power, but this requires $R_p > 1$ which resticts the practical sizing of the PGS and may require large fixed gear ratios (especially between the high speed flywheel and the PGS). The FWC synchronous and combined FDC/FWC transmission have potentially more practical R_p requirements for FESS use, but have significantly higher rated

variator power, increasing the mass and cost of the system. It is clear from these results that there is a case for investigating more mechanically complex multiple-regime transmissions which can combine the advantages of high efficiency with low variator power rating. Such a transmission is considered in the following section.

5.4. Multiple-regime FDC/DDC transmissions

The three 2-regime transmissions described in Section 5.3.2 all improve transmission efficiency relative to the direct variator configuration but do not achieve a significant reduction in the rated variator power compared to single regime PSTs. This is an important factor in achieving practical systems for high power applications such as rail vehicles. It has already been shown for the CGB-controlled transmission that FDC operation can be extended through use of DDC (dual-differential-coupled) power-split arrangements. This has been shown to achieve high efficiency with large reduction in the power requirement for the CGB, and the same configuration has therefore been applied using variator-control.

Using a 3-PGS configuration as illustrated in Figure 5-23, the system has 6 DOF (the 3 actual and 3 equivalent R^* values) making full optimisation of a time-step based numerical model time consuming. A much simpler approach is to use the characteristic charge and discharge equations derived in Chapter 4 to calculate performance during the brake and clutch controlled phases of operation. The performance of each variator-controlled phase can then be estimated by applying an assumed overall transmission efficiency to relate the initial and final conditions. A good estimate for this overall efficiency is achieved by assuming that 50% of the energy passes through the variator branch. This results in the following estimates of overall transmission efficiency during FDC and DDC variator-controlled phases;

FDC: $\eta_{ov} = \eta_{pgs}(1+\eta_{var})/2$

DDC: $\eta_{ov} = \eta_{pgs}^2(1+\eta_{var})/2$

These approximatations to the transmission efficiency during a variator-controlled phase of operation can be used to find the final vehicle and flywheel speeds for the phase, using conservation of energy with the initial speeds. By using this method, a quick and simple function minimisation procedure can be applied for complete flywheel discharge and charge events. This allows the ‘equalised modes’ method (described for the CGB-controlled PST in Chapter 4) to again be used to identify transmission performance and appropriate gearing

ratios. The results from this analysis can then be used in the full time-step based model of the transmission to obtain the final results.

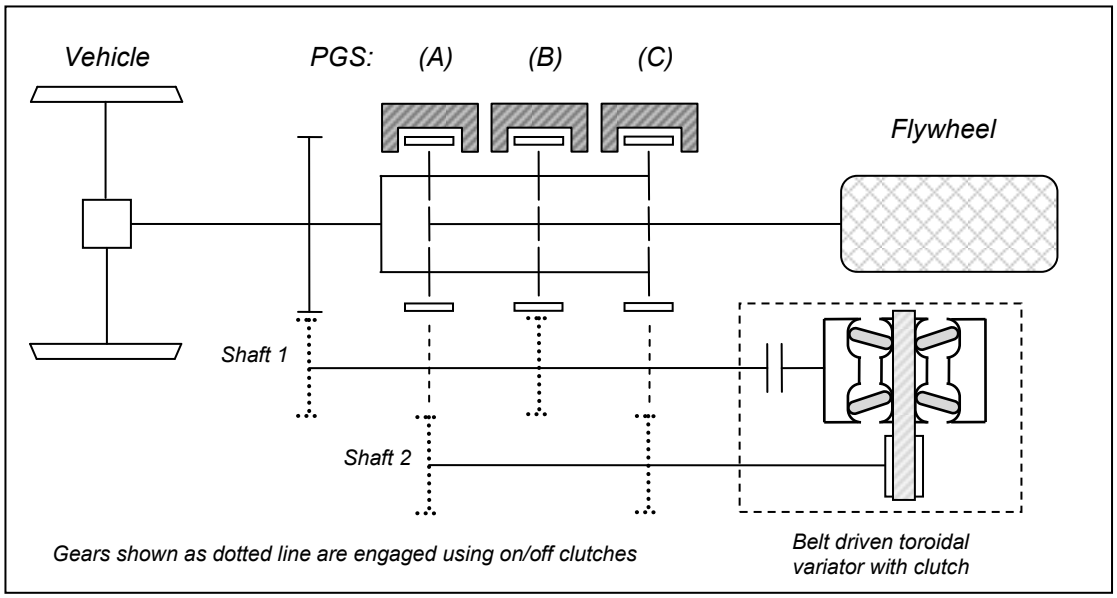


Figure 5-23 – Possible configuration for a 3-PGS FDC/DDC variator-controlled PST

The operating procedure for the 3-PGS variator-controlled PST is illustrated in Figure 5-24. This shows that the transmission consists of three consecutive regimes of clutch-variator-brake controlled operation as power-split is achieved by connecting;

i. Final drive and PGS A,
ii. PGSs A and B,
iii. PGSs B and C,

The brake-controlled phases are again shown with a variator speed ratio of zero for clarity – in reality the speed ratio of the variator would be kept at the final setting of the variator-controlled phase, as this corresponds with the required setting in the subsequent clutch-controlled phase.

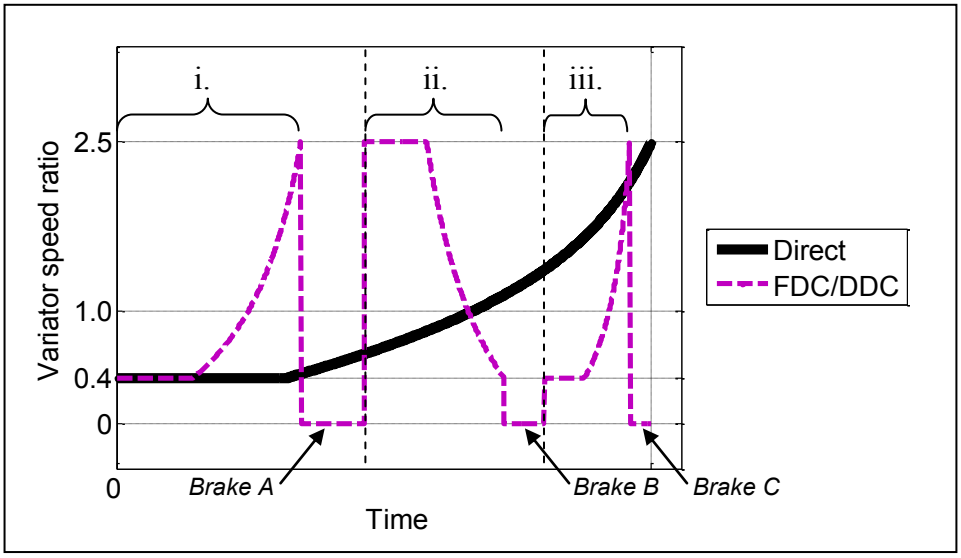


Figure 5-24 – Variator speed ratio as function of time during flywheel discharge with 'equalised modes' for $U = 60\%$

The design tool data for the 3-PGS variator-controlled transmission is presented in Figure 5-25. Together with the constraints of the 'equalised modes' analysis method (defined in Equations 4-60 and 4-61) this provides all the data required to assess the system performance and specify the gearing ratios for a particular application.

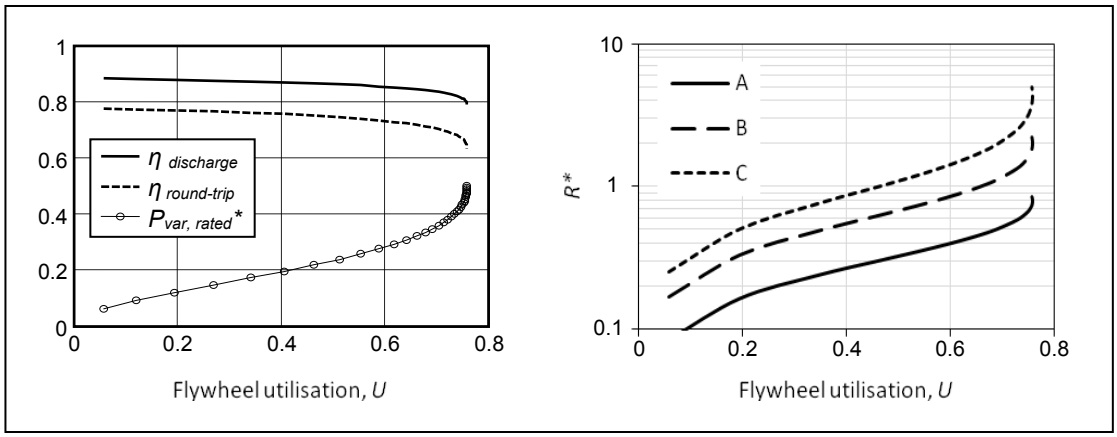


Figure 5-25 – Efficiencies, normalised rated variator power and normalised PGS ratios as functions of U for 3-PGS FDC/DDC variator-controlled PST ($\eta_{var} = 0.85$, $\eta_{pgs} = 0.95$)

These results show that high efficiency and low rated variator power can be achieved by using multiple PGSs in the combined FDC/DDC configuration. While this appears to be the most suitable option for high power applications such as rail, the overall system mass is an important factor. The specific energy capacity of the different variator-controlled flywheel

systems is therefore considered for the case of a typical regional diesel train in the following section.

5.5. Regional rail application of variator-controlled PSTs

The design tools which have been generated for each transmission configuration can be used to calculate a specific energy capacity for the FESS. By specifying the requirements of an FESS for regional rail (including a useful energy storage capacity), gearing ratios can be chosen in order to minimise mass. As in Chapter 4 the maximum specific energy capacity of the systems is presented as a function of the useful energy that can be delivered to the vehicle from a fully charged flywheel, with the energy available during braking limited to 40 MJ. These results are shown in Figure 5-27.

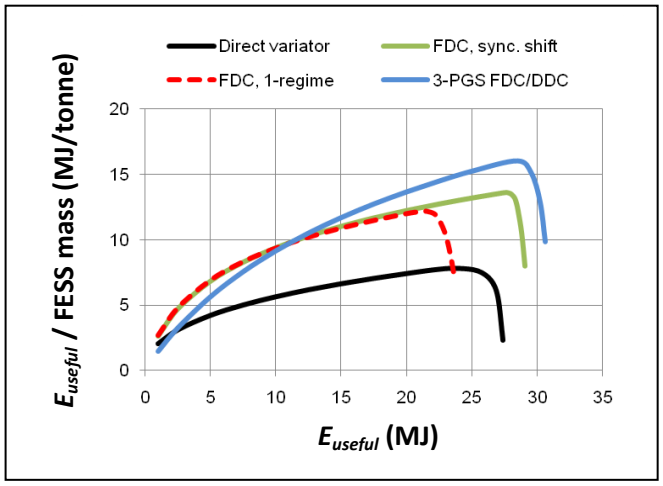


Figure 5-26 – Specific energy capacity of variator-controlled PSTs (E_{avail} = 40 MJ, η_{pgs}'s = 95%, η_{var} = 85%)

Figure 5-27 shows that the 3-PGS FDC/DDC variator-controlled PST is able to achieve the highest specific energy of around 16 MJ/tonne with a useful energy capacity of 28 MJ. The FDC synchronous shift PST also performs well in terms of the maximum *SE*, but requires a much larger variator and requires a very high gearing ratio between the flywheel and transmission (due to the constraint of $R > 1$). The 3-PGS FDC/DDC variator-controlled configuration therefore represents the most practical high performance flywheel transmission.

To assess whether the increased cost and complexity of using a variator component is justified, a direct comparison has been made between maximum specific energy of both the variator and 4-speed CGB controlled 3-PGS FDC/DDC configurations.

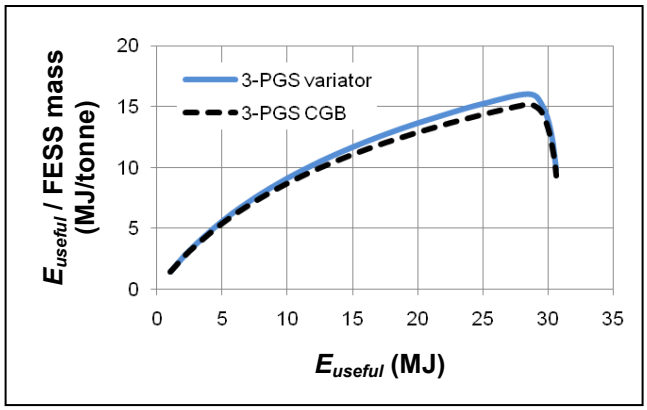


Figure 5-27 – Specific energy capacity of 3-PGS variator and CGB controlled PSTs (E_{avail} = 40 MJ, η_{pgs}'s and η_{cgb} = 95%, η_{var} = 85%)

The efficiency of the two 3-PGS transmissions shown in Figure 5-27 is similar for a given value of U, resulting in maximum specific energy occuring at a similar maximum useful energy capacity. The rated power requirement of the 4-speed CGB is however slightly higher than that of the variator. This results in a slightly lower maximum specific energy for the CGB-controlled configuration due to the larger mass of the CGB component. The actual difference in the weight of the two systems is however extremely small in relation to the total vehicle weight. The choice of system should therefore be based on practical issues such as the cost, reliability and maintenance requirements of the components. These issues require detailed consideration of the design, integration and control of the FESS, which could provide an interesting avenue for future research.

5.6. Summary

The use of the independent analysis method (IAM) has allowed a rigorous comparison of a range of variator-controlled transmission configurations. For the transmissions considered in this Chapter, the IAM has enabled the compromise between efficiency, useful energy capacity, mass, variator size and transmission complexity to be investigated. The flywheel utilisation factor defined in Chapter 4 has provided a basis for comparing the performance of different power-split configuration. The results of the IAM allow design tools to be produced for each configuration. Due to the high power flows that exist during regenerative braking applications in rail vehicles, the power-split configurations have been constrained to avoid power-recirculation during operation. It has been shown that high efficiency and specific

energy capacity can be achieved with a relatively small variator unit by using multiple PGSs to achieve multiple regimes of power-split operation. A comparison of the performance of variator and CGB controlled 3-PGS PSTs shows that the round-trip efficiency of the systems is very similar at around 70%, although the maximum specific energy of the variator-controlled FESS is around 5% higher for a regional rail application. A more detailed consideration of the transmission design and the vehicle duty-cycle is however required to make a final assessment of which system is most appropriate for the regional rail vehicle application.

The IAM has been shown to be an extremely powerful tool in comparing a range of transmission configurations and identifying appropriate system parameters for a given application. However, the resistance losses that occur at the vehicle and flywheel will affect the operation of the mechanical FESS. In order to assess the usefulness of the design tool data generated by the IAM, the affect of these losses on the transmission efficiency and flywheel state-of-charge as a function of transmission gear ratios must be investigated. This is considered in Chapter 6. The most promising PSTs that have been identified in Chapters 4 and 5 are then studied in Chapter 7 using detailed FESS component models integrated with the regional hydro-dynamic rail vehicle model described in Chapter 3.

6. Effect of vehicle and flywheel losses on FESS performance

The conclusions of Chapters 4 and 5 are based on the assumptions of the IAM (independent analysis method). The usefulness of the design tool data generated for each transmission configuration is therefore dependent on the accuracy of these assumptions. This can be quantified for any specific transmission configuration and application by comparing the results of a detailed FESS model (where vehicle and flywheel losses are included) with those predicted by the design tool. This allows us to determine whether the design tools can be used to accurately specify the system parameters, or whether they should only be used for comparative assessment of transmission configurations and to provide a starting point for further optimisation.

The aims of this Chapter are therefore to assess the accuracy of the IAM by investigating the following areas;

- The characterisation of losses at the vehicle and flywheel
- The inclusion of these loss models in the existing FESS models used in the IAM

A time-step based analysis can then be performed which includes these losses in order to test the approximations that have been used in the IAM for a range of different FESS configurations and applications. This new analysis is now dependent on parameters describing the vehicle, operating cycle and flywheel characteristics, and is therefore defined as the DAM (dependent analysis method). By using the same constant transmission component efficiencies, a direct comparison of results from the IAM and DAM can be made for a particular FESS configuration. These results are presented in this Chapter for regional train and passenger car applications, and demonstrate the value of the design tools presented in Chapters 4 and 5.

6.1. Characterisation of vehicle and flywheel losses

The application of a DAM requires that the losses occurring due to resistance forces acting on the vehicle and flywheel are accurately characterised. This enables detailed computational models of the vehicle and flywheel unit to be used in the time-step based model of a flywheel hybrid vehicle, allowing the effect of these factors on the operation of the FESS to be investigated.

6.1.1. Flywheel resistance losses

Flywheel energy storage devices incur losses relating to three main areas;

- the aerodynamic drag of the rotor
- the bearings
- the shaft seal required to achieve a mechanical connection to the transmission

These all apply a resistive torque to the flywheel which can be characterised as a function of flywheel rotational speed. This is achieved through experimental 'run down' testing as shown by Shah [29]. Theoretical relationships also exist to predict the resistive torque associated with each of the three loss mechanisms. Detailed design data for the geometry and operating conditions of the flywheel is however required in order to apply these equations. Furthermore, the aerodynamic losses associated with flywheels operating in a vacuum are not well characterised [29], and experimental testing of a particular flywheel design is therefore required in order to obtain an accurate measure of the losses. Consideration of the experimental data presented by Shah does however suggest that a simple approach to flywheel modelling can be implemented by assuming a constant percentage energy loss per minute. This allows the performance of flywheels of different energy capacity to be investigated without requiring a detailed consideration of the particular design. Based on values quoted in the literature for high performance flywheel units [64, 78, 105] a constant loss factor of 3% per minute has been used in this analysis. The resistance torque acting on the flywheel due to these losses, $T_{fw,\ loss}$, can be defined as shown in Equation 6-1, with the subsequent equation of motion for the flywheel defined in Equation 6-2.

$$T_{fw,loss} = \frac{1}{2} J_{fw} \omega_{fw} \left(\frac{\ln(0.97)}{60} \right) \tag{6-1}$$

$$\frac{d\omega_{fw}}{dt} = \frac{1}{J_{fw}} \left(T_{fw} + T_{fw,loss} \right) \tag{6-2}$$

Implementing Equation 6-2 in a timestep based model of a FESS allows the effect of flywheel losses to be investigated.

6.1.2. Vehicle resistance losses

As with the IAM, the vehicle is characterized by using the equivalent inertia at the transmission output. This is a function of the actual and equivalent rotational mass of the vehicle (m_v and m_r respectively), the wheel radius, r_w, and the final drive gear ratio, K_{fd}, as defined in Equation 6-2.

$$J_{fd} = \left(m_v + m_r\right)\left(\frac{r_w}{K_{fd}}\right)^2 \tag{6-3}$$

The effect of vehicle resistance is included in the vehicle model by characterising the resistance force as a function of vehicle speed. The instantaneous angular acceleration at the final drive can therefore be calculated as shown in Equation 6-3, where T_{fd} is the torque produced by the flywheel transmission at the input to the final drive.

$$\frac{d\omega_{fd}}{dt} = \frac{1}{J_{fd}}\left(T_{fd} - \frac{r_w F_{w,\,res}}{K_{fd}}\right) \tag{6-4}$$

The DAM has been applied to a regional rail application using the vehicle parameters described in Chapter 3. This data has already been used with the IAM design tools to identify the FESS parameters resulting in minimum mass for a given useful energy capacity, as described in Sections 4.1.6, 4.3.5 and 5.5 for brake, CGB and variator controlled transmissions respectively. The DAM allows the accuracy of these results to be tested.

The wider usefulness of the IAM is also demonstrated by considering the different application of flywheel energy storage for a typical passenger car. This particular application has been chosen as automotive vehicles are responsible for the majority of CO_2 emissions from transport and FESS technology represents a potentially low cost, efficient and robust means of achieving significant savings. Vehicle data for a Ford Focus passenger car has been used in the analysis, with the parameters described in Table 6-1.

Ford Focus vehicle parameter	Value
Gross vehicle weight (kg)	1441
Load weight (kg)	70
Equivalent rotating mass, m_r (kg)	$0.1m_v$
Frontal area, A_{front} (m^2)	2.06
Radius of wheels, r_w (m)	0.282
Final drive ratio, K_{fd}	3.84
Rolling friction coefficient, k_{roll}	0.009
Aerodynamic drag coefficient, c_D	0.312

Table 6-1 – Vehicle data for Ford Focus passenger car [107]

The equation describing the resistance force acting on the passenger car takes a different form to the Davis Equation used for rail vehicles, and is defined as follows;

$$F_{w,\,res} = \left(m_v g\, k_{roll} + \frac{1}{2} \rho_{air} c_D A_{front} v^2 \right) \tag{6-5}$$

Using these models of vehicle and flywheel losses the DAM can be performed for both regional train and passenger car applications, as discussed below.

6.2. Methodology for assessing accuracy of Independent Analysis Method

The modelling of a FESS for particular applications requires characterisation of the duty cycle in order to assess the effect of losses at the vehicle and flywheel. This is achieved by considering a simple drive cycle in which the periods of full flywheel discharge and charge are separated by 'dwell' and 'interval' periods, as illustrated in Figure 6-1. These are periods in which the FESS is not active, but losses at the flywheel dissipate kinetic energy causing the flywheel speed to reduce.

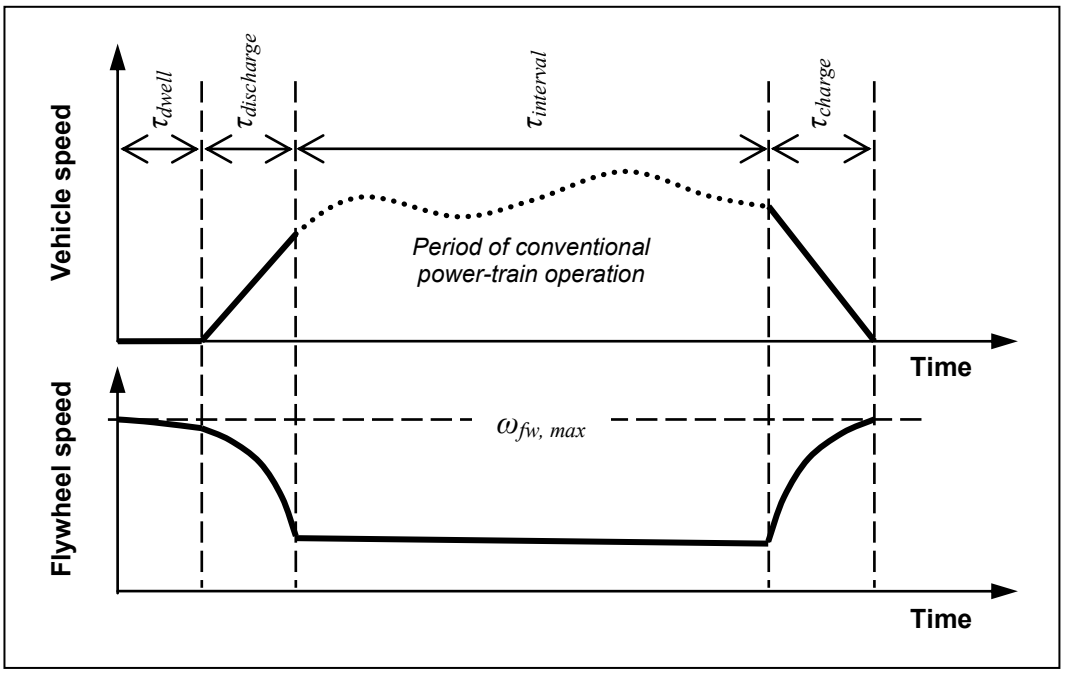


Figure 6-1 – Schematic illustration of time parameters for analysis of FESS performance including vehicle and flywheel losses

The characteristic times for full charge and discharge, τ_{charge} and $\tau_{discharge}$, are defined by the vehicle parameters, the FESS gearing ratios and energy storage capacity, the specified torque at the final drive and the initial flywheel speed. The model is therefore fully defined once representative values of τ_{dwell} and $\tau_{interval}$ have been chosen for a specific application.

The results of the independent analysis of an FESS using different transmissions have been applied to a regional rail application in previous sections. Focussing on the results for a given useful energy capacity allows the effect of vehicle and flywheel losses to be illustrated using the methodology described below.

i. Specify vehicle parameters for a given application
ii. Use design tool data to find gear ratios and J_{fw} values as a function of U required to achieve a given useful energy capacity
iii. Specify a percentage flywheel energy loss per second, duration of dwell time and duration of interval between flywheel discharge and charge
iv. Use these values in time step based model of FESS including vehicle and flywheel losses – this generates transmission efficiencies, variator rated power and overall system efficiency as functions of U

The effect of different torque levels on the efficiency of the flywheel transmission is dependent on the specific details of a drive cycle, and is considered for main-line and branch-line operation of a regional rail vehicle in Chapter 7. In order to assess the effect of vehicle and flywheel losses on the FESS performance the rated torque for the FESS has been used for both vehicle acceleration and deceleration, and constant efficiencies have been assumed for the PGS, CGB and variator components. The results of the DAM are discussed in the following sections.

6.3. FESS performance for regional train application including losses

In order to investigate the effect of losses on the performance of the FESS, three cases have been considered;

a. Design tool data from IAM (shown in black in Figures 6-2 to 6-4)
b. Results of DAM with the inclusion of vehicle resistance and flywheel losses of 3% per min (shown in red in Figures 6-2 to 6-4)
c. Results of DAM with the inclusion of vehicle resistance and flywheel losses of 3% per min, a 60s dwell time and a 5 minute interval between flywheel discharging and charging (shown in green in Figures 6-2 to 6-4)

The dwell and interval times used in case (c) are typical values for a regional rail vehicle operating on a main-line route (see Chapter 3). These three cases have been applied to the 1-regime FDC variator-controlled PST using the gearing ratios and flywheel inertias identified from the IAM (case a). Figures 6-2 to 6-4 are presented in terms of normalised PGS ratio, R^*, which together with the flywheel maximum speed and energy capacity define all the required FESS parameters. The actual values of R and J_{fw} will depend on the gear ratio in the flywheel unit, K_{fw}, and the maximum allowable flywheel rotor speed – while these are important parameters from a design perspective, they do not affect the mass or operating efficiency of the FESS. The following results have been all been generated using the FESS parameters identified from the IAM design tool for a useful energy capacity of 20 MJ.

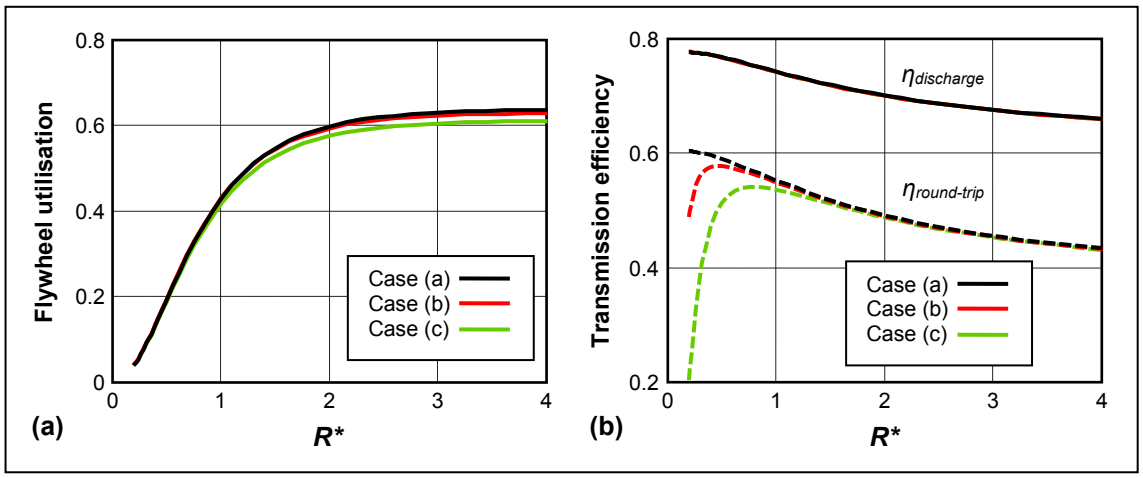


Figure 6-2 – (a) Flywheel utilisation and (b) transmission discharge (solid) and round-trip (dashed) efficiencies as a function of R^* for 1-regime FDC variator-controlled PST (E_{useful} = 20 MJ using IAM design tool)

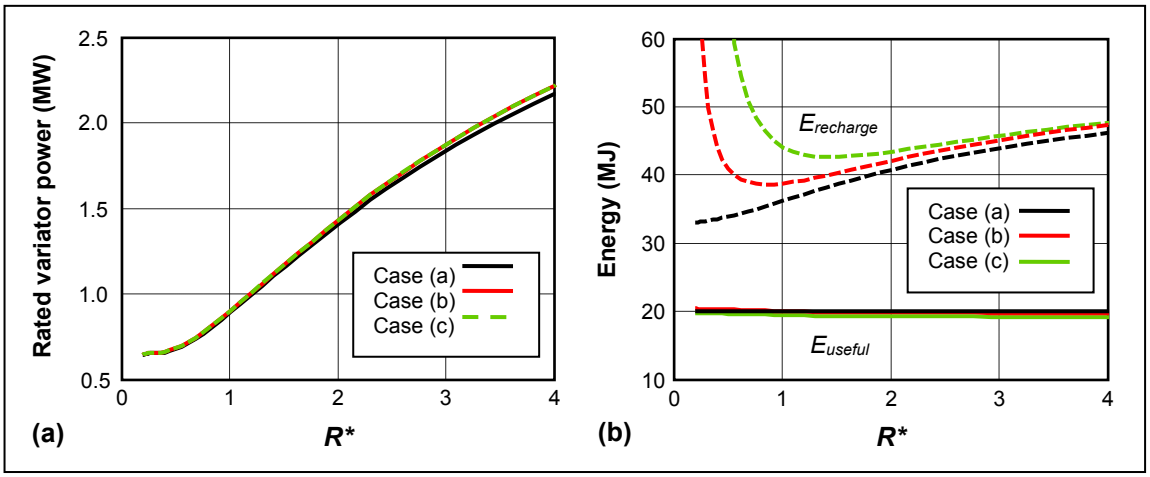


Figure 6-3 – (a) Rated variator power and (b) useful energy delivered to vehicle during flywheel discharge (E_{useful}, solid line) and minimum braking energy required to fully recharge flywheel ($E_{recharge}$, dashed line) as functions of R^* for 1-regime FDC variator-controlled PST (E_{useful} = 20 MJ using IAM design tool)

Figures 6-2 and 6-3 illustrate three important points relating FESS performance when vehicle and flywheel losses are included;

1. Transmission discharge efficiency, normalised rated variator power and useful energy capacity are very similar using the IAM and the DAM
2. The round-trip efficiency is similar at high U, but significantly lower at low U for the DAM results. This is due to losses at the flywheel and vehicle which increases the vehicle speed at which regenerative braking must be initiated in order to fully recharge

the flywheel. A higher proportion of energy is then dissipated during the initial brake-controlled phase of flywheel charging, reducing the overall charging efficiency.

3. The results of the DAM show that flywheel losses increase as U decreases. This is because the flywheel losses are being modelled as a constant percentage kinetic energy loss per minute. These losses can be limited by minimising the time-averaged kinetic energy of the flywheel. This is achieved by implementing a high DOD_{ov} and so limiting the kinetic energy of the flywheel when charged and discharged. In simple terms, in order to store 20 MJ of energy, a flywheel operating with kinetic energy varying between 5 and 25 MJ (DOD_{ov} = 80%) will have significantly lower losses than one operating between 20 and 40 MJ (DOD_{ov} = 50%). This effect is amplified when the flywheel losses that occur in the periods after regenerative braking and after flywheel discharge (characterised by the dwell and interval times respectively) are considered. The time-averaged kinetic energy (and therefore the flywheel losses) during these periods can again be reduced by using a relatively small flywheel with a high DOD_{ov}.

As the losses at the vehicle and flywheel reduce the total amount of energy that can be recovered and reused, an overall round-trip efficiency for the system (rather than for the transmission), $\eta_{round\text{-}trip,\ sys}$, is defined as follows ;

$$\eta_{round\text{-}trip,\ sys} = \frac{E_{useful}}{E_{recharge}} \tag{6-6}$$

This system efficiency can be calculated using the values of E_{useful} and $E_{recharge}$ presented in Figure 6-3. The results are shown in Figure 6-4 along with the specific energy of the FESS for the three cases (a, b and c).

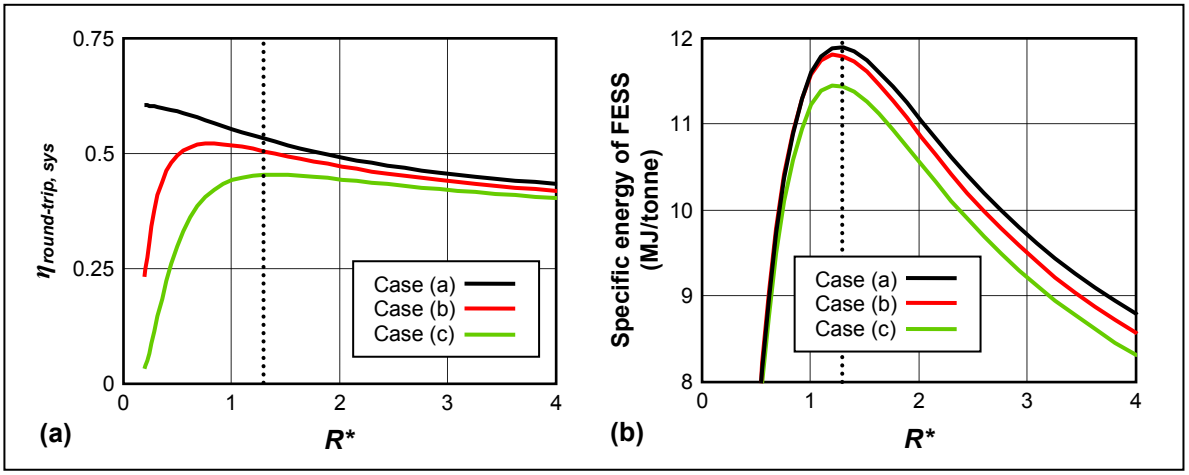


Figure 6-4 – (a) Overall round-trip system efficiency and (b) specific energy of FESS as a function of R^* for 1-regime FDC variator-controlled PST (E_{useful} = 20 MJ using IAM design tool)

The IAM design tool data suggests that $\eta_{round\text{-}trip,\ sys}$ (which is equal to the transmission round-trip efficiency when vehicle and flywheel losses are neglected) increases with decreasing U, and the FESS parameters have therefore been specified on the basis of minimising mass in Chapters 4 and 5. However, it is clear from Figure 6-4(a) that the results of the DAM show a maximum $\eta_{round\text{-}trip,\ sys}$ operating point exists for a given E_{useful}, which provides an alternative method of specifying the FESS parameters. It is therefore important to consider how the operating point identified to maximise specific energy from the IAM design tool compares with the operating points that achieve maximum specific energy and maximum $\eta_{round\text{-}trip,\ sys}$ in the DAM. It is clear from Figure 6-4 that the R^* value required to minimise mass using the IAM design tool (R^* = 1.30) is very close to the R^* values required to both minimise mass and maximise overall round-trip system efficiency in the DAM with flywheel losses of 3% per min, a dwell time of 30s and an interval time of 5mins. While this result is for the particular case of a 1-PGS FDC variator-controlled PST with E_{useful} = 20 MJ, further analysis shows that this is true for all practical values of E_{useful} and for other transmission configurations (see Appendix B). The IAM design tool therefore provides an accurate means of identifying appropriate gear ratios and flywheel capacity for the FESS. The major effect of vehicle and flywheel losses is to decrease the overall system round-trip efficiency compared to the values predicted by the IAM. For an application with a limited amount of braking energy available from the vehicle during a flywheel charging event, the reduced system efficiency limits the useful energy capacity of the FESS compared to the results of the design tool as shown in Figure 6-5 for the regional train application.

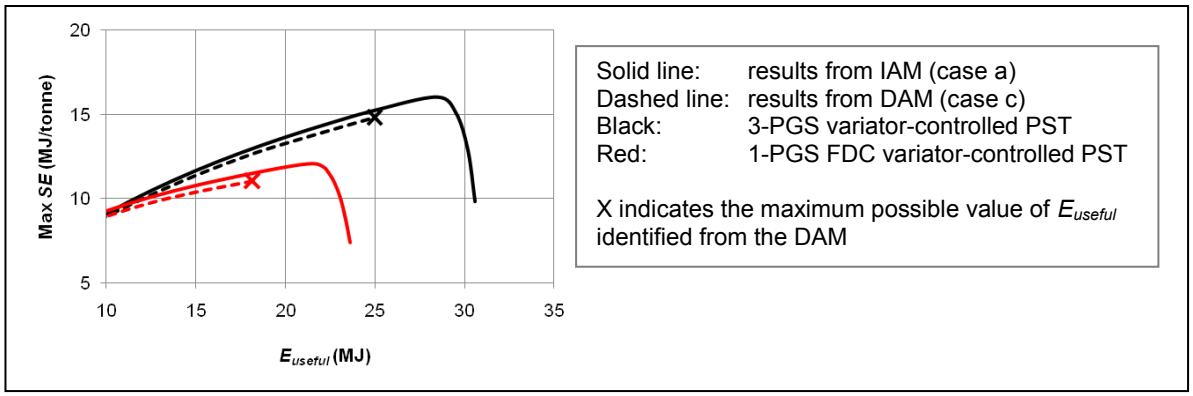


Figure 6-5 – Maximum *SE* as a function of useful energy capacity for regional train application using 1-PGS FDC and 3-PGS FDC/DDC variator-controlled FESSs with available braking energy limited to 40 MJ

The IAM design tool data suggests that operation at higher values of E_{useful} than the maximum *SE* condtion is possible at the expense of decreased *SE* (by increasing the size of the flywheel and reducing DOD_{ov}). The results of the DAM however, show that when vehicle and flywheel losses are included in the analysis the resulting small increase in discharge efficiency is counteracted by the large decrease in charging efficiency and increased flywheel losses. For the 1-PGS and 3-PGS variator-controlled PSTs respectively, the maximum possible *SE* is therefore 9% and 8% lower than that calculated using the IAM design tool, and is achieved with a reduction of 16% and 12% in the overall system efficiency, η_{sys}.

6.4. FESS performance for passenger car application including losses

The usefulness of the design tool data generated by the IAM for mechanical FESS systems has been demonstrated for a regional rail application. Much of the literature relating to mechanical transmissions for FESSs focusses on automotive applications, and the effect of vehicle and flywheel losses on the accuracy of the IAM is also therefore also considered for a passenger car operating a typical urban drive cycle. The simple stop-start drive cycle shown in Figure 6-6 has been extracted from the standard ECE urban drive cycle, and can be characterised by the stated ‘drive cycle characteristics’.

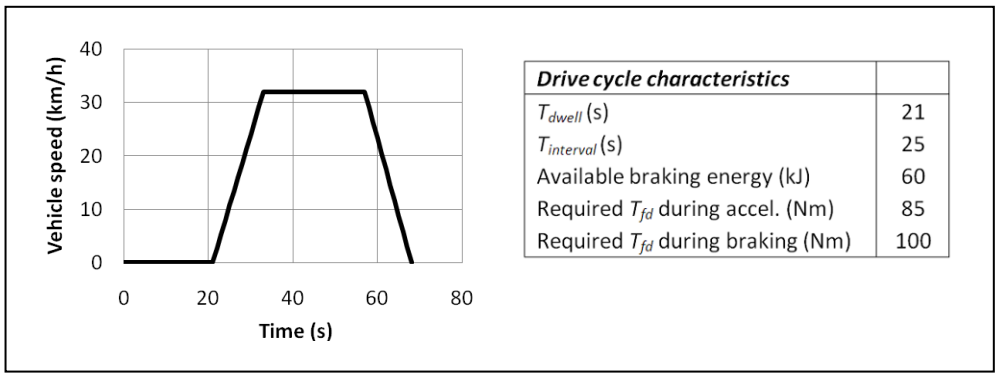


Figure 6-6 – Typical discharge/charge event for passenger car in urban driving (extracted from ECE urban drive cycle) and associated drive cycle characteristics used in the DAM

Using the gearing ratios and flywheel energy capacity identified from the IAM design tool as minimising FESS mass for a 3-PGS variator-controlled PST, the DAM can be performed producing the plot of maximum specific energy against useful energy capacity shown in Figure 6-7.

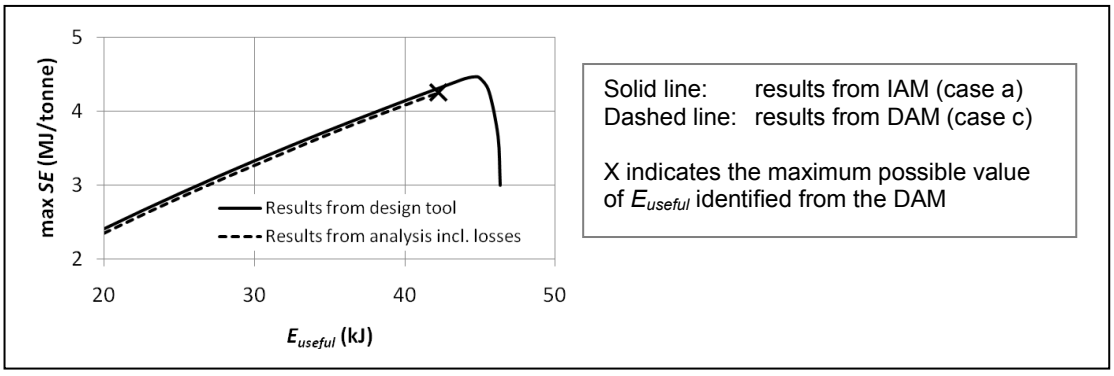


Figure 6-7 – Maximum *SE* as a function of useful energy capacity for 3-PGS variator-controlled PST in a passenger car application with available braking energy limited to 60 kJ

The relatively short dwell and interval times that characterise the passenger car application result in low flywheel losses and relatively high transmission efficiency. The DAM results presented in Figure 6-7 are therefore very similar to the IAM results, with a relative reduction in $\eta_{round\text{-}trip,\ sys}$ of only around 5% at the maximum *SE* operating point (compared to around 12% for the same transmission in a rail application as seen in Figure 6-5).

6.5. Summary

The analysis presented in this Chapter shows that the design tool generated using the Independent Analysis Method (IAM) provides a simple and accurate means of specifying the gearing ratios required to achieve a given useful energy storage capacity with minimum system mass for practical applications. The major effect of losses at the vehicle and flywheel is to reduce the amount of available braking energy that can be recovered and reused. The IAM design tool is shown to provides an accurate guide to identifying the required flywheel size (a function of the useful energy capacity) but overestimates the overall system efficiency of the FESS. This is illustrated by the analysis presented in this Chapter which shows that when losses are considered for the regional train application using a 3-PGS variator-controlled PST, the maximum FESS specific energy is achieved with a value of E_{useful} which is 88% of that predicted from the design tool (caused by a 12% reduction in $\eta_{round\text{-}trip,\ sys}$). A flywheel hybrid passenger car application for a typical urban drive cycle is shown to be less affected by the vehicle and flywheel losses, with a 5% reduction in $\eta_{round\text{-}trip,\ sys}$ at the maximum specific energy.

Having shown that the effects on FESS performance of resistance losses at the vehicle and flywheel are relatively small for the regional rail application, the following Chapter uses the IAM design tools to specifiy FESS parameters for a number of transmission configurations. Detailed computational models of these FESS systems (including torque dependent transmission losses) are integrated with the regional diesel train model described in Chapter 3. The performance of these flywheel hybrid regional trains (FHRTs) over main-line and branch-line routes is then assesed and compared to the conventional regional trains.

7. Investigation of flywheel hybrid regional train

This Chapter provides a demonstration of how the results of the IAM can be used to specify the system parameters for a particular application. This allows the effect on vehicle fuel consumption of a range of factors such as the energy capacity, control strategy and component efficiencies of the FESS to be investigated. The aim of this Chapter is therefore to investigate the operation of flywheel hybrid rail vehicles over realistic drive cycles using a range of vehicle control strategies. This is achieved by integrating the detailed time-step based models of the best performing FESSs (identified from the IAM results) with the conventional regional diesel train model described in Chapter 3. The FESS design tool data is used to specify the flywheel and transmission parameters for a range of energy storage capacities. The integrated flywheel hybrid regional train (FHRT) model is then used to investigate the effect of driving strategy and FESS control strategy on the total fuel consumption and journey time for main-line and branch-line routes. This allows a direct comparison between the fuel efficiency of the conventional and flywheel hybrid trains, and the benefits of the FESS are quantified. This detailed modelling also allows the torque and speed requirements of the flywheel transmission components to be accurately specified, and allows an effective FESS control strategy to be formulated.

7.1. FESS configurations considered for hybrid train

The best performing FESS considered in the previous Chapters have been shown to consist of multiple PGSs providing a number of power-split operating regimes. This leads to high transmission efficiency and a relatively low rated power requirement of the control component (either a variator or CGB). These multi-regime transmissions have been shown to achieve high specific energy for a regional rail application when used in FESSs with relatively large energy storage capacity (around 40 MJ), where the additional weight of the planetary gearing is offset by the reduced variator/CGB size and the improved system efficiency. Both the variator and CGB controlled options have been shown to have very similar operating characteristics. The variator controlled option is however considered for the flywheel hybrid train analysis presented in this Chapter due to the slightly higher predicted specific energy capacity.

For lower energy storage capacity systems (up to 20 MJ), the 4-PGS brake-controlled transmission has been shown to achieve similar specific energy to the more complex power-split configurations. The excess of braking energy available during flywheel recharging compensates for the relatively low transmission efficiency. This configuration has therefore also been considered as it can potentially provide a mechanically simple system for limited braking energy recovery.

7.2. Integration of FESS and conventional diesel regional train models

A computational FHRT model has been created by integrating the quasi-static time-step based models of the conventional diesel-hydrodynamic train with a detailed model of the chosen FESS configuration. In the IAM and DAM analysis discussed in Chapters 4, 5 and 6 the efficiency of the FESS transmission gearing components was assumed to be constant. The component losses are however a function of the operating speed and torque, and should be considered as part of a detailed analysis of FESS performance. The characterisation of the PGS and variator losses is therefore discussed in the following Section.

7.2.1. Torque and speed dependence of FESS component efficiencies

Detailed computational model of FESSs including the effect of torque on PGS and variator/CGB efficiencies have been created as part of an integrated FHRT model.

Variator loss model

As discussed in Chapter 2, the efficiency of a mechanical variator can be characterised as a function of input torque (as a function of the maximum allowable torque) and the speed ratio. An experimentally derived efficiency map for a push-belt type variator has been used in a number of studies to characterise variator losses in vehicle transmission applications [106-107, 134], and is shown in Figure 7-1.

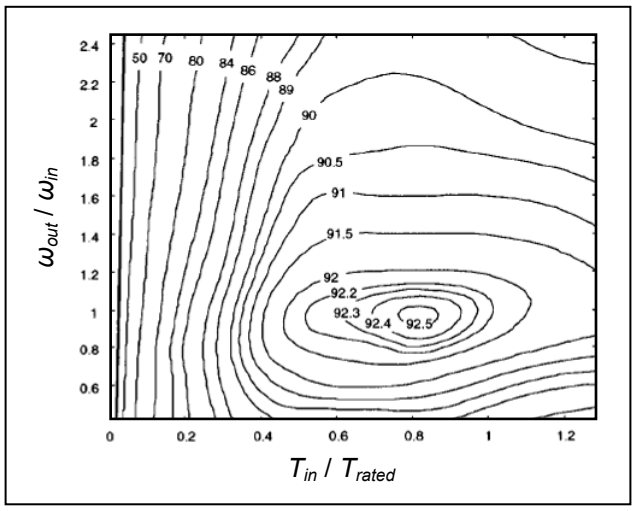


Figure 7-1 – Variator efficiency map (in percent, including hydraulic control system) as a function of speed ratio and normalised input torque [134]

This map requires a nominal maximum torque to be defined for the variator. A maximum variator torque can be identified from the IAM design tool results for a particular transmission configuration and FESS application, and this value has therefore used to normalised the variator input torque in the computational analysis of the FHRT. This map is used to calculate the efficiency of the variator during each time-step of the calculation procedure. As the application of the variator in an FESS requires it allow power flow in both directions, it is important to note that the efficiency is a function of the input torque. When applying this map in the FESS computational model the torque at the point where power is flowing into the variator is therefore used. Transmission operation in each power-split mode has been considered during flywheel charging and discharging in order to identify the appropriate torque and speed ratio required to calculate the variator efficiency. The variator efficiency allows the torque acting on the flywheel to be calculated for a given tractive force at the vehicle, vehicle speed and flywheel speed. The total variator energy losses can then be calculated over a drive cycle.

PGS loss model

Losses in a PGS are caused by a range of factors including friction at the gear teeth contact patch, bearing and seal losses, aerodynamic drag and lubrication churning losses. All these losses will depend on the gearing ratio, design and operating environment of the PGS unit as well as the torque and speed at the three branches, and are difficult to characterise without obtaining test data under operating conditions [133]. Several authors have presented methods

for assessing the meshing losses in a PGS [135-137]. These losses can be characterised by assuming a constant efficiency between an 'elemental' gear-pair in a frame of reference moving with the gear carrier. As a complete PGS can be defined by a number of gear-pair elements the meshing losses can then be calculated. The most rigorous method of this type is presented by Chen and Angeles [138] and is based on the concept of virtual power flow in a frame of reference of the gear carrier. In the present research, this analytical method has been applied to 2 degree-of-freedom, single stage PGSs with a practical characteristic gear ratio of $0.1 < R < 0.33$. Equations for the PGS efficiency as a function of the branch speeds are presented in Appendix C. These results suggest that meshing losses are relatively small, and do not account for torque dependent losses. An experimental investigation by Mantriota and Pennestri [139] measured the efficiency of a PGS under a range of operating conditions. The results show significant variation in PGS efficiency with both torque and speed. For the purposes of analysing the FESS performance, it was felt that sufficient accuracy could be obtained by using a simple affine relationship (as described by Guzzella [46]) to define efficiency as a function of the maximum PGS torque. The affine coefficients have been chosen in order to achieve a maximum efficiency of 95% and provide a good fit with published experimental results [139], as shown in Figure 7-2.

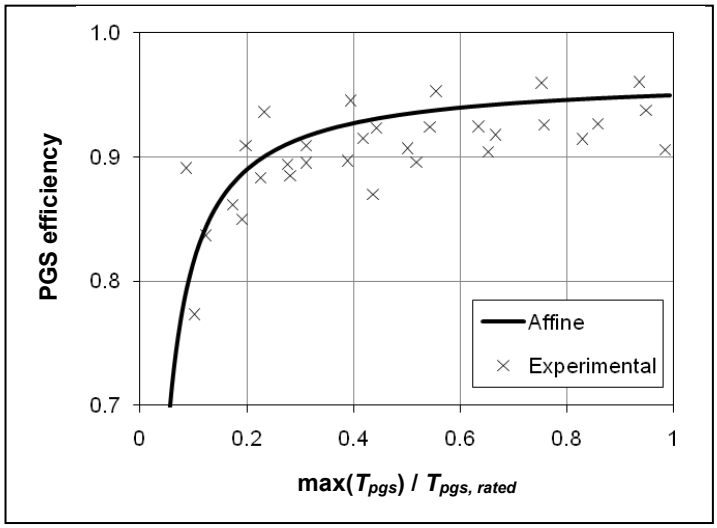


Figure 7-2 – PGS efficiency as a function of maximum torque in the three PGS branches divided by the PGS torque rating (experimental data from Mantriota [139])

The efficiency of the PGS is therefore defined as a function of the maximum instantaneous torque in the three PGS branches divided by the rated torque, and is calculated in the FHRT model during each time-step. This allows the torque acting on the flywheel during a time-

step to be calculated, and the total PGS gearing losses to be found for a drive cycle. The total gearing losses occurring in FESSs with brake and variator controlled transmissions can therefore be completely characterised.

7.2.2. FESS control strategy

A key requirement of the integrated FHRT model is a control strategy for the FESS, defining how the power-train of the FHRT responds to the 'power command' signal produced by the vehicle control module. This FESS control strategy therefore determines how the FESS is used to achieve charge and discharge of the flywheel. The basic structure of the FHRT computational model is described in Figure 7-3.

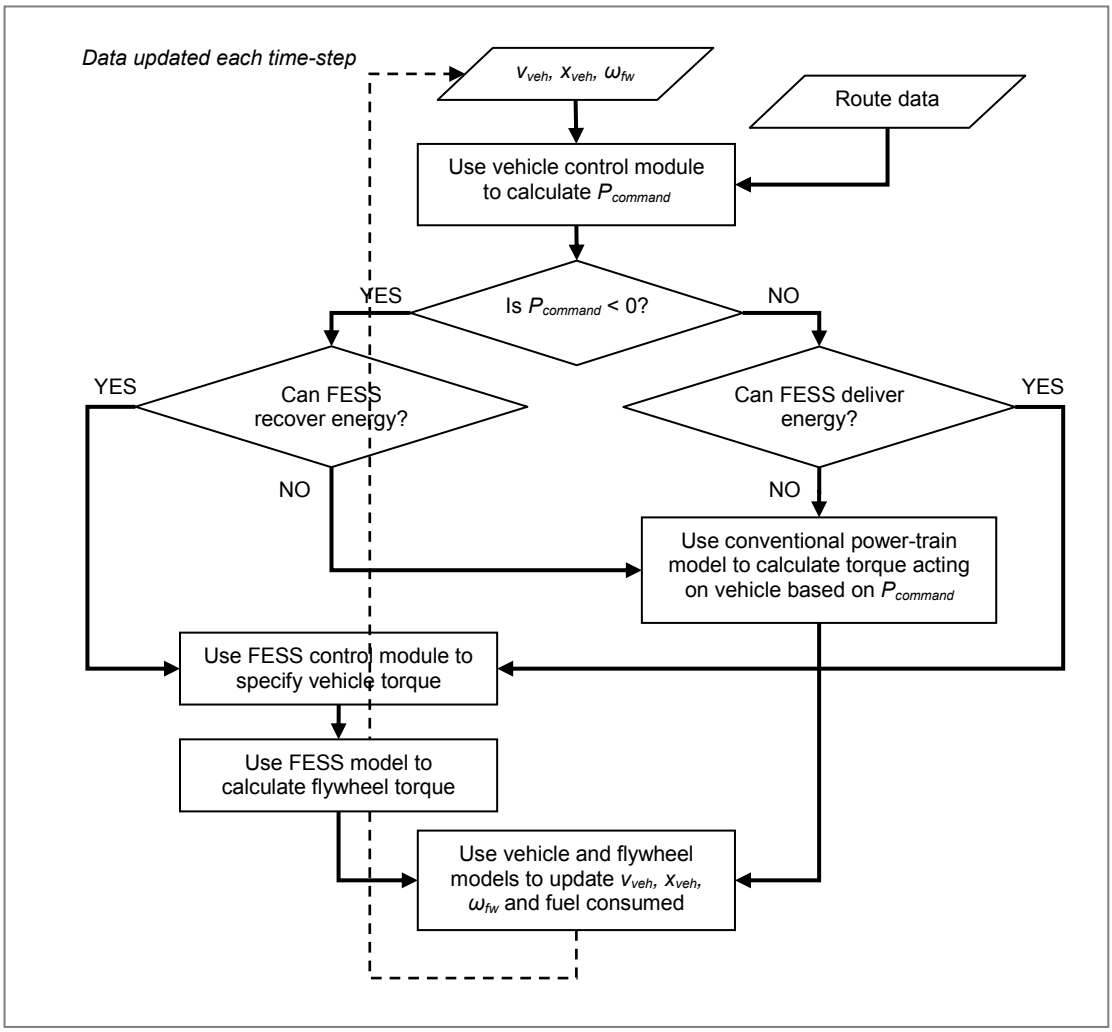


Figure 7-3 – Overview of the FHRT model structure

As with the conventional vehicle model described in Chapter 3, the operation of the FHRT can be defined in the three possible modes of vehicle control; powering, speed holding and speed reduction. In each of these modes a control strategy must decide whether the required tractive force should be provided by the FESS, the conventional power-train or a combination of both. If the FESS is able to provide tractive force then a decision must also be made regarding the magnitude of the torque applied at the final drive. The control strategies used in each of the three modes are described below.

Powering

Due to the poor efficiency of the conventional power-train at low vehicle speeds, the FESS is used to provide all the tractive effort whenever possible. The maximum rated flywheel transmission torque is used during powering in order to achieve high transmission efficiency and good vehicle acceleration performance. Once the FESS is discharged the conventional power-train is used.

Braking

The FESS components have been sized in order to provide a constant moderate braking torque to achieve the required deceleration of 0.5 m/s^2. The rated FESS torque is therefore used during regenerative braking.

Speed holding

Relatively low torque is required for smooth acceleration or braking during speed holding. As speed holding usually occurs at relatively high vehicle speeds, flywheel use under these conditions is infrequent. The decrease in efficiency of the transmission components at low torque could however be significant. The FESS is therefore used to provide any required braking torque during speed holding, but does not provide tractive force if the efficiency of the PGS or variator falls below 50%.

The study of FHRT performance presented in this Chapter focuses on using the flywheel system to provide tractive power and reduce the operation of the conventional power-train at low vehicle speed, and the auxiliary power requirement of the train is therefore always provided by the engine.

The decisions to use the FESS to deliver or recover tractive energy are based on the vehicle speed, flywheel speed and tractive torque demand. These factors determine whether

a FESS transmission operating phase can be used to achieve flywheel charge/discharge, and whether the speed and torque requirements of the FESS components are within the rated values. Two FESS control strategies have been considered and the rules that define FESS operation in each strategy are discussed below.

Control Strategy 1

- Flywheel charging only implemented when the flywheel *SOC* is less than 100%
- Use FESS whenever kinematic conditions allow charging/discharging of flywheel

Control Strategy 2

- Flywheel charging only implemented when the flywheel *SOC* is less than 100%
- Brake-controlled operation can be implemented at any time to provide the required vehicle tractive torque
- Variator/CGB controlled operation can only be implemented when the variator/CGB input and output speeds are less than the maximum rated value

These control strategies will determine how much braking energy can be recovered and reused by a particular FESS. The FESS systems considered for the hybrid regional train application are specified in the following Section, and the results of the FHRT models are presented.

7.3. Results of FHRT modelling

The kinematic and torque equations characterising the operation of the 3-PGS variator and 4-PGS brake controlled FESSs are described in Chapters 4 and 5. These equations have been implemented in a time-step based quasi-static computational model of each FESS, which are completely defined using the data in Tables 7-1 and 7-2. These models include the effect of torque on the efficiency of the variator and PGS components as described in Section 7.2.1, and have been integrated with the conventional regional diesel train model described in Chapter 3. This allows the performance of a mechanical flywheel hybrid train to be investigated. Based on the results of the generic hybrid regional train study in Chapter 3, useful energy capacities of 10, 20 and 30 MJ are considered for both the 3-PGS variator and 4-PGS brake controlled FESSs. The design tool data generated by the IAM for these two

transmission configurations has been used to specify the FESS parameters shown in Tables 7-1 and 7-2. These values have been identified as achieving minimum FESS mass for the stated useful energy capacity. The gear ratios have been chosen in order to achieve a maximum PGS ratio, R, of 0.33. This results in practical values for both the planetary and fixed ratio gears and the inertia and maximum speed of the flywheel unit.

E_{useful} (MJ)	10	20	30
max ω_{var} (rad/s)	300		
max T_{pgs} (kNm)	10		
J_{fw} (kg m^2)	94.6	74.9	67.2
max ω_{fw} (rad/s)	553	865	1112
R_A	0.082	0.079	0.077
R_B	0.184	0.179	0.177
R_C	0.330	0.330	0.330
K_o	7.17	4.84	3.86
K_A	6.58	4.46	3.56
K_B	5.37	3.66	2.93
K_C	3.60	2.45	1.96
max T_{var} (kNm)	1.05	1.56	1.96
FESS mass (tonnes)	1.10	1.47	1.82

Table 7-1 – Specifications for a 3-PGS variator-controlled FESS with a range of useful energy capacities in order to achieve minimum mass (using the design tool data presented in Chapter 5 with the stated maximum variator speed and PGS torque)

E_{useful} (MJ)	10	20	30
max T_{pgs} (kNm)	10		
J_{fw} (kgm^2)	131		
max w_{fw} (rad/s)	515	729	893
R_1	0.051		
R_2	0.110		
R_3	0.190		
R_4	0.330		
FESS mass (tonnes)	1.26	1.73	2.19

Table 7-2 – Specifications for a 4-PGS brake-controlled FESS with a range of useful energy capacities in order to achieve minimum mass (using the design tool data presented in Chapter 4 with the stated maximum PGS torque)

All the FHRT results have been calculated using a uniform coasting driving strategy with a range of D_{coast} values, and the effects of energy capacity, FESS efficiency and control strategy on the fuel consumption of the FHRT are considered in the following Section.

7.3.1. Effect of FESS control strategy on FHRT performance

For power-split transmissions either of the two control strategies defined in Section 7.2.2 can be used. The effect of these strategies on the fuel consumption of the 3-PGS variator-controlled FHRT for a range of uniform coasting conditions are presented in Figure 7-4. The fuel consumption is presented as a percentage saving over a conventional vehicle using a uniform coasting driving strategy to achieve the same journey time for the route. The maximum variator speed that occurs using FESS Control Strategy 1 (unlimited FESS operation) is shown in Figure 7-5.

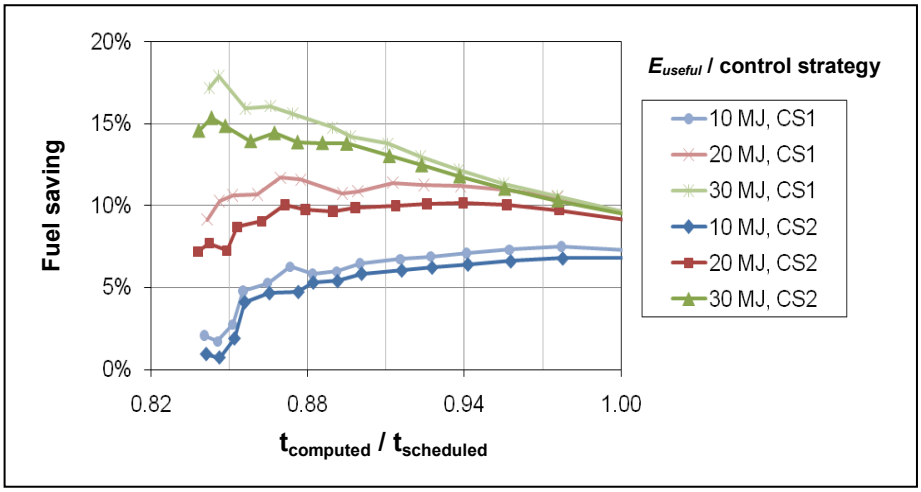


Figure 7-4 – Effect of FESS control strategy on fuel saving for 3-PGS variator-controlled FESS relative to conventional vehicle using a range of 'uniform coasting' conditions

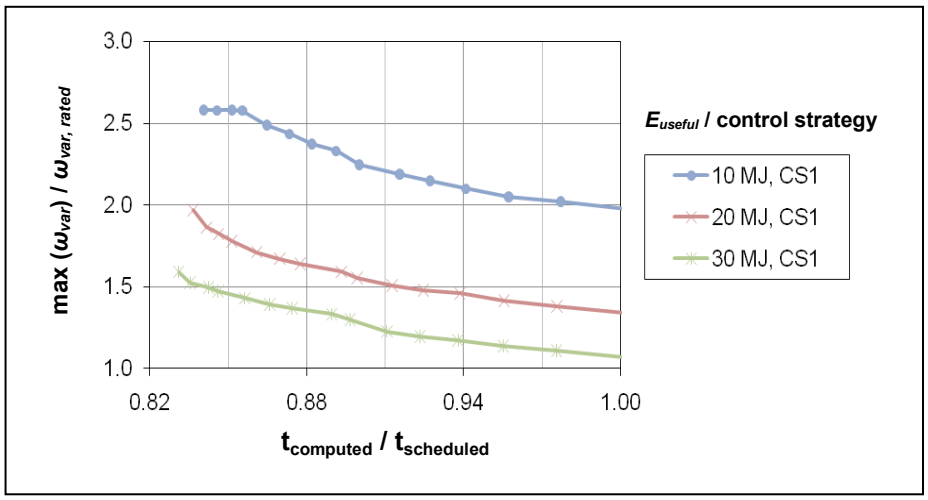


Figure 7-5 – Effect of FESS control strategy 1 on the maximum operating speed of the variator (relative to the rated value) in a 3-PGS variator-controlled FESS using a range of 'uniform coasting' conditions

It is clear from these results that a consistently larger fuel saving is possible using Control Strategy 1, though this requires the variator to operate above the rated speed. This can be understood by considering the vehicle and flywheel speed profiles obtained using Control Strategy 1 and 2 with the same uniform coasting driving strategy. Figure 7-6 shows the results for a FESS with a 20 MJ useful energy capacity and a journey time of approximately 90% of the scheduled time.

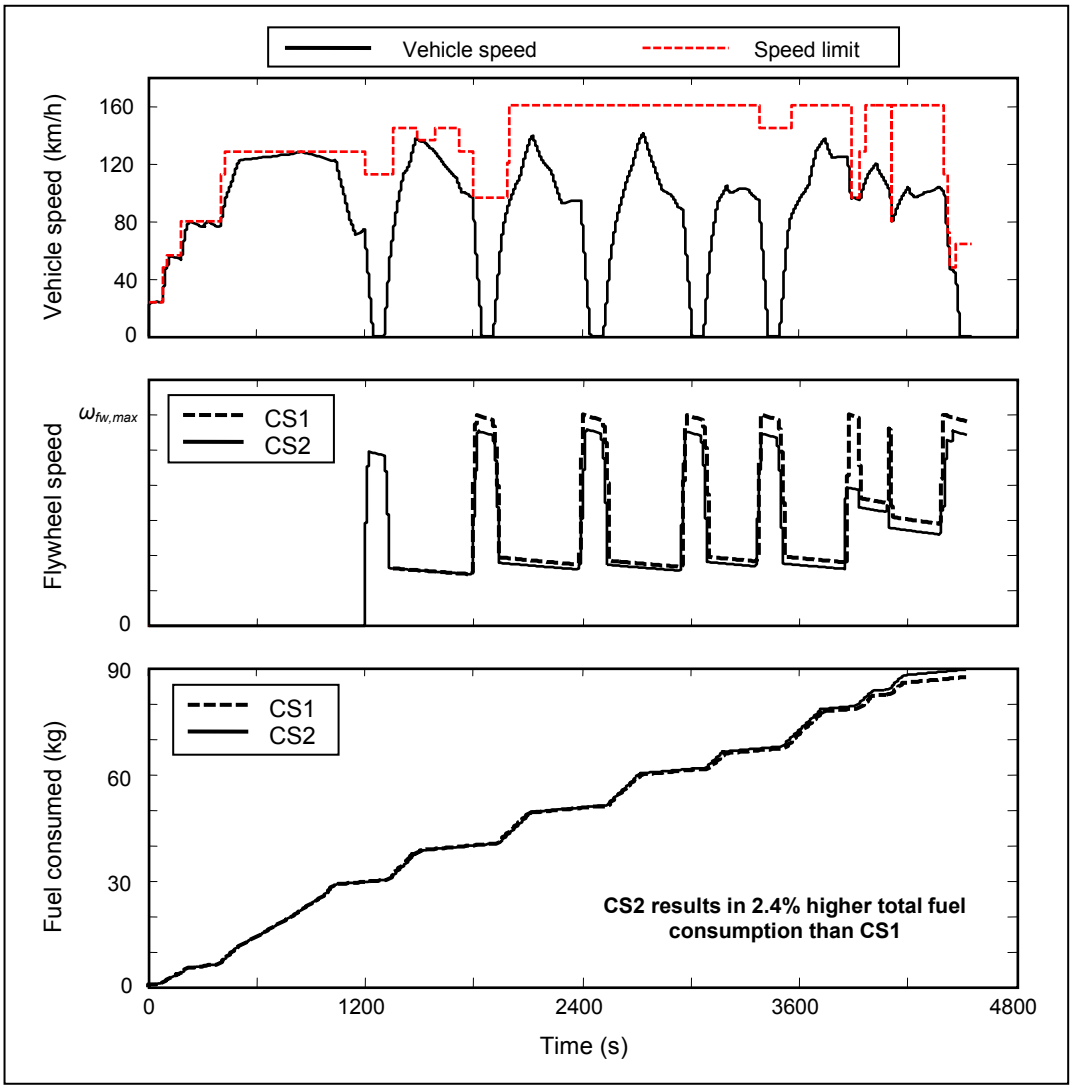


Figure 7-6 – An example of the effect of FESS control strategy (CS) on FHRT performance (with D_{coast} = 0.1 m/s^2)

Figure 7-6 shows that the main result of implementing Control Strategy 2 is to prevent the FESS from recovering and reusing significant amounts of the braking energy available during the high speed braking events, particulary the two speed reductions at around 4000s. This is because the FESS has been specified (using the IAM) to operate at or below the minimum vehicle speed required to fully recharge the flywheel. Using the FESS to apply a braking torque above this speed forces the FESS to operate outside of its design range, increasing the variator speed beyond its rated limit. As the useful energy storage capacity of the FESS is increased, a higher initial vehicle speed is required to fully recharge the system, and the maximum variator speed is therefore closer to its rated value as shown in Figure 7-5.

In practical terms, the rated variator speed should not be exceeded. The FESS operation shown in Figure 7-4 using Control Strategy 1 can therefore only be achieved by re-specifying

the gearing ratios of the FESS to reduce the variator speed. This would increase the maximum torque and therefore the mass and cost of the variator. However, Figures 7-4 and 7-6 show that the overall effect of control strategy on fuel consumption is relatively small. All further analysis of the 3-PGS variator-controlled FESS therefore uses the parameters specified in Tables 7-1 and 7-2 with Control Strategy 2 to limit the maximum variator speed.

The brake-controlled FESS has no components that have been specified on the basis of a rated speed, and is therefore able to operate whenever it is kinematically possible to charge or discharge the flywheel as required. Control Strategy 1 has therefore been used for all analysis of the FHRT with 4-PGS brake controlled FESS. It should however be noted that using the brake-controlled transmission at high vehicle speeds will result in higher levels of energy dissipation in the FESS control brakes than have been calculated using the IAM for the simple charge/discharge case (see Chapter 4). Computational modelling of a realistic drive cycle therefore plays an important role in identifying the design requirements of a practical system.

7.3.2. Effect of initial FESS condition on FHRT performance

The initial *SOC* of the flywheel device is an important consideration in assessing the potential benefit of a flywheel hybrid system for rail. The operational schedule may mean that a train is required to wait for long periods at the beginning or end of a route, and the vehicle is then likely to begin a journey with little or no kinetic energy stored in the flywheel. While operating a particular service however, the vehicle is likely to have a short dwell time. Two flywheel conditions have therefore been considered as described below;

i. 'Empty' refers to an initial flywheel state-of-charge, $(SOC)_{initial} = 0$
ii. 'Equal' refers to $(SOC)_{initial} = (SOC)_{final}$

The effect of these two initial flywheel conditions on the fuel saving achieved by the FHRT is shown in Figures 7-7 for the 3-PGS variator-controlled FESS.

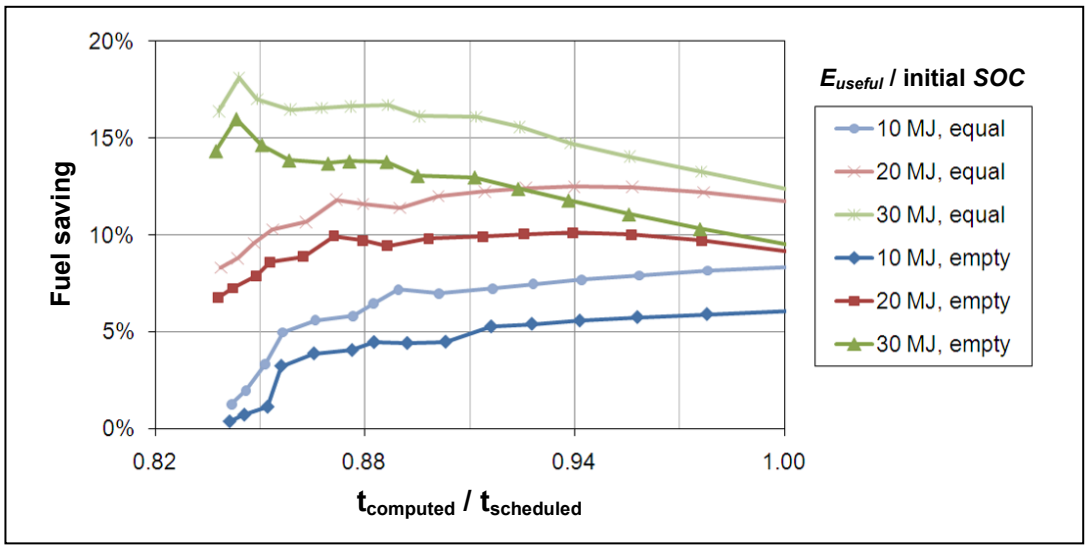


Figure 7-7 – Fuel saving relative to conventional vehicle using 3-PGS variator-controlled transmission and the stated FESS useful energy capacities with flywheel initially either fully charged or empty

The additional energy stored in the flywheel in the 'equal' case is seen to result in a consistently higher fuel saving for the FHRT. It is clear that the fuel saving possible is highly dependent on the useful energy capacity and the degree of coasting used in the driving strategy. This is discussed for both the 3-PGS variator and 4-PGS brake controlled FESSs in the following Section.

7.3.3. Comparison of mechanical FESSs for regional rail application

The performance of the 3-PGS variator and 4-PGS brake controlled flywheel systems can be understood by considering the total energy used during operation. This is presented in Table 7-3 for a conventional train and the two FHRT configurations operating on both the main-line and branch-line routes defined in Chapter 3. A uniform coasting strategy has been applied using the stated values of D_{coast} in order to achieve a total journey time of around 98% of the scheduled time, and the intial flywheel *SOC* has been specifed to match the final *SOC*. Average efficiency terms can be defined for the drive cycle that provide insight into the operation of the FESS. The mean FESS transmission discharge efficiency, $\eta_{FESS,\,dis}$, and the mean FESS turn-around efficiency, $\eta_{FESS,\,turn}$, are defined as follows;

$$\eta_{FESS,\,dis} = \frac{E_{FESS,\,out}}{\left(E_{FW,\,in} - E_{FW,\,loss}\right)} \tag{7-1}$$

$$\eta_{FESS,\,turn} = \frac{E_{FESS,\,out}}{E_{FESS,\,in}} \tag{7-2}$$

Where; $E_{FESS,\,out}$ is the total energy flowing out of the FESS,

$E_{FESS,\,in}$ is the total energy flowing into the FESS,

$E_{FW,\,in}$ is the total energy delivered to the flywheel,

$E_{FW,\,loss}$ is the total energy dissipated due to flywheel losses,

Vehicle type	**Conventional vehicle**		**4-PGS brake FESS**		**3-PGS variator FESS**	
Route	**BL**	**ML**	**BL**	**ML**	**BL**	**ML**
Value of D_{coast} for uniform coasting strategy	0.7	0.6	0.7	0.6	0.7	0.6
Journey time, s	5226	4909	5263	4929	5264	4924
Relative journey time, $t_{calculated}/t_{scheduled}$	0.974	0.968	0.978	0.975	0.975	0.977
Fuel consumed, kg	68.0	87.4	59.4	79.8	55.8	77.1
Fuel saving relative to conventional vehicle	-	-	12.7%	8.7%	17.9%	11.8%
Tractive energy delivered by conventional power-train	611	1044	542.9	968.9	501	938.7
Resistance losses at vehicle	418	838	418.3	837.9	418	838.7
Energy dissipated in conventional brakes	193	207	29.1	13.4	11.5	28.0
Resistance losses at flywheel	-	-	10.1	19.6	12.0	15.5
Energy dissipated in FESS PGSs	-	-	13.0	16.1	25.3	25.9
Energy dissipated in FESS control brakes	-	-	72.3	81.9	15.5	14.4
Energy dissipated in FESS control clutches	-	-	-	-	13.0	11.9
Energy dissipated in FESS variator	-	-	-	-	4.7	4.3
Total tractive energy out of FESS	-	-	67.5	76.7	108.9	108.7
Total tractive energy into FESS	-	-	153.7	183.3	181.2	178.8
Total energy delivered to flywheel	-	-	109.2	132.2	140.8	144.9
Mean FESS transmission discharge efficiency	-	-	68%	68%	85%	84%
Mean FESS turn-around efficiency			44%	42%	60%	61%
FESS transmission discharge eff. predicted by IAM			66.6%		83.1%	
FESS transmission round-trip eff. predicted by IAM	-	-	43.3%		69.8%	

Table 7-3 – Energy breakdown (in MJ's) for conventional and flywheel hybrid regional trains on main-line (ML) and branch-line (BL) routes using uniform coasting driving strategy (FESS useful energy capacity of 20 MJ, equal initial and final flywheel *SOC*)

Table 7-3 shows that both FESSs can accept a similar amount of braking energy during operation on either route. The higher transmission efficiency of the 3-PGS variator-controlled system means that a higher proportion of this energy can be returned to the vehicle, resulting in a mean FESS turn-around efficiency of approximately 60% during operation on both the main-line and branch-line route. The high 'control brake' losses that

occur in the 4-PGS brake-controlled FESS lead to a significantly lower mean turn-around efficiency of around 40%. In both systems, flywheel losses are shown to have a relatively small impact on the overall system performance. The PGS losses are also relatively small for the brake-controlled system, but are significantly higher in the variator-controlled system (where they are the biggest source of FESS losses). This increase in PGS losses has two causes. Firstly, the higher transmission efficiency allows a higher total energy flow through the transmission. Secondly, part-load operation of the PGSs always occurs during FDC or DDC power-split modes, where the output torque from the FESS (which is usually equal to the rated PGS torque during operation) is the sum of the output torques from the PGS output and the power-split branch or the two PGS outputs respectively. This part-load operation occurs even during full vehicle acceleration or braking and reduces the efficiency of the PGSs.

The mean transmission discharge efficiency of both FESSs is seen to be very close to that predicted by the IAM. The round-trip efficiency predicted by the IAM is also found to be reasonably close to the calculated turn-around efficiency of the FESS, although it should be stressed that these efficiencies have different definitions – the IAM round-trip efficiency is calculated for a simple charge-discharge cycle (including the energy dissipated in the required phase of conventional braking to bring the vehicle to a stop) with no resistance losses at the vehicle and flywheel, while the turn-around efficiency is simply the total output to input energy ratio for the FESS over a drive cycle. Nonetheless, the results of the IAM are shown to provide a good guide to the FESS performance under realistic operating conditions.

The specific FHRT cases detailed in Table 7-3 are shown to achieve significant fuel savings relative to the conventional vehicle. The following results show the fuel savings achieved by FHRTs using the variator and brake controlled FESSs with a range of useful energy capacities. This has been calculated for both the main-line and branch-line routes using the uniform coasting strategy defined in Chapter 3. The results are shown for the case when initial and final flywheel *SOC* are equal.

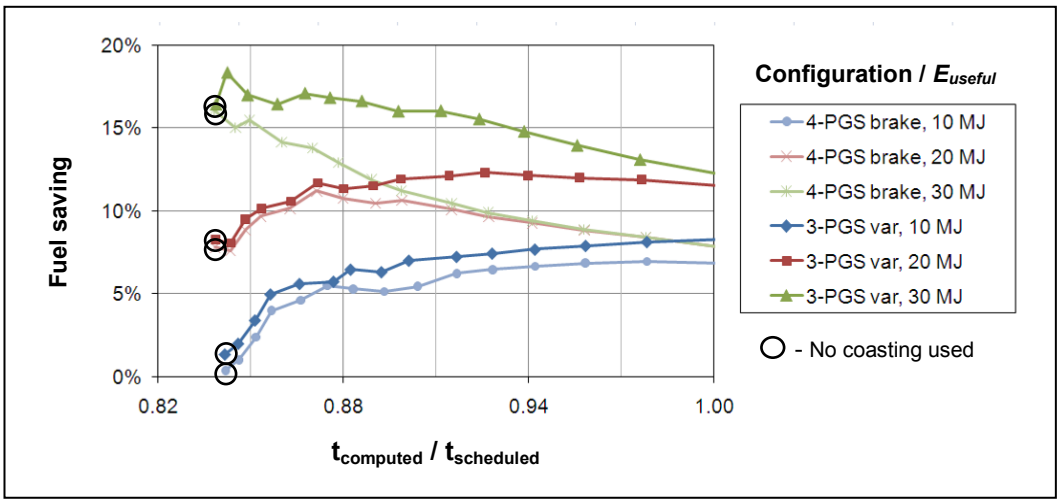


Figure 7-8 – Fuel saving relative to conventional vehicle for main-line operation using 4-PGS brake-controlled and 3-PGS variator-controlled PSTs and the stated FESS useful energy capacities with equal initial and final flywheel *SOC*

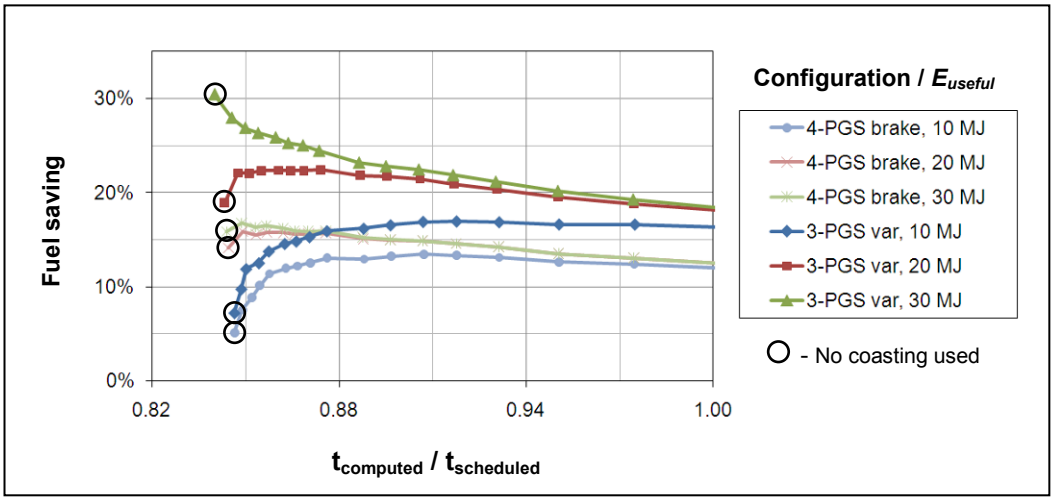


Figure 7-9 – Fuel saving relative to conventional vehicle for branch-line operation using 4-PGS brake-controlled and 3-PGS variator-controlled PSTs and the stated FESS useful energy capacities with equal initial and final flywheel *SOC*

It is clear from these results that the 3-PGS variator-controlled system achieves the highest fuel saving for a given FESS energy capacity under all operating conditions, due to the higher transmission efficiency. For a relatively small system of 10 MJ the 4-PGS brake-controlled FESS does however provide a similar level of performance. When sufficient coasting is used to meet the scheduled journey time the brake system achieves a maximum fuel savings of 6.7% and 12% for the main and branch lines respectively, compared to 8.4% and 16% for the variator-controlled system.

Increasing the energy capacity of the brake-controlled system achieves little further benefit when used with a high degree of coasting, as the available braking energy and the transmission efficiency are both limited. As less coasting is used more braking energy can be recovered and the fuel saving increases until the energy capacity of the system is insufficient to store the available energy.

Increasing the energy capacity of the variator-controlled system is seen to have a larger effect on the fuel saving due to the higher transmission efficiency. A maximum fuel savings of around 17% (main-line) and 30% (branch-line) are achieved with the 30 MJ system when very little coasting is used. When significant coasting is used the 30 MJ system is no longer fully charged, and approaches the performance of the 20 MJ system which achieves savings of around 12% (main-line) and 20% (branch-line) over a wide range of journey times.

The fuel savings calculated for the 3-PGS variator-controlled FESS are similar to those predicted for the 100% efficiency generic energy storage system with a power limitation of 1MW described in Chapter 3. This is due to the fact that the braking energy recovered by the generic hybrid was assumed to replace energy generated by the conventional power-train operating at the average efficiency for the drive cycle. The flywheel systems descibed in the course of this Thesis are capable of providing the entire tractive power for the initial vehicle acceleration, thereby eliminating the inefficient low speed operation of the conventional power-train. This has associated advantages such as reducing noise and emissions in the station environment which are outside the scope of this research. In terms of fuel consumption, even relatively simple flywheel regenerative braking systems have been shown to allow significant reductions in fuel consumption, and present an effective option for improving the efficiency of existing and new diesel powered rail vehicles.

7.4. Summary

The performance of flywheel hybrid regional trains has been investigated using an integrated computational model of the conventional vehicle power-train and an FESS (flywheel energy storage system). Calculations have been performed for two FESS configurations; the 3-PGS variator-controlled system (which has high efficiency but is mechanically complex) and the 4-PGS brake-controlled system (which has lower efficiency but a simpler design). The effect of FESS energy capacity, control strategy and component efficiencies on the overall fuel consumption has been assessed for representative main-line and branch-line routes using a range of uniform coasting driving strategies. The parameters of the FESSs have been

specified using the design tool data generated by the IAM, and have been chosen in order to achieve minimum mass for the given useful energy capacity. The results of the flywheel hybrid vehicle analysis show that this approach provides an excellent starting point for investigating the effect of application specific factors related to the vehicle drive cycle and FESS control requirements. Significant fuel savings are have been calculated for flywheel hybrid vehicle using both of the FESS configurations, and appropriate useful energy capacities have been identified. The results of the analysis presented in this Chapter therefore offer guidelines for the specification and design of practical mechanical FESSs for regional rail applications, and illustrate the inherent compromise between the mass, efficiency and complexity of the system.

8. Summary and conclusions

8.1. Summary of research and contributions

The research presented in this Thesis focuses on assessing the potential fuel savings possible through the hybridisation of regional trains and understanding the operation and performance of mechanical flywheel energy storage systems. Advanced flywheel devices used with variable mechanical transmissions are identified in Chapter 2 as representing a suitable energy storage option for enabling regenerative braking on rail vehicles. This is confirmed in Chapter 3, where a computational model of a conventional diesel powered regional train is described and the energy and power requirements for the energy storage system of a generic hybrid regional train are characterised. In the literature, the analysis of hybrid regional trains has been performed using defined drive cycles that represent relatively aggressive strategies. A key contribution of this research is to characterise the effect of driving strategy on the fuel savings possible through hybridisation. As efficient driving strategies have been identified as a low cost, short term means of reducing the energy consumption of rail vehicles, it is important to consider the efficient control of a conventional train as the base case for assessing the benefits of hybridisation. The results presented in Chapter 3 show that the potential fuel saving of a hybrid regional train is highest when an aggressive 'flat out' driving strategy is used, and falls to around half the maximum value when an efficient coasting strategy is used to achieve the scheduled journey time. With an efficient driving strategy and applying practical limitations to the energy storage system, fuel savings of around 10% and 20% are predicted for hybrid regional trains operating on a representative main-line and branch-line route respectively.

The design of potential mechanical flywheel energy storage systems to meet the requirements of the hybrid regional train application is considered in Chapters 4 and 5. The characterisation of these systems is a difficult process due to the variation in both flywheel and vehicle speed that occurs during charging and discharging. Continuously variable transmissions (CVTs) for mechanical flywheel systems are therefore required to operate over a much larger range of speed ratios than occur in conventional variable transmissions for engine applications. Common CVT components are discussed in Chapter 2, along with a range of proposed flywheel power-trains described in the literature for specific applications. There is however little fundamental information regarding the comparison of flywheel system

performance for different configurations or the identification of appropriate system parameters such as gearing ratios, flywheel energy capacity, flywheel depth-of-discharge and component power ratings for a particular application. An analysis method has therefore been developed which is independent of the flywheel application and provides fundamental insight into the performance of mechanical flywheel energy storage systems (FESSs) for regenerative braking applications. The strength of this analysis lies in understanding the interaction between the flywheel, transmission and vehicle. The efficiency of the transmission is a key factor in determining the overall operation of the system. The Independent Analysis Method (IAM) presented in Chapters 4 and 5 assumes that the resistance losses at the flywheel and vehicle are negligible, allowing the operation of the system to be completely characterised in terms of normalised gear ratios which are a function of the transmission gear ratios and the ratio of the equivalent inertias of the vehicle and flywheel at the transmission input and ouput. The results of the analysis are therefore independent of the application, and allow general design tools to be generated for flywheel systems.

The key component in all the flywheel transmissions considered in this research is the planetary gearset (PGS). When operated as a 2 degree-of-freedom device this allows torque to be transmitted between two of the PGS branches over a continuously variable speed range by applying a 'control' torque at the third PGS branch. While there are a wide range of PGS designs and connection options, the generic PGS analysis method described by White [94] applies to all types of differential gearing, and has been used throughout this research. The IAM is applied to simple brake-controlled PGS transmissions and more complex gearbox-controlled power-split transmissions in Chapter 4. Exact analytical expressions are derived relating the transmission efficiency and normalised component requirements (such as energy dissipation in the control brakes or the power rating of gearbox components) to the normalised gearing ratios of the transmission. A key contribution of this research is the ability to use this method of FESS analysis to identify appropriate normalised gear ratios for a given transmission configuration and produce 'design tools' which encapsulate the performance and design specifications of a flywheel system for any vehicle regenerative braking application (as defined by the equivalent vehicle and flywheel inertias). An important finding of the research is the relationship between the flywheel depth of discharge achieved using particular values of normalised gear ratios and the associated transmission discharge efficiency. This led to the definition of a flywheel utilisation factor, U, which reflects the proportion of the initial kinetic energy stored in a fully charged flywheel that can

be delivered to the vehicle during a full discharge event. This factor is very important in terms of the specific energy capacity of the system, as the maximum U occurs when the smallest possible flywheel can be used to deliver a fixed amount of energy to the vehicle. The U factor is also shown to provide a basis for identifying an appropriate range of operating conditions to define the design tools for the variator-controlled power-split transmission discussed in Chapter 5. Due to the high power requirements of a regenerative braking system for rail vehicle, the variator-controlled power-split transmissions considered have all been constrained to avoid operating with power recirculation. The U factor is shown to provide an absolute basis for performing a comparison of the transmission efficiency and variator power requirement of the different transmissions.

The design tools created using the IAM illustrate the range of system parameters which should be considered for a given application. The actual system parameters can be identified as the most appropriate on the basis of minimising the total mass of the flywheel and transmission required to deliver a fixed amount of useful energy to the vehicle during flywheel discharge. The results of this analysis for the regional rail application show that of all the transmission configurations considered, a novel multiple-regime power-split configuration consisting of 3 PGSs and either a variator or 4-speed discrete gearbox can achieve both high transmission efficiency and a high specific energy capacity. A mechanically much simpler 4-PGS brake-controlled transmission has also been identified as suitable for regenerative braking applications in situations where the useful energy capacity of the flywheel is significantly less than the energy available during braking, and high transmission efficiency is not therefore essential.

The accuracy of the results of the IAM are investigated in Chapter 6 by applying a Dependent Analysis Method (DAM) which is dependent on the characteristics of the vehicle and a simple drive cycle, and includes the effect of resistance losses at the vehicle and flywheel. The system parameters identified from the IAM design tools as minimising mass for a given useful energy capacity are found to achieve similar performance when applied to the DAM for both regional train and passenger car applications. The main difference is a small decrease in the round-trip efficiency for the system, caused by energy losses at the flywheel and a reduction in the transmission efficiency for a full flywheel charging event (as the required initial speed is now higher than that predicted by the IAM). The results of the IAM are therefore shown to provide a strong basis for specifying flywheel system parameters for realistic applications.

This is demonstrated in Chapter 7 which describes the computational modelling of flywheel hybrid regional trains using both the 3-PGS variator and 4-PGS brake controlled systems. A range of energy storage capacities are considered for both cases, and the system parameters are specified to achieve minimum mass using the IAM design tools. Compared to the conventional vehicle, the flywheel hybrid train using a 3-PGS variator-controlled system was found to achieve the largest reductions in fuel consumption. When combined with the efficient use of coasting, fuel savings of around 12% and 20% were calculated for the main-line and branch-line routes, and an appropriate useful energy capacity of 20 MJ was identified. Under these operating conditions the FESS was found to achieve a relatively high mean turn-around efficiency of approximately 60% which includes the effect of losses in the transmission components and at the flywheel. The lower mean turn-around efficiency of approximately 42% for the 4-PGS brake-controlled FESS was found to limit the possible fuel savings to around 8% and 12% for the same driving strategy and useful energy capacity. The results of this detailed computational analysis demonstrate the value of using the design tools generated by the IAM to specify the FESS parameters for practical applications, and show that flywheel systems can provide an effective regenerative braking solution for regional rail vehicles.

8.2. Recommendations for future work

There are several avenues for further research in the area of flywheel energy storage systems.

Firstly, detailed design work is required to assess whether the multiple-PGS power-split transmissions described in this Thesis represent a practical option for vehicle regenerative braking applications. Key factors are whether the required levels of clutch and variator control can be achieved with current technology to enable a smooth and continous tractive power flow throughout flywheel charging and discharging. Furthermore, the production cost, durability and maintenance requirements of these transmissions need to be investigated. The research presented in this Thesis provides useful guidlines for the detailed design process.

Secondly, the Independent Analysis Method described in this Thesis can be used to characterise a wide range of possible flywheel transmission configurations. This can include power-split transmissions which operate with power-recirculation. An interesting study would be to investigate the operation of a power-recirculating variator-controlled flywheel transmission and characterise the compromise between increasing the overall ratio coverage of the transmission while increasing the rated power requirement of the variator and the

associated losses. Combining this with detailed design work would allow a thorough comparison of the many different flywheel transmission options on the basis of efficiency, control requirements, mass and cost.

Finally, a comprehensive comparison of the proposed flywheel energy storage systems with alternative diesel-electric hybrid technology should be performed to identify the relative strengths of the different technologies and assess their suitablility for a range of applications.

Appendices

Appendix A – Identifying expression for normalised CGB speed

Normalisation of CGB output speed for FDC clutch-controlled PST during flywheel discharge is described as follows;

$$\omega_{cgb,o} = GK_p\omega_2 = \frac{GK_p}{1-R_p}\left(\omega_3 - R_p\omega_1\right)$$

$$\frac{1}{K_o}\frac{\omega_{cgb,o}}{\omega_{1,\max}}\sqrt{\frac{J_{fd}}{J_{fw}}} = \frac{GK_p}{K_o}\frac{1}{\left(1-R_p\right)}\left(\frac{\omega_3}{\omega_{1,\max}} - R_p\frac{\omega_1}{\omega_{1,\max}}\right)\sqrt{\frac{J_{fd}}{J_{fw}}}$$

$$= \frac{\left|\left(1-R_p\right)\right|}{\left(1-R_p\right)}\left(\frac{R_p*}{R_{eq}*}-1\right)\left(\left(\frac{\left|R_p*\right|}{R_p*}\right)\sqrt{\frac{KE_{veh}}{KE_{fw,\max}}} - R_p*\frac{\omega_1}{\omega_{1,\max}}\right)$$

Therefore,

$$\frac{1}{K_o}\left|\frac{\omega_{cgb,o}}{\omega_{1,\max}}\right|\sqrt{\frac{J_{fd}}{J_{fw}}} = \left(\frac{R_p*}{R_{eq}*}-1\right)\left|\left(\frac{\left|R_p*\right|}{R_p*}\right)\sqrt{U'} - \left(R_p*\right)\sqrt{\left(1-DOD'\right)}\right|$$

Where *U'* is the instantaneous flywheel utilisation and *DOD'* is the instantaneous flywheel depth of discharge corresponding to the instantaneous CGB output speed, $\omega_{cgb,o}$. For flywheel discharge, these will have initial values of zero (when the vehicle is stationary and the flywheel is fully charged) and final values of *U* and DOD_{ov} (when the transmission can no longer discharge the flywheel). As the values of *U* and DOD_{ov} are purely functions of the actual and equivalent PGS *R**'s and actual PGS and CGB efficiencies, it is clear that this expression corresponds to a normalised CGB output speed, $\omega_{cgb,o}$*.

$$\omega_{cgb,o}* = \frac{1}{K_o}\left|\frac{\omega_{cgb,o}}{\omega_{1,\max}}\right|\sqrt{\frac{J_{fd}}{J_{fw}}}$$

Appendix B – Further results from the Dependent Analysis Method

Figure B-1 shows the specific energy of FESS and overall round-trip system efficiency as functions of R^* for 1-regime FDC variator-controlled PST with a range of E_{useful} values.

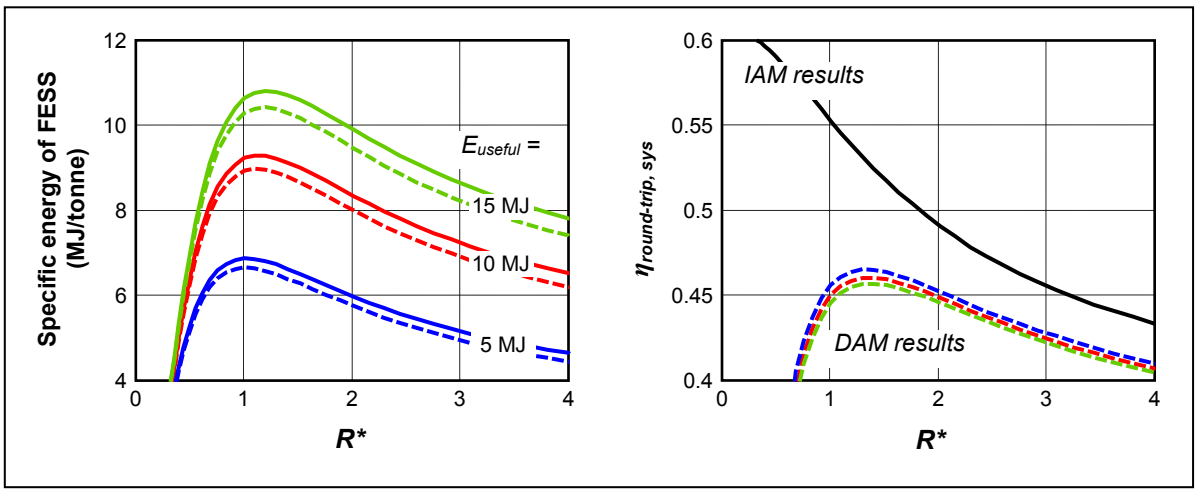


Figure B-1 – Specific energy and overall system round-trip efficiency for 1-PGS FDC variator-controlled FESS using using the IAM (solid lines) and the DAM with τ_{dwell} = 60 s and $\tau_{interval}$ = 5 mins (dashed lines)

These results show that for practical energy storage capacitites the maximum specific energy capacity of the FESS is very similar to that calculated using the IAM design tool, and occurs at the same value of R^*. The corresponding overall round-trip system efficiency is seen to remain close to the maximum value for the useful energy capacities considered.

Further results of the DAM for a regional rail application of the 3-PGS variator-controlled FESS are shown in Figure B-2. The specific energy of the FESS and the overall round-trip system efficiency are shown as functions of the largest of the three normalised PGS gear ratios, R_C^*.

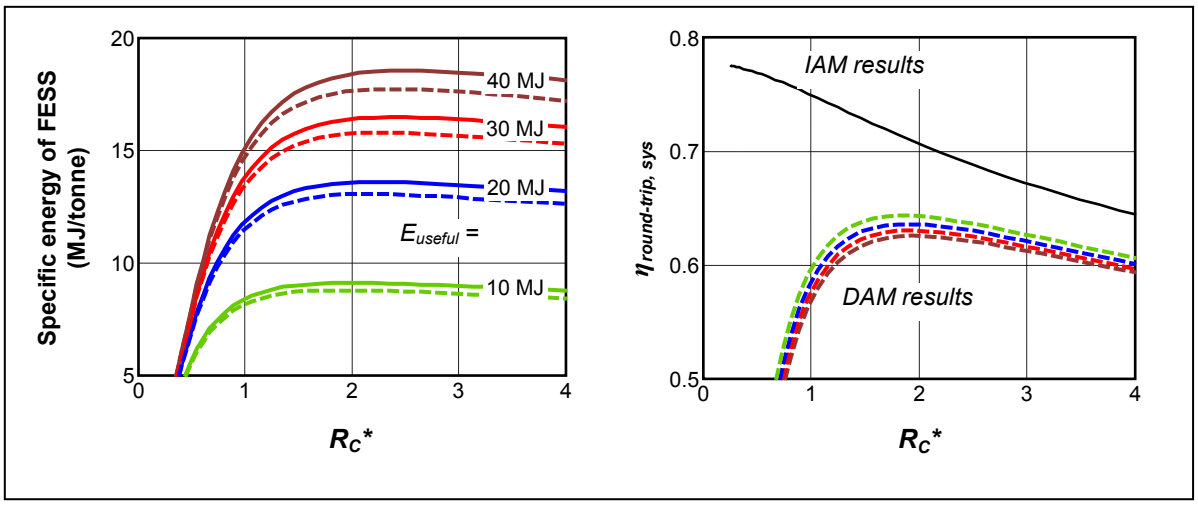


Figure B-2 – Specific energy and overall system round-trip efficiency for the 3-PGS variator-controlled FESS using the IAM (solid lines) and the DAM with τ_{dwell} = 60 s and $\tau_{interval}$ = 5 mins (dashed lines)

These results again show that for a given useful energy capacity, the R_C* value that achieves maximum specific energy capacity is very similar using the IAM and the DAM, and results in a close to maximum value of the round-trip system efficiency.

Appendix C – Consideration of PGS meshing losses

The virtual power method of analysing the meshing efficiency of planetary gearsets (PGSs) has been described by Chen and Angeles [ref]. This method has been applied here to the case of a single stage, 2 degree-of-freedom PGS with a characteristic gear ratio, R, in the range; $0 < R < 0.5$. This corresponds to the type of PGSs that have been identified as practical for FESS transmission.

The virtual power analysis requires loss factors, λ, to be specified, defined as the percentage transmission losses that occur for an elementary gear pair when the gear pair carrier is fixed. The losses that occur in the PGS can therefore be calculated by considering the virtual power flowing between the gear pair in a frame of reference moving with the carrier. Expressions for the PGS efficiency can then be derived for a range of power flow and speed conditions at the PGS branches.

Four general power flow scenarios typically occur for a 1-stage PGS with branch 1 connected to the flywheel and branch 3 connected to the vehicle final drive. These are shown below along with the derived expression for PGS efficiency, where λ_1 and λ_2 refer to the loss factors for the sun-planet and planet-ring gear pairs respectively.

i. Flywheel discharge with $\omega_2 < 0$

$$\eta = 1 - \left(\lambda_1 + \lambda_2 - \lambda_1\lambda_2\right)\left(1 - \frac{\omega_3}{\omega_1}\right)$$

ii. Flywheel discharge with $0 < \omega_2 < \omega_3$

$$\eta = \frac{\left(1-\lambda_1\right)\left(1-\lambda_2\right)\left(\frac{\omega_3}{R\omega_1}\right) + \left(\lambda_1 + \lambda_2 - \lambda_1\lambda_2\right)\left(\frac{\omega_3}{\omega_1}\right)}{\left(1-\lambda_1\right)\left(1-\lambda_2\right)\left(\frac{\omega_3}{R\omega_1}\right) + \lambda_1 + \lambda_2 - \lambda_1\lambda_2}$$

iii. Flywheel charging with $\omega_2 < 0$

$$\eta = \frac{1}{1 + \left(\frac{\lambda_1 + \lambda_2 - \lambda_1\lambda_2}{\left(1-\lambda_1\right)\left(1-\lambda_2\right)}\right)\left(1 - \frac{\omega_3}{\omega_1}\right)}$$

iv. Flywheel charging with $0 < \omega_2 < \omega_3$

$$\eta = \frac{\frac{\omega_3}{R\omega_1} - \lambda_1 - \lambda_2 + \lambda_1\lambda_2}{\left(\frac{1}{R} - \lambda_1 - \lambda_2 + \lambda_1\lambda_2\right)\left(\frac{\omega_3}{\omega_1}\right)}$$

It is clear from these equations that the PGS meshing losses depend on the speed ratio ω_3/ω_1, the loss factors and (when $0 < \omega_2 < \omega_3$) the characteristic gear ratio, R. The efficiency equations derived for a particular speed condition produce almost identical results for both flywheel charging and discharging. Assuming a typical gear pair transmission efficiency of 98% provides loss factors of 2%, and the efficiency of the PGS during both charging and discharging is illustrated in the Figure below for two practical R values for a single-stage PGS.

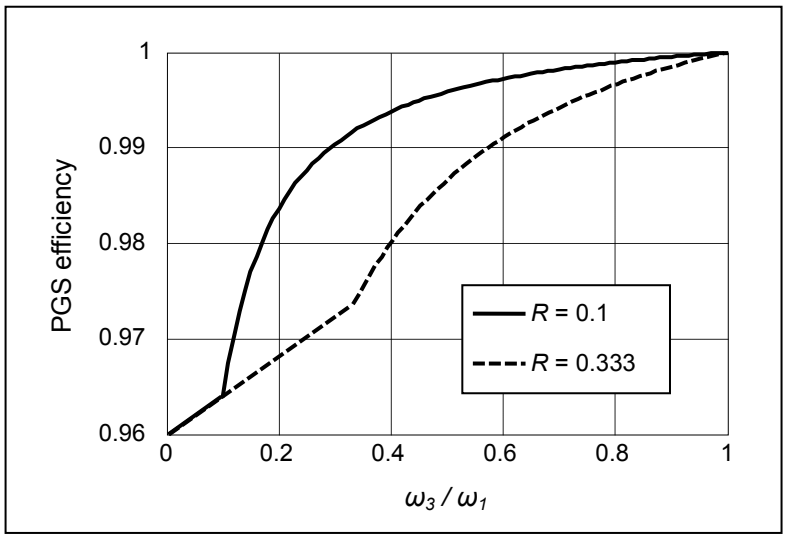


Figure C-1 – PGS efficiency calculated using virtual power analysis of meshing losses

This Figure illustrates the speed dependence of a practical PGS for flywheel transmission applications. The minimum efficiency is however relatively high and independent of torque, suggesting that other, torque dependent sources of energy loss need to be considered when characterising the overall PGS efficiency.

Bibliography

1. Stern, N., *Stern review on the economics of climate change*. 2006, Cambridge, UK: Cambridge University Press.
2. Metz, B., et al., *Contribution of Working Group III to the Fourth Assessment Report of the Intergovernmental Panel on Climate Change*. 2007, Cambridge, UK: Cambridge University Press.
3. *Energy Technology Perspectives 2008*, Paris: OECD/IEA.
4. *World Energy Outlook 2009*, Paris: OECD/IEA.
5. Levinson, D., et al., *The full cost of high-speed rail: an engineering approach.* Annals of Regional Science, 1997. **Vol 31**(Number 2): p. 189-215.
6. de Rus, G. and G. Nombela, *Is Investment in High Speed Rail Socially Profitable?* Journal of Transport Economics and Policy, 2007. **41**: p. 3-23.
7. *Study on further electrification of Britain's railway network*. 2007, Rail Safety and Standards Board: London.
8. *Network RUS, Electrification*. 2009, Network Rail: London.
9. *UK Climate Change Sustainable Development Indicator; 2008 Greenhouse Gas Emissions, Final Figures*. 2010, Department of Energy and Climate Change: London.
10. Anon., *Baseline energy statement - energy consumption and carbon dioxide emissions on the railways*. March 2007, ATOC.
11. Peckham, C., *Improving the efficiency of traction energy use*. 2007, Rail Safety and Standards Board: London.
12. Mellitt, B., Z.S. Mouneimne, and C.J. Goodman, *Simulation study of DC transit systems with inverting substations.* Electric Power Applications, IEE Proceedings B, 1984. **131**(2): p. 38-50.
13. Yii Shen, T., W. Ruay-Nan, and C. Nanming, *Electric network solutions of DC transit systems with inverting substations.* Vehicular Technology, IEEE Transactions on, 1998. **47**(4): p. 1405-1412.
14. *Delivering a Sustainable Railway - White Paper CM 7176*. 2007, Department for Transport: London.
15. *Evaluation of drivetrain technology for future diesel multiple units*. 2009, Rail Safety and Standards Board: London.
16. Chau, K.T. and C.C. Chan, *Emerging Energy-Efficient Technologies for Hybrid Electric Vehicles.* Proceedings of the IEEE, 2007. **95**(4): p. 821-835.
17. Chau, K.T. and Y.S. Wong, *Hybridization of energy sources in electric vehicles.* Energy conversion and management, 2001. **42**(9): p. 1059-1069.
18. Pay, S. and Y. Baghzouz. *Effectiveness of battery-supercapacitor combination in electric vehicles*. in *Power Tech Conference Proceedings, 2003 IEEE Bologna*. 2003.
19. Bentley, P., D.A. Stone, and N. Schofield, *The parallel combination of a VRLA cell and supercapacitor for use as a hybrid vehicle peak power buffer.* Journal of Power Sources, 2005. **147**(1-2): p. 288-294.
20. Briat, O., et al., *Principle, design and experimental validation of a flywheel-battery hybrid source for heavy-duty electric vehicles.* Electric Power Applications, IET, 2007. **1**(5): p. 665-674.
21. Chau, K.T. and Y.S. Wong, *Overview of power management in hybrid electric vehicles.* Energy conversion and management, 2002. **43**(15): p. 1953-1968.
22. Emadi, A., et al., *Topological overview of hybrid electric and fuel cell vehicular power system architectures and configurations.* Vehicular Technology, IEEE Transactions on, 2005. **54**(3): p. 763-770.

23. Vincent, C.A. and B. Scrosati, *Modern Batteries: An Introduction to Electrochemical Power Sources*. 1997, Oxford: Butterworth-Heinemann.
24. Chan, C.C. and K.T. Chau, *Modern Electric Vehicle Technology*. Monographs in Electrical and Electronic Engineering, ed. P. Hammond, T.J.E. Miller, and T. Kenjo. 2001, Oxford: Oxford University Press.
25. Larminie, J. and J. Lowry, *Electric Vehicle Technology Explained*. 2003, Chichester, UK: Wiley.
26. *Tesla Motors*. [cited 01/10/10]; Available from: http://www.teslamotors.com/.
27. *Nissan Motor Company*. [cited 01/10/10]; Available from: http://www.nissan.co.uk/.
28. Burke, A., *Ultracapacitors: why, how, and where is the technology.* Journal of Power Sources, 2000. **91**(1): p. 37-50.
29. Shah, S., *The design and development of a high speed composite flywheel for hybrid vehicles. PhD Thesis*, in *Department of Mechanical Engineering, Imperial College London*. 2006.
30. Hebner, R., J. Beno, and A. Walls, *Flywheel batteries come around again.* Spectrum, IEEE, 2002. **39**(4): p. 46-51.
31. Hayes, R.J., et al., *Design and Testing of a Flywheel Battery for a Transit Bus*, in *International Congress & Exposition*. 1999, SAE International: Detroit, MI, USA.
32. Hayes, R.J., et al., *Design and Performance Testing of an Advanced Integrated Power System with Flywheel Energy Storage*, in *Future Transportation Technology Conference*. 2003, SAE International: Costa Mesa, California.
33. *Flybrid Systems*. [cited 01/10/10]; Available from: http://www.flybridsystems.com/.
34. Flynn, M.M., J.J. Zierer, and R.C. Thompson, *Performance Testing of a Vehicular Flywheel Energy System*, in *SAE 2005 World Congress & Exhibition*. 2005, SAE International: Detroit, MI, USA.
35. Genta, G., *Kinetic energy storage : theory and practice of advanced flywheel systems* 1985, London: Butterworths.
36. Zierer, J.J., et al., *Design and Proof Testing of a Composite Containment System for Mobile Applications*, in *SAE 2004 World Congress & Exhibition*. 2004, SAE International: Detroit, MI, USA.
37. Wu, B., et al., *Optimal Power Management for a Hydraulic Hybrid Delivery Truck.* Vehicle System Dynamics, 2004. **42**(1): p. 23 - 40.
38. Hewko, L.O. and T.R. Weber. *Hydraulic Energy Storage Based Hybrid Propulsion System For A Terrestrial Vehicle*. in *Energy Conversion Engineering Conference, 1990. IECEC-90. Proceedings of the 25th Intersociety*. 1990.
39. Pourmovahed, A., *Durability testing of an elastomeric foam for use in hydraulic accumulators*, in *Proceedings of the Twenty-second Intersociety Energy Conversion Engineering Conference*. 1988, American Society of Mechanical Engineers: Denver, CO. p. 31-36.
40. Pourmovahed, A., N.H. Beachley, and F.J. Fronczak, *Modeling of a Hydraulic Energy Regeneration System: Part I - Analytical Treatment.* Journal of Dynamic Systems, Measurement, and Control, 1992. **114**(1): p. 155-159.
41. Pourmovahed, A., N.H. Beachley, and F.J. Fronczak, *Modeling of a Hydraulic Energy Regeneration System: Part II - Experimental Program.* Journal of Dynamic Systems, Measurement, and Control, 1992. **114**(1): p. 160-165.
42. Payne, G., et al., *Efficiency and dynamic performance of Digital Displacement™ hydraulic transmission in tidal current energy converters.* Proceedings of the Institution of Mechanical Engineers, Part A: Journal of Power and Energy, 2007. **221**(2): p. 207-218.

43. *Artemis Intelligent Power*. [cited 01/10/10]; Available from: http://www.artemisip.com/.
44. Christen, T. and M.W. Carlen, *Theory of Ragone plots.* Journal of Power Sources, 2000. **91**(2): p. 210-216.
45. Pell, W.G. and B.E. Conway, *Quantitative modeling of factors determining Ragone plots for batteries and electrochemical capacitors.* Journal of Power Sources, 1996. **63**(2): p. 255-266.
46. Guzzella, L. and A. Sciarretta, *Vehicle Propulsion Systems: Introduction to Modeling and Optimization*. 2nd ed. 2007, Berlin: Springer.
47. Kadhim, R., *Energy storage systems for railway applications - Phase 1*. 2009, Rail Safety and Standards Board: London.
48. Broussely, M., *Recent developments on lithium ion batteries at SAFT.* Journal of Power Sources, 1999. **81-82**: p. 140-143.
49. Saft, M., et al., *Saft lithium-ion energy and power storage technology.* Journal of Power Sources, 1999. **80**(1-2): p. 180-189.
50. Taniguchi, A., et al., *Development of nickel/metal-hydride batteries for EVs and HEVs.* Journal of Power Sources, 2001. **100**(1-2): p. 117-124.
51. Ehsani, M., et al., *Modern Electric, Hybrid Electric, and Fuel Cell Vehicles: Fundamentals, Theory, and Design*. 2005: CRC Press.
52. Anderman, M., *The challenge to fulfill electrical power requirements of advanced vehicles.* Journal of Power Sources, 2004. **127**(1-2): p. 2-7.
53. Jefferson, C.M. and R.H. Barnard, *Hybrid Vehicle Propulsion*. International Series on Advances in Transport. 2002, Southampton, UK: WIT Press.
54. Kanellos, M. *Nissan Prices the Leaf—$32,780—But Will They Make Money?* 30th March 2010 [cited 01/10/10]; Available from: http://www.greentechmedia.com/.
55. Lipman, T.E., *The Cost of Manufacturing Electric Vehicle Batteries*, in *Report for California Air Resources Board*. 1999, Institute of Transportation Studies, University of California: Davis.
56. Lipman, T.E. *Manufacturing and lifecycle costs of battery electric vehicles, direct-hydrogen fuel cell vehicles, and direct-methanol fuel cell vehicles*. in *Energy Conversion Engineering Conference and Exhibit, 2000. (IECEC) 35th Intersociety*. 2000.
57. Jung, D.Y., et al., *Development of ultracapacitor modules for 42-V automotive electrical systems.* Journal of Power Sources, 2003. **114**(2): p. 366-373.
58. Burke, A.F., *Batteries and Ultracapacitors for Electric, Hybrid, and Fuel Cell Vehicles.* Proceedings of the IEEE, 2007. **95**(4): p. 806-820.
59. Linzen, D., et al., *Analysis and evaluation of charge-balancing circuits on performance, reliability, and lifetime of supercapacitor systems.* Industry Applications, IEEE Transactions on, 2005. **41**(5): p. 1135-1141.
60. Acarnley, P.P., et al., *Design principles for a flywheel energy store for road vehicles.* Industry Applications, IEEE Transactions on, 1996. **32**(6): p. 1402-1408.
61. Henning, U., et al., *Ultra low emission traction drive system for hybrid light rail vehicles*, in *International Symposium on Power Electronics, Electrical Drives, Automation and Motion.* 2006. p. 1068-1072.
62. Murphy, B.T., D.A. Bresie, and J.H. Beno, *Bearing loads in a vehicular flywheel battery*, in *1997 International Congress and Exposition*. 1999, SAE Special Publications: Detroit, MI.
63. *ULEV-TAP 2 European Research Project*. [cited 01/10/10]; Available from: http://www.ulev-tap.org/.

64. Cross, D. and J. Hilton. *High Speed Flywheel Based Hybrid Systems for Low Carbon Vehicles*. in *Hybrid and Eco-Friendly Vehicle Conference, 2008. IET HEVC 2008*. 2008.
65. Reading, M.M., *Flywheel Energy Storage System*, in *Public Interest Energy Research Program*. 2004, California Energy Commission.
66. Lu, S., et al. *Analysis of energy storage devices in hybrid railway vehicles*. in *Railway Engineering - Challenges for Railway Transportation in Information Age, 2008. ICRE 2008. International Conference on*. 2008.
67. Fujii, T., N. Teraya, and M. Osawa, *Development of an NE Train.* JR East Technical Review, 2004(No. 4): p. 62-70.
68. Grantham, A. *Hybrid technology enters the real world*. 2007 [cited 01/10/10]; Available from: http://www.railwaygazette.com/.
69. *Diesel-battery hybrid trial ends*. 2008 [cited 01/10/10]; Available from: http://www.railwaygazette.com/.
70. Sameshima, H., M. Ogasa, and T. Yamamoto, *On-board Characteristics of Rechargeable Lithium Ion Batteries for Improving Energy Regenerative Efficiency.* Quarterly Report of RTRI, 2004. **45**(2): p. 45-52.
71. *MITRAC Energy Saver*. 2009 [cited 01/10/10]; Available from: http://www.bombardier.com/.
72. *MITRAC Hybrid - The Dual Power Propulsion Chain*. 2009 [cited 01/10/10]; Available from: http://www.bombardier.com/.
73. Steiner, M. and J. Scholten, *Energy storage on board of DC fed railway vehicles*, in *IEEE Power Electronics Specialists Conference*. 2004. p. 666-671 Vol.1.
74. Donnelly, F.W., R.L. Cousineau, and R.N.M. Horsley. *Hybrid technology for the rail industry*. in *Rail Conference, 2004. Proceedings of the 2004 ASME/IEEE Joint*. 2004.
75. Cousineau, R., *Development of a hybrid switcher locomotive the Railpower Green Goat.* Instrumentation & Measurement Magazine, IEEE, 2006. **9**(1): p. 25-29.
76. Miller, A.R., et al., *System design of a large fuel cell hybrid locomotive.* Journal of Power Sources, 2007. **173**(2): p. 935-942.
77. Nene, V.D., *Advanced Propulsion Systems for Urban Rail Vehicles*. 1985: Prentice-Hall, Inc.
78. Cook, L.M., et al., *Flywheel Energy Storage Switcher - Study Summary and Detailed Description of Analysis*. 1979, U.S. Department of Transportation, Federal Railroad Administration.
79. Griffin, T., *Ultra light rail developments.* Proceedings of the Institution of Mechanical Engineers, Part F: Journal of Rail and Rapid Transit, 2001. **215**(3): p. 149-156.
80. *Hydrodynamic Drive Solutions*. [cited 01/10/10]; Available from: http://www.voithturbo.com/.
81. Beachley, N.H., et al., *Continuously-variable transmission designs for flywheel hybrid automobiles*, in *Proceedings of the lnternational Symposium on Gearing & Power Transmissions*. 1981: Tokyo. p. 393-398,.
82. *Torotrak*. [cited 01/10/10]; Available from: http://www.torotrak.com/.
83. Fuchs, R., et al., *The Making of The Full Toroidal Variator.* JTEKT Engineering Journal, English Edition, 2009(No.1006E): p. 31-36.
84. van der Sluis, F., et al., *Efficiency Optimization of the Pushbelt CVT*, in *SAE World Congress & Exhibition*. 2007, SAE International: Detroit, MI, USA.
85. Yamamoto, T., K. Matsuda, and T. Hibi, *Analysis of the efficiency of a half-toroidal CVT.* JSAE review, 2001. **22**(4): p. 565-570.
86. Akehurst, S., et al., *Modelling of loss mechanisms in a pushing metal V-belt continuously variable transmission. Part 1: torque losses due to band friction.*

Proceedings of the Institution of Mechanical Engineers, Part D: Journal of Automobile Engineering, 2004. **218**(11): p. 1269-1281.
87. Akehurst, S., et al., *Modelling of loss mechanisms in a pushing metal V-belt continuously variable transmission: Part 2: pulley deflection losses and total torque loss validation.* Proceedings of the Institution of Mechanical Engineers, Part D: Journal of Automobile Engineering, 2004. **218**(11): p. 1283-1293.
88. Akehurst, S., et al., *Modelling of loss mechanisms in a pushing metal V-belt continuously variable transmission. Part 3: belt slip losses.* Proceedings of the Institution of Mechanical Engineers, Part D: Journal of Automobile Engineering, 2004. **218**(11): p. 1295-1306.
89. Ryu, W. and H. Kim, *Belt-pulley mechanical loss for a metal belt continuously variable transmission.* Proceedings of the Institution of Mechanical Engineers, Part D: Journal of Automobile Engineering, 2007. **221**(1): p. 57-65.
90. Macmillan, R.H. and P.B. Davies, *Analytical study of systems for bifurcated power transmission.* ARCHIVE: Journal of Mechanical Engineering Science 1959-1982 (vols 1-23), 1965. **7**(1): p. 40-47.
91. White, G., *Power–speed characteristics of differential transmissions.* Journal of Mechanical Engineering Science, 1967. **9**(4): p. 258-264.
92. White, G., *Multiple-stage, split-power transmissions.* Journal of Mechanisms, 1970. **5**(4): p. 505-520.
93. Beachley, N.H., C. Anscomb, and C.R. Burrows, *Evaluation of split-path extended range continuously-variable transmissions for automotive applications.* Journal of the Franklin Institute, 1984. **317**(4): p. 235-262.
94. White, G., *Properties of Differential Transmissions.* The Engineer, 1967. **224**(105).
95. White, G., *Compounded two-path variable ratio transmissions with coaxial gear trains.* Mechanism and Machine Theory, 1976. **11**(3): p. 227-240.
96. Villeneuve, A.M. *Dual Mode Electric Infinitely Variable Transmission*. in *2004 International CVT and Hybrid Transmission Congress*. Davis, CA, USA.
97. Mantriota, G., *Performances of a series infinitely variable transmission with type I power flow.* Mechanism and Machine Theory, 2002. **37**(6): p. 579-597.
98. Mantriota, G., *Performances of a parallel infinitely variable transmissions with a type II power flow.* Mechanism and Machine Theory, 2002. **37**(6): p. 555-578.
99. Mangialardi, L. and G. Mantriota, *Power flows and efficiency in infinitely variable transmissions.* Mechanism and Machine Theory, 1999. **34**(7): p. 973-994.
100. Field, M. and M. Burke, *Powertrain Control of the Torotrak Infinitely Variable Transmission*, in *SAE 2005 World Congress & Exhibition*. 2005, SAE International: Detroit, MI, USA.
101. Mantriota, G., *Power split continuously variable transmission systems with high efficiency.* Proceedings of the Institution of Mechanical Engineers. Part D: Journal of Automobile Engineering, 2001. **215**(3): p. 357-358.
102. Miller, J.M., *Hybrid electric vehicle propulsion system architectures of the e-CVT type.* Power Electronics, IEEE Transactions on, 2006. **21**(3): p. 756-767.
103. Clerk, R.C., *The Utilisation of Flywheel Energy.* SAE Transactions, 1964. **72**.
104. Frank, A.A., N.H. Beachley, and T.C. Hausenbauer, *The fuel efficiency potential of a flywheel hybrid vehicle for urban driving*, in *11th Intersociety Energy Conversion Engineering Conference*. 1976, American Institute of Chemical Engineers: State Line, Nev. p. 17-24.
105. Schilke, N.A., et al., *The design of an engine-flywheel hybrid drive system for a passenger car.* Proceedings of the Institution of Mechanical Engineers, Part D, 1986. **200**(44): p. 231-248.

106. Diego-Ayala, U., et al., *The mechanical hybrid vehicle: an investigation of a flywheel-based vehicular regenerative energy capture system.* Proceedings of the Institution of Mechanical Engineers; Part D; Journal of automobile engineering, 2008. **222**(11): p. 2087-2101.
107. Diego-Ayala, U., *An Investigation Into Hybrid Power Trains for Vehicles With Regenerative Braking*. PhD Thesis, 2006, Imperial College London.
108. Diego-Ayala, U., P. Martinez-Gonzalez, and K.R. Pullen. *A Simple Mechanical Transmission System for Hybrid Vehicles Incorporating a Flywheel*. in *Hybrid and Eco-Friendly Vehicle Conference, 2008. IET HEVC 2008*. 2008.
109. Cross, D. and C. Brockbank, *Mechanical Hybrid system comprising a flywheel and CVT for Motorsport & mainstream Automotive applications*, in *SAE World Congress & Exhibition*. 2008, SAE International: Detroit, MI, USA.
110. Brockbank, C. and W. Body, *Flywheel-based mechanical hybrid system: simulation of the fuel consumption benefits of various transmission arrangements and control strategies*, in *ASME 2010 International Design Engineering Technical Conferences & Computers & Information in Engineering Conference*. 2010: Montreal, Canada.
111. Martin, P. *Train performance and simulation*. in *Simulation Conference Proceedings, 1999 Winter*. 1999.
112. Toffolo, M.P., G.E. Dawson, and A.R. Eastham. *An improved train network simulator*. in *Electrical and Computer Engineering, 1994. Conference Proceedings. 1994 Canadian Conference on*. 1994.
113. Liu, R. and I.M. Golovitcher, *Energy-efficient operation of rail vehicles.* Transportation Research Part A: Policy and Practice, 2003. **37**(10): p. 917-932.
114. Howlett, P.G., I.P. Milroy, and P.J. Pudney, *Energy-efficient train control.* Control Engineering Practice, 1994. **2**(2): p. 193-200.
115. Howlett, P.G., P.J. Pudney, and X. Vu, *Local energy minimization in optimal train control.* Automatica, 2009. **45**(11): p. 2692-2698.
116. Wong, K.K. and T.K. Ho, *Coast control for mass rapid transit railways with searching methods.* Electric Power Applications, IEE Proceedings -, 2004. **151**(3): p. 365-376.
117. Hee-Soo, H., *Control strategy for optimal compromise between trip time and energy consumption in a high-speed railway.* Systems, Man and Cybernetics, Part A: Systems and Humans, IEEE Transactions on, 1998. **28**(6): p. 791-802.
118. Bocharnikov, Y.V., et al., *Optimal driving strategy for traction energy saving on DC suburban railways.* Electric Power Applications, IET, 2007. **1**(5): p. 675-682.
119. Hillmansen, S. and C. Roberts, *Energy storage devices in hybrid railway vehicles: a kinematic analysis.* Proceedings of the Institution of Mechanical Engineers. Part F, Journal of Rail and Rapid Transit, 2007. **221**(1): p. 135-143.
120. Jefferson, C. and J. Marquez. *Hybrid powertrain for a light rail vehicle*. in *Universities Power Engineering Conference*. 2004.
121. Destraz, B., P. Barrade, and A. Rufer. *Power assistance for diesel-electric locomotives with supercapacitive energy storage*. in *IEEE Power Electronics Specialists Conference*. 2004.
122. Wen, Q., S. Kingsley, and R.A. Smith, *Energy simulation of hybrid inter-city trains.* Proceedings of the Institution of Civil Engineers, Energy, 2007. **160**(3): p. 123-131.
123. Andrews, H.I., *Railway Traction*. 1986, London: Elsevier.
124. Rochard, B.P. and F. Schmid, *A review of methods to measure and calculate train resistances.* Proceedings of the Institution of Mechanical Engineers. Part F, Journal of Rail and Rapid Transit, 2000. **214**(4): p. 185-199.

125. Wipke, K.B., M.R. Cuddy, and S.D. Burch, *ADVISOR 2.1: a user-friendly advanced powertrain simulation using a combined backward/forward approach.* IEEE Transactions on Vehicular Technology, 1999. **48**(6): p. 1751-1761.
126. Edghill, C.M., *Hydrostatic and hydrodynamic transmissions*. Engineering design guides. Vol. 23. 1977, Oxford: Oxford University Press for the Design Council, the British Standards Institution, and the Council of Engineering Institutions
127. Lechner, G., *Automotive transmissions : fundamentals, selection, design and application*. 1999, Berlin: Springer.
128. Hinde, P. and C. Larsson, *The Energy Consumption of Rail Vehicles in Britain*. 2006, Joint study by ATOC, Bombadier Transportation, National Express Group.
129. *Class 170 diesel railcar datasheet*. [cited 01/12/09]; Available from: www.voithturbo.com.
130. Ricci, G., *Mass and rated characteristics of planetary gear reduction units.* Meccanica, 1992. **27**(1): p. 35-45.
131. White, G., *Design study of a 375 kW helicopter transmission with split-torque epicyclic and bevel drive stages.* Proceedings of the Institution of Mechanical Engineers, Part C, 1983. **197**(1983): p. 213-224.
132. Schofield, K., D. Horsley, and R. Bevan, *Investigating how the requirements for train brake systems affect vehicle mass: Addressing the issues arising*. 2008, Rail Safety and Standards Board: London.
133. White, G., *Derivation of high efficiency two-stage epicyclic gears.* Mechanism and Machine Theory, 2003. **38**(2): p. 149-159.
134. Soltic, P. and L. Guzzella, *Performance simulations of engine-gearbox combinations for lightweight passenger cars.* Proceedings of the Institution of Mechanical Engineers, Part D: Journal of Automobile Engineering, 2001. **215**(2): p. 259-271.
135. Pennestri, E. and F. Freudenstein, *A Systematic Approach to Power-Flow and Static-Force Analysis in Epicyclic Spur-Gear Trains.* Journal of Mechanical Design, 1993. **115**(3): p. 639-644.
136. Pennestri, E. and P.P. Valentini, *A Review of Formulas for the Mechanical Efficiency Analysis of Two Degrees-of-Freedom Epicyclic Gear Trains.* Journal of Mechanical Design, 2003. **125**(3): p. 602-608.
137. Macmillan, R.H., *Power flow and loss in differential mechanisms.* Journal of Mechanical Engineering Science, 1961. **3**(1): p. 37-41.
138. Chen, C. and J. Angeles, *Virtual-Power Flow and Mechanical Gear-Mesh Power Losses of Epicyclic Gear Trains.* Journal of Mechanical Design, 2007. **129**(1): p. 107-113.
139. Mantriota, G. and E. Pennestrì, *Theoretical and Experimental Efficiency Analysis of Multi-Degrees-of-Freedom Epicyclic Gear Trains.* Multibody system dynamics, 2003. **9**(4): p. 389-408.